



Understand the inversion mechanism of P-stereogenic compound using kinetic studies and in silico modeling

Guilhem Javierre

► To cite this version:

Guilhem Javierre. Understand the inversion mechanism of P-stereogenic compound using kinetic studies and in silico modeling. Theoretical and/or physical chemistry. Ecole Centrale Marseille, 2018. English. NNT : 2018ECDM0001 . tel-01798123

HAL Id: tel-01798123

<https://theses.hal.science/tel-01798123>

Submitted on 23 May 2018

HAL is a multi-disciplinary open access archive for the deposit and dissemination of scientific research documents, whether they are published or not. The documents may come from teaching and research institutions in France or abroad, or from public or private research centers.

L'archive ouverte pluridisciplinaire **HAL**, est destinée au dépôt et à la diffusion de documents scientifiques de niveau recherche, publiés ou non, émanant des établissements d'enseignement et de recherche français ou étrangers, des laboratoires publics ou privés.

Ecole Centrale de Marseille

Institut des Sciences moléculaires de Marseille (iSm2) / UMR 7313

Thèse présentée pour obtenir le grade de docteur de l'Ecole
Centrale de Marseille

Discipline : Sciences chimiques

ED250 – Sciences chimiques de Marseille

Understand the inversion mechanism of P- stereogenic compound using kinetic studies and *in silico* modeling

Présentée par :

Guilhem JAVIERRE

Directeur de thèse : Prof. Frédéric FOTIADU

Co-encadrant : Dr. Rémy FORTRIE

Soutenue le 16/01/2018 devant le jury :

Dr. Angela MARINETTI	Université Paris-Saclay	Rapporteur
Prof. Hélène GERARD	Université Pierre et Marie Curie	Rapporteur
Dr. Stéphane MOUTARD	Novachim	Examinateur
Prof. Stéphane HUMBEL	Université d'Aix-Marseille	Examinateur
Dr. Rémy FORTRIE	Ecole Centrale de Marseille	Examinateur
Prof. Frédéric FOTIADU	Ecole Centrale de Marseille	Directeur de Thèse

“Science is nothing but a series of questions that lead to more questions, which is just as well, or it wouldn’t be much of a career path, would it?”

Terry Pratchett

Je souhaite tout d'abord présenter mes remerciements à la docteure Angela Marinetti de l'Institut de Chimie des Substances Naturelles, et à la professeure Hélène Gérard de l'Université Pierre et Marie Curie - Paris 6, qui me font l'honneur d'être les rapporteuses de cette thèse et de participer à ce jury.

Je remercie également le professeur Stéphane Humbel de l'Université d'Aix-Marseille, et le docteur Stéphane Moutard de Novachim, qui ont accepté de juger cette thèse et de rejoindre le jury.

Je présente toute ma gratitude à mon directeur de thèse, le professeur Frédéric Fotiadu, directeur de l'Ecole Centrale de Marseille, pour m'avoir accueilli en tant que doctorant au sein de l'équipe Chirosciences de l'Institut des Sciences Moléculaires de Marseille. Je le remercie pour ses conseils et sa disponibilité qui ont été précieux dans le développement de cette thèse.

Je remercie tout particulièrement le docteur Rémy Fortrie pour m'avoir encadré tout au long de ma thèse. Je lui exprime toute ma reconnaissance pour son engagement, ses conseils et sa patience, et le remercie particulièrement pour ses encouragements tout au long de ces trois années qui m'ont poussé à toujours m'améliorer.

Je remercie également la docteure Delphine Moraleda, qui m'a encadré au laboratoire, pour son aide et sa patience lors des synthèses avec le théoricien que je suis, ainsi que le docteur Jean-Valère Naubron pour ses bons conseils et sa disponibilité chaque fois que j'avais besoin de son aide.

Je souhaite aussi remercier l'Ecole Centrale de Marseille et la Région Provence-Alpes Côte d'Azur qui ont permis le financement de cette thèse.

Je remercie les chercheurs avec qui j'ai collaboré lors de mes travaux de thèse : le docteur Nicolas Vanthuyne et Mme Marion Jean pour l'HPLC chirale, la docteure Roselyne Rosas et docteur Gaëtan Herbette pour la RMN. Leur participation et leurs explications m'ont beaucoup aidé dans l'avancée de nos travaux.

J'aimerais également remercier le professeur Gérard Buono, et les docteurs Laurent Giordano, Damien Héraut, Sébastien Lemouzy et David Gatineau, qui m'ont aidé à prendre mes marques dans la chimie du phosphore lors de mon arrivée.

Je présente également toute ma gratitude à tous les membres de l'Ecole Doctorale 250, son directeur le professeur Thierry Constantieux pour sa disponibilité, et la secrétaire Mme Corinne Esquiva-Criado pour son attention.

Je remercie le professeur Alexandre Martinez qui m'a accueilli au sein de Chirosciences. Merci également à toute l'équipe pour son accueil et sa bonne humeur, plus spécialement au récemment docteur Rui Liu avec qui j'ai eu le plaisir de partager le bureau pendant trois ans. Je remercie aussi chaque permanent, doctorant, post-doc et stagiaire pour nos discussions scientifiques et autres. Ce fut un plaisir de partager ces trois années en si bonne compagnie.

Je remercie également mes amis, dont le docteur Guillaume Maurin qui m'a aidé lors de la rédaction, sans oublier tous ceux qui m'ont suivi et supporté pendant toutes ces années directement ou en ligne. Merci à chacun d'entre vous.

Enfin, je remercie ma famille pour leur soutien inconditionnel. Je pense particulièrement mes parents « sans qui je ne serais pas là » où j'en suis aujourd'hui, mes grands-parents pour tout ce qu'ils m'inspirent, ainsi que ma sœur et toute ma famille qui m'ont toujours aidé et soutenu. Je n'en serais pas là sans vous.

LIST OF ABBREVIATION

- AC: Associated complex
AdHP: Adamantyl *hydrogeno*-phenylphosphinate
AdOH: 1-adamantanol
AlkHP: alkyl *hydrogeno*-phenylphosphinate
CD: Circular dichroism
 CH_2Cl_2 : Dichloromethane
CIP: Cahn-Ingold-Prelog
COSMO: Conductor-like screening model
CPCM: conductor-like polarizable continuum model
CPD: composite pulse decoupling
d.e.: diastereomeric excess
e.e.: enantiomeric excess
EtOH: Ethanol
DFT: Density functional theory
DMSO: Dimethylsulfoxide
EtHP: ethyl *hydrogeno*-phenylphosphinate
GGA: Generalized gradient approximation
HHP: *hydrogeno*-phenylphosphinic acid
HPLC: High performance liquid chromatography
i-PrHP: *Iso*-propyl *hydrogeno*-phenylphosphinate
i-PrOH: *Iso*-propanol
LDA: Local density approximation
MeHP: Methyl *hydrogeno*-phenylphosphinate
MeLi: Methylolithium
MenHP: Menthyl *hydrogeno*-phenylphosphinate
MeOH: Methanol
MenOH: Menthol
MeP⁻: Methoxyphenylphosphonide
NMR: Nuclear magnetic resonance

n-PrOH: *n*-propanol
n-PrHP: *n*-propyl *hydrogeno*-phenylphosphinate
PES: Potential energy surface
PhPCl₂: Dichlorophenylphosphine
SAS: Solvent accessible surface
SES: Solvent excluded surface
SMD: Solvation model based on density
S_N2: Nucleophilic substitution
S_N2@P: Nucleophilic substitution at phosphorus atom
SPO: Secondary phosphine oxide
TBP: triangle-based bi-pyramidal
t-BuLi: *tert*-butyllithium
t-BuOH: *Tert*-butanol
t-BuSPO: *tert*-butyl *hydrogeno*-phenylphosphine oxide
THF: Tetrahydrofuran
TEA: Triethylamine
TEAO: Triethylamnne oxide
TMA: Trimethylamine
TMAO: Trimethylamine oxide
TPP: Triphenylphospine
TS: Transition state
UV: Ultraviolet

SUMMARY

INTRODUCTION	1
CHAPTER 1:	3
PRESENTATION OF ALKYL HYDROGENO-PHENYLPHOSPHINATES	3
1.1 FROM ASYMMETRIC CATALYSIS TO HYDROGENO-PHOSPHINE OXIDES.....	5
1.1.1 Organophosphorous compounds in asymmetric catalysis.....	5
1.1.2 Description of secondary phosphine oxides.....	6
1.2 SYNTHESIS OF SECONDARY PHOSPHINE OXIDES.....	9
1.3 NUCLEOPHILIC SUBSTITUTIONS AT PHOSPHORUS ATOM	13
1.4 PSEUDOROTATIONS OF PENTACOORDINATED PHOSPHOROUS COMPOUNDS.....	15
1.4.1 Description of a pentacoordinated phosphorus.....	15
1.4.2 The Berry pseudorotations.....	16
1.5 AIM OF THE THESIS	18
CHAPTER 2:	21
METHODOLOGIES FOR SYNTHESIS, ANALYSIS, THEORETICAL MODELING AND KINETIC STUDIES	21
2.1 INTRODUCTION	23
2.2 THEORETICAL CHEMISTRY	23
2.2.1 The Schrödinger Equation.....	24
2.2.2 Density Functional Theory	25
2.2.3 Implicit solvation.....	27
2.2.4 Effect of the temperature	27
2.3 SYNTHESIS OF ALKYL HYDROGENO-PHENYLPHOSPHINATES	28
2.4 ANALYSIS METHODS AND QUANTIFICATION	31
2.4.1 Nuclear magnetic resonance	31
2.4.2 Chiral high performance liquid chromatography.....	32
2.5 KINETICS	33
2.5.1 Reaction rate and transition standard Gibbs free energy.....	33
2.5.2 A case of study: the racemization of ethyl phenylphosphinate	35
2.6 CONCLUSION	36
CHAPTER 3:	39
SYSTEM OF INTEREST AND EQUILIBRIUM IN SOLUTION	39
3.1 INTRODUCTION	41
3.1.1 Context	41
3.1.2 Choice of the system	42
3.2 CONFORMATION OF THE METHYL HYDROGENO-PHENYLPHOSPHINATE.....	42
3.3 PROTOTROPIC EQUILIBRIUM	43
3.4 ACIDOBASICITY SCALE	45
3.4.1 How to build an acidobasicity scale.....	45
3.4.2 Determination of the pKa of the compounds of interest	46
3.5 METHOXIDE AND PHOSPHONIDE	49
3.5.1 Deprotonation of phosphinate by an alkoxide.....	49
3.5.2 Inversion of configuration of a phosphinide	52

3.6 CONCLUSION	53
CHAPTER 4:	55
TRANSESTERIFICATION MECHANISM OF METHANOL ON ALKYL HYDROGENO-PHENYLPHOSPHINATE	55
4.1 INTRODUCTION	59
4.1.1 <i>Context</i>	59
4.1.2 <i>Methodology</i>	60
4.2 ADDITION OF METHANOL ONTO THE PHOSPHORUS ATOM	62
4.2.1 <i>Possible approaches of methanol onto phosphinate</i>	62
4.2.2 <i>A study of the 6 mechanisms for S_N2</i>	65
4.3 INFLUENCE OF THE PENTACOORDINATED INTERMEDIATE ON THE GLOBAL MECHANISM	68
4.3.1 <i>Further evolution on the pentacoordinated intermediate</i>	68
4.3.2 <i>Berry pseudorotations of the pentacoordinated intermediate</i>	72
4.4 KINETIC STUDY	76
4.4.1 <i>Experimental measurements</i>	76
4.4.2 <i>Observations</i>	78
4.4.3 <i>Discussion</i>	81
4.4.4 <i>Kinetic adjustment</i>	82
4.5 RELIABILITY OF SIMULATIONS	84
4.6 CONCLUSION	86
CHAPTER 5:	89
EFFECT OF BASIC CATALYSIS ON THE TRANSESTERIFICATION MECHANISM OF ALKYL HYDROGENO-PHENYLPHOSPHINATES BY ALCOHOL.....	89
5.1 INTRODUCTION	93
5.1.1 <i>Context</i>	93
5.1.2 <i>Methodology</i>	94
5.2 EXPERIMENTAL STUDY: KINETIC OF ENANTIOMERIZATION.....	94
5.2.1 <i>Observations</i>	94
5.2.2 <i>Kinetic modeling</i>	97
5.3 EQUILIBRIUM OF THE SYSTEM IN BASIC CONDITIONS.....	100
5.3.1 <i>Tautomerism and coordination of TMA</i>	100
5.3.2 <i>Deprotonation of reactants</i>	101
5.3.3 <i>Conclusion</i>	102
5.4 ADDITION MECHANISM IN BASIC CONDITIONS	103
5.4.1 <i>Addition on phosphinous acid form</i>	103
5.4.2 <i>With one equivalent of TMA</i>	104
5.4.3 <i>With 2 equivalents of TMA</i>	106
5.4.4 <i>Deprotonated phosphinate</i>	108
5.4.5 <i>The mysterious catalyst</i>	110
5.4.6 <i>Conclusion</i>	112
5.5 CONCLUSION	113
CHAPTER 6:	117
EFFECT OF THE HINDRANCE ON THE ENANTIOSTABILITY OF ALKYL HYDROGENO-PHENYLPHOSPHINATES	117
6.1 INTRODUCTION	119
6.1.1 <i>Context</i>	119
6.1.2 <i>Methodology</i>	119

6.2	INFLUENCE OF THE ALKYL GROUP ON SN ₂ @P IN NEUTRAL CONDITIONS.....	120
6.3	KINETIC STUDY IN BASIC CONDITIONS USING ³¹ P-CPD NMR	124
6.3.1	<i>Choice of the system</i>	124
6.3.2	<i>Observations</i>	125
6.4	EARLY CONCLUSION	128
GENERAL CONCLUSION		129
BIBLIOGRAPHY		133
ANNEXES.....		137

Introduction

The whole work presented in this thesis has been done in the Chirosciences team at the “Institut des Sciences Moléculaires de Marseille, iSm2”, UMR 7313 CNRS, Aix Marseille University. Fundings have been provided by the Ecole Centrale de Marseille and the Conseil Régional de la Région Provence-Alpes-Côte-d’Azur, with the kind partnership of Novachim as socio-economical partner.

The Chirosciences team is under the direction of Prof. Alexandre Martinez, and is specialized in the synthesis of chiral compounds, such as phosphorous ligands or hemicryptophanes, their separation and their use for asymmetric catalysis. This manuscript is about phosphine oxides, a compound widely studied in the lab with the work of Buono *et al.*, that can be used as ligands for enantioselective synthesis through organometallic catalysis as shown with the work of Hérault or Giordano in our lab. In this context, we here explore the reactivity of such chemicals, focusing onto phosphinate compounds, using both theoretical and experimental ways.

The first chapter presents a bibliographic study about phosphine oxides. First, we quickly describe the evolution of synthesis methodologies, from the first synthesis to the last results from our lab. Then, we explain various properties of organophosphorous compounds and how they might impact their reactivity. From these elements, we subsequently introduce the main topic of this thesis.

The second chapter is organized as a toolbox where both experimental and theoretical methodologies are explained. We first present the theoretical level used in the thesis and explain our choice for this level of theory. Then, we describe the synthesis of compounds of interest, and the associated analysis methods used to identify them, and how kinetic studies were made. The aim of this chapter is to allow a better understanding of the methodologies presented in this thesis.

In the third chapter, we determine the form of various compounds considered in the manuscript and their interactions in solution by using theoretical calculations and by building an ad hoc acidobasicity scale. Based on the relative stabilities of the studied systems, we have been able to identify the most abundant forms of involved species at the equilibrium.

The relative reactivity between compounds of interest is studied in chapter four, where the nucleophilic substitution of alcohol onto alkyl *hydrogeno*-phenylphosphinate is investigated. We hereby present an extensive study of all possible approaches of methanol onto methyl phosphinate using theoretical modeling, and identify the most favored one. In order to validate our model, a kinetic study has been done, which results are compared to theoretical studies.

During the study in neutral conditions, we noticed that the presence of basic compound acted on the kinetic of enantiomerization. We thus decided to experimentally study the effect of triethylamine on the inversion of configuration of ethyl phosphinate in ethanol. Using kinetic modeling, we could determine some possibilities of reaction in solution. Then, we performed simulations about the addition of methanol onto phosphinate with trimethylamine, and crossed experimental and theoretical results to elaborate first conclusions about the catalytic mechanism.

The sixth and final chapter presents additional results that concern the effect of hindrance in the addition of alcohol onto phosphinates. Theoretical calculations are jointly done about compounds with various alkyl group to see the effect of this hindrance on the energy barrier in neutral conditions. In parallel, kinetic studies were done in basic conditions using phosphorus NMR.

Chapter 1:

Presentation of alkyl *hydrogeno-*-phenylphosphinates

RESUME EN FRANÇAIS

Afin d'améliorer les méthodes de synthèse énantiosélectives, les ligands organophosphorés P-stéréogéniques ont montré d'excellents résultats dans divers processus asymétriques. Parmi eux, les composés oxydes de phosphines secondaires (SPO) monodentates, portant une liaison P-H, semblent très prometteurs, ceci dû à leur possible tautomérie où l'hydrogène passe du phosphore à l'oxygène doublement lié. Ce phénomène est fortement orienté vers la forme pentacoordinée P(V) de l'oxyde plutôt que vers l'acide phosphineux P(III) correspondant, mais cet équilibre est inversé en présence d'un métal de transition ce qui permet la coordination par le phosphore de deux ligands acide phosphineux, l'un protoné et l'autre déprotoné, qui agissent alors comme un ligand bidentate.

Depuis leur première synthèse par Williams et Hamilton en 1952, les méthodes de synthèse se sont concrètement améliorées et notre groupe y a activement participé avec les travaux de Buono et *al.* en 2007 et 2015 grâce à la synthèse énantiosélective de SPO à partir d'*hydrogénophénylphosphinate d'alkyle* (AlkHP) réagissant avec un réactif de Grignard via une S_N2. En 2015, il fut noté que le groupement alkyle porté par le phosphinate agissait sur l'excès énantiomérique (e.e.) final, passant de 86 % avec un phosphinate de menthyle à 99% avec celui d'adamantyle. Il fut également remarqué que le groupement alkyle agissait sur la stabilité relative de l'énantiomère pur : moins le groupement est encombré, plus l'énantiomère

isolé racémise rapidement. Il semble probable que ces deux phénomènes soient liés, c'est pourquoi nous avons décidé d'étudier l'effet du groupement alkyle sur la substitution nucléophile S_N2@P d'alcool sur les phosphinates.

Il est possible de trouver dans la littérature des études théoriques sur les S_N2@P, mais la plupart portent sur des composés cycliques ou ioniques. À notre connaissance, les études les plus exhaustives de S_N2 sur les phosphinates ont été réalisées par Bickelhaupt et *al.* entre 2006 et 2009. Leurs études montrent que les barrières d'activation pour l'addition d'un nucléophile dépendent activement de l'environnement du phosphore. Si l'ajout d'un modèle de solvant et le choix de la conformation la plus stable au départ de la réaction agissent, la nature des substituants autour du phosphore et du nucléophile montrent également une grande importance. Il est donc nécessaire de bien choisir notre modèle afin de ne pas fausser les résultats.

Ces études ont également montré que les S_N2@P passent régulièrement par des phosphore P(V) à 5 substituants sous forme de bipyramide trigonale (TBP). On appelle équatoriaux les ligands situés sur les angles de la base triangulaire, et apicaux ceux situés au sommet des pyramides. Ces composés P(V) peuvent subir des pseudorotations, c'est à dire un réarrangement des ligands autour du phosphore central. Ces isomérisations sont régies par les règles d'apicophilie, c'est-à-dire le fait que certains substituants, notamment les plus électronégatifs, favorisent la position apicale pour diminuer l'énergie de la molécule. Comme nous étudions dans cette thèse des composés organophosphorés non-ioniques et non-cycliques, la bibliographie indique que les mécanismes de pseudorotations les plus probables étaient les pseudorotations de Berry qui consistent en l'échange simultané de deux ligands apicaux et équatoriaux passant par un état de transition (TS) en pyramide à bas carrée.

Maintenant que nous avons étudié l'état de l'art en ce qui concerne les S_N2@P, nous savons qu'il est important de bien choisir son modèle pour ne pas fausser le mécanisme et qu'il nous faudra probablement étudier la possibilité de pseudorotation et tautomérie des composés qui nous intéressent.

1 Presentation of alkyl *hydrogeno*-phenylphosphinates

1.1 From asymmetric catalysis to *hydrogeno*-phosphine oxides

1.1.1 Organophosphorous compounds in asymmetric catalysis

Within the framework of constantly improving sustainable chemical processes, asymmetric catalysis plays a key role. Indeed, making synthesis stereoselective significantly contributes to a drastic reduction of waste and energy consumption.¹ This is especially true for pharmaceutical drugs, where stereochemistry must be strictly tuned.^{2, 3, 4, 5, 6}

The use of organophosphorous ligands in asymmetric organometallic catalysis showed good results since their first use in 1968, when Knowles & *al.* used such compounds for the stereoselective hydrogenation of alkenes.⁷ They have notably synthetized the CAMP (cyclohexyl *o*-anisylmethylphosphine) which allowed them to obtain an 88% enantiomeric excess (e.e.) in the stereoselective hydrogenation of olefin.^{8, 9} But because monophosphines oxidize easily under air, their development is difficult and their storage even more.

In 1971, Kagan synthetizes the first diphosphine: the DIOP (2,3-*O*-isopropylidene-2,3-dihydroxy-1,4-bis(diphenylphosphino)butane).¹⁰ Since then, diphosphines have been widely used for asymmetric synthesis because of their stability under air and moist which make them easier to store and use. Biphosphorous compounds are still used today at the industrial scale for asymmetric hydrogenation, such as BINAP (2,2'-bis(diphenylphosphino)-1,1'-binaphthyl)¹² or DIPAMP (Ethane-1,2-diylbis[(2-methoxyphenyl)phenylphosphane])¹¹ which notably showed success in the L-DOPA process (Figure 1-1).^{9, 13, 14}

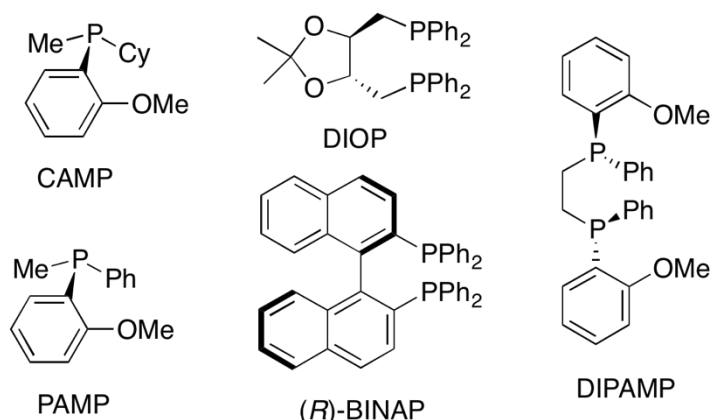


Figure 1-1: Various chiral organophosphorous ligands used in asymmetric catalysis; Cy = cyclohexyl, Ph = Phenyl, Me = Methyl

In 2003, monophosphines have come back in asymmetric catalysis with the work of Jiang et al. using secondary phosphine oxides (SPO, Figure 1-2) as a preligand for a stereoselective hydrogenation.¹⁵ Their oxidative aspect avoids the degradation of the compound under air conditions allowing easiest storage and synthesis. Since this work, studies about monophosphines oxides increased, showing promising results.^{14, 16, 17, 18, 19}

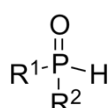


Figure 1-2: Secondary phosphine oxide, R = alkyl, aryl

1.1.2 Description of secondary phosphine oxides

1.1.2.1 *Definition of a secondary phosphine oxide*

A phosphine oxide is a pentavalent phosphorous compound with four ligands. It contains one phosphorus atom doubly bound to an oxygen in its structure. Several families can be defined, such as phosphine oxide, phosphinate (with one OR group), phosphonate (with two OR groups), or phosphate (with three OR groups) depending on the nature of substituents (Figure 1-3).

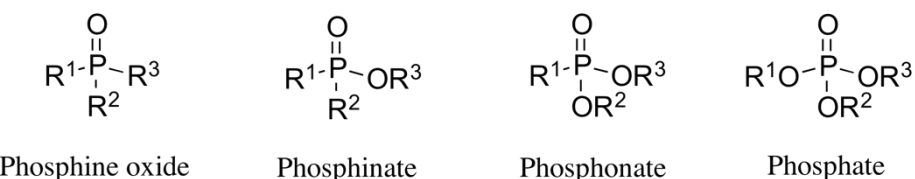


Figure 1-3 : Monophosphine oxides

As a result, and as can be seen in Figure 1-4, phosphinic and phosphonic acids correspond respectively to phosphinate and phosphonate where the R groups borne by OR substituents are hydrogen atoms.

For monoester phosphine oxides such as phosphinate, we hereby use a nomenclature where the R³ group borne by the OR³ substituent is placed first and separated from the rest of the structure. As an example: ethyl *hydrogeno*-phenylphosphinate will be the phosphinate form where R³ = ethyl, R² = hydrogen and R¹ = phenyl. Using the same nomenclature, a diester phosphine oxide like diethyl phenylphosphonate bears two ethyl groups for OR substituents (R² and R³), with R¹ = phenyl.

For acidic phosphine oxides, the rules for ester-like apply the same. Ethyl phenylphosphonic acid bears an ethyl group on one OR and a hydrogen on the second, while the R¹ group on the phosphorus atom would be a phenyl. Ethyl phosphinic acid bears only one OR group where R

$= \text{H}$ (here R^3), then substituents on the phosphorus atom are ethyl and phenyl (here respectively R^1 and R^2).

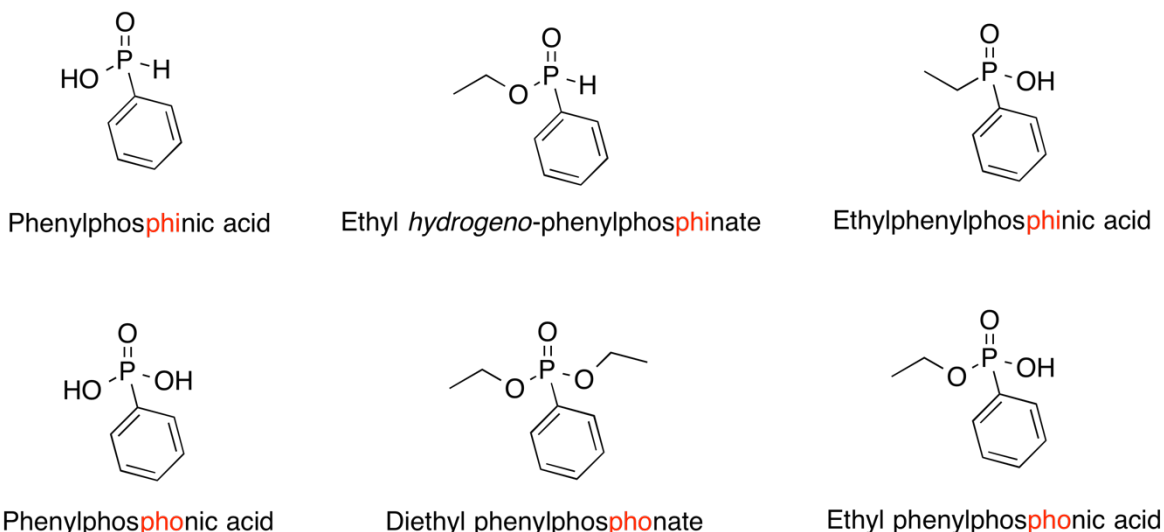


Figure 1-4: Nomination of diverse phosphine oxides depending on the OR group they bear.

We are hereby interested in secondary phosphine oxides (SPO) for which one of the R groups bound to the phosphorus atom is a hydrogen atom. An interesting property of SPO is that they can undergo tautomerism with the H atom being transferred from the phosphorus to the double bound oxygen (Figure 1-5).²⁰ This prototropic equilibrium switches the central phosphorus atom from a pentavalent form P(V) to a trivalent P(III).



Figure 1-5 : Tautomeric equilibrium of secondary phosphine oxide from P(V) (left) to P(III) (right)

1.1.2.2 Tautomerism in SPO

Numerous studies have been made on tautomerism at phosphorous compounds, and showed that the P(V) form is generally favored over the P(III). In 2001, Wesolowski et al. have shown that the equilibrium between P(V) and P(III) for the phosphine oxide OPH_3 shifts toward the P(V) by approximately $30 \text{ kJ}\cdot\text{mol}^{-1}$.²¹ In addition to the relative stability, the transition Gibbs free energy of tautomerism in gas phase has been determined around $240 \text{ kJ}\cdot\text{mol}^{-1}$ which indicates that the mechanism should not happen for a molecule alone. (Figure 1-6, up)^{21, 22} Later, Babin and Mamaev studied the impact of dimerization on this energy barrier. They have

shown that it could be lowered to approximately $190 \text{ kJ}\cdot\text{mol}^{-1}$ by a dimeric mechanism (Figure 1-6, bottom), but the equilibrium stays in favor of the P(V) form.^{23, 24}

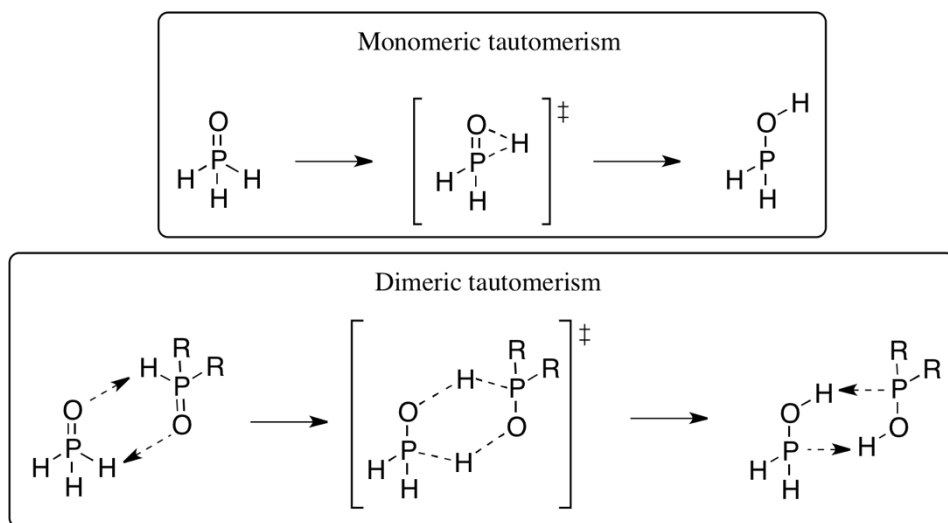


Figure 1-6: Tautomerism mechanisms of OPH_3 for a monomer (up) and a dimer (bottom)

In a more recent study, Janesko et al. have shown that protic solvents can participate to a prototropic exchange and diminishes the energy barrier of the equilibrium between P(V) and P(III).²⁵ Using B3LYP/6-31++G(3df,3pd) level of calculation, they have determined that participation of two molecules of water lowers the transition Gibbs free energy to $120 \text{ kJ}\cdot\text{mol}^{-1}$ for OPH_3 . However, the equilibrium is still in favor of the P(V) form by $22 \text{ kJ}\cdot\text{mol}^{-1}$. (Figure 1-7)

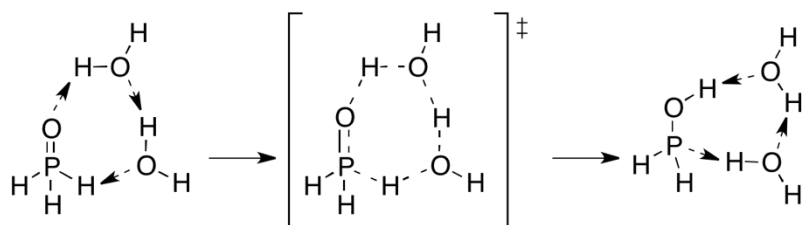


Figure 1-7: Prototropic exchange between OPH_3 and two molecules of water

Tavakol et al. have studied the proton exchange between methanol and *hydrogeno-dimethylphosphine oxide* or dimethyl *hydrogeno-phosphonate* using wB97XD/aug-CC-PVTZ level of theory with a polarizable continuum model as implicit solvent CPCM(MeOH). This model applies a dielectric constant to the system to simulate its interactions with molecules of solvent (cf. section 2.2.3, p.27).²⁶ They showed that the P(V) form is still favored by a Gibbs free energy of approximately $31 \text{ kJ}\cdot\text{mol}^{-1}$, with a transition state around $150 \text{ kJ}\cdot\text{mol}^{-1}$. (Figure 1-8)

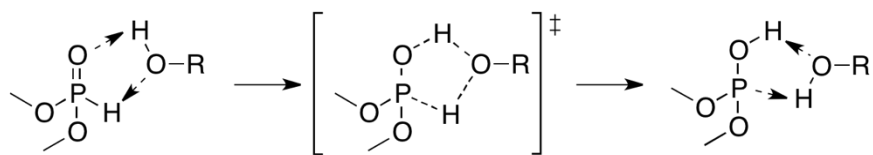


Figure 1-8: Prototropic exchange between dimethyl *hydrogeno*-phosphonate oxide and a single molecule of ROH

In 2005, Hoge et al. have showed that electron acceptor groups like CF_3 tend to stabilize the P(III) form and shift the equilibrium in its favor.²⁷ Indeed, they have managed to synthesize the phosphinous acid $(\text{C}_6\text{F}_5)_2\text{POH}$ and have shown its stability at room temperature. In addition, using calculation at the B3PW91/6-311G(3d,p) level, they have worked on $(\text{CF}_3)_2\text{POH}$ and showed that the P(III) form was more stable than its P(V) form by $14 \text{ kJ}\cdot\text{mol}^{-1}$. They explained this phenomenon by the withdrawing effect of CF_3 groups, and maybe hydrogen interactions with the OH group closer to CF_3 in the acid form.

This inversion of equilibrium is also possible in the presence of a transition metal where the acidic form allows the phosphorus atom to coordinate onto the metal (Figure 1-9).^{28, 29} This characteristic of SPO explains how they can be used in catalysis as preligands in organometallic catalysis. It is especially interesting when both R borne by the SPO are different because it allows those to be used in asymmetric catalysis as P(III) ligands.^{14, 30}

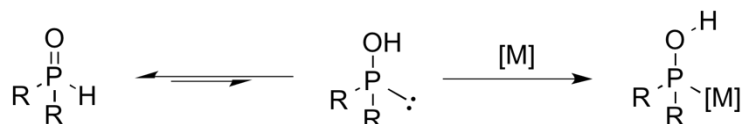


Figure 1-9 : Coordination of a secondary phosphine oxide onto a transition metal [M]

1.2 Synthesis of secondary phosphine oxides

The first SPO in literature is the dihexylphosphine oxide synthetized in 1952 by Williams and Hamilton. To do so, they have used dialkyl phosphonate with a Grignard reagent and got a 29% yield (Figure 1-10). They also synthetized di-octylphosphine oxide from dialkyl phosphinic acid chloride for a 54% yield.³¹

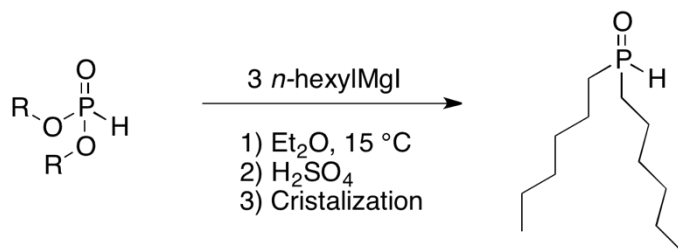


Figure 1-10: Synthesis of di-*n*-hexylphosphine oxide from dialkyl phosphonate developed by Williams and Hamilton

In 1955, the same team has synthetized an SPO from diethyl *hydrogeno*-phenylphosphonate using a Grignard reagent with a 70% yield for the dibenzylphosphine oxide.³² Based on this work, Mislow & *al.* have done in 1967 the enantioselective synthesis of a tertiary phosphine oxide from a diastereopure (-)-menthyl (R_P)-dialkylphosphinate.^{33, 34} This compound was diluted in benzene with a Grignard reagent, and the solution heated at 70 °C in order to obtain the corresponding tertiary phosphine oxide with an inversion of configuration at phosphorus atom (Figure 1-11).

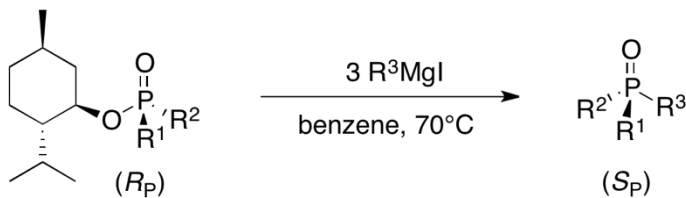


Figure 1-11: Synthesis of tertiary phosphine oxides developed by Korpiun and Mislow

In 2007, Buono & *al.* have synthetized an SPO by diluting diastereopure (-)-menthyl (R_P)-*hydrogeno*-phenylphosphinate ((R_P)-MenHP) in diethyl ether with 3 equivalents of organolithium compound.³⁵ This process shows excellent yields, especially with *tert*-butyllithium (*t*-BuLi) to synthesize *tert*-butylphenylphosphine oxide (*t*-BuSPO) with an 86% yield and 80% e.e. with inversion of configuration at phosphorus atom (Figure 1-12).

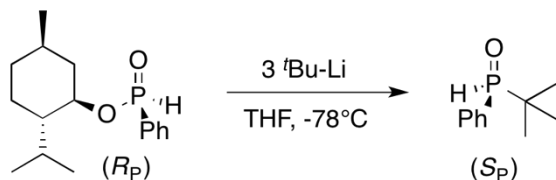


Figure 1-12: Synthesis of *tert*-butylphenylphosphine oxide by Buono et *al.*

The reactant (R_P)-MenHP can be synthetized from dichlorophenylphosphine (PhPCl_2) reacting with enantiopure (-)-menthol in benzene with pyridine. After 2 h at room temperature, the solution is hydrolyzed to obtain both corresponding diastereomers of MenHP with a 93% yield

and 40% diastereomeric excess (d.e.).³⁶ The R_P diastereomer can be isolated by recrystallization for a final 25% yield and a 100% d.e. (Figure 1-13)

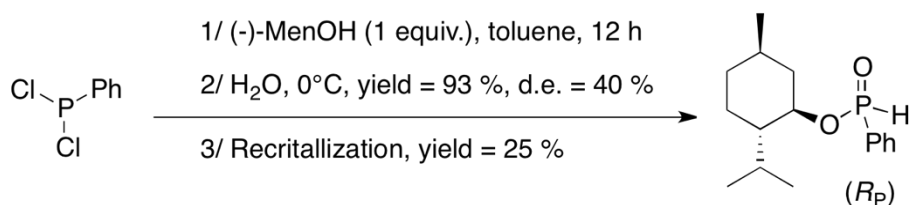


Figure 1-13: Synthesis of (-)-menthyl (R_P)-hydrogeno-phenylphosphinate by Emmick and the recrystallization step added by Mislow

The synthesis of *t*-BuSPO has been improved in 2015 when Buono & *al.* used the same methodology as in 2007, but replacing (R_P)-MenHP by the enantiopure adamantyl *hydrogeno-phenylphosphinate* (AdHP) for a 95% yield and 99% e.e..³⁷ AdHP can be synthetized easily by diluting PhPCl₂ and 1-adamantanone in dichloromethane (CH₂Cl₂) with 1 equivalent of distilled pyridine (annex 1.1.4, p.141). Both enantiomers can then be separated by chiral high-performance liquid chromatography (chiral HPLC) to give an access to enantiopure (R_P)-AdHP and (S_P)-AdHP, while diastereopure (R_P)-MenHP can only be obtained in the (R_P) configuration with a low final yield. As a result, the use of AdHP allows to access both enantiomers of an SPO, in addition of being more easily synthetized than (R_P)-MenHP.

The mechanism of synthesis for SPO from alkyl *hydrogeno-phenylphosphinate* (AlkHP) is detailed in Figure 1-14. It consists in the deprotonation of phosphorus atom by one equivalent of alkyllithium, followed by the addition of a second equivalent on the opposite side of the ester group. The addition of alkyllithium involves the departure of an alkoxide and an inversion of the stereogenic phosphorous center.

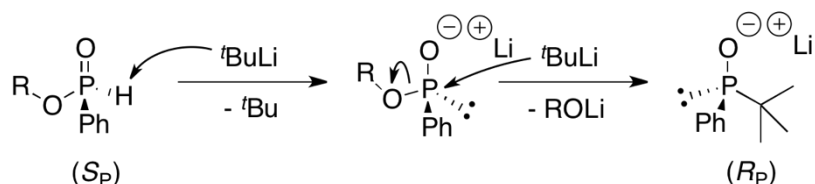


Figure 1-14: Mechanism of addition of *tert*-butyllithium onto phosphinate in the Buono synthesis

According to Han *et al.*, some alkyllithium could react on the phosphorous center with a S_N2.³⁸ To support this hypothesis, they used only one equivalent of alkyllithium on a solution of ethyl *hydrogeno-phenylphosphinate* (EtHP) diluted in diethyl ether, and observed the formation of the corresponding secondary alkylphenylphosphine with a good 89% yield for methylolithium.

Other phosphinates and alkylolithiums have been used with a 39% to 82% yield depending on the hindrance.

In both Buono or Han mechanisms, the leaving alkoxide from phosphinate is able to react with other phosphinates the same way alkylolithiums do, as shown with the red arrows in Figure 1-15. This reactivity involves an inversion of the configuration at phosphorus atom of reactant phosphinate, which changes the final e.e. of the enantioselective synthesis of SPO.

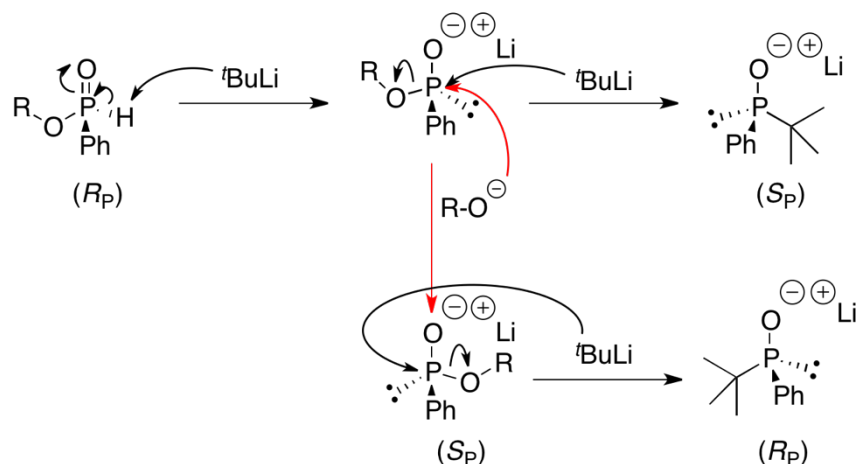


Figure 1-15: Mechanism of the synthesis of SPO from alkyl phosphinate and the possible parallel reaction with the freed alkoxide (red arrows)

The action of alkoxides has been studied by Buono *et al.* in our lab by diluting diastereopure (*R_P*)-MenHP (d.e. = 99 %) in tetrahydrofuran (THF) at -80 °C with 1 equivalent of lithium diisopropylamide to deprotonate the phosphinate.³⁷ Then, one equivalent of (-)-menthol was added to the solution which was stirred for 2 h. After that, the solution was hydrolyzed, and the phosphinate was taken back with diethyl ether.

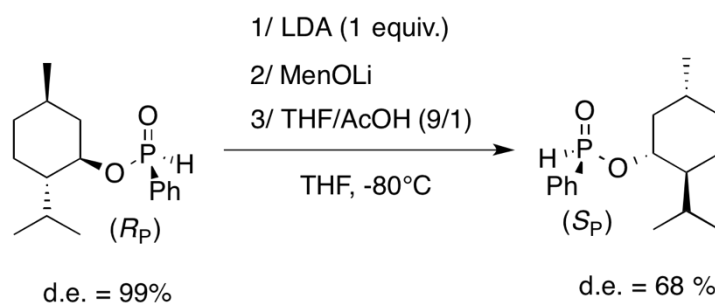


Figure 1-16: Inversion of configuration of (*R_P*)-MenHP with lithium menthol after deprotonation by Lithium Diisopropylamide

They observed a diminution of the d.e. from initially 99% to 68%, which can be related to the loss of enantioselectivity for the SPO synthesis with (*R_P*)-MenHP. To conclude, they deduced

that the nature of the alkoxide changes its kinetic of addition. As an example, in the case of (R_P)-MenHP compare to AdHP, the use of adamantyl improves the final enantiomeric excess respectively from 86% to 99%. This could be explained by the hindrance or the nature of the alkyl group which act nucleophilic property of the alkoxide.

While Buono & *al.* were looking for a good reactant for the synthesis of SPO from AlkHP in their study of 2015, they noticed that enantiopure ethyl and *iso*-propyl *hydrogeno*-phenylphosphinates were racemizing respectively in a few minutes or a few hours, while enantiopure AdHP was stable.³⁷ This observation, in addition of the difference of e.e. during the synthesis of SPO, raised an interrogation about the influence of this alkyl group on reactivity. It is a good assumption to think that both of these observations are related, so we decided to first focus on the inversion at stereogenic phosphorus atom through nucleophilic substitution (S_N2). These mechanisms have been researched before and can be named “ S_N2 at phosphorus” ($S_N2@P$).

1.3 Nucleophilic substitutions at phosphorus atom

As we saw in the previous section, the $S_N2@P$ are an important part of the synthesis on phosphorous chemistry, especially for phosphine oxides.³⁹ This methodology for synthesis has been widely used since their first synthesis in 1952 up until now for the synthesis of SPO.¹⁴ Theoretical studies of nucleophilic substitutions at phosphorus can be found in literature since the 1980's. But the majority of these studies are about halogenated phosphorous compounds,⁴⁰,⁴¹ trivalent phosphorus atoms,⁴⁰ cyclic phosphorous intermediates,^{42, 43, 44} and sometimes phosphonium salts,⁴⁵ all of which we do not talk about in this thesis. Nevertheless, those studies showed the importance of taking into account the empty 3d orbitals of the phosphorus, low in energy, that can participate as acceptor in some molecules. This implies the use of an extended orbital basis.

To our knowledge, the only theoretical studies about $S_N2@P$ for non-halogenated nor ionic phosphine oxides were made by Bickelhaupt *et al.* between 2006 and 2009 within their work about ionic compounds such as Cl^- or MeO^- reacting with neutral phosphine oxides.^{46, 47, 48, 49}

We could here argue that using ions generally needs to take the solvent explicitly into account since it acts on their stabilization or destabilization. The absence of explicit solvation makes this study not linkable to experiments. However, they are still useful to determine what acts on the shape of reactive pathways for $S_N2@P$.

In 2006, Bickelhaupt & *al.* have published their first work about the energy barriers of S_N2 at phosphine oxides, and the shape of the potential energy surfaces (PES) depending on substituents at phosphorus atom.⁴⁶ Using theoretical chemistry at OLYP/TZ2P level in gas phase, they showed that electronic and steric effects of those substituents could act on reactivity, thus on the shape of PES. As a result, the modeling of a nucleophilic substitution with Cl⁻ as a reactant and leaving group while changing the substituents on the phosphorus atoms between H, OMe or Cl gives three different shapes of PES, respectively with one, two or three wells. Their deduction was that not only the energy, but even the shape of the PES depends on steric hindrance and electronic properties of substituents. The central barrier of S_N2 is absent with Cl, but present with OMe because of the hindrance induced by methyls which destabilizes the pentacoordinated phosphorus atom. As a result, this conformation becomes a transition state for OMe substituents, while it is an intermediate for the less hindered H and Cl, making the profile of the PES with two wells for Cl, and one well for H. They also showed that the hindrance of OMe increases the energy barrier by 4 kJ.mol⁻¹ (65 kJ.mol⁻¹ for R = Cl to 69 kJ.mol⁻¹ for R = OMe).

In 2007, Bickelhaupt et *al.* have worked on OH⁻ reacting on diakylphosphinic acids P(O)R₂OH to study the importance of conformations on the reaction profile.⁴⁷ They observed that the reaction path which begins from the most stable conformer of reactant shows a reaction profile 5 kJ.mol⁻¹ lower than the others, following the Hammond's postulate which specifies that a TS following an intermediate is close to its structure and energy. As a result, a TS should be lower in energy if it comes from a less energetic conformation. This effect has been noted in this study, where a less stable conformer results in a higher TS. Consequently, going from a more energetic structure acts on the whole PES because the entire mechanism is based on this first conformation. Starting with the most stable conformer should lower the whole PES. This result was also presented in their study of 2009 with P(O)(OMe)₂X.⁴⁹ To conclude, this observation implies that diminishing the size of reactants in simulation can influence the energy profile, so the model used for theoretical studies has to be chosen very carefully.

In 2008, Bickelhaupt et *al.* have worked on the effect of solvation on S_N2@P for diverse P(III) and P(V) species substituted by Cl⁻. To model the effect of solvent, chose as water, they have used the COnductor-like Screening Model of solvent (COSMO).⁴⁸ They observed that transition states were lowered from 20 kJ.mol⁻¹ for P(O)Cl₃ to 37 kJ.mol⁻¹ for P(O)(CH₃)₂Cl, which shows the influence of solvent on the whole PES.

The last study of Bickelhaupt *et al.* about S_N2@P was in 2009 on the effect of substituents at phosphorus atom.⁴⁹ They tested S_N2 with Cl, OH and OMe as substituted groups onto the phosphorus atom, and showed that the PES shape was changing from two wells with the addition of Cl⁻, to three wells with MeO⁻ and HO⁻. They conclude that the steric effect acts on the shape of PES not only for substituents on the phosphorus atom, but also on the reactant.

Those diverse studies show how important it is to consider every part of the system around the phosphorous compound: substituents, reactants and solvent; since each of those acts on the profile of the PES. To conclude, we need to be very careful while choosing the system of interest for our study.

1.4 Pseudorotations of pentacoordinated phosphorous compounds

1.4.1 Description of a pentacoordinated phosphorus

As was described in the previous section, S_N2@P can go through a pentavalent phosphorous intermediate that bears 5 different substituents, and form a pentacoordinated compound with a triangle-based bi-pyramidal (TBP) geometry as shown in Figure 1-17. We can separate ligands depending on their position: apical ligands are the two at top vertices of the bi-pyramid (blue), and equatorial ligands the three at vertices of the triangle base (red).

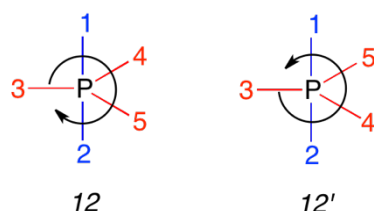


Figure 1-17: Triangle based bi-pyramidal pentacoordinated phosphorus. Groups in apical position are in blue, groups in equatorial are in red. Isomers are named after their apical groups, the heaviest one by Cahn-Ingold-Prelog rules on top. The enantiomers are named with a prime.

To name the different isomers, we use Cahn-Ingold-Prelog (CIP) rules⁵⁰ on substituent groups and numerate them from 1 to 5, 1 being the most important and 5 the least. (Figure 1-17) An isomer is named after the groups in apical position, putting the most important group up. As an example, the isomer with the ligands 1 and 2 in apical position will be named 12.

If both apical ligands and the three equatorial groups are different from each other, the isomer *12* has two enantiomers depending on the order of equatorial groups. In this case, the original molecule *12* is the isomer where equatorial ligands are clockwise. Its enantiomer, where equatorial ligands are in the opposite order, is named with a prime. An example can be seen in Figure 1-17 with the isomer *12*, where equatorial ligands are clockwise respecting the CIP rule (3-4-5), and its enantiomer *12'* where equatorial groups in the opposite order (5-4-3).

The position of ligands in the TBP depends on their apicophilicity, i.e. their relative preference to be in apical position. It depends on several characteristics, the most important being their electronegativity, since the more electronegative groups favor the apical position because of their inductive effect. 3d orbitals from the phosphorus atom that acts as an acceptor, which tends to stabilize its positive polarization.⁵¹ For groups with an equivalent electronegativity, the more sterically hindered groups will prefer the equatorial position because the 120° angle gives them more space than the 90° angles of apical positions.⁵² Based on various observations, several apicophilicity scales have been made respecting those rules.^{53, 51, 52}

1.4.2 The Berry pseudorotations

TBP based phosphorous molecules are known for their ability to undergo reorganization of ligands around the phosphorus. In those cases, two equatorial ligands switch their positions with both apical ligands, while the remaining ligand does not move during the process as shown on the Figure 1-18.⁵⁴

We can divide those mechanisms in three different kinds. The first two are regular mechanisms which do not need to break a bond: Berry pseudorotation and turnstile isomerization. Berry are known to be about five times lower in energy than turnstile according to previous studies, which makes the last mechanisms less probable than the first.^{55, 56, 57} Opposite to regular processes, irregular processes go through the breaking of a bond. It generally happens for cyclic phosphorous molecules which are not presented in this thesis. We thus hereby exclusively work on Berry pseudorotations.

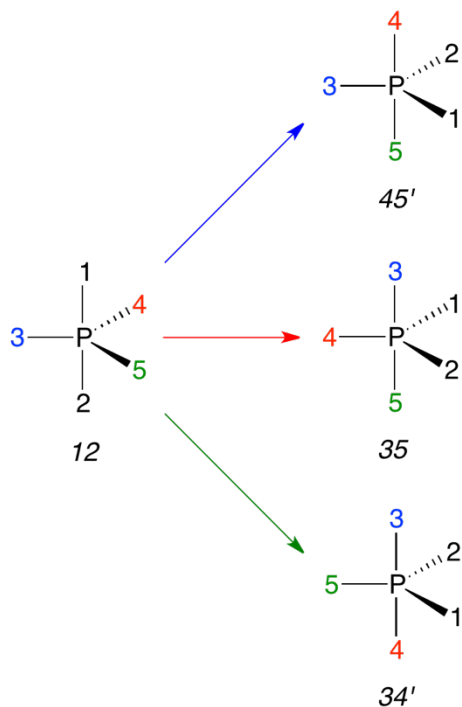


Figure 1-18: The three possible isomerizations from *12* around each possible pivot in equatorial position: 3 (blue), 4 (red) and 5 (green). The color of each arrow is assorted to the color of the ligand acting as a pivot that remains in equatorial position during the isomerization

In Berry's mechanisms shown in Figure 1-19, four of the ligands borne by the phosphorus atom rotate around the fifth one which stays unchanged as a pivot. Both apical ligands in blue have their angle go from 180° to 120° , while two equatorial ligands in red have their angle increase from 120° to 180° . Those two movements are coordinated so the transition state (TS) appears to be a squared base pyramid.

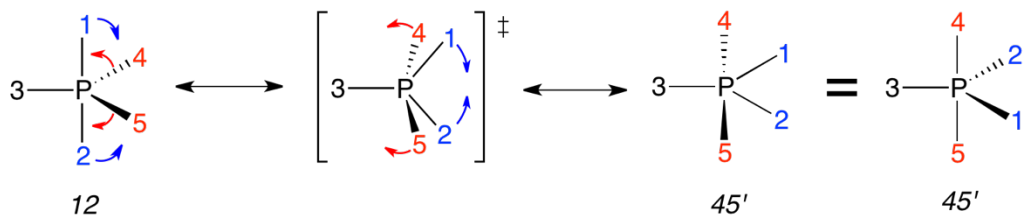


Figure 1-19: Berry pseudorotation from the pentacoordinated compound *12* to *45'* around the equatorial ligand 3 (pivot), 1 and 2 go from apical position to equatorial, 4 and 5 go from equatorial to apical.

We can represent the pseudorotations and the isomers they connect with a de Bruin diagram as shown in Figure 1-20.⁵⁸ Technically, if all five ligands are different in such a pentacoordinated structure, there are 20 different ways of positioning them around the phosphorous center so it can undergo 30 different pseudorotations.

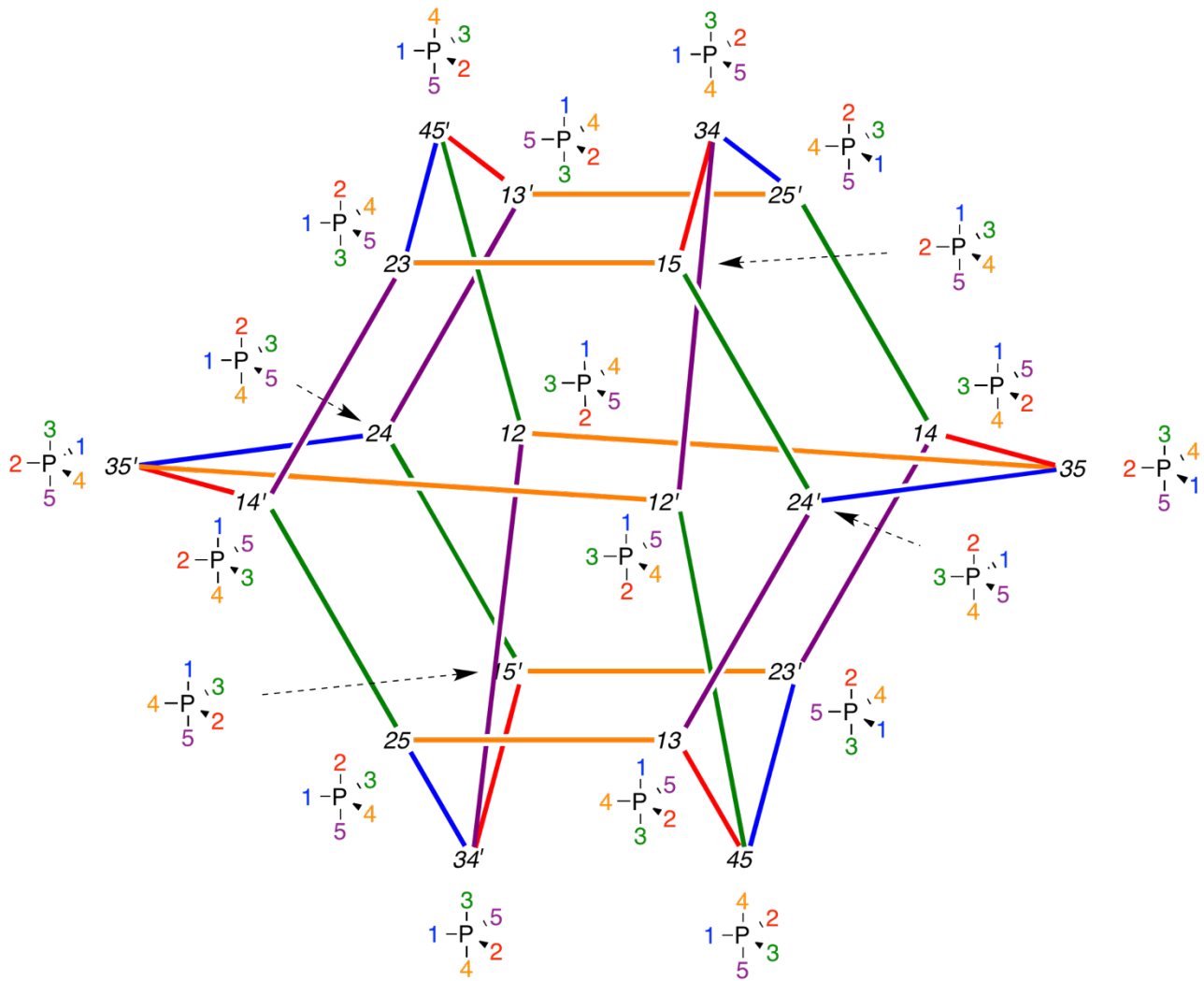


Figure 1-20 : Complete list of all 20 pentacoordinated intermediates that can be transformed into each other through pseudorotations in case all groups bound to the phosphorus center are different, and all 30 pseudorotations that bind them. The color of each line representing a pseudorotation is assorted to the color of the ligand acting as a pivot that remains in equatorial position during the pseudorotation.

1.5 Aim of the thesis

As was described in the first part of this section, chiral phosphorous molecules have successfully been used as ligands within several asymmetric catalytic processes.^{9, 59} P-stereogenic ligands, in particular, have shown to be efficient^{60, 14, 61} and, among them, monodentate P-stereogenic secondary phosphine oxides are thought to be very promising.^{62, 19, 18, 63} During the past decades, our group has significantly contributed to the making of such ligands with the development of an enantioselective synthesis of P-stereogenic SPO from AlkHP via a S_N2 mechanism with a Grignard reagent.^{35, 37}

It has been noticed that the nature of the alkyl group of the alkoxide borne by the phosphorus atom acts on the enantiomeric excess at the end of the reaction: the less hindered it is, the lower

the e.e.. They also noticed that this alkyl group acts on the stability of the enantiomer: the more hindered the alkyl, the more stable the enantiomer. It is a reasonable assumption to think that both of these phenomena are related. We then decided to study the effect of this alkyl group on S_N2@P by alcohols and their derivatives at phosphinates using experimental and theoretical chemistry.

Previous researches done by Bickelhaupt *et al.* showed how important it is to take the entire environment of phosphorus atom in consideration if we want to correctly describe the behavior of phosphorous compound. Consequently, we need to pay attention not to simplify too much our system of reference by lowering the hindrance of substituents or modifying their electronegativity. We will also study pseudorotations which, in certain case, could participate to inversion of configuration through isomerization of TBP intermediates.

However, before we head to the choice of our system of interest, we first need to choose theoretical and experimental methodologies we will use in this study. In the next section, we present those methodologies used during this thesis, and explain why they have been chosen.

Chapter 2:

Methodologies for synthesis, analysis, theoretical modeling and kinetic studies

RESUME EN FRANÇAIS

Afin d'étudier la réactivité des AlkHP, nous allons utiliser des méthodes de chimie théorique et expérimentale présentées dans cette section. Pour les études mécanistiques, nous avons choisi la théorie de la fonctionnelle de la densité (DFT) qui se base sur les théorèmes de Kohn-Sham, développés en 1965, selon lesquels la densité électronique d'un système permet de connaître toutes ses propriétés. Ce niveau théorique est plus rapide qu'en utilisant une méthode Hartree-Fock, puisqu'on ne considère plus les noyaux et électrons d'un système un par un, mais sa densité électronique et son évolution au fil de la réaction. Nous avons choisi d'utiliser la fonctionnelle M06-2X/6-31++G(d,p) qui a été optimisée pour les études énergétiques, géométriques, vibrationnelles et mécanistiques, associée au modèle de solvant SMD développé et testé avec cette fonctionnelle.

Pour tenir compte de l'effet de la température à laquelle les expériences sont menées, nous avons utilisé les fonctions de partition dans les approximations de la translation libre, de l'oscillateur harmonique et du rotateur rigide. Cela permet d'ajouter la prise en compte des états vibrationnels, rotationnels et translationnels du système.

La synthèse de l'*hydrogénophénylphosphinate d'éthyle* EtHP utilisé dans cette thèse est réalisée à partir de dichlorophénylphosphine PhPCl₂ réagissant avec de l'éthanol. L'identité de la molécule synthétisée est ensuite confirmée par RMN du phosphore et du proton. A l'issue de la synthèse, on a noté la présence d'un second produit non-identifié qui semble être le

phénylphosphonate de diéthyle d'après une analyse COSY-NMR. Cela n'a pas pu être confirmé car le produit n'a pas été isolé. La méthode de synthèse des EtHP n'étant pas énantiométrique, la séparation de deux énantiomères a été réalisée par Marion Jean via chromatographie chirale (Chiral HPLC). L'excès énantiomérique est déterminé via UV-visible après chromatographie chirale. Ces méthodes d'analyse pourront être utilisées dans le cadre d'études cinétiques.

Les études cinétiques seront réalisées de manière à obtenir des 1^{ers} ordres apparents. Cela permettra d'extraire facilement les constantes de vitesse k_{app} et d'en déduire les enthalpies libres de transition.

Un 1^{er} ordre est souvent relié à une réaction monomoléculaire, mais peut également correspondre à une réaction où l'un des réactifs voit sa concentration virtuellement constante au fil du temps. Pour cela, plusieurs modèles cinétiques, chacun décrivant une réaction différente caractérisée par sa propre constante de vitesse, pourront être construit. Leurs enthalpie libres de transition seront fittées pour approcher celle mesurée expérimentalement. La comparaison entre les valeurs du modèle et de l'expérience permettra de déterminer la validité du la réaction modèle.

Le développement par Rémy Fortrie d'un programme d'ajustement de modèles cinétiques peut permettre, à terme, de prendre en compte la participation de plusieurs mécanismes dans un modèle, et de pondérer leur participation pour recouper les résultats expérimentaux et déduire les mécanismes en solution.

2 Methodologies for synthesis, analysis, theoretical modeling and kinetic studies

2.1 Introduction

In the first chapter, we explored the history of monophosphine oxides, their properties and applications. We presented the researches made in our team by Buono & *al.* where they showed the influence of the alkyl group borne by the phosphinate on its enantioselectivity and reactivity (Figure 2-1).³⁷

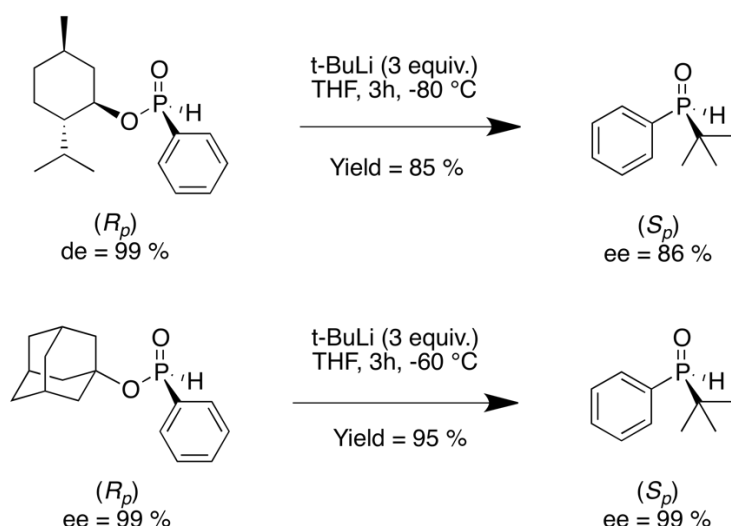


Figure 2-1 : Substitutions of alkoxy groups on P-stereogenic alkyl *hydrogeno*-phenylphosphinates in similar experimental conditions using *tert*-butyl as a nucleophilic species. Leaving alkoxy groups are (-)-menthoxide (top), and 1-adamantoxide (bottom)³⁷

To study this property, we will use various methodologies described in the following sections. First, we will describe the level of theory chosen for the mechanistic studies. Then, we will focus on the experimental methodologies, describe the synthesis of phosphinates and the analysis methods with NMR and chiral high performance liquid chromatography, to end with a presentation of kinetic chemistry.

2.2 Theoretical chemistry

The purpose of this part is not to give mathematical explanation of Density Functional Theory (DFT), but to present its major principles, strength and weaknesses. We will here focus on its origin and concepts to explain our choice for the level of theory.

2.2.1 The Schrödinger Equation

In 1926, Schrödinger publishes his well-known equation⁶⁴ which purpose is to determine the energy of a system:

$$\hat{H}\Psi_i(\vec{x}_1, \vec{x}_2, \dots, \vec{x}_N, \vec{R}_1, \vec{R}_2, \dots, \vec{R}_M) = E_i \Psi_i(\vec{x}_1, \vec{x}_2, \dots, \vec{x}_N, \vec{R}_1, \vec{R}_2, \dots, \vec{R}_M) \quad \text{Eq. 2-1}$$

where M is the number of nuclei, N the number of electrons in the system, and Ψ_i the wave function of the system in its i^{th} state. E_i is the energy of the system determined by applying the Hamilton operator \hat{H} to the wave function Ψ_i .

While it cannot be observed, the wave function Ψ_i contains every possible information about the system. It can be interpreted with the form $|\Psi(x_1, x_2, \dots, x_N)|^2 d\vec{x}_1 d\vec{x}_2 \dots d\vec{x}_N$ which represents the probability for electron 1 to N to be simultaneously in volume elements $d\vec{x}_1 d\vec{x}_2 \dots d\vec{x}_N$. It depends on the $3N$ spatial coordinates $\{\vec{r}_i\}$ of the electrons, the N spin coordinates $\{\vec{s}_i\}$ which are collectively named $\{\vec{s}_i\}$, and the $3M$ spatial coordinates of the nuclei $\{\vec{R}_I\}$.

The operator \hat{H} is the Hamilton operator. It is the differential operator representing the total energy of isolated systems which can be described in atomic units as:

$$\hat{H} = -\frac{1}{2} \sum_{A=1}^N \nabla_A^2 - \frac{1}{2} \sum_{A=1}^M \frac{1}{M_A} \nabla_A^2 - \sum_{i=1}^N \sum_{A=1}^M \frac{Z_A}{r_{iA}} + \sum_{i=1}^N \sum_{j>i}^M \frac{1}{r_{ij}} + \sum_{A=1}^M \sum_{B>A}^M \frac{Z_A Z_B}{R_{AB}} \quad \text{Eq. 2-2}$$

The data A and B run over the M nuclei in the system, while i and j denote the N electrons. The first two terms in the Eq. 2-2 represent the kinetic energy, respectively of electrons and nuclei, where the Laplacian operator is defined by:

$$\nabla_q^2 = \frac{\partial^2}{\partial x_q^2} + \frac{\partial^2}{\partial y_q^2} + \frac{\partial^2}{\partial z_q^2} \quad \text{Eq. 2-3}$$

In Eq. 2-2, M_A represents the mass of the nucleus A . It is different from M which represents the total number of nuclei in the system as previously defined. The remaining three parts of Eq. 2-2 determine the potential parts of the Hamilton operator with electrostatic interactions between particles. We can find respectively the attractive part due to attraction between nuclei and electrons, and the repulsive parts due to electron-electron and nucleus-nucleus interactions. R_{AB} and r_{ij} represent the distance between i and j or A and B respectively, such that $r_{ij} = |\vec{r}_i - \vec{r}_j|$. The objective of theoretical chemistry is to solve the Schrödinger equation, but the exact resolution is impossible to get for more than 2 particles. For this reason, several approximations are necessary, keeping in mind that the objective is to approach as nearly as possible the exact solution.

To do so, another method than using wave functions consists in using electronic density to determine properties of a system. This theory is called Density Functional Theory (DFT), and several levels of methodologies have been developed. We hereby present their major concepts in the following section.⁶⁵

2.2.2 Density Functional Theory

2.2.2.1 Building DFT methodology

Because of numerous different values calculated ($3N$ spatial coordinates and N spins), the cost of one calculation using post Hartree-Fock methods increases a lot with the size of systems, making the study of large chemical systems complex if not impossible. To make it easier, Kohn and Sham had the idea to replace the wave function Ψ_i by the electronic density $\rho(\vec{r})$, which contains all important information from the system.⁶⁶ In their publication, they notably define the first theorem of DFT which shows that if two systems at their fundamental state have the same energy, which means that they are defined by the same electronic density under the same external potential. From this theorem, it is possible to determine the energy of the system with the Schrödinger equation, but using electronic density instead of wave functions as shown in Eq. 2-4:

$$E_0[\rho_0] = T[\rho_0] + E_{ee}[\rho_0] + E_{Ne}[\rho_0] \quad \text{Eq. 2-4}$$

In this equation, $T[\rho_0]$ define the kinetic energy of electrons, $E_{ee}[\rho_0]$ the energy due to interactions between electrons, and $E_{Ne}[\rho_0]$ the energy due to interactions between electrons and nuclei. In this equation, we can separate the part we can solve from the one we cannot, and get the following equation:

$$E[\rho] = T_S[\rho] + J[\rho] + E_{XC}[\rho] + E_{Ne}[\rho] \quad \text{Eq. 2-5}$$

where $T_S[\rho]$ is the part of kinetic energy determined in the approximation of a perfect electron gas where particles do not interact with each other, $J[\rho]$ the Coulomb energy of the electron-electron interaction, and E_{XC} the exchange-correlation energy which contains everything we cannot determine. Knowing E_{XC} and its related potential V_{XC} could give us the exact value of E_0 , but the exact expression of those two components is not known. For this reason, several approximations have been developed, thus several DFT methods exist, each with a different resolution of these terms which affects the behavior of the studied system. Consequently, the level of theory has to be chosen carefully.

In our case, we have chosen the functional M06-2X as theoretical level. It is a hybrid GGA-functionals (GGA: Generalized Gradient Approximation) which means that it contains both HF

and DFT resolution for Exc in order to approach the real solution. Hybrid GGA functionals generally give good equilibrium geometries, vibrational frequencies and atomization energies, which make them a good choice for mechanistic studies.^{68, 69} Additionally, M06-2X functional has been parametrized for better render mechanistic and vibrational properties, so it is a good level of theory for our studies.

2.2.2.2 Description of non-covalent bonds

Since DFT describes interactions between two atoms only when there is an overlap of their respective densities, it cannot describe instantaneous variations in the electronic density nor long interactions such as hydrogen bonds. For this reason, the modeling of non-covalent interactions has long been a problem until the implementation of electronic dispersion.⁷⁰ This addition to the DFT acts on the system by simulating an attractive interaction on electrons in one region.

The simplest way to describe the dipole interaction is with a $1/r^6$ term, where r describes the interatomic distance. In their review of 2012, Klimes and Michaelides call this approach the ground-binding dispersion, and propose a classification of the different dispersion models depending on their ability to give better accuracy on their own.⁷⁰ Ground-binding dispersion is considered as less reliable because of the absence of description for long range interactions, but it can still be used for weakly bound systems or with a dataset which compensates the lack of description in the dispersion. This is the case for *Minnesota functionals*, such as M06-2X, which use a simple description of the long-range interactions coupled with a dataset that allows to describe the other interactions than long-range weak bonds.

It may seem problematic to add empirical data to a level of theory, but according to the mean unsigned error obtained with M06-2X on various benchmarks, this description of long-range interactions is fairly good compare to other level of theory which contains less empirical dispersion.⁷¹ The optimization of dispersion for the description of energies and geometries along reaction path for simple systems works well,⁷⁰ which is good for our application. Still, in following mechanistic studies, we will prefer to start from the first associated complex of reactants in order to avoid the risk of bad description of association-dissociation energies. We also decided to test the effect of an additional term of dispersion with supplementary calculation using the GD3 model of dispersion on the most relevant parts of studied mechanisms. Results of this comparison will be presented later in the study.

2.2.3 Implicit solvation

The solvent has always been an important part of reactions in experimental works, and so it is for the study of mechanisms. However, the explicit simulation of solvent, which consists in modeling all molecules of solvent in the system, would increase a lot the calculation cost. For this reason, many methods have been developed to model the solvent as a continuum, also called implicit solvent model.^{69, 72}

The principle is to put the molecule of interest in an electrostatic cavity where the solvent is excluded because of the molecule's repulsion. This surface is called solvent excluded surface (SES), outside of which we find the solvent accessible surface (SAS), which shape is determined by a spherical probe which rolls on the SES. This probe represents the solvent and is defined by the van der Walls volume of its molecule. The shape drawn by the trajectory of the probe's center determines the surface of the SAS. In the SAS, the solvent is described with a dielectric constant that simulates its influence on the molecule's atoms. In the SES, the effect of the solvent is represented with a lower dielectric constant to simulate the repulsion effect.

As for DFT, several models of implicit solvation have been developed. In our case, we use the Solvation Model Density (SMD)⁷³ which consider the full density of the solute is used instead defining the individual charge of each atom, and was parametrized to fit with *Minesotta functionals* like M06-2X we used for this study. This way, we ensure that our choice was already optimized.

2.2.4 Effect of the temperature

Once the whole system is defined and the methodology chosen, we can calculate the minimum energy for the ground state. However, in realistic conditions, molecules translate, rotate and vibrate and these properties have to be taken into account for comparison with non-0K experimental data. Fortunately, they can be approximate from DFT calculations using molecular partition functions.⁷⁴ In our case, molecules are solutes and the solute thermodynamic standard state is used, i.e. $c^0=1 \text{ mol.L}^{-1}$. However, partition functions in condensed phase are hardly accessible and we consequently made the assumption that the properties of these solute could be approximated using gas phase partition functions instead. We have actually no definitive proof that such an approximation is accurate, but it has been proved to be reliable in previous studies.

The electronic partition function is defined as Eq. 2-6, where E_{elec} is the electronic energy of the system of interest multiplied by the degeneracy of the electronic state.

$$Z_{\text{elec}} = \exp\left(-\frac{E_{\text{elec}}}{k_B T}\right) \quad \text{Eq. 2-6}$$

For a system exhibiting N_{vib} vibrational modes, the vibrational partition function Z_{vib} can be calculated with the Eq. 2-7, where ν_i represents the vibrational frequency of mode i . It includes the zero-point energy and is only strictly valid within the framework of the harmonic approximation.

$$Z_{\text{vib}} = \prod_{i=0}^{N_{\text{vib}}} \frac{\exp\left(-\frac{\hbar\nu_i}{2k_B T}\right)}{1 - \exp\left(-\frac{\hbar\nu_i}{2k_B T}\right)} \quad \text{Eq. 2-7}$$

The value of the rotational partition function of a molecular system depends on its symmetry. The general relation Eq. 2-8 is verified, in case the molecular system is assumed rigid while rotating, where I_i represents the inertial momentum of the molecule with respect to its axis, and σ is a symmetry factor equal to the number of rotations that let the molecular system unchanged.

$$Z_{\text{rot}} = \frac{\sqrt{\pi}}{\sigma} \prod_i \left(\frac{2I_i k_B T}{\hbar^2} \right)^{1/2} \quad \text{Eq. 2-8}$$

In this study, since we use the solute thermodynamic standard state, we consider the system in the canonical ensemble where T , V and N (number of particle) are constant. In this ensemble, the translational partition functional of a non-interacting molecular system can be defined by the Eq. 2-9, where m is the weight of the system and V its volume.

$$Z_{\text{trans}} = V \left(\frac{mk_B T}{2\pi\hbar^2} \right)^{3/2} \quad \text{Eq. 2-9}$$

All those equations are grouped in the total partition function Z_{tot} defined in the Eq. 2-10.

$$Z_{\text{tot}} = Z_{\text{elec}} Z_{\text{vib}} Z_{\text{rot}} Z_{\text{trans}} \quad \text{Eq. 2-10}$$

It is equal to the product of its electronic, vibrational, rotational and translational partition functions, all of which determine the participation of their respective movements to the total energy with Eq. 2-11.

$$G = -RT \ln(Z_{\text{tot}}) \quad \text{Eq. 2-11}$$

2.3 Synthesis of alkyl *hydrogeno*-phenylphosphinates

All phosphinates presented in this thesis have been synthetized at the laboratory. Other chemicals were purchased.

To synthetize ethyl *hydrogeno*-phenylphosphinates, we used a method presented in A. Leyris' thesis in our lab,⁹⁵ a simplified version of Emmick's method in 1968.³⁶ A volume of 100 mL of dry THF is put in a dry bicol flask under nitrogen. THF is cooled to 0 °C before 65 mmol of

PhPCl₂ are added. Then, 40 mL of ethanol is added dropwise at 0 °C while stirring. The stirring is maintained for 20 hours at room temperature. Then, the solvent is evaporated under reduced pressure to get the ethyl *hydrogeno*-phenylphosphinate with a 95.3 % yield (10.5 g). The product is identified by nuclear magnetic resonance (NMR) ³¹P (singlet 24.5 ppm in ³¹P-CPD) and ¹H (CDCl₃, annex 1.1.2, p.140).

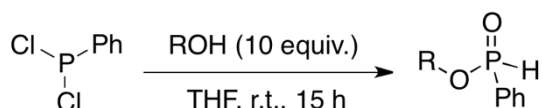


Figure 2-2: Synthesis of AlkHP from PhPCl₂ reacting with ROH, R=ethyl, *iso*-propyl

Phosphinates can degrade under air to form the corresponding phosphinic acid (Figure 2-3). It can be found at the end of the synthesis or by reacting with water. This impurity can be easily removed with a work up using sodium bicarbonate NaHCO₃ and diethylether or ethyl acetate to extract the phosphinate.

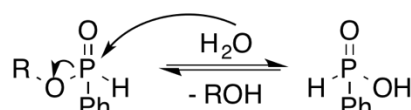


Figure 2-3: Formation of alkyl *hydrogeno*-phenylphosphinic acid from alkyl *hydrogeno*-phenylphosphinate

At the end of the synthesis of phosphinate, it is possible to find another phosphorous compound as side product. This impurity shows no P-H bond in ³¹P NMR and is not eliminated by the work up so we can conclude it is a non-acidic compound. To identify this impurity, we did a correlation spectroscopy (COSY) NMR on an ethyl *hydrogeno*-phenylphosphinate sample containing the side product. This procedure is able to measure the effect of substituent's neighbors so we can link different peaks together and determine more easily the nature of the analyzed compound. The resulting signal is presented in Figure 2-4.

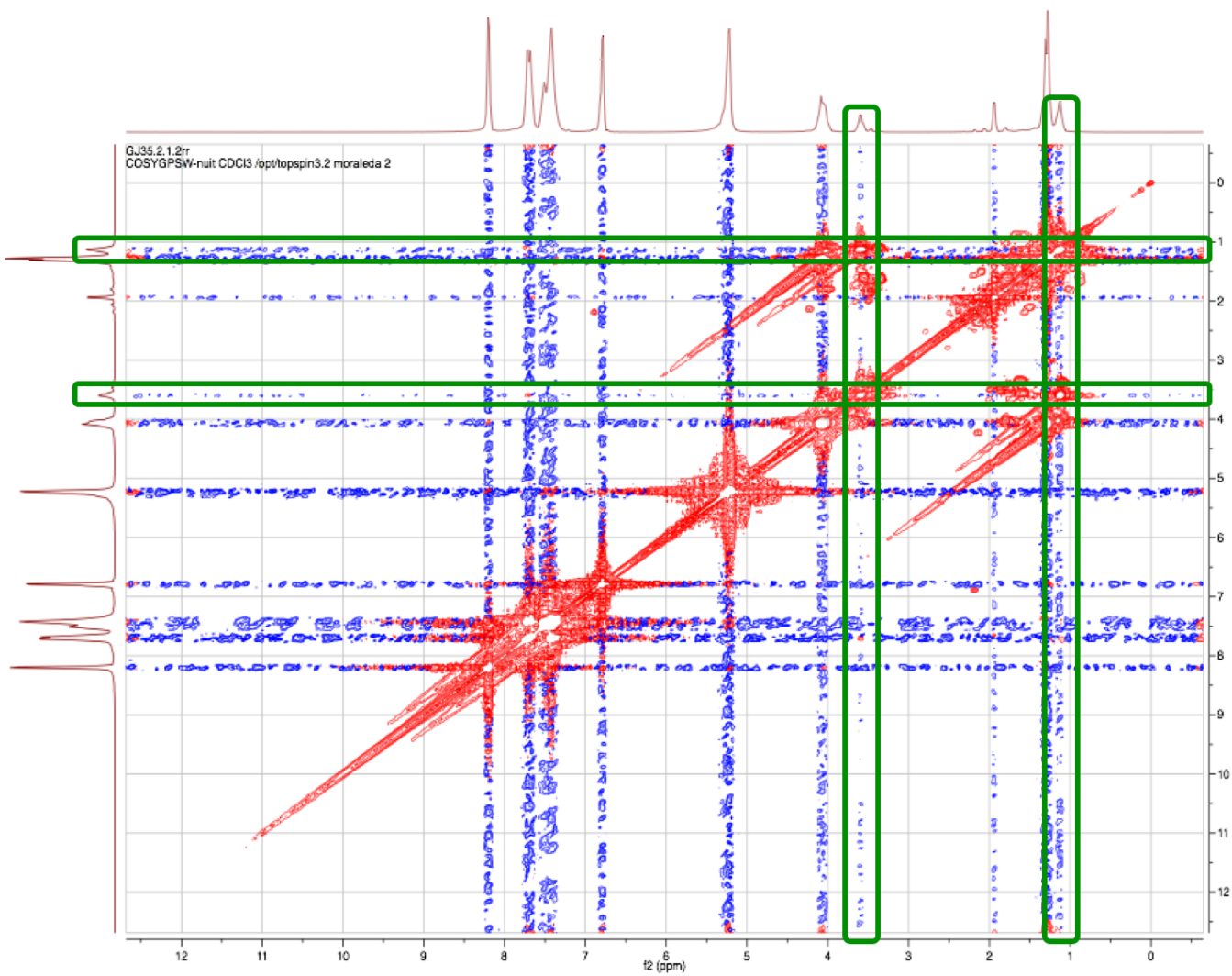


Figure 2-4: COSY ^1H NMR 400 MHz of the alkyl *hydrogeno*-phenylphosphinate in CDCl_3 . Peaks circled in green are unidentified and related to each other.

Considering peaks unrelated to the ethyl phosphinate, circled in green on the signal, we can see that two of those are linked: one is a quadruplet at 3.59 ppm, the other a triplet at 1.12 ppm. Those peaks are characteristics for ethoxy groups and are not corresponding to the signal of ethanol nor ethyl acetate. For this reason, we think that the impurity is the diethyl phenylphosphonate (respectively dialkyl depending on the alcohol used as reactant, Figure 2-5). However, this has not been confirmed since we could not isolate the compound.

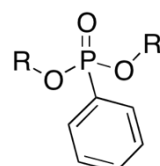


Figure 2-5: Possible side product from the synthesis of alkyl phénylphosphinate: dialkyl phenylphosphonate.

2.4 Analysis methods and quantification

2.4.1 Nuclear magnetic resonance

As previously seen, the main method used to identify chemical compounds is the Nuclear Magnetic Resonance.⁷⁴ In our case, we mainly use the NMR signals of ^{31}P with a $\frac{1}{2}$ spin using 85% phosphoric acid as external reference for signal calibration. When bound to a hydrogen atom, this signal is a large doublet. The quantification is thus more difficult with larger error than thin peaks, especially if several molecules are in solution since their respective signals may superpose. For this reason, we generally use a decoupling technic called composite pulse decoupling (CPD) ^{31}P to obtain a thin singlet, easiest to follow in quantitative studies.

This technic consists in applying a second magnetic field to the sample. This field acts only on hydrogen atoms, so phosphorus feels a mean value of their influence. The problem of this method is that we create an interaction between H and P atoms which influences the surface of the NMR peak.⁷⁶ This interaction is called the Overhauser effect and consists in transferring the excitation from a nucleus to another during the relaxation, which implies that the integration of the peak can be overestimated.⁷⁷ This error can be neglected if the decoupling field is canceled during the measurement so we still have the decoupling effect without the Overhauser one.

The position of a ^{31}P -CPD peak depends on the environment of the studied nucleus, i.e. the substituents around the phosphorus atom and other chemicals in solution that interact with the molecule. For this reason, it is classic to see a shift of the signal depending on the solution and chemicals therein.

The surface of the resulting signal depends on the quantity of analyzed nuclei in solution with the formula $\frac{n_A}{n_B} = \frac{S_A/a}{S_B/b}$, where n_A is the molar concentration of the compound A , S_A the surface of its NMR signal, and a the number of analyzed nuclei in solution. In our case, since we study monophosphorous compound, $a = b = 1$, so $\frac{n_A}{n_B} = \frac{S_A}{S_B}$. The proportionality from n to S can vary with the sample, but NMR signals are calibrated on an 85% phosphoric acid external reference that should minimize the potential error. A complete sampling would allow us to study the potential variation of the surface of the peak depending on its composition, but this methodology has been used before with good reliability. This allows us to use the ^{31}P -CPD NMR to study kinetics such as the exchange of alcohol on AlkHP.

Since deuterated solvent are expensive, we can use not-deuterated solvent in the NMR tube, and add a capillary which contains an NMR solvent for the device. It is also useful if a quantification is needed since we can add in the capillary a reference which concentration is

known, and compare the surface of its signal to the peak of interest. Since the reference is in a capillary, it will not interfere with the reaction in solution.

2.4.2 Chiral high performance liquid chromatography

In order to separate two enantiomers, an efficient method is the chiral high-performance liquid chromatography (chiral HPLC) which was performed by Marion Jean at the laboratory. The difference with classical liquid chromatography is that a chiral compound is fixed on the silica gel. One of the product's enantiomer will thus interact more with the column and stays coordinated with the gel longer than the other. This way, it is possible to separate both enantiomers. To be sure that the separation worked, we use a polarimeter. An example is given in Figure 2-6 with the separation of enantiomers of racemic ethyl *hydrogeno*-phenylphosphinate, where the ultraviolet-visible (UV-visible) signal in black allows us to determine the quantity of one enantiomer, and the polarimeter signal in green to identify its configuration.

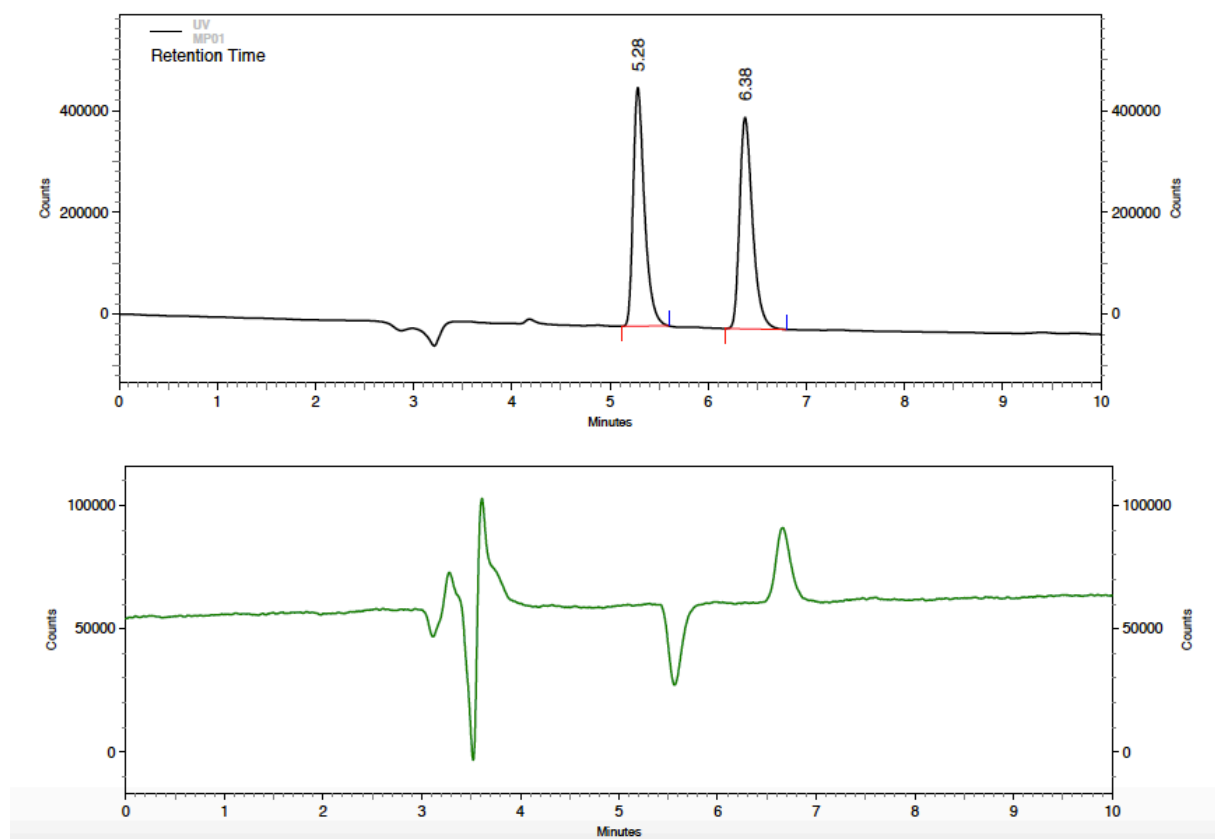


Figure 2-6: Chiral HPLC of ethyl *hydrogeno*-phenylphosphinate; analytical separation on Lux Cellulose-2 in hexane/ethanol (1/1) at 1 mL/min and 25 °C with UV detection at 254 nm (black line) and polarimeter (green line). The first peaks in the polarimeter signal (around 3'30") are due to the injection, not to the presence of another compound.

2.5 Kinetics

2.5.1 Reaction rate and transition standard Gibbs free energy

The quantification of compounds from analysis methodologies is useful to follow the evolution of a reaction. To do so, several rules have been developed in the field of kinetic. The ones used in this thesis are presented within this section.

2.5.1.1 *First order kinetic*

First order kinetic are related to monomolecular reaction of compound A, which concentration $[A]$ changes over time. If we trace the logarithm of the evolution of ratio $[A]/[A_0]$, we obtain a straight line characterized by a function corresponding to the kinetic law for first order reactions:

$$\ln\left(\frac{[A]}{[A]_0}\right) = k_r t \quad \text{Eq. 2-12}$$

Therefore, we can extract k_r from Eq. 2-12, which is the kinetic constant of reaction. From this value, we can determine the transition Gibbs free energy $\Delta_r G^{0\dagger}$ from experimental data with the Eyring equation:

$$\Delta_r G^{0\dagger} = -RT \ln\left(\frac{k_r h}{k_B T}\right) \quad \text{Eq. 2-13}$$

where R is the ideal gas constant, T the temperature in Kelvin, h the Planck constant, and k_B the Boltzmann constant.

2.5.1.2 *Apparent first order kinetic*

For a bimolecular reaction A+B, the equation describing the reaction flow can be written as:

$$\frac{d[A]}{dt} = k_r [A] \frac{[B]}{c^0} \quad \text{Eq. 2-14}$$

However, when one of the concentration is a lot higher than the others, it can be considered as constant over the reaction.⁷⁴ In that case, we talk about an “apparent first order reaction”, where the kinetic of reaction is characterized by the apparent kinetic constant k_{app} :

$$\frac{d[A]}{dt} = k_{app} [A] \quad \text{Eq. 2-15}$$

In this equation, k_{app} includes the constant concentration $[B]$ such that $k_{app} = k_r [B]/c^0$. This is only possible because $[B]$ is constant over the reaction, or if $[B] \gg [A]$ so the quantity of B virtually does not change. Consequently, it is important to extract $[B]$ from the apparent constant in order to get the k_r characteristic of the reaction. As a result, Eq. 2-13 is now:

$$\ln\left(\frac{[A]}{[A]_0}\right) = \ln(k_{app}) t$$

$$\Delta_r G_r^{0\ddagger} = -RT \ln\left(\frac{k_r h}{k_B T [B]/c^0}\right) \quad \text{Eq. 2-16}$$

where $c^0 = 1 \text{ mol.L}^{-1}$ is the standard solute concentration for perfect solution.

2.5.1.3 Model adjustment

During kinetic studies, it is also possible that several reactions, each characterized by their own $\Delta_r G_r^{0\ddagger}$ and k_r , happen simultaneously in solution. In that case, each one of those reactions participate to the global $\Delta_r G_{app}^{0\ddagger}$. To determine their participation, we can build a kinetic model containing several reactions. This model is defined by its kinetic constant k_{mod} , such that:

$$k_{mod} = \sum_r C_r k_r$$

where $k_r = \exp\left(-\frac{\Delta_r G_r^{0\ddagger}}{RT}\right)$, and C_r is the concentration of reactants involved in the reaction characterized by this k_r . The transition Gibbs free energy $\Delta_r G_r^{0\ddagger}$ has been fit to approach the measured $\Delta_r G_{app}^{0\ddagger}$, as if only this reaction was happening in solution. The value C_r allows us to weight the participation of k_r to k_{mod} , so we can vary those concentrations and get as close as possible to the measured k_{app} . In addition, it allows us to determine the participation of each reaction to the global k_{mod} .

In the end, we calculate $\Delta_r G_{mod}^{0\ddagger}$ using k_{mod} in the Eyring equation, and compare $\Delta_r G_{mod}^{0\ddagger}$ to the experimental $\Delta_r G_{app}^{0\ddagger}$ to test the validity of the model.

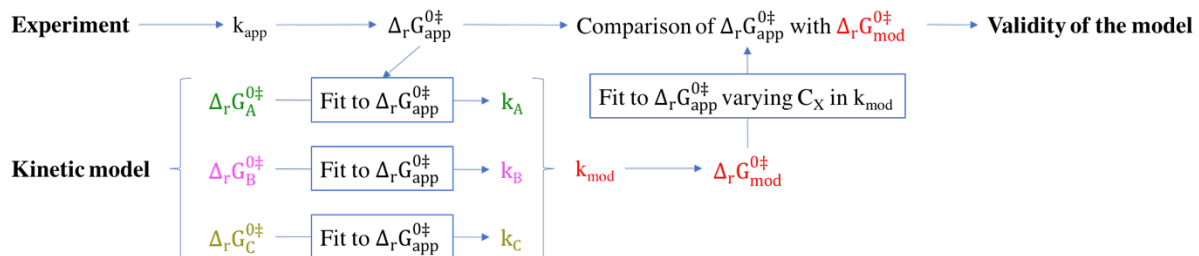


Figure 2-7: Schematic description of the kinetic model adjustment. From experimental data $\Delta_r G_{app}^{0\ddagger}$, we can imagine several theoretical reactions X (here X = A to C) for which we determine the theoretical $\Delta_r G_X^{0\ddagger}$. This $\Delta_r G_X^{0\ddagger}$ is fit to $\Delta_r G_{app}^{0\ddagger}$ as if reaction X was the only one happening in solution. From this value, k_X is determined. Then, we cumulate several reaction X in a model characterized by $k_{mod} = \sum_X C_X k_X$, where C_X is the ratio of reactants involved in reaction X for the model mod. By varying C_X , k_{mod} changes so we can fit $\Delta_r G_{mod}^{0\ddagger}$ to get

closer to $\Delta_f G_{app}^{0\ddagger}$ and compare their respective values. This comparison allows us to know the validity of our model.

2.5.2 A case of study: the racemization of ethyl phenylphosphinate

In this section, we will define the kinetic equations we use later in the manuscript for the kinetic of racemization of enantiopure EtHP diluted in ethanol. In these kinetic studies, we follow the evolution of the e.e. over time. Technically, kinetic measurements are here performed in pure ethanol, which implies that ethanol should be considered with respect to its pure liquid thermodynamic standard state. Nevertheless, in order to stay coherent with the synthetic reaction of initial interest (section 1.5, p.18) and with the DFT models, we chose to consider ethanol with respect to its solute thermodynamic standard state. This variation can be described with the formula:

$$ee = \frac{|[R] - [S]|}{[R] + [S]} = \frac{|[R] - [S]|}{C_P} \quad \text{Eq. 2-17}$$

where $[R]$ and $[S]$ stands for the concentration of respectively enantiomer R and S, $C_P = [R] + [S]$ is the total concentration of phosphinate in solution, and the e.e. represents a fraction which could subsequently be transformed in a percentage after a multiplication by 100. Here, we will consider R as major enantiomer at the beginning of the reaction. We can then write the expressions of concentration for each enantiomer:

$$[R] = \frac{c_P}{2}(1 + ee) \quad \text{Eq. 2-18}$$

$$[S] = \frac{c_P}{2}(1 - ee) \quad \text{Eq. 2-19}$$

As a result, we can define the enantiomeric excess depending on R as:

$$ee = \frac{2}{c_P} [R] - 1 \quad \text{Eq. 2-20}$$

and its evolution over time for the inversion of R into S:

$$\frac{dee}{dt} = \frac{2}{c_P} \frac{d[R]}{dt} \quad \text{Eq. 2-21}$$

However, this enantiomerization can also happen backward, inverting S to form the R enantiomer. Whatever enantiomer is inverting, the reaction is characterized by the same kinetic constant k_0 . The evolution of concentration for each enantiomer can thus be defined as:

$$\frac{d[R]}{dt} = k_{app}[S] - k_{app}[R] \quad \text{Eq. 2-22}$$

$$\frac{d[S]}{dt} = k_{app}[R] - k_{app}[S] \quad \text{Eq. 2-23}$$

As a result, from Eq. 2-21, we get the following expression for variation of enantiomeric excess:

$$\frac{dee(t)}{dt} = -2k_{app}ee(t) \quad \text{Eq. 2-24}$$

Taking back Eq. 2-16, the apparent transition Gibbs free energy is here defined as:

$$\Delta_r G_{app}^{0\ddagger} = -RT \ln \left(\frac{k_{app}h}{k_B T} \right) \quad \text{Eq. 2-25}$$

From this equation and with the experimental data C_P , C_E and T , we can determine the theoretical value of $\Delta_r G_{app}^{0\ddagger}$ for the inversion mechanism and compare it to experimental values to deduce its reliability.

2.6 Conclusion

In this chapter, we first presented DFT and its exchange correlation functionals. After a presentation of how DFT and solvent modeling work, we chose to use SMD//M06-2X/6-31++G(d,p) for its optimization in the mechanistic and thermodynamic studies. In order to reproduce the experimental conditions with more accuracy, we will use partition functions to describe the effect of temperature, and place ourselves in the approximation of rigid rotator and oscillator for rotation and vibration partition functions.

Then, we presented the synthesis protocol for ethyl *hydrogeno*-phenylphosphinates used in this thesis and how to separate phosphinic acid from phosphinate. We also noted the presence of an unknown impurity. Using COSY-NMR, we suspect it corresponds to diethyl phenylphosphonate.

The analysis method, NMR and chiral-HPLC with UV-visible, have also been presented. These will be used in kinetic studies. Kinetic work will be done in the apparent first order approximation, where one of the reactant's concentrations is a lot higher than the other. For this reason, the obtained kinetic constant will not be representative of the mechanism actually happening in solution. Kinetic modeling should allow us to fit the participation of various possible mechanisms based on experimental concentrations.

Now that the methodologies for theoretical, analytical and kinetic studies have been described and chosen, it is necessary to study chemicals of interest and their interaction to elaborate a system to study, which we do in the next chapter.

Chapter 3:

System of interest and equilibrium in solution

RESUME EN FRANÇAIS

Avant de travailler sur le phénomène de substitution nucléophile, nous devons définir le système de référence que nous avons utilisé durant la thèse. Afin de simplifier le système autant que possible sans pour autant négliger la nature des espèces en jeu, nous avons décidé de commencer l'étude par l'attaque du méthanol MeOH sur l'*hydrogéno-phénylphosphinate de méthyle* MeHP. La conformation la plus stable a été identifiée comme étant celle où les hydrogènes du méthoxy interagissent avec le système π du phényl et l'oxygène doublement lié au phosphore. Pour la même raison, le groupement phényl est coplanaire avec cette même liaison.

De prime abord, nous nous sommes intéressé à la tautomérie. Conformément aux études précédemment menées dans la littérature, la forme P(V) MeHP est favorisée de 10 kJ.mol⁻¹ par rapport à l'acide correspondant avec une barrière d'activation de 267 kJ.mol⁻¹. Avec la participation du méthanol, la forme P(V) est toujours favorisée par -10 kJ.mol⁻¹ avec une barrière de 152 kJ.mol⁻¹. De telles différences d'enthalpie libre suggèrent que la forme P(III) ne participera pas ou très peu en milieu neutre. Nous avons donc choisi de ne pas la considérer dans cette étude.

La partie suivante a déjà été partiellement présentée dans notre publication J. Mol. Mod. (2017) 23:168.⁹⁶ Théoriquement, chacun des réactifs MeOH et MeHP peut agir en tant que base ou acide. Afin de déterminer leur caractère acido-basique, nous avons modélisé une échelle acido-basique à partir de modélisations DFT pondérées par des références expérimentales. Nous

avons ainsi obtenu les pKa de -9.8 pour $\text{MeOH}_2^+/\text{MeOH}$, 17.9 pour MeHP/MeP^- , -3.6 pour $\text{MeHPh}^+/\text{MeHP}$, et +29.0 pour MeOH/MeO^- . De telles valeurs indiquent qu'aucune réaction d'échange de proton ne devrait se produire spontanément, donc que les molécules resteront neutres en solution.

Nous avons néanmoins étudié quel serait le comportement du méthanolate vis-à-vis du MeHP si le méthanol venait à être déprotoné. Les modèles d'addition de l'ion sur le phosphore n'ont montré aucune barrière d'enthalpie libre, de même que la déprotonation du phosphore par MeO^- . Ceci suggère que ces deux mécanismes sont des phénomènes spontanés. Cependant, les calculs DFT indiquent que le complexe associé (AC) du phosphinate déprotoné avec le méthanol est 61 kJ.mol^{-1} plus stable que le phosphore TBP le plus bas en énergie. Une telle différence d'enthalpie libre suggère qu'un méthanolate favorise la déprotonation du phosphinate plutôt que l'addition pour former un intermédiaire TBP.

Ce phénomène est intéressant si on le compare à la théorie de Han et *al.* en 2008 selon laquelle les organolithiens peuvent s'additionner directement sur le phosphore lors de la synthèse des SPO, sans passer par la déprotonation du phosphinate. Pour soutenir cette observation, ils s'étaient basé sur le rendement de 86 % obtenu avec un seul équivalent de Methylolithium réagissant sur de l'*hydrogénophénylphosphinate d'éthyle*. D'autres réactifs avaient été testés, avec un rendement de plus en plus bas avec l'accroissement de l'encombrement des groupements alkyles.

Or, d'après le mécanisme communément admis, l'ajout d'un lithien sur le phosphinate provoque le départ d'un alcoolate. D'après nos modèles, ce dernier favoriserait la déprotonation des phosphinates restants afin de retrouver sa forme neutre. Il est donc tout à fait possible que les lithiens ne s'additionnent non sur des phosphinates neutres, mais sur des phosphinates déprotonés par les alcoolates. Ceci expliquerait le bon rendement obtenu par Han et *al.* malgré l'utilisation d'un seul équivalent de lithien.

En conclusion de ce chapitre, nous avons vu que la forme la plus probable de MeHP en présence de MeOH en solution neutre est leur forme neutre. Ce modèle a été utilisé lors de l'étude suivante sur la substitution nucléophile du méthanol sur le MeHP.

3 Theoretical study of equilibrium in neutral condition

3.1 Introduction

3.1.1 Context

As previously described in the section 1.5, Buono & *al.* noticed, while they were developing an efficient way to synthesize SPO from AlKHP, that the alkyl group borne by the phosphinate acts on the enantiomeric excess at the end of the synthesis of SPO.³⁷ As can be seen in the Figure 3-1, the less hindered the alkyl, the lower the e.e.

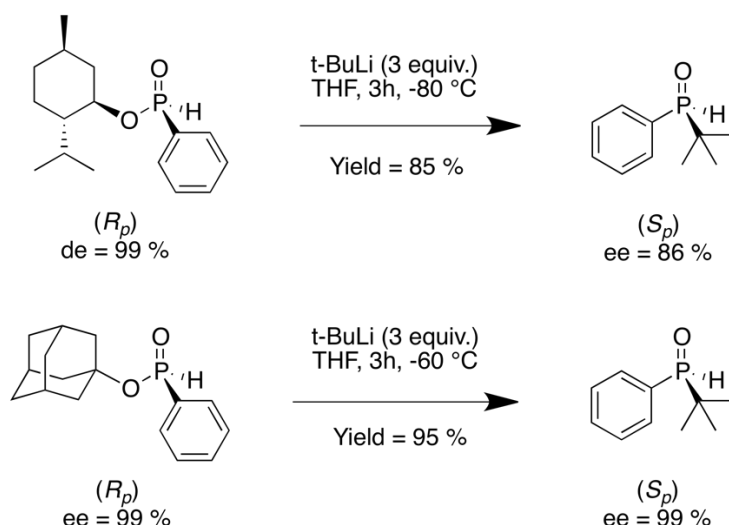


Figure 3-1: Substitutions of alkoxy groups on P-stereogenic alkyl *hydrogeno*-phenylphosphinates in similar experimental conditions using *tert*-butyl lithium as a nucleophilic species. Leaving alkoxy groups are (-)-menthol (top), and 1-adamantanol (bottom)

They also noted that EtHP was racemizing by his own in a few minutes and iPrHP in a few hours, whereas the AdHP remains stable over time. This phenomenon shows that the alkyl group also acts on the configurational stability, in addition of the enantiopurity of the synthesis of SPO. It appears that the effect of hindrance is more complicated than we thought. For this reason, we decided to begin our study the inversion of configuration at phosphorus atom through nucleophilic substitution in neutral condition to understand the effect of alkyl groups. The objective of this chapter is to determine the more stable form of the chemicals used in solution based on their various possible interactions. Parts of this section has already been published in our paper: J. Mol. Mod. (2017) 23:168.⁹⁶

3.1.2 Choice of the system

Since we here aim to deal only with the intrinsic reactivity of compounds of interest, we only keep the relevant chemical functions of these compounds to avoid subsidiary substituent effects. Therefore, we chose methyl *hydrogeno*-phenylphosphinate **1** (MeHP), and methanol **2** (MeOH) as reactants. (Figure 3-2)

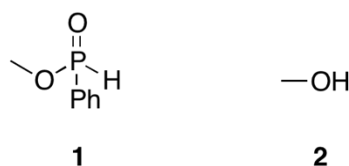


Figure 3-2: Molecules used for simulation of mechanism: methyl *hydrogeno*-phenylphosphinate **1** (left) and methanol **2** (right).

Any further simplification, like replacing the phenyl group for example, would lead to questionable results. It would indeed significantly change the electronic properties of the phosphine oxides substituents, which Bickelhaupt *et al.* has shown to strongly influence the nucleophilic substitution mechanism.^{46, 49}

3.2 Conformation of the methyl *hydrogeno*-phenylphosphinate

In order to determine the correct values of activation barriers, we need to know the less energetic conformation of reactants which will be used as a first step. In our case, we are mostly interested in MeHP **1** since the conformation of methanol is known as the staggered position for the alcohol. To do so, we first studied the rotation of the ester group, and obtained several conformations characterized by their dihedral angle O=P-O-Me and their own Gibbs free energy as detailed in Table 3-1.

Dihedral (Me-O-P=O) (°)	$\Delta_r G^{\circ\ddagger}$ (kJ.mol ⁻¹)
-56.92	0.0
60.11	+ 3.4
178.77	+ 9.4

Table 3-1: Values of the dihedral angle Me-O-P=O and their corresponding Gibbs free energy

After identifying the most stable position for this group, we rotated the phenyl and obtained the following conformations and their Gibbs free energies described in the Table 3-2.

We consequently identified the most stable conformation for **1** as the one presented in Figure 3-3. The stability of this conformation can be explained by two weak long-range bonds: one between hydrogen atoms of the methyl and the π bonds of the phenyl, the second between π system from the phenyl and the double bound oxygen. This conformation will be used along the whole study as molecule **1**.

Dihedral (C=C-P=O) ($^{\circ}$)	$\Delta_r G^{\ddagger}$ (kJ.mol $^{-1}$)
174.1	0.0
-141.5	+ 9.3

Table 3-2: Values of the dihedral angle C=C-P=O and their corresponding Gibbs free energy

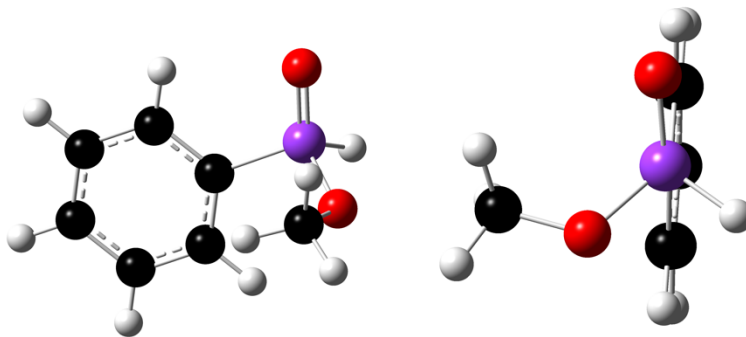


Figure 3-3: Pictures of the most stable conformation determined for MeHP **1**

3.3 Prototropic equilibrium

In the part 1.1.2 (p.9), we described how alkyl *hydrogeno*-phenylphosphinates can undergo prototropic exchange when the hydrogen borne by the phosphorus P(V) is transferred to the double bound oxygen to form the corresponding phosphinous acid P(III).^{20, 22} Previous studies showed that, in conditions like ours, this equilibrium is strongly displaced toward the P(V) form.^{22, 24, 23}

Our calculations on this exchange from MeHP **1** to methoxyphenylphosphinous acid **3** lead exactly to the same result since we obtain a transition Gibbs free energy $\Delta_r G^{\ddagger} = +267$ kJ.mol $^{-1}$ at 25°C (+271 kJ.mol $^{-1}$ at 50°C), as shown in the Figure 3-4. We obtained the same result for the equilibrium in favor of the P(V) by -12 kJ.mol $^{-1}$.

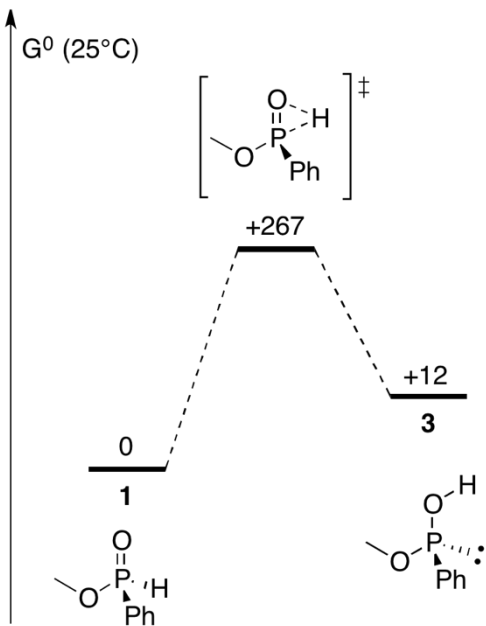


Figure 3-4: Tautomeric mechanism of **1** determined using SMD(THF)//M06-2X/6-31++G(d,p)

As shown in previous studies described in the part 1.1.2.2 (p.7), we can encounter a proton exchange between SPO and protic compounds like methanol.^{25,26} Hence, we need to determine if they can exchange a proton, as was shown in the studies from Tavakol *et al.* who determined that this exchange could happen with a 150 kJ.mol⁻¹ energy barrier.

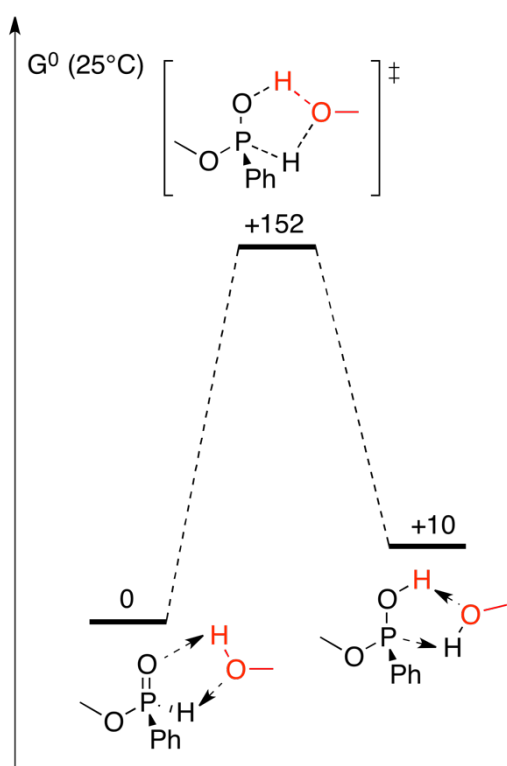


Figure 3-5: Prototropic exchange between **1** and **2** determined using SMD(THF)//M06-2X/6-31++G(d,p).

Reference is the associated complex of **1+2**.

Our results are consistent with their observation since we determined the Gibbs free energy difference between associated complexes (AC) **3** or **1** coordinated to **2** to be in favor of the P(V) form by -10 kJ.mol^{-1} with a transition state of $\Delta_r G^{\ddagger} = 152 \text{ kJ.mol}^{-1}$ (Figure 3-5).

As a conclusion, we can reasonably assume form such difference of energy that the phosphinous acid form **3** is absent from the reactive mixture according to Boltzmann distribution. Thus, we decide not to take the tautomerism into account in our study, and focus exclusively on the addition of methanol onto MeHP.

3.4 Acidobasicity scale

3.4.1 How to build an acidobasicity scale

From a reactivity point of view, methanol can act as a base, an acid or a nucleophile. Kinetically, methanol can protonate the oxygen atom from MeHP molecule that is doubly bound to the phosphorus atom, leading to MeHPH^+ **4** and MeO^- **5** (Figure 3-6), or, on the contrary, deprotonate the MeHP molecule by removing the proton that is directly bound to the phosphorus atom, leading to MeP^- **6** and MeOH_2^+ **7** (Figure 3-6).

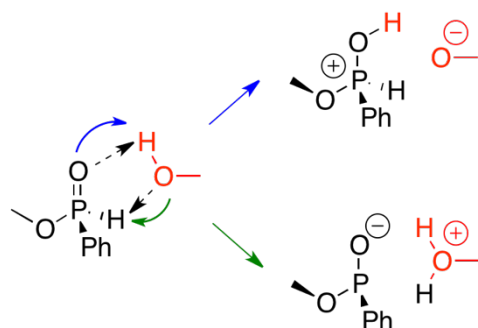
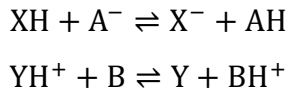


Figure 3-6: Conceivable proton exchange reactions between methyl *hydrogено*-phenylphosphinate **1** and methanol **2**.

Now, we need to determine which neutral, protonated or deprotonated forms of methanol and MeHP coexist at the equilibrium. Unfortunately, we did not find experimental pKa values in THF for those compounds. We consequently have to compare the relative acidities of these species on the basis of our calculations, which we do through by building a relative acidity scale of all involved species.

A method used in previous studies to determine pKas of compounds from calculations consists in choosing an acidobasic pair as a reference and estimate the energy associated to a proton

transfer between this reference species and the species of interest. In the present case, two pairs are used, that exhibit opposite charges, XH/X^- and YH^+/Y , which avoid charge separation issues.^{78, 79} We then study the proton exchange reaction between the unknown pair of interest, AH/A^- or BH^+/B , and the reference bearing the same charge:



We have then access to the pKa of pairs XH/X^- and YH^+/Y , relatively to pairs A^-/AH and B/BH^+ , through the following formula:

$$\text{pKa}_{\text{unkown}} = \text{pKa}_{\text{reference}} - \frac{\Delta_r G^0}{R T \ln(10)} \quad \text{Eq. 3-1}$$

According to previous studies such as Li in 2006 and Zhang in 2010 who used this same methodology, this empirical method generally gives acceptable results for a qualitative model of pKa scale.^{78, 79} However, such method has a tendency to distend the acidobasicity scale which means that the resulting pKa can be in the right order but too far apart from each other. A way to improve this is to use compounds for which we know the pKa as a reference. The difference between its calculated and measured pKa will give a scaling factor N which, applied to the Eq. 3-1, will lower the distortion of the calculated acidobasicity scale. Consequently, the theoretical pKa value determined from Eq. 3-1 gets closer to the experimental one when the factor N is applied. The resulting formula is:

$$\text{pKa}_{\text{unkown}} = N \left(\text{pKa}_{\text{reference}} - \frac{\Delta_r G^0}{R T \ln(10)} \right) \quad \text{Eq. 3-2}$$

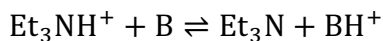
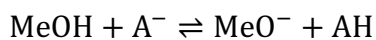
Note that this N factor is here purely arbitrary and has no other purpose than to make the predicted values as close as possible from the known ones. Applying such an arbitrary correction, with no underlying theory, is not fully satisfying, but it leads to an approximate acidity scale, which approximatively shows the relative positions of the acidobasic pairs of interest, which is sufficient for our purpose.

3.4.2 Determination of the pKa of the compounds of interest

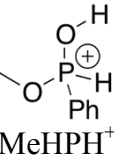
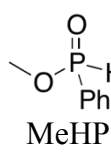
We now apply the method previously described to chemicals we are interested in: MeHP and MeOH. In order to make sure that we are not diverging too much from reality, we first build the acidity scale in dimethylsulfoxide (DMSO), a solvent for which we got the most pKa information. The dielectric constant of DMSO (47.24 at 293.2 K) is stronger than the one of THF (7.52 at 293.2 K),⁸⁰ but it is also aprotic. This solvent has been chosen on account of the numerous experimental and predicted pKa values that are already available within the literature.

Note that, in this part, DFT calculations in DMSO are performed using the default DMSO parametrization of the SMD implicit solvent model.

To build this acidobasicity scale in DMSO, we chose MeOH/MeO⁻ (29.0 at 298 K)⁸¹ and Et₃NH⁺/Et₃N (9.0 at 298 K)^{82, 83} as references. Proton transfer reaction standard Gibbs free energies Δ_rG⁰ are then calculated for the following reactions, in which no charge separation takes place.



In order to scale the pKa difference, we chose two compounds which structures are sufficiently different from both reference pairs and which pKa in DMSO are known to estimate scaling factors N that are applied to both scales that refer to positively charged and negatively charged acidobasic pairs respectively. Pairs are AcOH/AcO⁻ (12.6 at 298 K)⁸⁴ and 1-hydroxypyridinium/1-oxopyridinium (Pyr-OH⁺/Pyr-O, 1.63 at 298 K).⁸⁵ The scaling factors for the negatively and positively charged scales are estimated to 0.33 and 0.26 respectively. These scaling factors appear high and do not give exact pKa values, but they allow us to have a qualitative pKa scale which is enough for us to determine the potential acido-basic reactivity. Finally, a third pair of acidobasic pairs is used, which structures are again sufficiently different from other used pairs, and which pKa in DMSO are known, to check the validity of the estimated scale. These are benzophenone oxime (Oxime/Oxime⁻) and its corresponding deprotonated form (20.1 at 298 K)⁸⁶ and QuinuclidineH⁺/Quinuclidine (Quinu⁺/Quinu, 9.8 at 298 K).⁸⁷ The resulting pKa, determined using Eq. 3-2, are in the Table 3-3 and the resulting acidity scale is represented in Figure 3-7.

Acidobasic pair		Proton exchange Gibbs free energy at 25°C (kJ.mol ⁻¹)	Unscaled pKa difference	Scaled pKa difference	Estimated pKa	Expected pKa
Acid	Base					
 MeHPH ⁺	 MeHP	119.43	-48.18	-12,6	-3,6	

		95.55	-38.55	-12,9	16,1	
		178.94	-72.19	-18,8	-9,8	
		0.00	0.00	0,0	29,0	29,0
		0.00	0.00	0,0	9,0	9,0
		121.38	-48.97	-16,4	12,6	12,6
		70.11	-28.29	-7,4	1,6	1,6
		-1.27	0.51	0,1	9,1	9,8
		82.10	-33.12	-11,1	17,9	20,1

Table 3-3: Acidobasic pairs used to elaborate the acidobasicity scale in DMSO, their calculated Gibbs free energy difference between the acidic and basic form, the determined pKa value and the scaled pKa value calculated using Eq. 3-2, the expected pKa determined by experimental studies.

It can be seen in Table 3-3 and Figure 3-7 that both pairs used to test the validity of the estimated pKa scale are almost at the right position, 9.1 instead of 9.8 for QuinuclidineH⁺/Quinuclidine and 17.9 instead of 20.1 for benzophenone oxime and its corresponding deprotonated form. This is very reasonable on a scale that runs from -10 up to 30. In particular, this degree of precision is highly sufficient to conclude that MeHP and methanol cannot deprotonate each

other spontaneously, since the corresponding pairs differ about 26 pKa units in case methanol deprotonate MeHP, and about 33 pKa units in case MeHP deprotonate methanol. Moreover, since the dielectric constant of THF is significantly lower than that of DMSO, it is even more unlikely in THF that both neutral MeHP and methanol molecules deprotonate each other and generate separated ions.

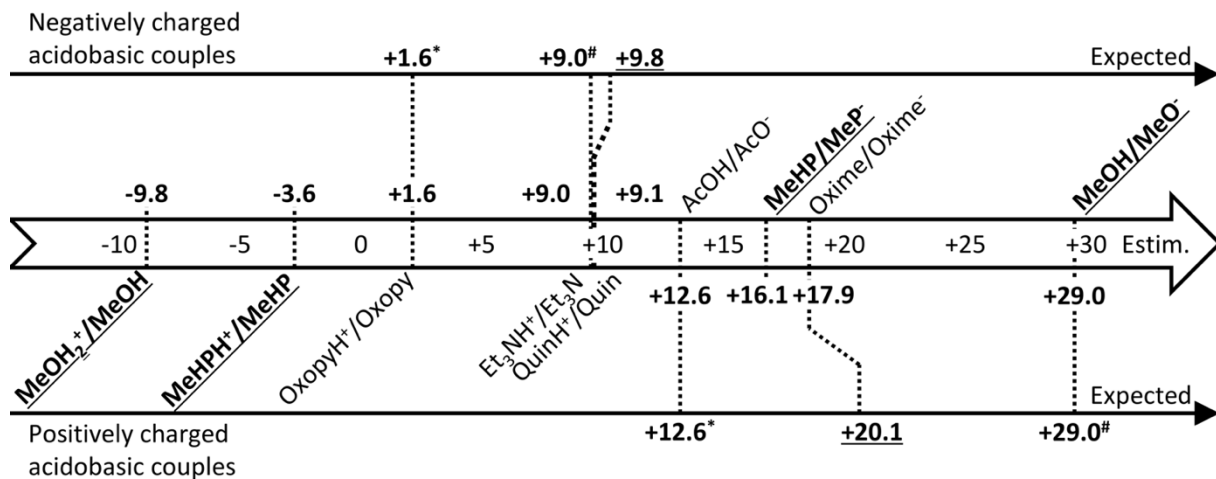


Figure 3-7: Estimated acidity scale in DMSO (middle) and comparison with expected values from literature for negatively charged acidobasic pairs (top) and positively charged acidobasic pairs (bottom). Values used as anchor points are marked with # (MeOH/MeO⁻ at 29.0 and Et₃NH⁺/Et₃N at 9.0). Those used for calculating scaling factors are marked with * (AcOH/AcO at 12.6 and 1-hydroxypyridinium/1-oxyridinium at 1.6). Those used as tests are underlined (OXIME at 20.1 and QuinuclidineH⁺/Quinuclidine at 9.8). Pairs with particular interests within the present study are bolded and underlined

3.5 Methoxide and phosphonide

3.5.1 Deprotonation of phosphinate by an alkoxide

Despite the low probability of a deprotonation of methanol **2**, we wanted to study what could happen if a phosphinate was in presence of an alkoxide. This sends us back to the original problem presented in the section 1.2, where the work of Buono *et al.* on the synthesis of SPO lead to the conclusion that alkoxide could react on phosphinates with a nucleophilic substitution or a deprotonation of the phosphorous compound.³⁷

To model the deprotonation of phosphinate by alkoxide, we made a relaxed scan where the proton borne by the phosphorus atom approaches the methoxide until it is bound to it (variation of distance H—OMe). More precisely, at the beginning of the scan, $d_{H-OMe} = 1.6 \text{ \AA}$ and the hydrogen is bound to the phosphorus atom, while at the end $d_{H-OMe} = 1.1 \text{ \AA}$ and the hydrogen is bound to the alcohol, so the calculation was stopped. Those distances seem low, but it can be

explained by the ionic nature of both reactants that will interact with the hydrogen whatever compound it is bound to. The variation of the non-thermalized Gibbs free energy depending on the distance H--OMe is reported in the Figure 3-8.

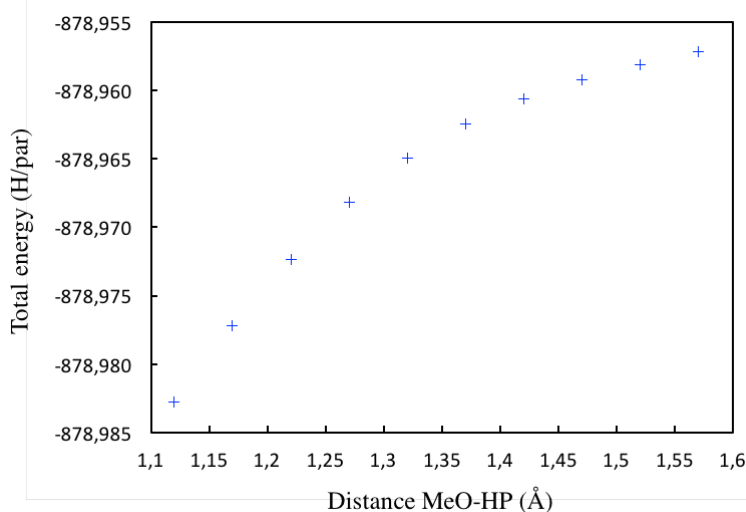


Figure 3-8: Evolution of the non-thermalized Gibbs free energy of the system in Hartree depending on the distance between the hydrogen and the alkoxide **6** (distance H – OMe) (SMD//M06-2X/6-31++G** level of theory, with THF as solvent). At 1.1 Å, the hydrogen is bound to the phosphorus, at 1.6 Å it is bound to the alcohol.

More calculations with different coordinates would be useful to fully represent the reactivity, but we can still observe that the energy keeps diminishing while the proton leaves the phosphorus atom and finally coordinates to the alkoxide to form the alcohol. This mechanism happens without any transition state, which means that the proton transfer from phosphorus to alcohol is spontaneous.

When we tried to get the associated complex of methoxide with phosphinate, the alkoxide systematically deprotonated the phosphorus atom. The AC **9** from Figure 3-8 has never been obtained, no matter how we proceed. We concluded that the presence of alkoxide with phosphinate spontaneously results in the formation of AC **8**. This is consistent with the previous work of Bickelhaupt who noted that methoxide systematically deprotonated the hydroxide groups of methoxyphosphonic acid P(O)(OH)₂OMe.⁴⁹

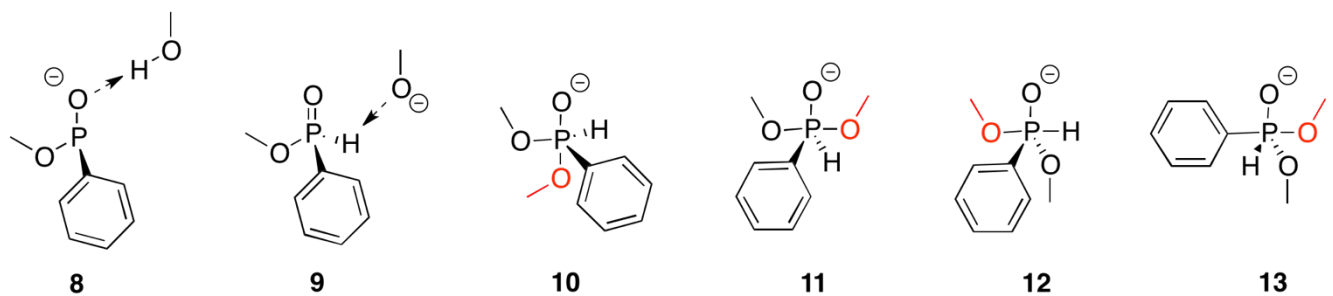


Figure 3-9: All possible anionic systems with MeHP, MeOH and their respective anionic form. Represented TBP are the one immediately after addition of MeO^- onto MeHP.

Another possibility would be the addition of methoxide onto the phosphorus atom. Such mechanism also shows no transition state and result in the formation of an anionic TBP. The four possible conformations of P(V) are represented in Figure 3-9 with the two possible anionic associated complexes (AC), and their respective Gibbs free energy of all ionic systems are given in Table 3-4.

We can observe that the difference of Gibbs free energy between **8** and the less energetic TBP **11** is $61 \text{ kJ}\cdot\text{mol}^{-1}$ in favor of the AC. We need to note that such TBP compound can evolve in various way, like undergo pseudorotations. Still, those models suggest that the most favored system is the deprotonation of phosphinate.

System	Relative Gibbs free energy ($\text{kJ}\cdot\text{mol}^{-1}$)
8	0
9	Optimization in 8
11	61
12	94
13	95
10	128

Table 3-4: Relative Gibbs free energies calculated at DFT level for $T = 25^\circ\text{C}$. Energetic reference is the original ionic system of interest **9**, the AC with MeHP **1** coordinated to methoxide **5**.

This observation is mostly interesting when relied to the hypothesis from Han about the synthesis of SPOs in their publication from 2008, when they managed to obtain a yield of 86% of SPO from ethyl phosphinate using only 1 equivalent of methyl lithium (MeLi).³⁸ According to previous work, this equivalent of MeLi should be consumed to deprotonate the phosphorus,³⁵

but this good yield made them think that an important amount of MeLi could directly react with phosphinate without proceeding to a deprotonation first.

However, this hypothesis does not take into account the formation of alkoxide after the addition of MeLi onto phosphinate. Our simulations suggest that the released alkoxide would deprotonate the phosphorous compound, allowing methylolithium to proceed to the S_N2 on the deprotonated phosphorus to form the SPO. This result alone does not prove that the hypothesis of Han is wrong, but it shows that their result can be due to another reactivity than a secondary mechanism of alkylolithium onto phosphinate.

3.5.2 Inversion of configuration of a phosphinide

Now that we have shown that alkoxide would deprotonate the phosphinate, we need to know the configurational stability of the phosphonide ion. In their publication of 2015, Buono et al. have tested the enantioselectivity of methyl phosphinate.³⁷ To do so, they have put MenHP in THF with one equivalent of lithium diisopropylamide, and stirred the solution at T = -80 °C, the temperature of synthesis of SPO. They observed a loss of only 2 % of enantiomeric excess after 2h, which is far less than the loss of enantioselectivity during the synthesis of SPO (11 %). They have deduced that deprotonated phosphinate is actually enantioselective enough, and the variation of enantioselectivity does not find its origin in its inversion.

Our DFT model of the inversion of configuration at ionic phosphonide **6** is presented in Figure 3-10. We can see that the transition Gibbs free energy is high: 232 kJ.mol⁻¹ for 25 °C. This is consistent with the conclusion of Buono et al. about the relative stability of the anion. We can conclude that an anion alone would not invert unless another compound is involved.

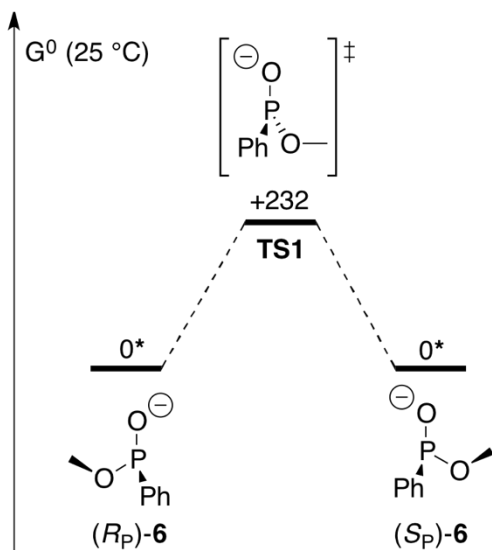


Figure 3-10: Inversion of MeP⁻ **6** in kJ.mol⁻¹ for T = 25 °C.

3.6 Conclusion

In this section, we wanted to determine the most probable form of MeHP in solution. To do so, we first modeled its various conformations, and saw that the most stable was the one where hydrogen atoms from the methyl group interact with both phenyl and oxygen, while the phenyl is coplanar with the double bond P=O. Then, we showed that prototropic exchange are not favored since the P(V) form is still lower in energy than P(III) by 10 kJ.mol⁻¹ for MeHP alone, to 12 kJ.mol⁻¹ with the participation of methanol.

We studied interactions between compounds of interest, MeHP and methanol, by modeling an acidobasicity scale. Using our level of theory, we managed to evaluate their pKa: -9.8 for MeOH⁺/MeOH, 17.9 for MeHP/MeP⁻, -3.6 for MeH⁺/MeHP and +29.0 for MeOH/MeO⁻. Those differences of values between those acidobasic pairs indicate that we should only find neutral compounds in our neutral conditions.

In order to cover all interactions, we still decided to study how the alkoxide could react with MeHP. Our model showed that the deprotonation of phosphinate by MeO⁻ or its addition onto phosphorus atom to form a TBP intermediate occurs with no energy barrier, thus spontaneously. The AC **8** of MeP⁻ with MeOH is 61 kJ.mol⁻¹ more stable than the less energetic TBP, which shows that the ion should first deprotonate the phosphorus atom to form the alcohol. The resulting ionic phosphonide would then be enantiomerically stable as showed by the high energy barrier of 232 kJ.mol⁻¹ determined by DFT and the experiments of Buono et al.³⁷ This results brings another explanation to results from Han in 2008,³⁸ where the synthesis of SPO from AlkHP with only MeLi could be due to a deprotonation by alkoxide in solution before addition of the alkyllithium.

The conclusion of this section is that MeHP and methanol only exist as neutral molecules in neutral reactive mixture. We then confidently head nucleophilic attacks as the only reactions that may take place when both molecules collide. This reaction will be studied in the next chapter.

Chapter 4:

Transesterification mechanism of methanol on alkyl hydrogeno-phenylphosphinate

RESUME EN FRANÇAIS

Cette section a déjà été partiellement publiée dans notre article J. Mol. Mod. (2017) 23:168.⁹⁶

Après avoir déterminé quelles sont les espèces présentes en solution dans le chapitre précédent, nous avons exploré les différentes possibilités pour l'alcool MeOH de réagir avec le phosphinate de méthyle MeHP. Nous avons alors réalisé des modélisations à l'aide de la méthode PM6 (méthode semi-empirique) en approchant le méthanol du phosphore sous divers angles susceptibles de permettre son addition. D'après ces modèles, la seule réaction possible était l'addition du MeOH sur le MeHP avec coordination de l'hydrogène sur un des oxygènes du phosphinates.

Nous avons obtenu 6 mécanismes possibles divisés en 2 groupes : les mécanismes V1 (F2-V1, F3-V1 et F4-V1) où l'hydrogène du méthanol se coordine à l'oxygène doublement lié pour former un intermédiaire TBP, et les mécanismes V2 (F1-V2, F3-V2 et F4-V2) où l'hydrogène du méthanol se coordine à l'oxygène du groupement méthoxy entraînant le départ d'un méthanol pendant que l'alcool d'origine remplace le méthoxy.

Les résultats théoriques ont montré que les mécanismes V2 conservent la configuration du phosphinate et présentent des enthalpies libres de transition très élevées (F1-V2, **TS5**: 268 kJ.mol⁻¹; F3-V2, **TS6**: 205 kJ.mol⁻¹; F4-V2, **TS7**: 204 kJ.mol⁻¹). Les mécanismes V1, en revanche, terminent sur un intermédiaire TBP susceptible d'évoluer, et présentent des barrières

d'enthalpie libre bien moindre (F2-V1, **TS2**: 113 kJ.mol⁻¹, F3-V1, **TS3**: 133 kJ.mol⁻¹ and F4-V1, **TS4**: 130 kJ.mol⁻¹). Le mécanisme F2-V1, notamment, est celui qui présente la barrière d'énergie la plus basse en plus de donner l'intermédiaire le plus stable.

Nous en déduisons que le mécanisme le plus probable entre le MeOH et MeHP est F2-V1, soit la *syn*-addition du méthanol sur la double liaison P=O pour former l'intermédiaire TBP avec deux méthoxy en position apicale.

Cet intermédiaire peut ensuite évoluer, soit via une rotation du groupement hydroxy qui permet alors au groupement OMe originel de quitter la molécule en tant qu'alcool et ainsi de reformer un MeHP de configuration opposée, soit via des pseudorotations. Les simulations DFT ont montré que les pseudorotations pouvaient être compétitives avec une barrière d'enthalpie libre atteignant 115 kJ.mol⁻¹, soit 2 kJ.mol⁻¹ au-dessus de l'addition de l'alcool. Ainsi, suivant le groupement alkyle porté par l'alcool, l'intermédiaire TBP peut s'inverser via pseudorotation avant d'éliminer l'alcool.

La cinétique de racémisation du phosphinate d'éthyle dans l'éthanol pur à 78 °C a été réalisée en utilisant l'HPLC chirale (mesures par Marion Jean). L'expérience a montré des cinsétiques de premier ordre apparent dont les barrières de transition ont ainsi été mesurées étaient autour de 127 kJ.mol⁻¹ en se basant sur un modèle monomoléculaire.

Ces cinétiques de 1^{er} ordre apparent sont également compatibles avec notre modèle DFT bimoléculaire EtOH + EtHP résultant sur une inversion. En considérant l'éthanol comme un réactif, on obtient des barrières expérimentales (environ 136 kJ.mol⁻¹) en très bon accord avec nos calculs DFT EtHP + EtOH (135 kJ.mol⁻¹) ce qui va dans le sens d'une validation de notre modèle. Cependant, on observe une dépendance à la concentration de phosphinate diluée selon la formule : $133.4 - 0.65 \log_{10}(C_p/C^0)$.

Pour expliquer cette dépendance, nous avons eu recours au modèle cinétique. Si l'on prend en compte un modèle cinétique prenant en compte une dimérisation et l'inversion d'un des monomères après celle-ci, les valeurs cinétiques de ce modèle correspondent bien aux valeurs expérimentales. On en déduit que plus il y a de phosphinate en solution, plus la formation de dimère est probable, et cette dimérisation semble agir comme une catalyse sur la substitution nucléophile par l'alcool.

En conclusion, les données expérimentales et théoriques sont compatibles avec le mécanisme de *syn*-addition d'alcool sur le phosphinate terminant sur une inversion de configuration. Ce mécanisme est néanmoins assujetti aux pseudorotations compétitives selon

les groupements alkyles portés par le phosphinate ou l'alcool. L'activité des dimères semblent accélérer la réaction d'après le modèle cinétique, probablement par catalyse basique ou acide.

4 Transesterification mechanism of methanol on alkyl *hydrogeno*-phenylphosphinates

4.1 Introduction

4.1.1 Context

As previously reported in the section 1.5 (p.18), our interest follow the observations of Buono *et al.* who showed that the alkyl group borne by the alkoxy substituent of phosphinates acts on their reactivity and enantioselectivity.³⁷ We suspected that this last phenomenon is related to the first, and decided to explore the reactivity of phosphinate with alcohol.

In section 3.4, we made an acidobasicity scale (Figure 4-1) and modeled the reactivity of compounds of interest to determine that only phosphinates and alcohols are present simultaneously in neutral conditions. In this chapter, we want to know the different mechanisms for an S_N2@P between those two compounds and identify the most probable one using DFT modeling. Parts of this section have already been published in our paper: J. Mol. Mod. (2017) 23:168.⁹⁶

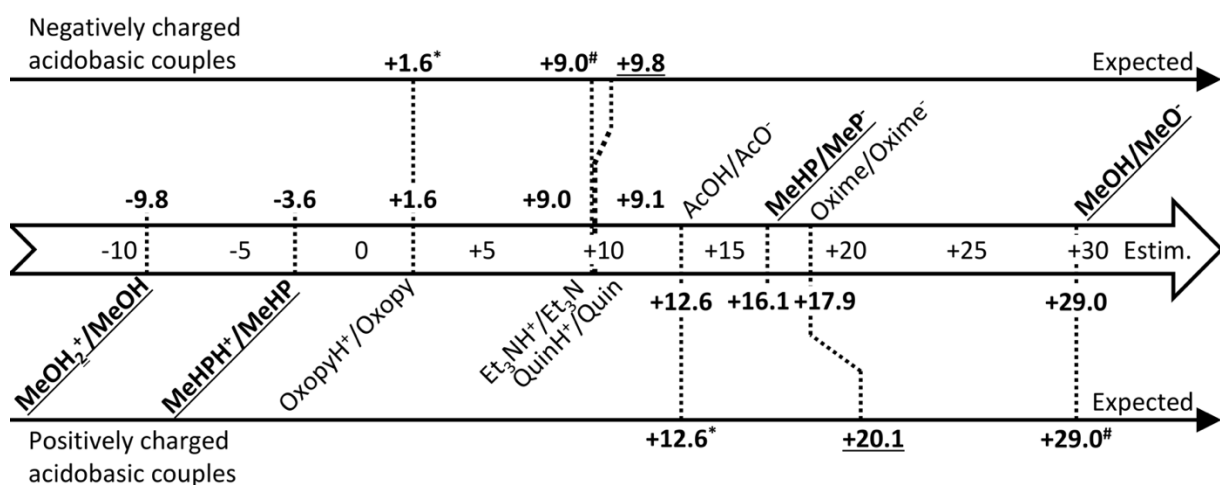


Figure 4-1: Estimated acidity scale in DMSO (middle) and comparison with expected values from literature for negatively charged acidobasic pairs (top) and positively charged acidobasic pairs (bottom). Values used as anchor points are marked with # (MeOH/MeO⁻ at 29.0 and Et₃NH⁺/Et₃N at 9.0). Those used for calculating scaling factors are marked with * (AcOH/AcO at 12.6 and 1-hydroxypyridinium/1-oxypyridinium at 1.6). Those used as tests are underlined (OXIME at 20.1 and QuinuclidineH⁺/Quinuclidine at 9.8). Pairs with particular interests within the present study are bolded and underlined.

4.1.2 Methodology

Geometrically, all four substituents of the phosphorus atom in MeHP are located at the vertices of a tetrahedral structure as shown in Figure 4-2. Vertices, faces and edges of this tetrahedron are hereafter numbered using the CIP rules.⁵⁰ In the present case, substituents have the following order: double bound oxygen, methoxy, phenyl, hydrogen. Faces are numbered using the same rules, but applied to the opposite substituent of each face. Finally, edges are numbered using the neighboring vertices.

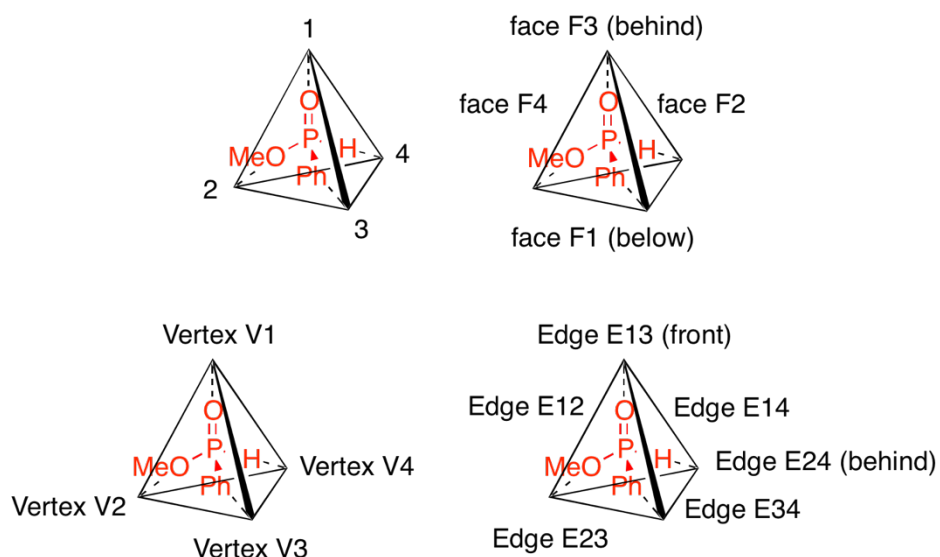


Figure 4-2: Tetrahedral geometry of the methyl *hydrogeno*-phenylphosphinate molecule around its P stereogenic center. Vertices are numbered using the Cahn-Ingold-Prelog rules applied to the corresponding substituents.

During the nucleophilic attack of methanol onto MeHP, the oxygen atom of methanol approaches the phosphorous center through the middle of one face of the tetrahedron (F1 to F4). At the same time, the hydrogen atom from the hydroxy function of methanol is placed either in the neighborhood of a vertex (V1 to V4) or in the middle of an edge (E12 to E34) as represented in Figure 4-3.

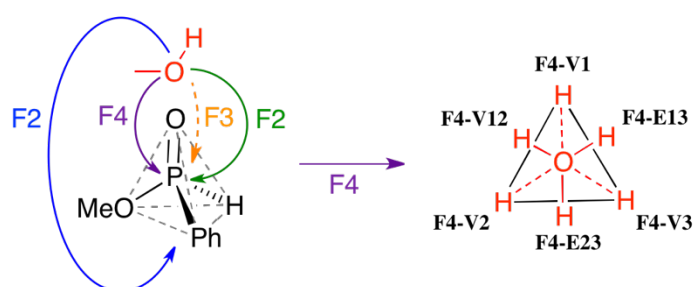


Figure 4-3: Description of all 24 possible attacks of methanol when it reacts nucleophilically with methyl *hydrogeno*-phenylphosphinate; example given on the face F4.

To each face of the tetrahedron are consequently associated 6 possible hydrogen positions, which makes globally 24 possible attacks (Figure 4-4). These last are named using the face index followed by the position of the hydrogen atom. For example, F4-V1 corresponds to the approach of the methanol on the opposite to the hydrogen substituent (face F4), with the hydrogen atom located in the vicinity of the doubly bonded oxygen atom (vertex V1).

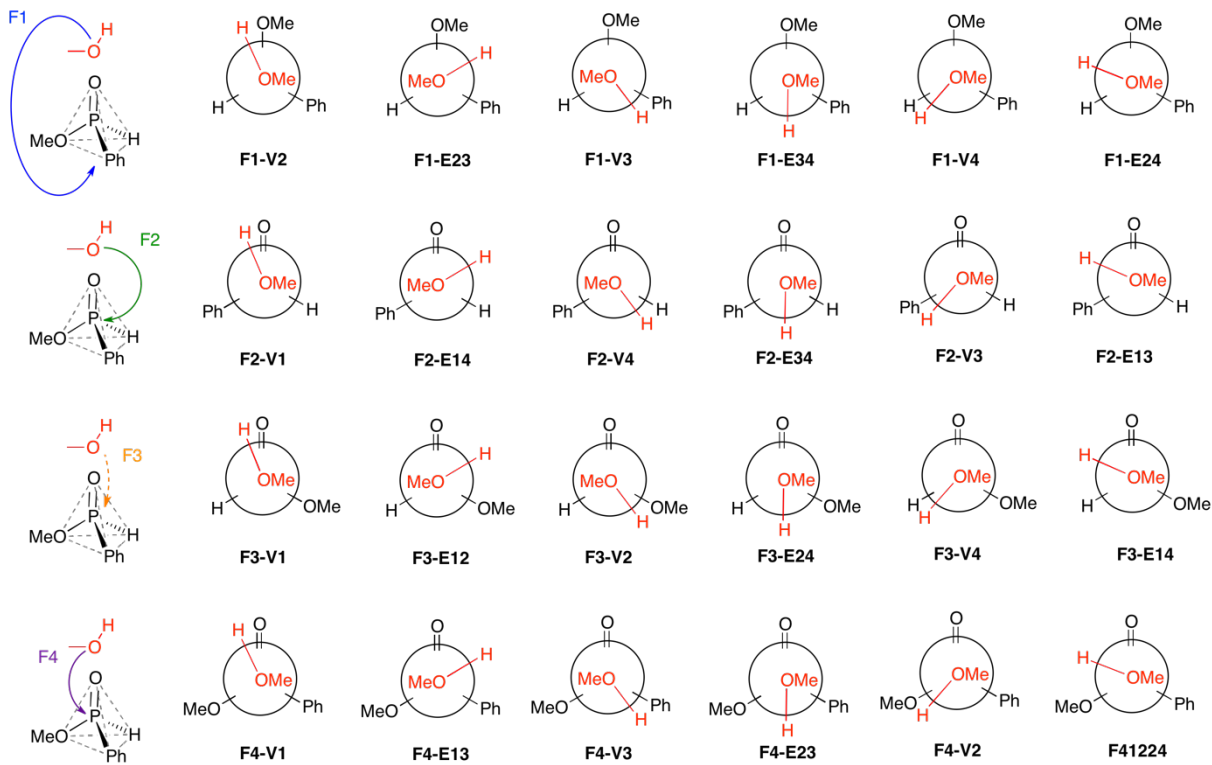


Figure 4-4: Representation of all 24 investigated nucleophilic attacks of methanol onto methyl *hydroxyphenylphosphinate*

During this study, we will use the intermediate **14** as an energetic reference, which simply corresponds to the association of both reactants through an H-bond with the lowest energy modeled during the study. (Figure 4-5) This choice has voluntarily been made on account of our expertise in this area, which has proven us that estimating precisely association-dissociation energies in condensed phase using DFT is a difficult task because of long-range interactions (section 2.2.2.2, p.26). We consequently prefer to estimate them separately from the reaction mechanism and avoid any contamination of the calculated barrier by those uncertain data in case they would be inaccurate.

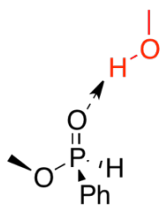


Figure 4-5: Intermediate **14** used as energetic reference

In the present case, the reaction standard Gibbs free energy corresponding to the association of MeHP **1** and methanol **2** into intermediate **14** at 25°C obtained from DFT (SMD(THF)//M06-2X/6-31++G**) is +8 kJ.mol⁻¹. This value is not discussed further here, but will be in the kinetic section 4.4, where its reliability is explicitly checked.

4.2 Addition of methanol onto the phosphorus atom

4.2.1 Possible approaches of methanol onto phosphinate

Each of the 24 possible approaches of the methanol onto the phosphorus atom for a nucleophilic attack is first investigated using PM6 semi-empirical method (Ampac).⁸⁸ To do so, we used an initial positioning for the alcohol with the hydroxyl oriented in the position of interest. Then, we progressively approached it to the phosphorus atom until we observed a reaction. If the hydroxyl changed its position relatively to phosphinate, we performed another calculation but freezing the hydroxyl group position to be sure that we did not miss any addition mechanism, even if not favored. Note that forcing the position of the hydroxyl group of methanol does normally not determine the whole position of the methanol, because its methyl group should still exhibit several degrees of freedom with rotations. However, at PM6 level (vide infra for modeling details), this methyl group exhibits, for all 24 attacks, a single acceptable position. The position of the hydroxyl group of methanol during the nucleophilic attack consequently fully determines the position of the whole methanol molecule.

Every addition mechanism has been tested with a scan using the PM6, which consists in approaching progressively a reactant to another and calculate the energy of the system at each step to get a reaction profile. The resulting reactive pathways were subsequently modeled using Density Functional Theory (Gaussian09).⁸⁹ Reaction intermediates and transition structures were all vibrationally characterized. Internal released channel (IRC) calculations, which allowed us to determine the correct intermediates around a specific TS, were performed on transition structures in order to locate the intermediates that are directly related to them.

Our results showed that the position of hydrogen from methanol is highly favored if coordinated to an oxygen from phosphinate. If not, the alcohol cannot be added onto the phosphorous center,

and no S_N2 can occur. As a result, we observed no reaction for V3 and V4 approaches showed in Figure 4-6.

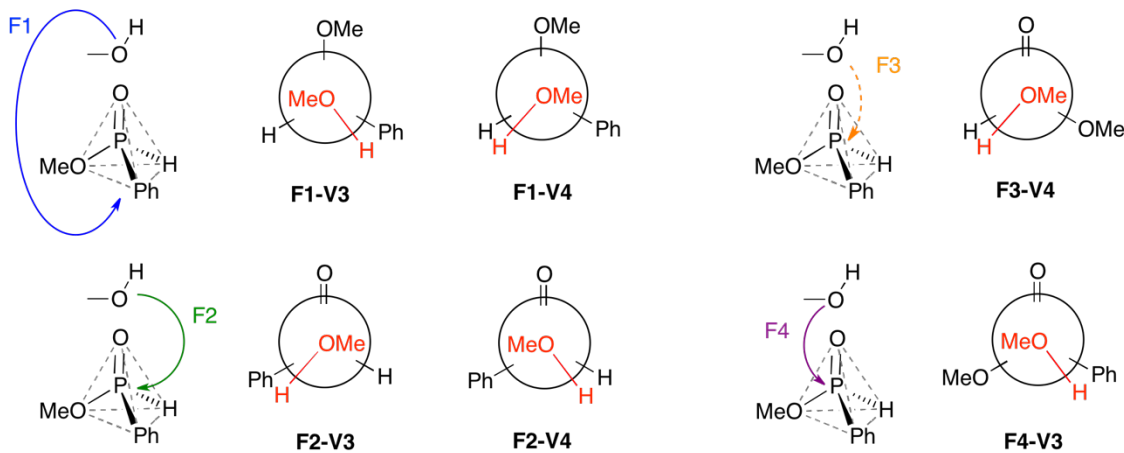


Figure 4-6: Approaches V3 and V4 that do not end up on an addition of the alcohol.

When the hydrogen is close to an oxygen, such in the case of E13, E14, E23 and E34 in Figure 4-7, the approach of alcohol favors the coordination of hydroxyl group to an oxygen, which corresponds to V1 or V2 approaches. If the hydrogen atom is between two oxygen atoms from phosphinate (E12), the addition favors the more electronegative double bond for a V1 addition.

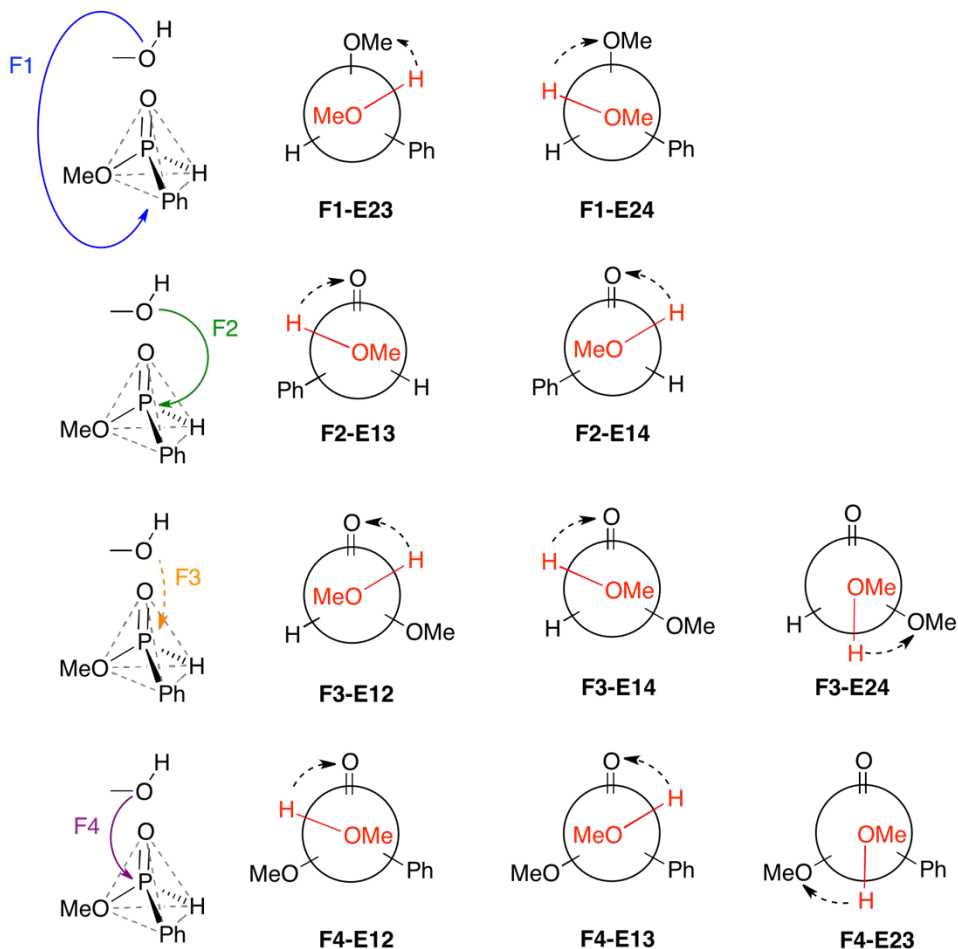


Figure 4-7: Approaches where the hydrogen atom is near an oxygen and the interaction it favors.

As a result, we end up with 6 mechanisms where the hydrogen atom from the methanol molecule exhibits a hydrogen bond with one of both oxygen atoms borne by the phosphorous center. This coordination can either be with the V1 doubly bound oxygen atom (F2-V1, F3-V1, F4-V1) or with the V2 methoxy oxygen atom (F1-V2, F3-V2, F4-V2). (Figure 4-8) These six relevant reaction pathways are confirmed by DFT calculations, and their respective behavior are presented in the next section.

From now on, the addition will be represented as in Figure 4-8, with MeHP as a pyramid where the colored face is the one attacked by the alcohol, and the vertex of coordination of the hydrogen is shown by a red circle.

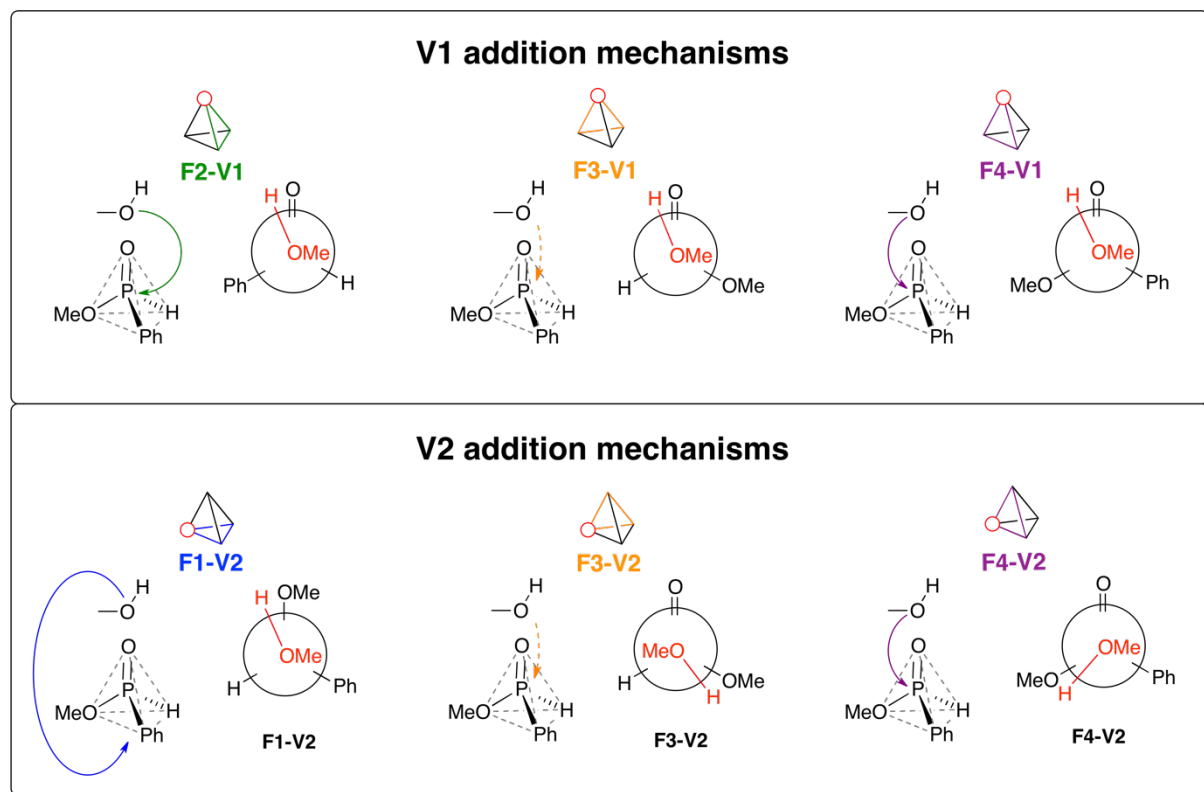


Figure 4-8: Positions of the alcohol and its hydrogen on the tetrahedral phosphinate for the 6 mechanisms that end up on the addition of methanol onto phosphinate. Pyramids are schematic representation of phosphinate and its reactivity with the alcohol (colored triangles) and the vertex coordinated to hydrogen (red circle). As will be seen in the next section, V1 mechanisms at top result in the formation of TBP phosphorous intermediates after the *syn*-addition of the hydroxide to the double bond P=O; V2 mechanisms at bottom are conjugated mechanism resulting from the coordination of hydroxide onto the MeO group.

4.2.2 A study of the 6 mechanisms for S_N2

4.2.2.1 Mechanisms V1

V1 attacks consist in *syn*-additions of the methanol molecule onto the P=O double bond. As shown in Figure 4-9, in these mechanisms, the methoxy part from methanol molecule is added to the phosphorous center, while its hydrogen atom is transferred to the oxygen atom V1 that was initially doubly bound to the phosphorous center. They lead to penta-coordinated intermediates **15** to **17**, through transition structures **TS2** to **TS4**.

These pentacoordinated intermediates can give subsequently access to racemization or transesterification products by eliminating the second methoxy substituent borne by the phosphorous center through a mechanism symmetric to the addition mechanism. In case of a transesterification reaction, the configuration at phosphorous center is expected to be inverted, except if TBP intermediates can undergo pseudorotations, which would possibly lead to a complete loss of stereoselectivity. This process is detailed within the section 4.3.

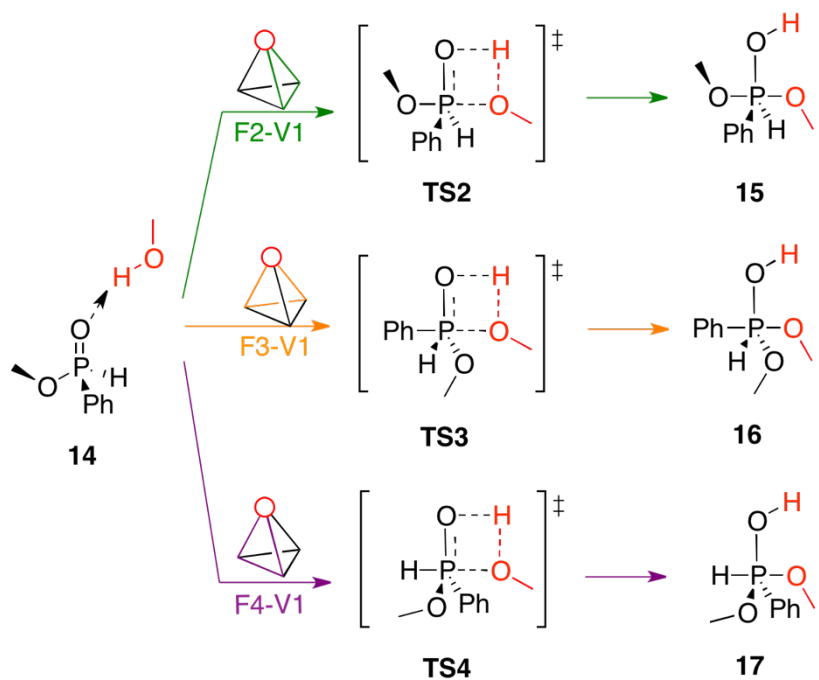


Figure 4-9: First activated steps of the mechanisms V1. Associated complex **14** is here used as a common energetic reference for all investigated routes. Pyramids are schematic representation of phosphinates and where the alcohol approaches (colored triangles) and the vertex coordinated to the hydrogen (red circle).

4.2.2.2 Mechanisms V2

In V2 attacks, the alcohol exchange reaction on the phosphorous center occurs in a single step. The hydrogen atom of methanol is transferred to the methoxy substituent V2 borne by the phosphorous center through transition structures **TS5** to **TS7**.

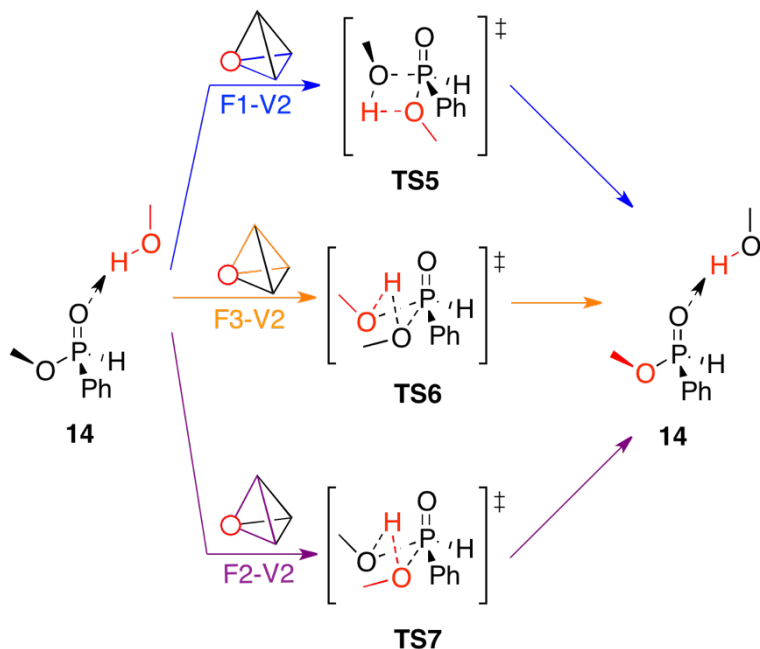


Figure 4-10: First activated steps of mechanisms V1. Structure **14** is here used as a common energetic reference for all investigated routes. Pyramids are schematic representations of phosphinate and the face where the alcohol approaches (colored triangles) and the vertex coordinated to the hydrogen (red circle).

This substituent is subsequently eliminated, while the methoxy part from methanol molecule is being added to the phosphorous center as shown in Figure 4-10. No racemization takes place through this mechanism. In case of an exchange of alcohol, the configuration of the phosphorous center here remains unchanged.

4.2.2.3 Discussion and conclusion

Gibbs free energies for all addition mechanisms have been calculated and can be found in Figure 4-11. We can see that V2 mechanisms are associated to much higher transition standard Gibbs free energies (F1-V2, **TS5**: 268 kJ.mol⁻¹; F3-V2, **TS6**: 205 kJ.mol⁻¹; F4-V2, **TS7**: 204 kJ.mol⁻¹) than V1 mechanisms (F2-V1, **TS2**: 113 kJ.mol⁻¹, F3-V1, **TS3**: 133 kJ.mol⁻¹ and F4-V1, **TS4**: 130 kJ.mol⁻¹). Additionally, within the V1 series, the F2-V1 (**TS2**) mechanism, in which the methanol is added on the opposite side of the methoxy substituent V2, exhibits a significantly lower transition standard Gibbs free energy (113 kJ.mol⁻¹) than both F3-V1 (**TS3**) and F4-V1 (**TS4**) mechanisms (133 kJ.mol⁻¹ and 130 kJ.mol⁻¹).

From a kinetic point of view, these differences are discriminating. Indeed, at room temperature, if we use the Eyring equation (section 2.5 p.33) to calculate the corresponding k_{F4-V1} and k_{F2-V1} , which are to both lowest transition structures, the difference between these is equal to $1.05 \cdot 10^{-3}$. Additionally, reaction intermediate **15**, which is reached through attack F2-V1 (**TS2**), is respectively 39 kJ.mol⁻¹ and 32 kJ.mol⁻¹ lower than intermediates **16** and **17** reached through

attacks F3-V1 (**TS3**) and F4-V1 (**TS4**). Consequently, attack F2-V1 (**TS2**, **15**) is simultaneously associated to the lowest transition structure and to the lowest reached reaction intermediate.

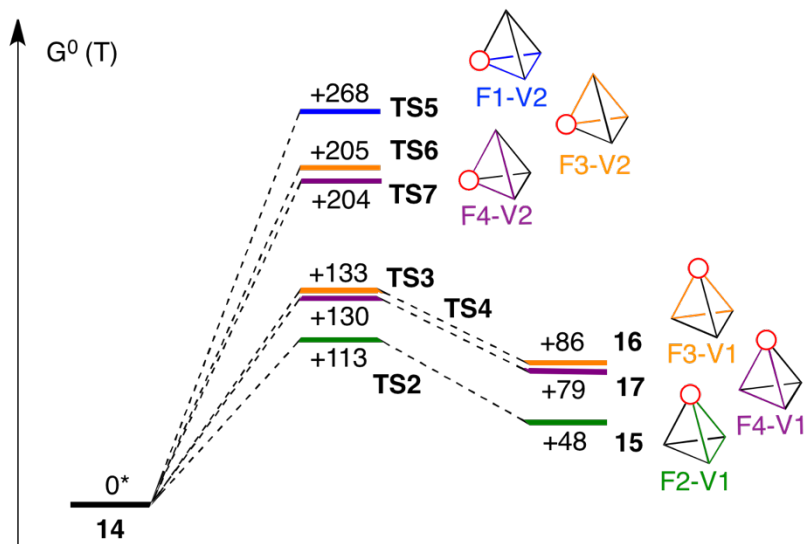


Figure 4-11: Reaction and their transition standard Gibbs free energies associated to mechanisms V1 and V2. Pyramids are schematic representations of phosphinate with the face where the alcohol approaches (colored triangles) and the vertex coordinated to the hydrogen (red circle). Numerical values are calculated at 25°C using DFT (SMD(THF)//M06-2X/6-31++G**) for solute standard states. Structure **14** is here used as an energetic reference.

From this comprehensive study, we conclude that the nucleophilic attack of methanol onto MeHP consists in a syn-addition of the hydroxy part of the methanol molecule onto the P=O double bond, on the opposite side, with respect to the phosphorous center, of the methoxy substituent (attack F2-V1, transition structure **TS2**, reaction intermediate **15**).

4.3 Influence of the pentacoordinated intermediate on the global mechanism

4.3.1 Further evolution on the pentacoordinated intermediate

Once intermediate **15** has been formed, it can evolve forwards and lead to the elimination of the methoxy group that was initially bound to the phosphorous center. A full picture of the addition-elimination mechanism is provided in Figure 4-12.

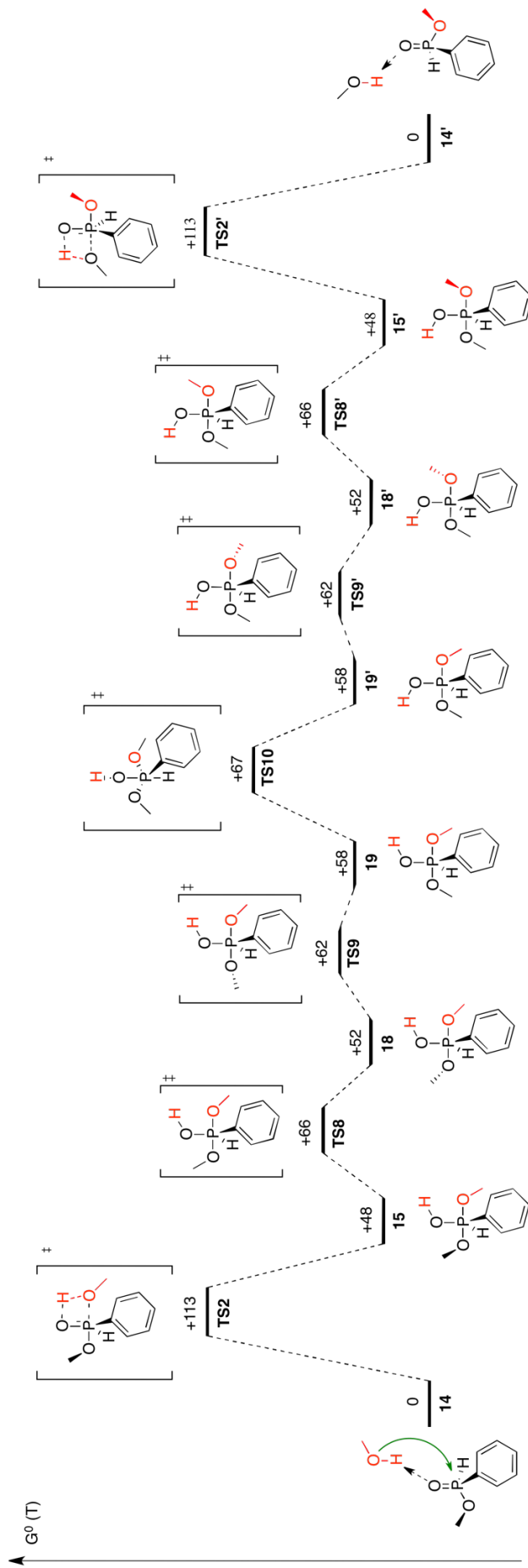


Figure 4-12: Nucleophilic attack of methanol onto MeHP: addition-elimination mechanism with the lowest energy profile. Standard Gibbs free energies are calculated at 25 °C using DFT (SMD(THF)//M06-2X/6-31++G***) for solute standard states. Structure **14** is here used as an energetic reference. Primes designate enantiomeric structure (SMD(THF)//M06-2X/6-31++G***) for solute standard states. The scale has not been respected for **TS10**, central point of this mechanism, to give more visibility to the symmetry of this transesterification.

This process first consists in small conformational changes based on the rotation of the methyl group from phosphinate (**TS8** and **TS9**). Then comes a rotation of the hydroxyl group (**TS10**). Its hydrogen atom, that was initially directed toward the incoming methoxy group, rotates toward the leaving one. The added methoxy group, that will remain attached to the phosphorous center, then rotates twice (**TS9'** and **TS8'**), and methanol is finally eliminated (**TS2'**). As a result, the mechanism is totally symmetric with the rotation of hydroxyl group **TS10** as central step.

For **TS10**, the hydrogen atom from the hydroxy group rotates over the hydrogen atom borne by the phosphorous center. In principle, it could also rotate over the phenyl group, but this route is strongly unfavorable as shown in the Figure 4-13. The corresponding transition structure **TS10b** is indeed 38 kJ.mol⁻¹ higher than **TS10**.

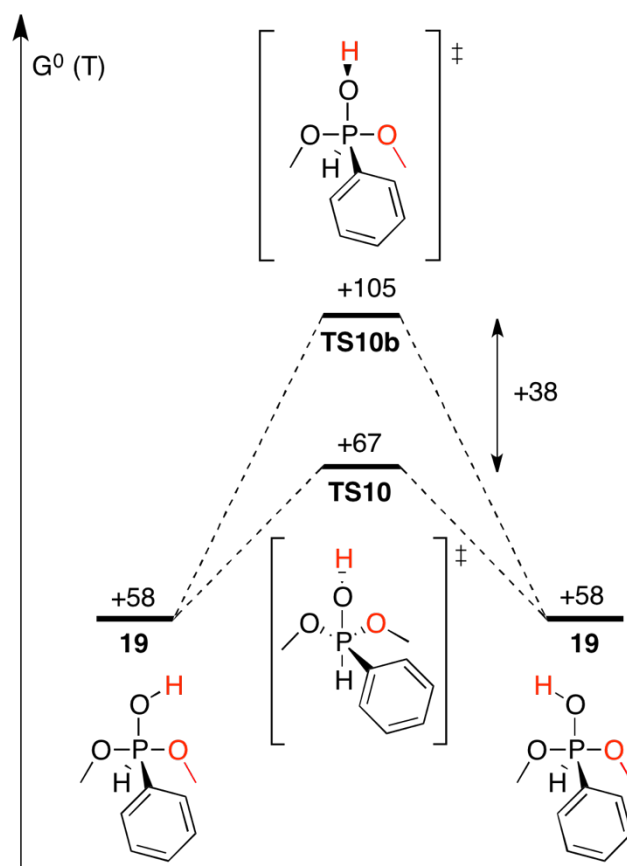


Figure 4-13: Comparison of energy profiles of the hydrogen rotation. **TS10** occurs on the side of the P-H bond, **TS10b** on the side of the phenyl group. Standard Gibbs free energies are calculated at 25°C.

The origin of this behavior can be found in the fact that the over-H region is less sterically hindered than the over-phenyl region, but also in the flexibility of the TBP. Indeed, both methoxy groups can accompany and stabilize the rotating hydrogen atom through H-bonds during its whole rotation over the H-side, as can be seen in Figure 4-14, where the angle OMe-

P-OMe goes from 180° to 120° while the angle HO-P-H goes from 120° to 180° , like a pseudorotation. However, this conformation only exists as a transition state. This mechanism is not possible over the phenyl-side due to the steric hindrance induced by the phenyl group which prevent this reorganization.

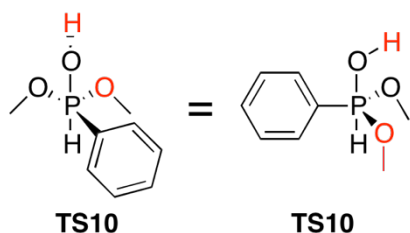


Figure 4-14: Representation of **TS10** from different perspectives.

Along the energy profile (Figure 4-12), all transition structures **TS8** to **TS8'** are much lower in energy than the transition structures **TS2** and **TS2'** ($113 \text{ kJ}\cdot\text{mol}^{-1}$), with a maximum of $67 \text{ kJ}\cdot\text{mol}^{-1}$. Statistically, this means that the whole conformational space ranging from intermediates **15** to **15'** becomes thermalized long before any backward or forward alcohol elimination takes place. In other words, kinetically, intermediates **15** to **15'** are permanently at the equilibrium and act as a single reaction intermediate, whereas transition structures **TS2** and **TS2'** are rate determining for the overall alcohol exchange reaction.

Finally, it can be observed in Figure 4-12 that this mechanism is fully symmetric with respect to **TS10**. This situation is of course due to the fact that both incoming and leaving alcohol molecules are here represented by methanol. In case of a transesterification where both involved alcohol molecules are different, energies on both side of **TS10** may consequently differ. We can even imagine that, in extreme cases, the incoming alcohol can be added, but reacts finally backwards because the departure of the leaving alcohol is kinetically hindered.

The backward elimination process preserves *a priori* the stereochemistry of the phosphorous center, whereas the alcohol exchange mechanism inverts *a priori* this stereochemistry. This result might however be very different if the penta-coordinated intermediate undergoes Berry pseudorotations previous to the backward or forward elimination. This possibility is investigated in details within the next section.

4.3.2 Berry pseudorotations of the pentacoordinated intermediate

As described in section 1.4, molecular structures containing TBP pentacoordinated phosphorous centers are known for their ability to undergo Berry pseudorotations, in which two equatorial ligands switch their positions with both apical ligands.⁵⁴ Technically, a

pentacoordinated structure where all five ligands are different can spread in 20 different manners around the phosphorous center and undergo 30 different pseudorotations. In the present case however, both alkoxy ligands are identical methoxy groups, which reduce the possibilities down to 10 different structures, among which 3 enantiomeric pairs and 15 pseudorotations (Figure 4-15).

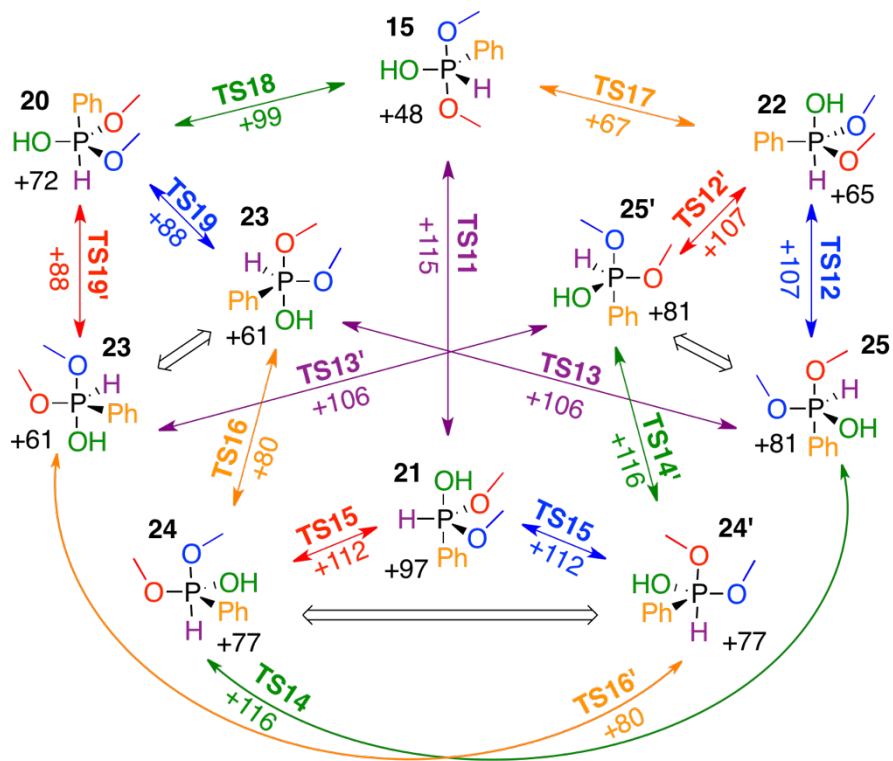


Figure 4-15: Left: Complete list of all 10 pentacoordinated intermediates **15** and **20** to **25** that can be transformed into each other through pseudorotations, and all 15 pseudorotations that bind them. Wide double arrows represent enantiomeric relationships. Primes are used for enantiomeric structures. The color of each arrow representing a pseudorotation is assorted to the color of the pivot ligand that remains in equatorial position during the pseudorotation. Energetic reference: structure **14**.

In Figure 4-15, every reaction intermediate corresponds to the less energetic structure obtained by IRC calculations performed from the surrounding transition structures. Within the previous section, we calculated the energies involved in methyl, phenyl and hydroxyl rotations (Figure 4-12), and we can see that they are small if compared to the energies involved in pseudorotations (Figure 4-15) and in methanol eliminations (Figure 4-12). Therefore, not taking them explicitly into account has no influence over the predicted global kinetic of the alcohol exchange reaction, and conformers that differ only by such rotations are consequently considered in Figure 4-15 as single species. For example, intermediate **24** is surrounded by transition structures **TS14**, **TS15** and **TS16**. IRC calculations lead, from these transition structures, to intermediates **24-**

IRC14, **24-IRC15** and **24-IRC16** that only differ by methyl, phenyl and/or hydroxyl rotations. Intermediate **24** simply designates the most stable of these conformers.

From the standard Gibbs free energies reported in Figure 4-15, it appears that not all ligands have the same affinity for apical positions. From the available numerical values (**15**, **23**, **24**, **25**), the following apicophilicity scale is established, OMe > OH > H > Ph. This result is in agreement with previous observations,^{90, 51} which we take as a confirmation of the validity of our modeling. Note that apicophilicities are numerically not additive, which is due to hydrogen bonds and other additional electronic effects.

The most interesting result that comes out of Figure 4-15 is that, from intermediate **15**, pseudorotations are actually competitive (highest calculated TS: 116 kJ.mol⁻¹) with the addition-elimination step (113 kJ.mol⁻¹). This means that the penta-coordinated intermediate obtained after an alcohol molecule has been added to an alkyl *hydrogeno*-phenylphosphinate molecule may racemize before any alcohol molecule is eliminated from this intermediate. The de Bruin diagram for AlkHP where both alkyl groups are different from each other is represented in Figure 4-16. We can see several possible racemization routes leading from **12**, which is equivalent to **15** if R₁=R₂=OMe, to **12'**, which is its enantiomeric version; for example **12'-34-25-14-23-15-34-12** (highest calculated TS: 116 kJ.mol⁻¹ between **25** and **14**).

It is of course expected that the exact nature of involved groups may significantly influence the actual transition standard Gibbs free energies of an inversion of configuration. Depending on these values, four scenarios can take place.

- First, the energy barrier associated to the formation of the pentacoordinated phosphorus is high enough to prevent it within the conditions of the experiment. In such a case, the alkyl *hydrogeno*-phenylphosphinate is chemically and stereochemically stable.
- Second, the energy barrier associated to the formation of the pentacoordinated phosphorus is low enough to make it possible within the conditions of the experiment. Then, the resulting penta-coordinated intermediate is either stereochemically stable or can invert through pseudorotations.
- Third, the energy barrier associated to the inversion without a pseudorotation is too high to make it possible and the only possible way to invert is through pseudorotation if the barrier is not too high either.
- Finally, the energy barrier is low enough to make the inversion possible without pseudorotation. The alkyl *hydrogeno*-phenylphosphinate is then chemically unstable,

i.e. its configuration has been changed and the phosphorous center has been inverted, or has possibly racemized through pseudorotations.

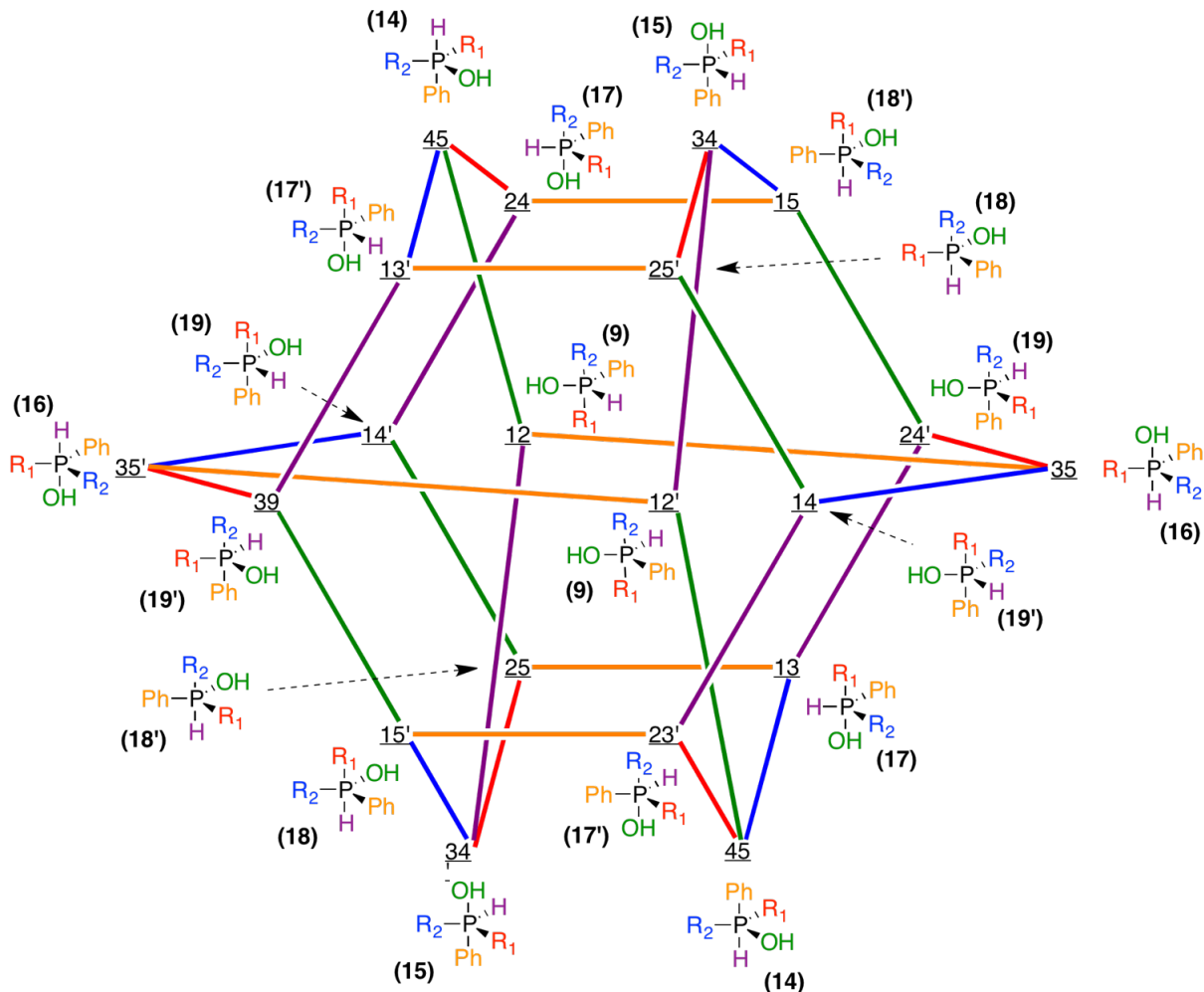


Figure 4-16: Complete list of all 20 pentacoordinated intermediates that can be transformed into each other through pseudorotations in case both alkoxy groups (R_1 and R_2) are different, and all 30 pseudorotations that bind them. The color of each line representing a pseudorotation is assorted to the color of the ligand that remains in equatorial position during the pseudorotation. The corresponding structures in case $R_1=R_2=OMe$ are provided between brackets

The four possible scenarios from the formation of the pentacoordinated intermediate are shown on the Figure 4-17: with and without pseudorotations (respectively bottom and top of the figure), with and without inversion (respectively left and right on the figure).

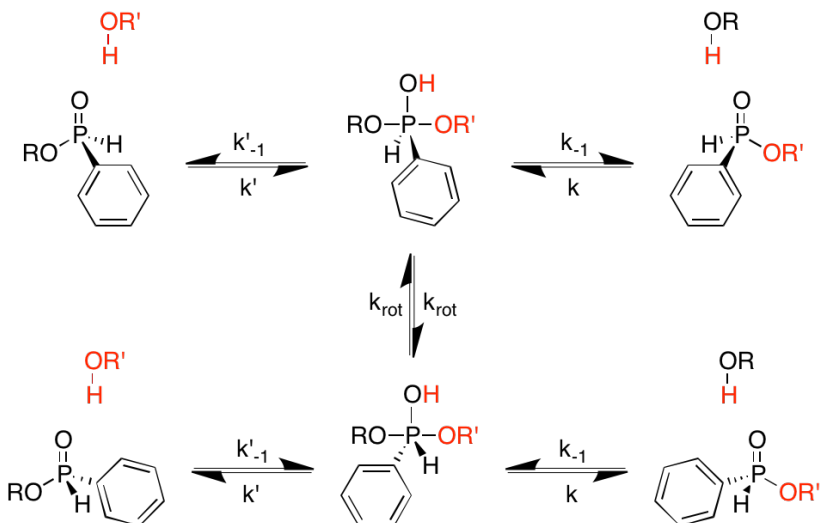


Figure 4-17: Schematic summary of all possible formal reactive routes within the framework of a nucleophilic attack of an alcohol molecule onto an alkyl *hydrogено*-phenylphosphinate molecule

4.4 Kinetic study

4.4.1 Experimental measurements

In order to validate the mechanism that we proposed within the previous sections, we have measured experimentally the racemization kinetic of EtHP **26** in presence of ethanol **27**. We really would have liked to measure the racemization kinetic of methyl *hydrogено*-phenylphosphinate in presence of methanol, but MeHP has unfortunately revealed to be chemically unstable and to denature faster than the time required for the racemization kinetic measurements to be performed. On account of this phenomenon, we have run the experiments, not with methanol, but with the smallest alcohol after it, i.e. ethanol.

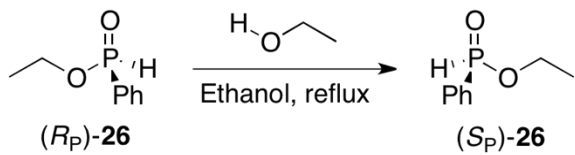


Figure 4-18: Racemization of EtHP **26** in ethanol under reflux

After several attempts, it became quite clear that the reaction of interest was really slow with respect to human time scales. We consequently progressively warmed up the reactive mixture and increased the concentration of ethanol to make measurements reliable. Practically, we finally used pure ethanol as solvent and measured the racemization kinetic at its boiling temperature ($78 \pm 1^\circ\text{C}$). Four experiments have been performed with these conditions, where the phosphinate concentration has been varied from $1.30 \cdot 10^{-4} \text{ mol.L}^{-1}$ to $1.31 \cdot 10^{-2} \text{ mol.L}^{-1}$. The

racemization kinetic has been followed using chiral HPLC (see experimental section), where the error on measurements written in the values have been calculated based on the precision of devices.

To do so, 30 mL of a solution of ethanol with enantio-enriched EtHP **26** of known concentration were refluxed. The decrease of enantiomeric excess is monitored over time for several days by chiral HPLC: 2 to 50 µL of the solution depending on the initial concentration are taken and then injected on Lux-Cellulose-2 (Heptane/ethanol 8/2, 1 mL/min, UV 254 nm). Raw experimental data are reported in Table 4-1 and Table 4-2.

Experiment	EtHP concentration (mol.L ⁻¹)	Initial enantiomeric excess (%)
1	(1.31 ± 0.04) 10 ⁻²	97,9 ± 1,0
2	(1.31 ± 0.04) 10 ⁻²	97,1 ± 1,0
3	(2.60 ± 0.07) 10 ⁻⁴	96,0 ± 1,0
4	(1.30 ± 0.04) 10 ⁻⁴	95,6 ± 1,0

Table 4-1. Synthetic description of racemization kinetic experiments. Solvent: ethanol. Temperature: 78 ± 1 °C (ethanol boiling point).

Data	Exp	Duration (min)	ee (%)
1	1	341,0 ± 1,0	96,0 ± 1,0
2	1	1331,0 ± 1,0	90,0 ± 1,0
3	1	1707,0 ± 1,0	87,7 ± 1,0
4	1	2777,0 ± 1,0	80,7 ± 1,0
5	1	2834,0 ± 1,0	80,4 ± 1,0
6	1	3234,0 ± 1,0	78,6 ± 1,0
7	1	4205,0 ± 1,0	74,0 ± 1,0
8	1	4612,0 ± 1,0	72,0 ± 1,0
9	1	5695,0 ± 1,0	66,4 ± 1,0
10	1	6118,0 ± 1,0	64,8 ± 1,0
11	1	7178,0 ± 1,0	60,9 ± 1,0
12	2	97,0 ± 1,0	96,5 ± 1,0
13	2	1151,0 ± 1,0	89,9 ± 1,0
14	2	1598,0 ± 1,0	87,0 ± 1,0
15	2	2587,0 ± 1,0	80,3 ± 1,0

Data	Exp.	Duration (min)	ee (%)
16	3	68,0 ± 1,0	95,8 ± 1,0
17	3	1086,0 ± 1,0	91,3 ± 1,0
18	3	1510,0 ± 1,0	89,7 ± 1,0
19	3	2491,0 ± 1,0	85,7 ± 1,0
20	3	2968,0 ± 1,0	83,2 ± 1,0
21	3	3901,0 ± 1,0	80,1 ± 1,0
22	4	404,0 ± 1,0	94,1 ± 1,0
23	4	1339,0 ± 1,0	90,3 ± 1,0
24	4	1807,0 ± 1,0	88,2 ± 1,0
25	4	2970,0 ± 1,0	83,7 ± 1,0
26	4	4299,0 ± 1,0	78,9 ± 1,0
27	4	6124,0 ± 1,0	73,3 ± 1,0
28	4	7269,0 ± 1,0	68,9 ± 1,0
29	4	9974,0 ± 1,0	61,2 ± 1,0

Table 4-2. Data points that have been collected during racemization kinetic measurements. “Exp” refers to experiments described in Table 4-1.

4.4.2 Observations

4.4.2.1 Monomolecular model

The observed first order kinetic corresponds to a monomolecular model where only phosphinate reacts by an inversion of configuration. By tracing the kinetic curve defined by Eq. 4-1 from the Eq. 2-24 previously developed in section 2.5.2 (p.35), we determine the apparent kinetic constant k_{app} from this model.

$$\frac{dee(t)}{dt} = -2 k_{app} ee(t)$$

$$-\frac{1}{2} \ln \left(\frac{ee(t)}{ee(0)} \right) = k_{app} t \quad \text{Eq. 4-1}$$

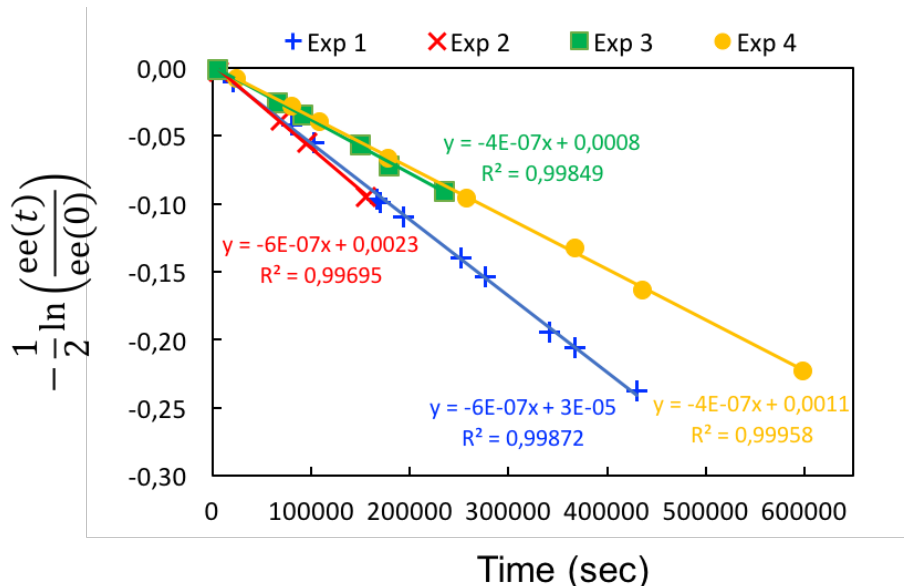


Figure 4-19: Evolution of the kinetic of reaction for EtHP diluted in ethanol under reflux (78 °C) with various concentrations: $1.31 \cdot 10^{-2}$ (experiment 1 in blue and experiment 2 in red), $2.6 \cdot 10^{-4}$ (experiment 3 in green), $1.3 \cdot 10^{-4}$ (experiment 4 in yellow).

From there, we extract the transition standard Gibbs free energy for monomolecular model using the Eyring equation. As a result, we obtain values presented in Table 4-3.

Experiment	EtHP concentration (mol.L ⁻¹)	Apparent transition standard Gibbs free energy (kJ.mol ⁻¹)
1	(1.31 ± 0.04) 10 ⁻²	126.6 ± 0.2
2	(1.31 ± 0.04) 10 ⁻²	126.7 ± 0.3
3	(2.60 ± 0.07) 10 ⁻⁴	127.7 ± 0.2
4	(1.30 ± 0.04) 10 ⁻⁴	127.8 ± 0.2

Table 4-3: Apparent transition Gibbs free energies of racemization kinetic of EtHP diluted in ethanol under reflux (78 °C) with various concentrations.

These values for $\Delta_r G_{app}^{0\ddagger}$ are valid in the approximation of the monomolecular model, which corresponds to the observed first order. However, as explained in section 4.2.2.2, the apparent first order visible in Figure 4-19 can also be coherent with other reactions, such as a bimolecular model. For this reason, we wanted to test the reliability of the bimolecular mechanism proposed during the DFT studies where ethanol and EtHP react together.

4.4.2.2 Bimolecular model

Here, we consider that ethanol reacts with phosphinate through a nucleophilic substitution as presented in the DFT study. In this transesterification mechanism, both incoming and leaving alcohols used experimentally are identical. Hence, the overall kinetic scheme, where the inversion of configuration can be related to transesterification or pseudorotations, simplifies into a single reactive pathway with, formally, a single reaction intermediate (**15**) and two symmetric transition structures (addition-elimination steps). On the basis of the DFT modelling, in which pentacoordinated intermediates are shown to be significantly higher in energy than the sum of reactants and products Gibbs free energies (**15** is 48 kJ.mol⁻¹ higher than **14** at 25°C), the quantity of the formally unique reaction intermediate is here assumed permanently negligible with respect to the quantities of the reactants and products.

It is then easily shown that the racemization kinetic obey the following law (Eq. 4-2), in which ee(t) represents the enantiomeric excess at time *t*, and *k*₀ the kinetic constant of bimolecular model associated to the reaction step that leads from separated ethanol and EtHP molecules to the reaction intermediate, as defined in Figure 4-17.

$$\frac{dee(t)}{dt} = -2k_0 \frac{[EtOH]}{c^0} ee(t) \quad \text{Eq. 4-2}$$

The racemization reaction produces exactly as much ethanol as it consumes. The concentration of ethanol consequently remains constant, and this last differential equation integrates as follows, where ee₀ represents the initial enantiomeric excess.

$$ee(t) = ee_0 \exp \left(-2k_0 \frac{[\text{EtOH}]}{c^0} t \right) \quad \text{Eq. 4-3}$$

Every single data point reported in Table 4-2 is consequently converted into a measure of k. To do so, the actual concentration of ethanol is required, which we here calculate from the density of ethanol at its boiling point ($16.06 \pm 0.02 \text{ mol.L}^{-1}$).⁸⁰ The resulting values of k, determined for each point of the experimental study, are reported in Figure 4-20. We obtained these overall values: 22.4 for experiment 1, 23.5 for experiment 2, 15.5 for experiment 3, and 14.7 for experiment 4.

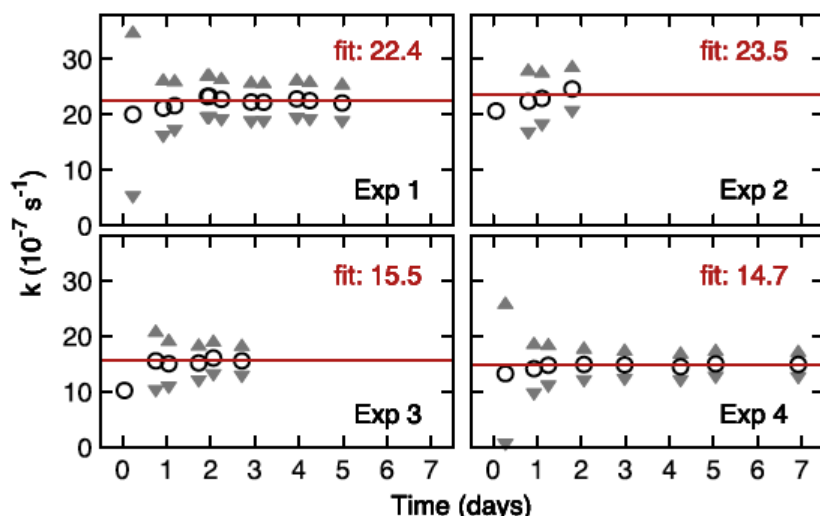


Figure 4-20: Values of k obtained from the experimental data listed in Table 4-2 (circles). Triangles represent the associated uncertainty ranges. Horizontal red lines are obtained by fitting k values with a constant. The uncertainties associated to the first data points of experiments 2 and 3 are larger than the vertical range used in the figure and the corresponding triangles are consequently not visible

Fitting is here achieved by minimizing the average quadratic deviation between measured and predicted values of k. The inverse of the square of the uncertainty is here used for weighting each fitted data. Finally, transition standard Gibbs free energies for bimolecular model $\Delta_r G_0^{0\ddagger}$ are extracted from the fitted k_0 values using Eyring equation. These energies are reported in Table 4-4.

$$\Delta_r G_0^{0\ddagger} = -\frac{1}{2} R T \ln \left(\frac{k_0 h}{k_B T} \right)$$

Experiment	EtHP concentration (mol.L ⁻¹)	Transition standard Gibbs free energy (kJ.mol ⁻¹)
1	(1.31 ± 0.04) 10 ⁻²	134.7 ± 0.2
2	(1.31 ± 0.04) 10 ⁻²	134.6 ± 0.3
3	(2.60 ± 0.07) 10 ⁻⁴	135.8 ± 0.2
4	(1.30 ± 0.04) 10 ⁻⁴	135.9 ± 0.2

Table 4-4. Transition standard Gibbs free energies extracted from the experiments described in Table 4-1 using the kinetic model deduced from the DFT modeling.

4.4.3 Discussion

First, we observe that measured Gibbs free energies determined for a bimolecular reaction 134.7 kJ.mol⁻¹ to 135.9 kJ.mol⁻¹, are very close to the DFT model 136 kJ.mol⁻¹. This good agreement shows that our DFT model is coherent with experimental results. Second, the obtained kinetic constant is actually different from an experiment to another, and depends on the phosphinate concentration. Indeed, multiplying this concentration by about 100 (from experiment 4 to experiment 1) increases k by about 50 % (from $1.5 \cdot 10^{-6} \text{ s}^{-1}$ to $2.2 \cdot 10^{-6} \text{ s}^{-1}$).

Figure 4-21 represents this dependency through the transition standard Gibbs free energies that are extracted from the fitted k values. It points out that this dependency is actually reproducible (experiments 1 and 2 on the right-hand side of the figure) and that it is a reality, i.e. not an experimental artefact, since it corresponds to an evolution of the transition standard Gibbs free energies that is significantly larger than the associated uncertainties (triangles in Figure 4-21).

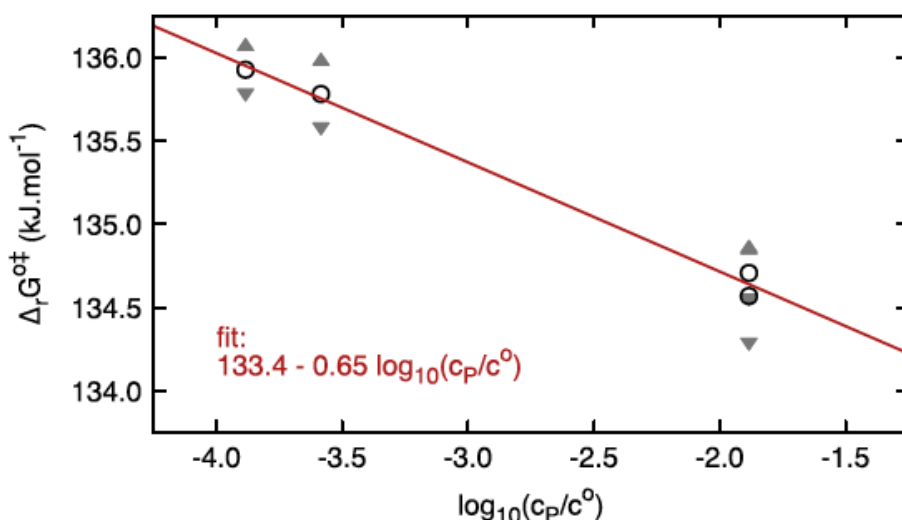


Figure 4-21: Dependency of the transition standard Gibbs free energies (Δ_rG^{\ddagger}) extracted from the fitted k values reported in Table 4-4 with respect to the phosphinate concentration (C_P)

This dependency is not expected if the mechanism consists only in the proposed bimolecular reaction, which suggests that this single reaction does not render the full picture of the actual reaction mechanism. This means that another mechanism happens simultaneously in solution, and that its participation to the global kinetic depends on the phosphinate concentration. Consequently, a reasonable hypothesis is the possibility for EtHP to dimerize in solution. A second phosphorous compounds could then act as a catalyst, which would make the addition of the ethanol easier and accelerate the racemization. This hypothesis is supported by the acidity scale Figure 3-7 presented in the section 3.4.2, in which MeHP is shown to be simultaneously more basic and acidic than methanol. If two reactions happen simultaneously, one monomeric and the other dimeric, it would explain the increasing kinetic constant with phosphinate concentration. Indeed, since the dimerization is easier with high concentrations, the participation of dimeric mechanism to the global kinetic becomes more important. Consequently, if this dimerization acts as a catalysis, the measured k_{app} increases with higher concentration.

More in the detail, such a catalysis may occur in different ways. A first EtHP molecule may, for example, activate the electrophilic character of the phosphorous center of a second EtHP molecule by building an H-bond with an oxygen atom that are directly bonded to the phosphorous center (=O or -OEt). It would be an acidic catalysis. In the second case, it may activate the nucleophilic character of ethanol by building an H-bond with the hydrogen atom of the alcoholic hydroxyl group. It would be a basic catalysis. These hypotheses are verified using kinetic modeling.

4.4.4 Kinetic adjustment

We previously showed that experimental measurements were in agreement with a bimolecular reaction. Here, we will consider two additional reactions in the model: the dimerization of phosphinate, and the nucleophilic substitution of a dimerized phosphinate by ethanol to proceed in the inversion. Each reaction is characterized by its own kinetic constant and transition Gibbs free energy that participates to the global $\Delta_r G_{mod}^{0\ddagger}$:

- bimolecular reaction R_0 between ethanol and phosphinate, with k_0 and $\Delta_r G_0^{0\ddagger}$
- the dimerization equilibrium $\Delta_r G_{DIM}^0$
- the addition reaction R_D of alcohol onto the dimer, k_D and $\Delta_r G_D^{0\ddagger}$. Note that, in the dimeric mechanism, only one EtHP is inverting while the other acts as a catalyst.

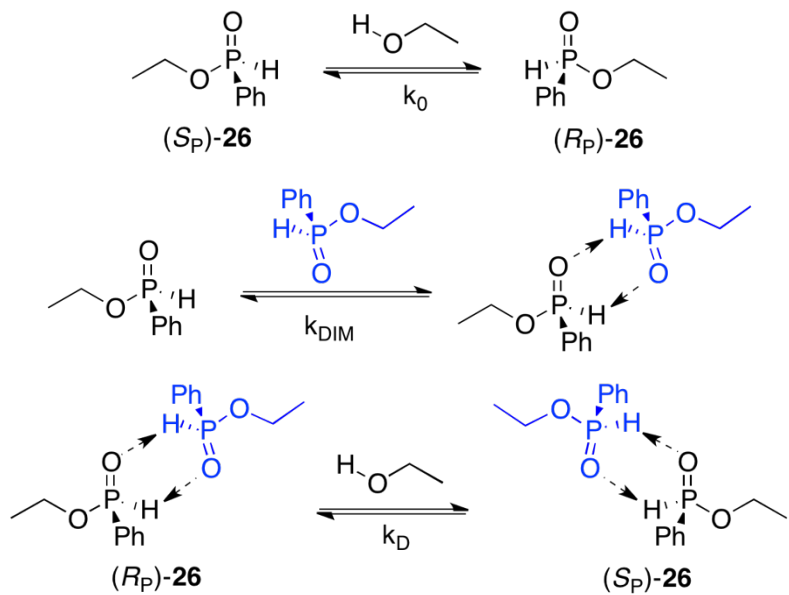


Figure 4-22: All mechanisms used in the kinetic modeling: direct addition on the monomer (top), dimeric association (middle), and addition after dimerization (bottom). The blue monomer in the dimer mechanism acts as catalyst and remains unchanged in the reaction.

All these reactions have been implemented in the kinetic model adjustment as presented in section 2.5.1.3 (p.34). According to the model, $\Delta_r G_0^{0\ddagger} = 135.9 \text{ kJ.mol}^{-1}$, and $\Delta_r G_D^{0\ddagger} = 120.6 \text{ kJ.mol}^{-1}$. The dimeric equilibrium does not go through a TS, but the difference of Gibbs free energy between the dimer and two monomers is -8 kJ.mol^{-1} in favor of the former. After an adjustment considering the three reactions, we obtain the following values for $\Delta_r G_{\text{mod}}^{0\ddagger}$ compared to experimental $\Delta_r G_{\text{app}}^{0\ddagger}$ in Table 4-5.

$C_p (\text{mol.L}^{-1})$	Measured $\Delta_r G_{\text{app}}^{0\ddagger} (\text{kJ.mol}^{-1})$	Predicted $\Delta_r G_{\text{mod}}^{0\ddagger} (\text{kJ.mol}^{-1})$
$1,31 \cdot 10^{-2}$	$126.6 \pm 2.0 \cdot 10^{-1}$	$126.57 \pm 2.50 \cdot 10^{-2}$
$1,31 \cdot 10^{-2}$	$126.7 \pm 3.0 \cdot 10^{-1}$	$126.57 \pm 2.50 \cdot 10^{-2}$
$2,60 \cdot 10^{-4}$	$127.7 \pm 2.0 \cdot 10^{-1}$	$127.74 \pm 2.26 \cdot 10^{-2}$
$1,30 \cdot 10^{-4}$	$127.8 \pm 2.0 \cdot 10^{-1}$	$127.76 \pm 2.30 \cdot 10^{-2}$

Table 4-5: Concentrations of phosphinate in solution and their corresponding measured $\Delta_r G_{\text{app}}^{0\ddagger}$. Predicted $\Delta_r G_{\text{mod}}^{0\ddagger}$ has been determined from kinetic modeling with consideration of both direct and dimeric addition.

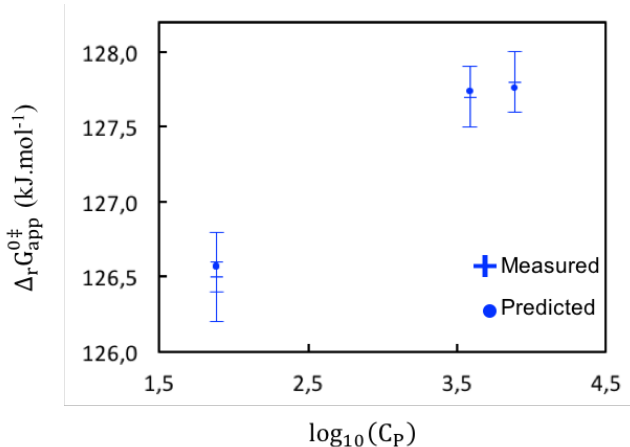


Figure 4-23: Comparison of measured and predicted $\Delta_r G_{app}^{0‡}$. Predicted values come from kinetic modeling with two reactions: direct addition and dimeric addition.

We can see that predicted values fit well with experiments. This good agreement suggests that both monomeric and dimeric mechanisms happen in solution. It is consistent with the dependency of the experimental $\Delta_r G_{app}^{0‡}$ with the concentration of phosphinate: the more EtHP in solution, the more dimer formed, the lower the $\Delta_r G_{app}^{0‡}$. As a result, we think that considering both reactions is a good model for our study. A DFT study would bring more information about this result, but the dimeric mechanism has not been modeled yet.

4.5 Reliability of simulations

The other aspect that now has to be investigated is the compatibility of the collected experimental data with the reaction mechanism that we proposed previously in this article. Considering the initial association of reactants **1** and **2** into intermediate **14** ($\Delta_r G^0(25^\circ\text{C})$: 8 kJ/mol⁻¹) and the energy barrier **TS2** between intermediates **14** and **15** ($\Delta_r G^{0‡}(25^\circ\text{C})$: 113 kJ/mol⁻¹), the overall transition standard Gibbs free energy expected from the DFT modelling is 121 kJ/mol⁻¹ at 25°C. This value changes a bit when the temperature is increased up to 78°C and reaches 128 kJ/mol⁻¹, with 13 kJ/mol⁻¹ that corresponds to the association of the reactants and 115 kJ/mol⁻¹ that corresponds to the energy barrier. This value is close to the 134-136 kJ/mol⁻¹ energy range that has been obtained experimentally, and we would like to conclude that our DFT model is in good agreement with the experimental data that we have collected. However, before we do so, we have to check the reliability of the DFT modeling.

This aspect is here investigated by changing both the functional and the implicit solvent model used for the key data of the DFT modelling (Figure 4-24). Our most significant results are modeled with the same basis set, but using the now classical B3LYP functional and the CPCM

implicit solvent model (THF solvent with default thresholds).^{91, 92} This second DFT modeling aims to test the methodology independency of the chemical conclusions that we draw at the end of this part.

Finally, a last question has to be addressed. Experiments have indeed been performed for ethyl groups, whereas modellings have been done for methyl groups. Additional modellings have consequently been performed for structures **1**, **2**, **14**, **TS2** and **15**, which are here kinetically determining, but in which methyl groups have been replaced by ethyl groups. The corresponding structures are named **26**, **27**, **28**, **TS20** and **29** and the associated numerical values are reported in Figure 4-24.

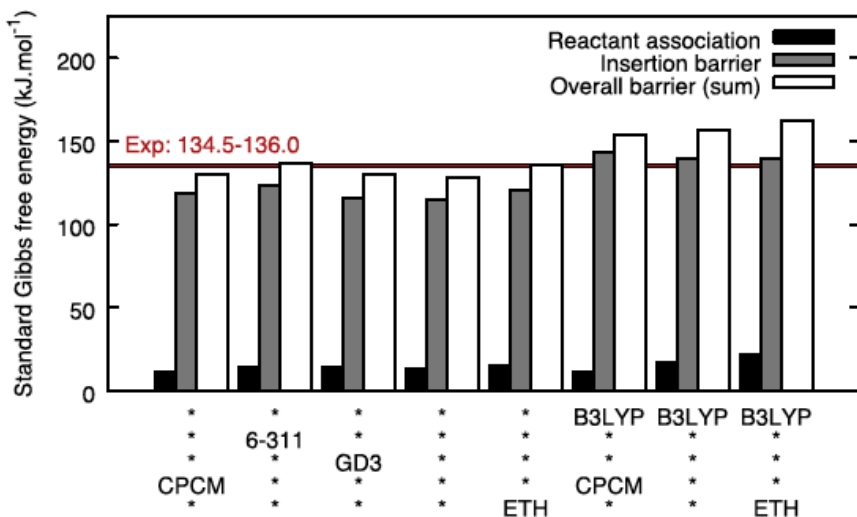


Figure 4-24: Partial and overall transition standard Gibbs free energies of the rate determining step of the proposed mechanism, but recalculated using functional B3LYP, implicit solvent model CPCM, and basis set 6-311++G(d,p) instead of M06-2X, SMD, and 6-31++G** (default values), or by adding GD3 as an empirical dispersion correction. * indicates that default values are used. ETH indicates that alkyl groups are ethyl groups.

Several important conclusions can be drawn from these results. First, changing the implicit solvent model or adding GD3 as an empirical dispersion correction has almost no effect on the predicted energies. Second, the association energy is very similar ($\pm 4 \text{ kJ.mol}^{-1}$) for all functional and solvent model combinations, which means that, on the contrary of what we had first frightened, this value seems reliable. Third, changing alkyl groups from methyl to ethyl increases slightly the calculated energy barriers ($+5\text{--}6 \text{ kJ.mol}^{-1}$), but this variation is small if compared to that resulting from a change of functional. Indeed, changing the functional from M06-2X to B3LYP increases the overall energy barrier by about $25\text{--}30 \text{ kJ.mol}^{-1}$. This difference may first look gigantic if compared with the precision of the values obtained experimentally, but it is actually a reasonable difference within the framework of energy barrier

predictions, and we can consequently conclude that barriers predicted from DFT are consistent. Since they additionally occupy an energy range that includes the values obtained experimentally, we can confidently assess that the mechanism we proposed from DFT calculations is compatible with the experiment.

4.6 Conclusion

In this chapter, we explored in a systematic way all reactive roots that may be taken when an alcohol molecule meets an alkyl *hydrogeno*-phenylphosphinate molecule. It has been found that the alcohol molecule acts as a nucleophile and attacks the phosphinate molecule directly on the phosphorous center with a *syn*-addition mechanism, along a direction which is exactly opposite to the alkoxy group borne by this atom (mechanism F2-V1).

This attack leads to a pentacoordinated intermediate that is significantly more energetic than the reactants and can consequently not be isolated. This intermediate may racemize through Berry pseudorotations, and evolve, either towards the elimination of the alcohol molecule that has just been added, or towards the elimination as an alcohol, of the alkoxy group that was initially borne by the phosphinate molecule.

According to DFT modelling, the highest transition standard Gibbs free energy of pseudorotation along the less energetic route that ends on the racemization of pentacoordinated intermediate is, with the same energetic reference, $124 \text{ kJ}\cdot\text{mol}^{-1}$ at 25°C , which is $3 \text{ kJ}\cdot\text{mol}^{-1}$ above the addition step. Pseudorotations of the pentacoordinated intermediate are consequently competitive with the elimination of an alcohol molecule.

The racemization kinetic of ethyl *hydrogeno*-phenylphosphinate in pure ethanol at 78°C has experimentally been monitored using chiral HPLC. The formal kinetic model predicted from DFT calculations has then been found to fit pretty well with these experimental data and experimental transition standard Gibbs free energies have been extracted with a good precision ($\pm 0.3 \text{ kJ}\cdot\text{mol}^{-1}$).

These energies unexpectedly exhibit a weak, but real, dependency to the phosphinate concentration, which is characterized by the following equation (unit: $\text{kJ}\cdot\text{mol}^{-1}$): $133.4 - 0.65 \log_{10}(C_p/c^0)$. This slight dependency has been interpreted as a possible acidobasicity catalytic action of a second phosphinate molecule in the alcohol exchange reaction. Using kinetic modeling, we have shown that using both monomer and dimer mechanism of addition shows an excellent agreement with experimental studies. Since this is consistent with the decreasing of $\Delta_r G_{\text{app}}^{0\ddagger}$ when C_p increases which implies more formation of dimer, we conclude that our

model of mechanism for the monomer is still the major one, but another mechanism happens onto phosphinate dimer. In the future, a DFT modeling of this dimeric mechanism would bring more information about its effect in solution.

As a conclusion, experimental and predicted transition standard Gibbs free energies have been proven to be compatible with the transesterification mechanism F2-V1. This makes us rather confident in the fact that the proposed mechanism is realistic. More studies will be done in the future to determine the participation of dimers that seem to take a part in the inversion of configuration according to kinetic modeling.

Chapter 5:

Effect of basic catalysis on the transesterification mechanism of alkyl hydrogeno-phenylphosphinates by alcohol

RESUME EN FRANÇAIS

Précédemment, nous avons vu que le mécanisme majoritaire de racémisation du phosphinate d'alkyle dilué dans l'alcool était une transestérification dû à une *syn*-addition de l'alcool sur la double liaison P=O. Le modèle cinétique a montré que la dimérisation du phosphinate en solution agissait comme un catalyseur. Nous avons donc décidé de nous intéresser à ce phénomène, plus précisément à la catalyse basique.

Dans ce chapitre, nous avons étudié expérimentalement l'impact de la présence d'un catalyseur basique, la triéthylamine TEA, sur le $\Delta_r G_{app}^{0\ddagger}$ d'énantiomérisation du phosphinate d'éthyle dans l'éthanol. Pour cela, nous avons mesuré la cinétique de racémisation du EtHP lors de 20 expériences, chacune caractérisée par une concentration de phosphinate C_p et de base C_b qui lui était propre.

Nous avons remarqué que les barrières d'énantiomérisation étaient significativement plus basses en présence de base qu'en milieu neutre, la valeur la plus élevée en milieu basique étant de 121,5 kJ.mol⁻¹ contre environ 135 kJ.mol⁻¹ dans le cas neutre. De plus, la barrière d'enthalpie libre était également de plus en plus basse avec l'augmentation du ratio C_b/C_p . Ces deux résultats montrent l'effet de catalyse basique de la TEA sur la racémisation du phosphinate d'éthyle dans l'éthanol.

Nous avons également noté que l'évolution de $\Delta_r G_{app}^{0\ddagger}$ en fonction du ratio C_B/C_P était différente selon si on faisait varier ce ratio en ajoutant du phosphinate ou de la TEA. Ce comportement montre qu'en plus de dépendre du rapport base / phosphinate, la vitesse de réaction dépend de la quantité propre de chaque réactif. Il semble donc que la molécularité de la réaction, la participation de chaque réactif à la cinétique globale, soit plus complexe qu'un simple mécanisme de transestérification entre les deux composés.

Pour tenter d'expliquer ce phénomène, nous avons eu recours à l'ajustement de modèle cinétique. À ce jour, 7 réactions ont été testée : addition directe R_0 , activation par la TEA de l'éthanol R_{EA} , du phosphinate R_{PA} ou des deux réactifs simultanément R_{EPA} , déprotonation du phosphinate R_{PD} , et activation par une molécule inconnue X de l'éthanol R_{EAX} ou du phosphinate R_{PAX} . A l'issue de ces comparaisons, un bon accord a été trouvé uniquement pour les réactions R_{EA} et R_{EAX} pour $C_B/C_P > 1$. R_{EPA} montre un comportement proche des données expérimentales notamment pour $C_B/C_P < 1$, mais ne fitte pas avec les valeurs expérimentales. Ces correspondances partielles font de ces modèles des pistes intéressantes pour les études à venir, mais ils ne suffisent pas pour décrire le comportement de la cinétique à eux seuls.

Les calculs DFT montrent que les enthalpies libres de transition pour l'addition du méthanol sur le phosphinate de méthyle sont plus basses en présence de triméthylamine que celles du mécanisme neutre. On obtient ainsi : 56 kJ.mol⁻¹ pour R_{EA} et 88 kJ.mol⁻¹ pour R_{PD} , contre 113 kJ.mol⁻¹ pour F2-V1 en conditions neutres. L'intermédiaire AC pour l'addition R_{EPA} n'a pas pu être optimisé, mais on a obtenu $\Delta_r G_{app}^{0\ddagger} = 99$ kJ.mol⁻¹ en se référant aux réactifs isolés, soit 22 kJ.mol⁻¹ en-dessous du mécanisme neutre en référence équivalente. Le mécanisme R_{PA} n'a pas pu être modélisé malgré de nombreuses tentatives car la TMA ne restait pas coordinée au phosphinate lors de l'approche de l'alcool.

La baisse des enthalpies libres de transition montre également qu'il existe un effet de catalyse basique sur l'addition. On observe également une bonne cohérence entre les modèles cinétiques et les calculs DFT : l'échec du calcul R_{PA} pour garder la base coordiné sur le phosphinate peut expliquer la mauvaise description de son modèle cinétique, et il le fait que l'addition la moins énergétique soit calculée pour R_{EA} montre qu'il s'agit probablement de la coordination la plus favorable, ce qui expliquerait la bonne description du modèle cinétique en cas d'excès d'alcool.

Lors des calculs du mécanisme R_{PD} , nous avons également modélisé la rotation de l'hydroxyl, étape centrale du mécanisme de transestérification. Nous avons alors obtenu une

enthalpie libre de transition de $111 \text{ kJ}\cdot\text{mol}^{-1}$, soit $23 \text{ kJ}\cdot\text{mol}^{-1}$ plus élevée que la barrière d'addition qui était de $89 \text{ kJ}\cdot\text{mol}^{-1}$. Ce résultat implique que, dans le cas d'un mécanisme de transestérification, l'étape la plus élevée en énergie pour R_{PD} , donc cinétiquement déterminante, n'est plus l'addition de l'alcool. Il est possible que ce soit également le cas pour d'autres types d'additions, ce qui montre l'importance de modéliser l'entièreté du mécanisme lors de catalyse basique.

Dans la continuité de l'étude, il nous est possible de considérer d'autres mécanismes dans le modèle cinétique, voire de faire comme lors du mécanisme neutre où plusieurs réactions étaient considérées afin de déterminer la participation de chacune d'entre elle. Ces modèles cinétiques seront accompagnés de calculs DFT dans lesquels il faudra modéliser les mécanismes de transestérification au complet afin de s'assurer de connaître l'étape cinétiquement déterminante en milieu basique.

5 Effect of basic catalysis on the transesterification mechanism on alkyl *hydrogeno*-phenylphosphinates

5.1 Introduction

5.1.1 Context

In the previous chapter, we explored, both theoretically and experimentally, the general reactivity of alkyl *hydrogeno*-phenylphosphinates with alcohols. We showed that alcohols act as nucleophiles, and attack phosphinate molecules directly on their phosphorous center with a *syn*-addition mechanism, along a direction which is exactly opposite to the alkoxy group borne by this atom. Such an attack leads to a pentacoordinated intermediate that may racemize through Berry pseudorotations, and/or evolve toward the elimination of the alcohol molecule that has just been added, or toward the elimination of the alkoxy group that was initially borne by the phosphinate molecule (Figure 5-1).

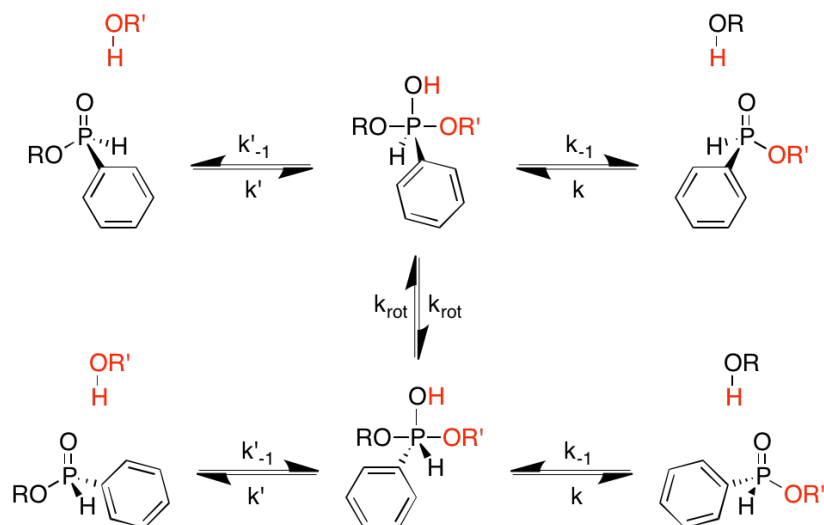


Figure 5-1: Schematic summary of the possible reactive routes within the framework of a nucleophilic attack of an alcohol on an alkyl *hydrogeno*-phenylphosphinate

As we were preparing the experimental part for this particular study, we encountered unexpected difficulties in reproducing the kinetic measurements that we were performing. We finally realized that this lack of reproducibility was simply due to inadequacies of the preparative treatment performed on the glass vessel before its use. Indeed, traces of the basic conditioning treatment that was performed on the glass vessel before delivery were actually

remaining subsequently to the preparative treatment that we were applying, and these traces were actually catalyzing the reaction.

This phenomenon was, in our case, unexpected and unwanted, but it was not surprising since phosphinate species are known to epimerize more easily in the presence of bases,^{93, 35, 37} and it corresponds to what we observed previously with the influence of dimerization. As a consequence, in this chapter, we explore both theoretically and experimentally this catalytic phenomenon.

First, the reactivity of AlkHP with alcohols is experimentally investigated within a controlled basic environment. Second, several scenarios are proposed that account for these experimental observations. Finally, the realistic characters of the most relevant scenarios are investigated using density function theory models.

5.1.2 Methodology

The system we study in the experimental section is EtHP **26** reacting with EtOH **27** as a solvent, with triethylamine (TEA) **30** used as a base for its basic but not nucleophilic properties. Since ethanol is used as solvent, it is in sufficient quantity to consider its concentration as constant over the reaction. We can then use the formula described in the part 2.5.1.2 (p.33). We will also use the kinetic model adjustment explained in the section 2.5.1.3 (p.34) to determine the active mechanisms from the experimental data.

Then, experimental results will be compared to the theoretical study on MeHP **1** reacting with methanol **2** following the mechanism F2-V1 previously determined in section 4.3.1, but with the addition of trimethylamine (TMA) **31**. To do so, we use the same level of theory as previously, SMD(THF)//M06-2X/6-31++G**, in the software Gaussian09, which reliability has previously been tested in section 4.5 (p.84).

5.2 Experimental study: kinetic of enantiomerization

5.2.1 Observations

The experimental study was made by M. Jean with the collaboration of Dr. N. Vanthuyne. It consisted in monitoring the racemization kinetic of EtHP in presence of ethanol within a controlled basic reactive environment (Figure 5-2). To do so, we used the same methodology as in section 4.4 (p.76) by diluting enantiopure ethyl phenylphosphinate in ethanol, but with the addition of trimethylamine (TEA) as a basic agent. The choice of TEA has been made on several arguments: (1) it is more basic than nucleophilic, (2) it is not an alcohol, (3) is it not a possible byproduct of the reaction, (4) it is an electrically neutral molecule.

In the previous study, which was in ethanol without base, the half-life time is about one week at 78°C, so about 70 years at 25°C. As the enantiomerization appeared to be much faster with triethylamine, we had to work at 25°C to observe a half-life time of several hours. Solutions M_n containing EtHP **26**, TEA and ethanol was placed in a vial and thermostated at 25°C in the autosampler of the HPLC system (Agilent G1329B with Peltier system).

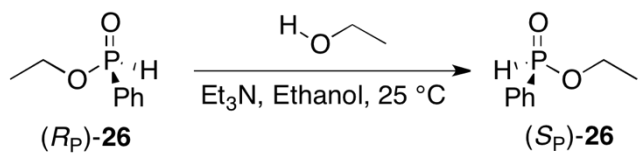


Figure 5-2: Racemization of EtHP **26** in ethanol with TEA

Since we hereby wanted to understand the effect of basic catalysis and its mechanism, we need to determine the participation of each product in solution to the global reaction. To do so, we did two parallel studies: one with a variation of the phosphinate's concentration, the other with a variation base's concentration. This methodology should allow us to know the molecularity of the reaction, and so the participation of one or more molecule to the global mechanism.

We here ran a first set of ten experiments in which we varied the phosphinate concentration (C_p) from $5.06 \cdot 10^{-5} \text{ mol.L}^{-1}$ to $9.88 \cdot 10^{-5} \text{ mol.L}^{-1}$, but kept the concentration of TEA constant $C_B = 3.36 \cdot 10^{-3} \text{ mol.L}^{-1}$. A second set has been made, also with ten samples, but keeping C_p constant ($3.16 \cdot 10^{-3}$) and varying C_B from $1.07 \cdot 10^{-1} \text{ mol.L}^{-1}$ to $2.10 \cdot 10^{-4} \text{ mol.L}^{-1}$. The concentration of ethanol $C_E = 1.71 \cdot 10^{+1} \pm 1.87 \cdot 10^{-1}$ was kept constant in all solutions. More details about the procedure are provided in annex 1.2.2.2 (p.144). Their apparent kinetic constants and transition Gibbs free energies are given in Table 5-1, and the evolution of $\Delta_r G_{\text{app}}^{0\ddagger}$ depending on $\log_{10}(C_B/C_p)$ is represented in Figure 5-3 for both sets.

Solution	$C_p (10^{-3} \text{ mol.L}^{-1})$	$C_B (10^{-3} \text{ mol.L}^{-1})$	C_B/C_p	$k_{\text{app}} (10^{-6} \text{ s}^{-1})$	$\Delta_r G_{\text{app}}^{0\ddagger} (\text{kJ.mol}^{-1})$
M ₁	50.60 ± 0.62	3.36 ± 0.12	0.07	$1.2 \cdot 10^{-2} \pm 0.001$	118.2 ± 0.4
M ₂	25.30 ± 0.36	3.36 ± 0.12	0.13	$3.9 \cdot 10^{-2} \pm 0.002$	115.3 ± 0.2
M ₃	12.65 ± 0.20	3.36 ± 0.12	0.27	$7.2 \cdot 10^{-2} \pm 0.003$	113.8 ± 0.2
M ₄	6.32 ± 0.11	3.36 ± 0.12	0.53	$6.0 \cdot 10^{-1} \pm 0.004$	108.5 ± 0.2
M ₅	3.16 ± 0.06	3.36 ± 0.12	1.06	1.2 ± 0.01	106.7 ± 0.2
M ₆	1.58 ± 0.03	3.36 ± 0.12	2.12	2.6 ± 0.02	104.9 ± 0.2

M ₇	$(7.91 \pm 0.17) 10^{-1}$	3.36 ± 0.12	4.24	5.0 ± 0.03	103.3 ± 0.2
M ₈	$(3.95 \pm 0.09) 10^{-1}$	3.36 ± 0.12	8.49	7.9 ± 0.04	102.1 ± 0.2
M ₉	$(1.98 \pm 0.05) 10^{-1}$	3.36 ± 0.12	16.98	13.0 ± 0.04	100.9 ± 0.2
M ₁₀	$(9.88 \pm 0.24) 10^{-2}$	3.36 ± 0.12	33.96	19.1 ± 0.2	100.0 ± 0.2
M ₁₁	3.16 ± 0.06	107.39 ± 3.39	33.96	35.8 ± 0.2	98.4 ± 0.2
M ₁₂	3.16 ± 0.06	53.70 ± 1.70	16.98	19.7 ± 0.1	99.9 ± 0.2
M ₁₃	3.16 ± 0.06	26.85 ± 0.87	8.49	10.7 ± 0.1	101.4 ± 0.2
M ₁₄	3.16 ± 0.06	13.42 ± 0.45	4.24	5.3 ± 0.03	103.1 ± 0.2
M ₁₅	3.16 ± 0.06	6.71 ± 0.23	2.12	2.6 ± 0.02	104.9 ± 0.2
M ₁₆	3.16 ± 0.06	3.36 ± 0.12	1.06	1.2 ± 0.01	106.7 ± 0.2
M ₁₇	3.16 ± 0.06	1.68 ± 0.06	0.53	$4.5 10^{-1} \pm 0.004$	109.2 ± 0.2
M ₁₈	3.16 ± 0.06	$(8.39 \pm 0.30) 10^{-1}$	0.27	$6.4 10^{-2} \pm 0.001$	114.1 ± 0.2
M ₁₉	3.16 ± 0.06	$(4.20 \pm 0.15) 10^{-1}$	0.13	$4.0 10^{-3} \pm 0.001$	120.9 ± 0.6
M ₂₀	3.16 ± 0.06	$(2.10 \pm 0.08) 10^{-1}$	0.07	$3.0 10^{-3} \pm 0.001$	121.5 ± 0.9

Table 5-1: Concentrations of phosphinate and TEA diluted in pure ethanol in solutions M_n used for the kinetic study of racemization and their resulting apparent kinetic constant k_{app} and transition Gibbs free energies Δ_rG_{app}^{0‡}

for T = 25 °C. Concentration of ethanol C_E = $1.71 10^{+1} \pm 1.87 10^{-1}$.

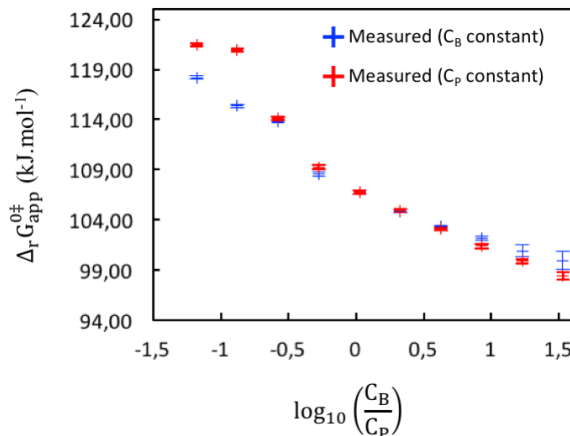


Figure 5-3: Evolution of the Δ_rG_{app}^{0‡} of enantiomerization of enantiopure EtHP in EtOH in presence of TEA depending on log₁₀(C_B/C_P). Two sets of experiments were done: varying C_P while C_B remained constant (blue), and the reverse case (red).

First of all, we can see in Table 5-1 that k_{app} increases with the C_B/C_P ratio. This phenomenon shows a catalytic influence of the basic compound. We also observe in Figure 5-3 that both

curves behave differently despite the same concentration ratios. Indeed, except for the central point at 1 equivalent of TEA ($\log_{10} = 0$), the $\Delta_r G_{app}^{0\ddagger}$ is different for every point. For low C_B/C_P , the kinetic of enantiomerization is faster for C_B constant than for C_P constant ($\Delta_r G_{app}^{0\ddagger} = 118.2 \text{ kJ.mol}^{-1}$ for C_B constant, $121.5 \text{ kJ.mol}^{-1}$ for C_P constant), while this is inverted for high C_B/C_P ($\Delta_r G_{app}^{0\ddagger} = 100.0 \text{ kJ.mol}^{-1}$ for C_B constant, 98.4 kJ.mol^{-1} for C_P constant).

In addition, we observe various rupture in the curves depending on C_B or C_P variation. With C_P constant, we can see a clear rupture in the curve between 0.13 and 0.27 equivalent of TEA ($\log_{10}(C_B/C_P) = -0.88$ and -0.58) which suggests that the reactivity changes. For C_B constant, this rupture appears later, between 0.27 and 0.53 equivalent of TEA ($\log_{10}(C_B/C_P) = -0.58$ and -0.28). After this point, $\Delta_r G_{app}^{0\ddagger}$ decreases faster for C_P constant than C_B .

As a conclusion, the kinetic of racemization depends not only on the C_B/C_P ratio, but also on which of those compounds is added. This suggests that several reactions happen in solution with various molecularity. The kinetic model adjustment, presented in section 2.5.1.3 (p.34) and already used in section 4.4.4 (p.82), should be useful to determine what type of reactivity is encountered in this study.

5.2.2 Kinetic modeling

Within the present section, we assume different scenarios that could explain the catalytic activity of TEA and we evaluate their legitimacy by fitting their parameters using the experimental data collected within the previous section. To this day, seven theoretical reactions have been tested:

- R_0 where ethanol is directly added onto phosphinate as presented in section 4
- R_{PA} where TEA activates EtHP by coordinating onto the H bound to the phosphorus atom
- R_{EA} where TEA activates ethanol by coordinating onto the H bound to the oxygen atom
- R_{PAX} where the activation of phosphinate is related to an unknown compound X brought by TEA, and which concentration is proportional to TEA
- R_{EAX} where the activation of ethanol is related to an unknown compound X brought by TEA, and which concentration is proportional to TEA
- R_{EPA} where both ethanol and EtHP are activated by TEA
- R_{PD} where EtHP has been deprotonated

Data used as input are C_P , C_E , C_B and T. The modeling process tries to use them to correctly reproduce the observed $\Delta_r G_{app}^{0\ddagger}$ values. The results of these models are presented in Figure 5-4.

As was done in section 4.4.4 (p. 82) with the dimeric model in neutral conditions, the $\Delta_r G_r^{0\ddagger}$ of these reactions and all equilibria they involve will be fitted to experimental measurements. From there, their respective k_r will be determined, and the participation of each k_r to the global k_{mod} , kinetic constant of the model, will be weighted, so the resulting $\Delta_r G_{mod}^{0\ddagger}$ gets as close as possible to the experimental $\Delta_r G_{app}^{0\ddagger}$. Then, the resulting curves of $\Delta_r G_{mod}^{0\ddagger}$ will be compared to experimental ones. If we find a complete good accordance with experimental curves, it means that our model is reliable. In the other cases, our model is not good to describe what happens in solution. However, if it partially fits to experiment, it could mean that it partially participates to the global model.

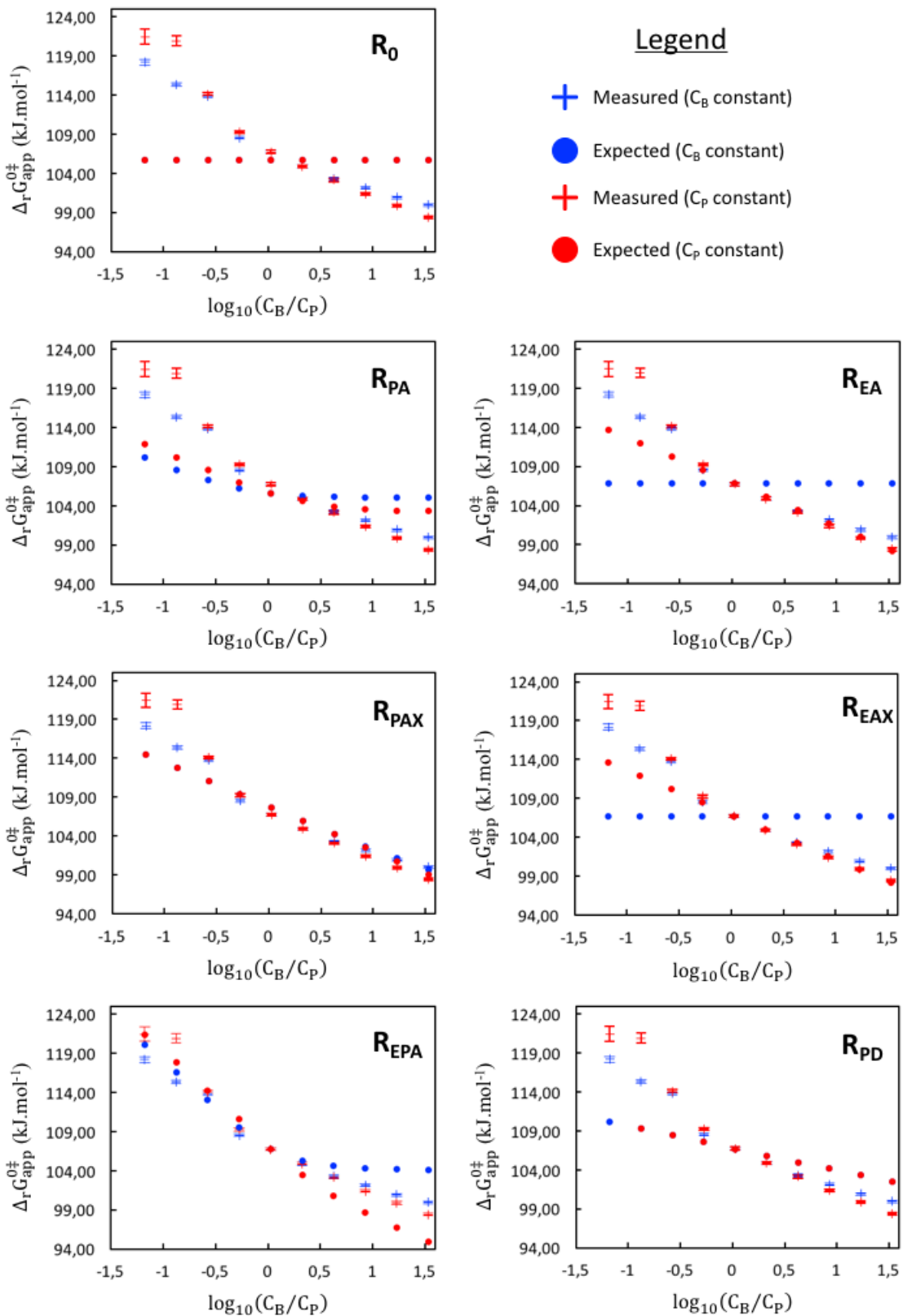


Figure 5-4: Transition Gibbs free energies for all kinetic models done to this day. From left to right, top to bottom: direct addition R_0 , activation of phosphinate by TEA R_{PA} , activation of ethanol by TEA R_{EA} , activation of phosphinate by X R_{PAX} , activation of ethanol by X R_{EAX} , activation of both phosphinate and ethanol R_{EPA} , after deprotonation of phosphinate by TEA R_{PD} .

We first observe that no mechanism alone fits well with experimental results. This means either that the right mechanism has not been found yet, or that several mechanisms happen simultaneously, so the actual mechanism has not been elucidated through the proposed scenarios.

We note that R_{EA} and R_{PAX} mechanism gives a good description of reactivity when $C_B/C_P > 1$ ($\log_{10} > 0$) respectively for C_P or C_B constant. This description is not different with R_{EAX} where we consider the activation of ethanol by X. The fact that this mechanism does not describe well the reactivity before 1 equivalent of TEA means that it is not a good overall model. But it suggests that, while increasing the ratio C_B/C_P , the basic compound would favor the coordination to solvent ethanol.

In the event of the participation of an impurity brought by TEA, the comparison of R_{EA} or R_{EAX} show similar behavior. However, the quantity of impurity would change from one TEA sample to another, which should appear as a different behavior in the variation of $\Delta_r G_{app}^{0\ddagger}$ depending on C_B .

The model R_{EPA} , where both reactants are activated, has a behavior close to experiment for both curves for $C_B/C_P < 1$, but does not fit with experimental data and diverges too much with high C_B/C_P ratios. We can conclude that, even if this model does not well describe the reactivity, the activation of both reactants could be interesting to develop in future study.

Since no proposed reactions fit well with the whole experimental results, either there is another mechanism which has not been tested yet, or we need to consider several simultaneous mechanisms in our model. In the meantime, we modeled some of the theoretical reactions at DFT level to check on the reliability of kinetic models and bring some new information.

5.3 Equilibrium of the system in basic conditions

Before we head to the theoretical study of $S_N2@P$, we need to determine the possible new equilibrium between compounds of interest in basic conditions. To do so, we used the same model as previously with MeHP and MeOH, and added TMA as a model for TEA.

5.3.1 Tautomerism and coordination of TMA

First, we studied the tautomeric equilibrium between **1** and **3** to check if the addition of base in the system could affect this equilibrium. We thus compared the Gibbs free energies of associated complexes **32** for MeHP, and **33** for the phosphinous acid as shown in Figure 5-5.

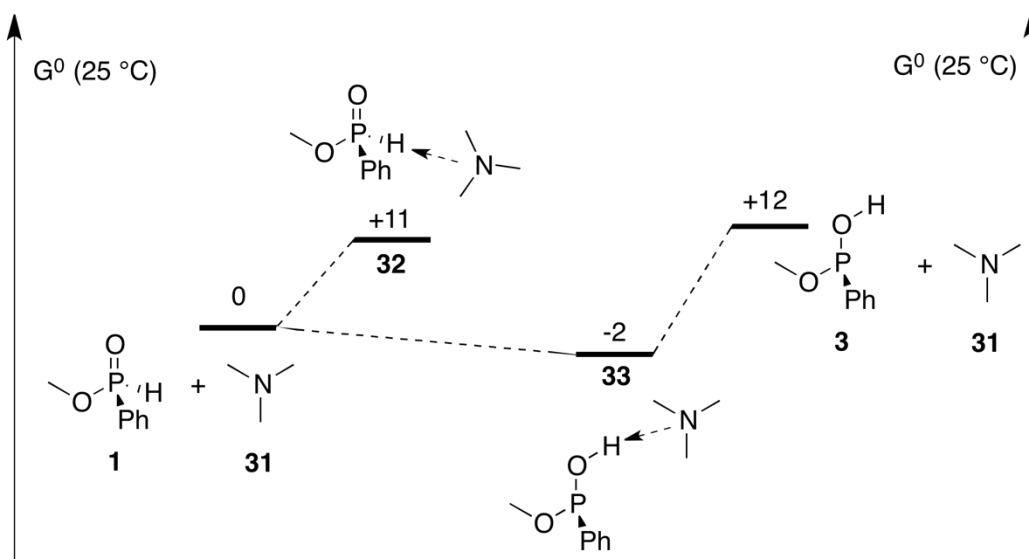


Figure 5-5: Relative Gibbs free energy of association for TMA **31** interacting with MeHP **1** giving the AC **32**, and its corresponding acidic form **3** giving the AC **33**. The energetic reference is the sum of isolated reactants **1** + **31** (left).

We can see that the equilibrium between **1** and **3** interacting with TMA is in favor of **33** by -14 kJ·mol⁻¹. Consequently, in the case of a prototropic exchange between **32** and **33**, the influence of TMA could make the P(III) form **33** more favored than the P(V) **32**, as opposite to equilibrium in neutral conditions where the P(V) form **1** is favored by -12 kJ·mol⁻¹ (section 3.3, p.43). Unfortunately, we have not been able to determine the mechanism nor the energy of transition for the tautomerism between **32** and **33**. We would have liked to know the probability of the mechanism to occur, but this should not be a problem since tautomerism does not act directly on enantiomerization. Nevertheless, the inversion of equilibrium means that both complexes can be found in solution depending on the concentration of reactants, and the P(III) form could act as a most stable form for our system. However, in our kinetic models, **33** appears as a **32** conformation. Consequently, its possible effect on the transition Gibbs free energy cannot be extracted from kinetic modeling.

5.3.2 Deprotonation of reactants

The presence of basic compound could, at some point, favors the deprotonation of a reactant. Using the previously built acidobasicity scale in Figure 3-7 (p.49), we see that the pKa of MeOH/MeO⁻ is estimated to 29.0, TEAH⁺/TEA 9.0, and MeHP/MeP⁻ 16.1. We thus conclude that the alcohol cannot be deprotonated by the basic compound, but the difference between TEA and MeHP is actually not as big. Thus, we investigated the mechanism of deprotonation of phosphinate **1** by trimethylamine **31** described in the Figure 5-6 and obtained a 56 kJ·mol⁻¹

Gibbs free energy of transition for **TS21** at 25 °C, resulting on the system **34** ($\Delta_r G^0 = 48 \text{ kJ.mol}^{-1}$).

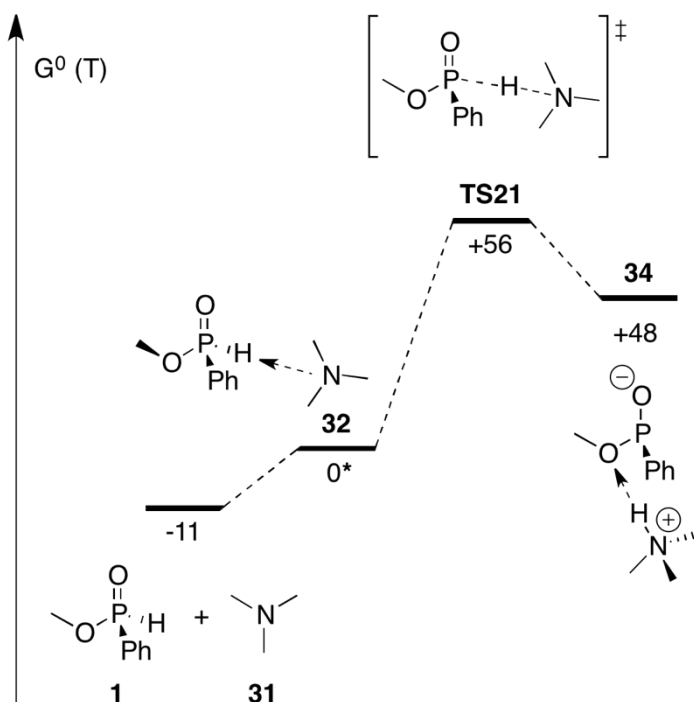


Figure 5-6: Deprotonation mechanism of MeHP **1** by TMA **31** at DFT level for T = 25 °C.

We must note that we are in the situation of a separation of charge, so the solvent simulation can give a bad description of this mechanism. In our case, however, both charges are in the same system and interact with each other, so our description should be reliable. The barrier of **TS21** seems low enough for the deprotonation to occur, but the resulting ionic system **34** is a lot higher than the neutral one so it could only be useful as a reaction intermediate, like an activation of phosphinate.

We also tried to model the deprotonation of phosphinous acid form **3**, but did not manage to do so despite all of our try. This should not be a problem because if such reaction would occur, then we obtain system similar to **34** where phosphonide and protonated TMA coexists. Thus, we will not consider this possibility in this study.

5.3.3 Conclusion

We here observed that the acidic form coordinated to TMA **33** is favored by 13 kJ.mol⁻¹ over the phosphinate **32**, and that the deprotonation of the phosphinate is possible with a 56 kJ.mol⁻¹ Gibbs free energy of transition, resulting on **34** ($\Delta_r G^0 = 48 \text{ kJ.mol}^{-1}$). We conclude that, in

order to cover all possibilities, both the acidic and deprotonated forms of phosphinate must be taken into account in the following study about the addition mechanism.

5.4 Addition mechanism in basic conditions

Based on kinetic modeling and theoretical investigations of equilibrium in basic conditions, we here present various possibilities for the addition mechanism of methanol onto phosphinate in basic conditions. The original mechanism is the F2-V1 previously reported in neutral conditions in section 4.2.2 (p.65).

We will start to study the possibility of addition for an alcohol onto phosphinous acid **3** which appeared to be more favored according to DFT model. Afterward, we investigate the reactivity of MeHP **1**.

5.4.1 Addition on phosphinous acid form

The addition mechanism involving the phosphinous acid **3** is interesting since it could involve a simultaneous departure of the alkoxy group as shown in Figure 5-7. This way, the substitution would happen in one step instead of involving the rotation of the OH bond.

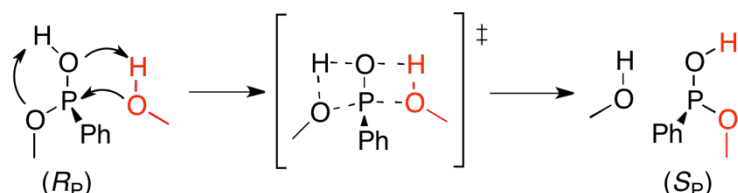


Figure 5-7: Addition-elimination mechanism of methanol **2** on phosphinous acid **3** in neutral conditions.

While this mechanism was unlikely to happen in neutral conditions because **3** was $12 \text{ kJ}\cdot\text{mol}^{-1}$ higher than **1**, we saw in the previous section that coordination of TMA changes the equilibrium in favor of the acid, which AC **33** is $14 \text{ kJ}\cdot\text{mol}^{-1}$ lower than **32**. There are three possibilities of coordination depending on the number of TMA involved (Figure 5-8):

- One TMA coordinated to the H of methanol (1)
- One TMA coordinated to the H of phosphinous acid (2)
- Two TMA, one on each hydrogen atom (3)

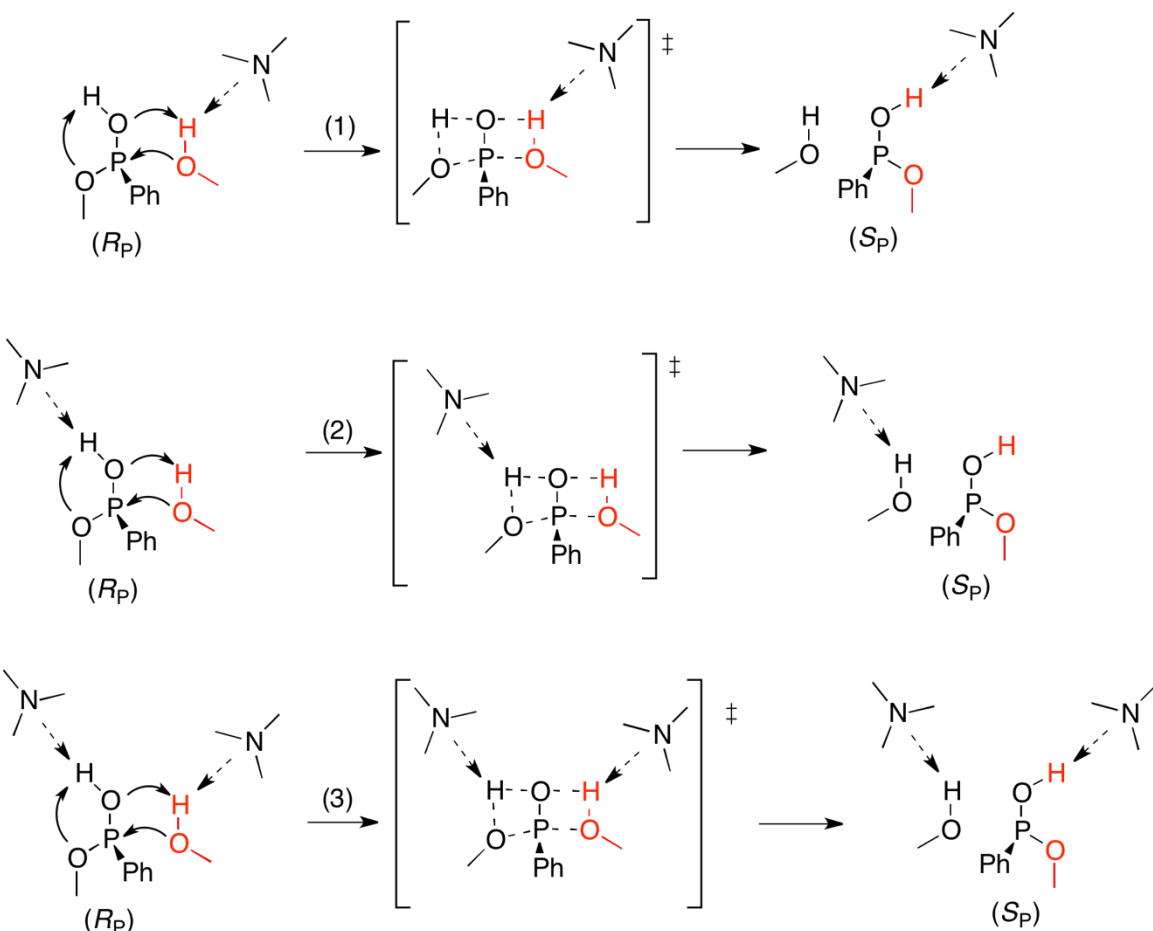


Figure 5-8: Addition-elimination mechanism of methanol **2** on the phosphinic acid **3** with the participation of TMA **31**, mechanisms could not be simulated

Despite all of our tries, we have not been unable to model these mechanisms. Optimizations of transition states systematically fail, and relaxed scans show no addition nor elimination in any case. It is too early to conclude that those mechanisms are impossible, but since we did not manage to model them we will consider that they do not occur.

5.4.2 With one equivalent of TMA

5.4.2.1 TMA coordinated to P-H: R_{PA}

The coordination of TMA on the phosphinate P–H bond, which corresponds to reaction R_{PA} , is considered as an activation of the phosphorus to facilitate the addition of the alcohol. Unfortunately, no approach of methanol on the AC resulted in the coordination of methanol to phosphinate.

We determined a 2.4 Å distance between the hydrogen borne by the phosphorus atom and the nitrogen for the AC **32**. This distance makes us think that the two compounds do not interact enough with each other to act on the reactivity. This is supported by relaxed scans where, when methanol gets closer to phosphinate, TMA does not stay coordinated to the hydrogen atom and

leaves the molecule as far as 2.9 Å. Because of this flexibility, we did not manage to get the addition mechanism on **32** yet. The fact that we did not manage to model the addition is consistent with the failure of kinetic model R_{PA} to fit with experimental measurements.

5.4.2.2 TMA coordinated to the alcohol

Another possibility for basic catalysis is the reaction R_{EA} , where the alcohol is activated by TMA coordinated to the hydroxyl hydrogen **35**. This mechanism has been simulated and results are shown in Figure 5-9.

We note that, when going from AC **35** to **TS22**, the distance H-N between the alcohol's hydrogen atom and the nitrogen goes from 1.7 Å to 1.1 Å, while the distance O-H of the hydroxyl group increases from 1.0 Å to 1.7 Å. In addition, while we were modeling the mechanism at 0 K, we obtained an additional step before the addition that consisted in an intermediate which geometry was close to **TS22**. Based on this, it seems that TMA activates the alcohol with a slight deprotonation before the addition happens. However, when reported at 25 °C, this step has a Gibbs free energy higher than the previous TS. As a consequence, the corresponding intermediate does not thermalize and spontaneously evolves forward or backward.

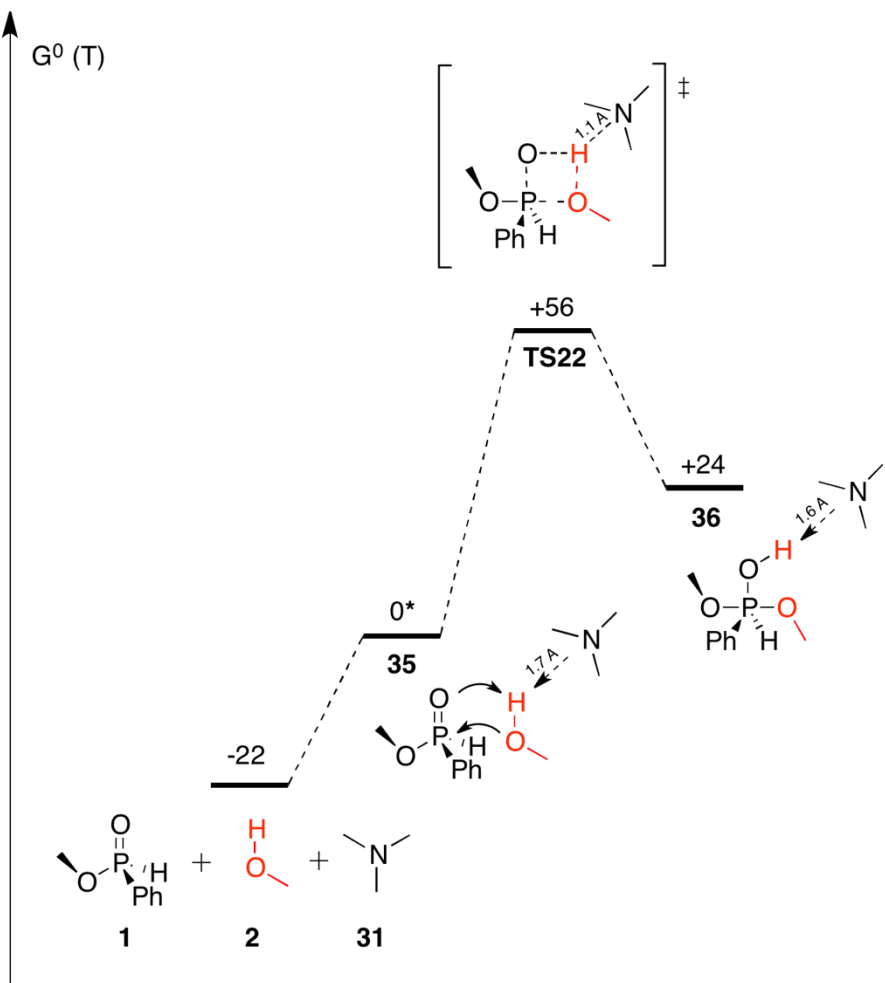


Figure 5-9: Addition mechanism of methanol **2** on phosphinate **1** with the methanol's hydrogen coordinated with TMA **31** at $T = 25\text{ }^{\circ}\text{C}$. The energetic reference for the G^0 values is the AC noted with *.

The DFT model shows a transition Gibbs free energy $\Delta_r G^{0\ddagger} = 56 \text{ kJ.mol}^{-1}$ for $T = 25\text{ }^{\circ}\text{C}$. This value is 57 kJ.mol^{-1} lower than in neutral condition ($\Delta_r G^{0\ddagger} = 113 \text{ kJ.mol}^{-1}$), which shows the catalytic participation of TMA to the addition mechanism.

As a conclusion, we can see that the participation of TMA induces a large diminution of the transition Gibbs free energy for the addition, from 113 kJ.mol^{-1} in neutral conditions to 56 kJ.mol^{-1} with TMA. This mechanism seems to go through a slight deprotonation of methanol which is simultaneous to the addition **TS22**. The catalytic effect is consistent with the kinetic model that showed a good agreement between R_{EA} and experimental measurement.

5.4.3 With 2 equivalents of TMA

Once the TMA catalyst is in excess, one molecule can be coordinated to each reactant. The resulting AC, where one TMA is borne by the P-H and the other by the alcohol, is presented as

37 in the Figure 5-10. Up until now, we did not manage to model the first AC intermediate due to the complex flexibility. Thus, we refer the Gibbs free energy of transition to the sum of reactants.

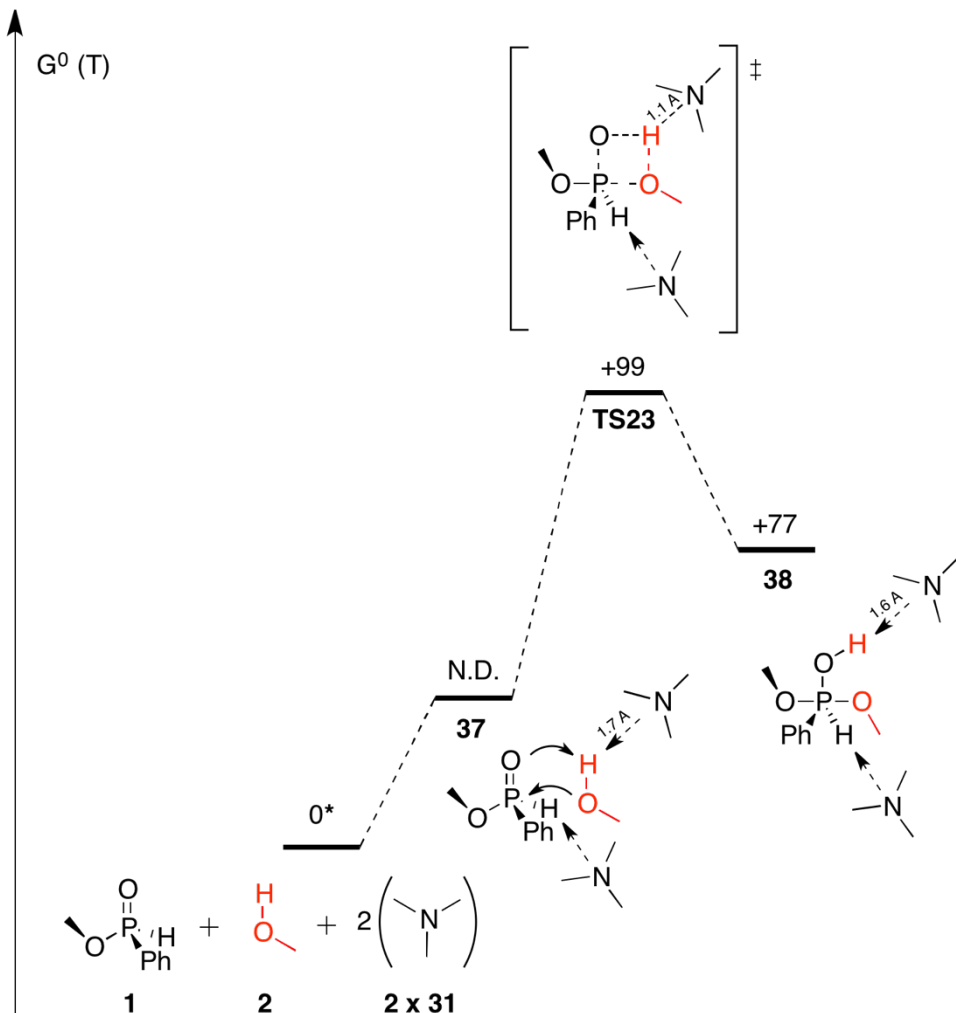


Figure 5-10: Addition mechanism of methanol **2** on phosphinate **1** with both methanol's and phosphinate's hydrogen coordinated with TMA **31** at $T = 25\text{ }^{\circ}\text{C}$. The energetic reference for the G^0 values is the sum of reactants noted with *. The Gibbs free energy of the AC **37** has not been determined.

We see that $\Delta_f G^{0\ddagger}$ for **TS23** is 99 kJ.mol^{-1} , which makes it 21 kJ.mol^{-1} higher than **TS22** from R_{EA} if referred to the sum of reactants ($22 + 56 = 78\text{ kJ.mol}^{-1}$). In the model, we determined the distance H-N between TMA and P-H to be 2.9 \AA for both **TS23** and **38**.

It is possible that, due to a long distance between MeHP **1** and TMA **31**, their coordination does not influence the addition as in the previous attempt with R_{PA} . The addition is mostly influenced by the activation of alcohol, while the coordination of MeHP **1** with TMA **31** just destabilizes the system. As a conclusion, theoretical model seems to show that it R_{EPA} is not more efficient

nor favored than R_{EA} , which is consistent with the kinetic model where R_{EPA} does not fit well experimental measurements despite a close behavior.

5.4.4 Deprotonated phosphinate

In case of a deprotonation of phosphorus atom giving phosphonide **6**, the addition of methanol would result on the formation of AC **8**. We can proceed to an addition with the same mechanism than in neutral conditions, but onto **6** instead of **1**. As a result, we obtain the mechanism showed in Figure 5-11. First, we observe that the complex **8** is lower in energy than isolated reactants by $-10 \text{ kJ}\cdot\text{mol}^{-1}$. Then, we can see that the addition of alcohol is $-23 \text{ kJ}\cdot\text{mol}^{-1}$ lower than the neutral conditions with a $\Delta_r G^{0\ddagger} = 88 \text{ kJ}\cdot\text{mol}^{-1}$ referred to **8**, but $+32 \text{ kJ}\cdot\text{mol}^{-1}$ higher than R_{EA} .

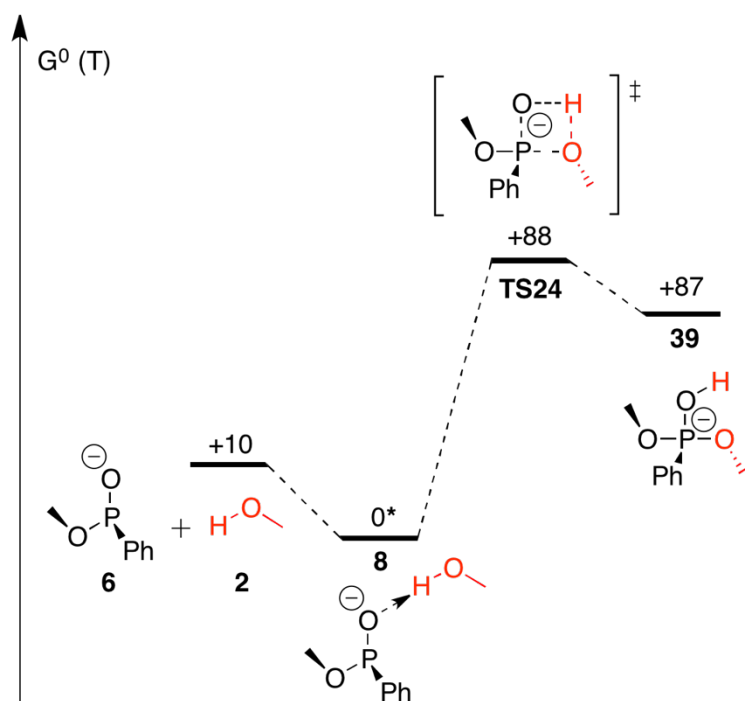


Figure 5-11: Addition mechanism of methanol **2** on the AC **8** at $T = 25^\circ\text{C}$. The energetic reference is noted with a * as **8**, the lower AC in the mechanism. The scale has not been respected for **8** to underline the lowering in energy going from separated reactants to the AC.

It is interesting to compare the value of intermediate **39**, where the incoming H is bound to the oxygen atom, and the previously modeled **11** where H is bound to the phosphorus atom (section 3.5.1 p.49, Figure 5-12). When we compare their respective Gibbs free energies, we see that **39** is actually $27 \text{ kJ}\cdot\text{mol}^{-1}$ higher than **11** as shown in Table 5-2. This suggests that, if **39** is formed, there may be a prototropic equilibrium in favor of **11** because of the electronegativity of the oxygen atom which better stabilizes the negative charge than the phosphorus atom. This

equilibrium has not been studied yet, but the conformation of **11** could prevent any departure of methoxide since the proton would be bound to the phosphorus, too far away from the leaving group to react ($d_{PH-OMe} = 2.2 \text{ \AA}$).

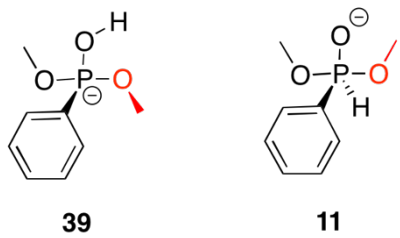


Figure 5-12: TBP **39** and **1**

TBP	Relative Gibbs free energy (kJ.mol ⁻¹)
39	0
11	-23

Table 5-2: Relative Gibbs free energy of TBP **11** compare to **39** determine at DFT level for T = 25 °C.

If this tautomerism does not occur, we previously showed that the TBP intermediate evolves with rotations of methyl groups to allow the rotation of the hydrogen **TS10**, second highest step of the transesterification mechanism with a 67 kJ.mol⁻¹ transition Gibbs free energy according to our previous study in neutral conditions (Figure 4-12, p.69). We here modeled the anionic equivalent of **TS10**, here **TS25**, as can be seen in Figure 5-13, and obtained a 111 kJ.mol⁻¹ energy barrier, 23 kJ.mol⁻¹ higher than the addition step **TS24**.

Consequently, the addition-elimination step is no longer the highest step, thus no longer the rate determining step for R_{PD}, as opposed to the neutral mechanism of transesterification. Since we do not have computed the overall R_{PD} mechanism yet, we cannot definitely tell which step is the new determining one for now. But this little study shows the importance to consider the whole mechanism for future studies, especially when relied to experimental work where the identification of the highest step is of primary interest.

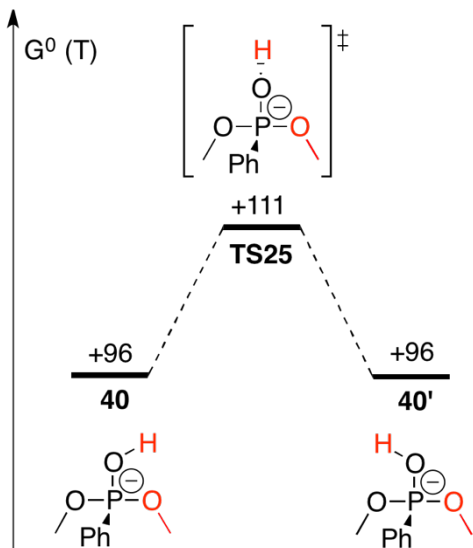


Figure 5-13: DFT model of the hydrogen rotation for the ionic intermediate. Energetic reference is 8.

5.4.5 The mysterious catalyst

In the kinetic modeling section 5.2.2 (p.97), we saw that kinetic model R_{EAX} , where an unknown impurity X coming with TEA participates to the reaction, fits well with experimental data after 1 equivalent of TEA. The first hypothesis about the nature of X is water or maybe triethylamine oxide (TEAO) which would act as an additional catalyst. Both possibilities have been investigated.

The most classical impurity present in solution with alcohol and TEA is water **41**. Even after distillation, a very small amount of it can still be present in solution. DFT simulations of the addition mechanism catalyzed by H_2O is however different from the one with TMA as shown in the Figure 5-14. Once coordinated with MeHP to form the AC **42**, water takes the hydrogen of the alcohol during its addition **TS26**, while it gives one of its hydrogens to the double bonded oxygen. The resulting Gibbs free energy of transition is $80 \text{ kJ}\cdot\text{mol}^{-1}$ at 25°C .

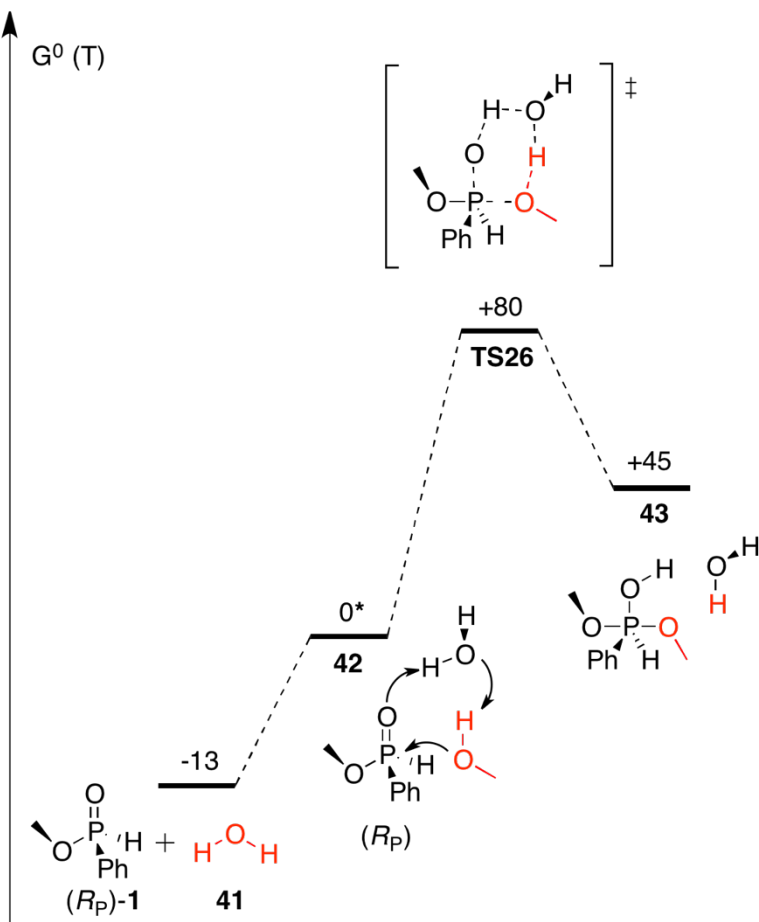


Figure 5-14: DFT simulation of the addition mechanism of methanol **2** on MeHP- H_2O associated complex **42** catalyzed by H_2O **41** at $25\text{ }^\circ\text{C}$. Energetic reference is the AC **42** noted with a *.

While this is still $33\text{ kJ}\cdot\text{mol}^{-1}$ lower than the addition in neutral conditions, this mechanism is $24\text{ kJ}\cdot\text{mol}^{-1}$ higher than R_{EA} . Consequently, R_{EA} should be favored over R_{EAX} , but the participation of water still decreases the energy barrier could participate to the catalysis.

We then wanted to model the mechanism catalyzed by TMAO but, up until now, we have not been able to do so because the system is too flexible. However, first results showed a path similar to the one with TMA, in which there is a slight deprotonation of the alcohol before the addition (Figure 5-9, p.106). Nevertheless, it is too early to get any ensured numerical data, thus to conclude anything from it.

5.4.5.1 NMR study of the alcohol exchange with H_2O or trimethylamine oxide

To get more information about the action of H_2O and amine oxides, we did experiments with both of those impurities. We first diluted 0.3 mmol of EtHP in 5 mL of *n*-propanol (*n*-PrOH), then added 1 equivalent of either water or trimethylamine oxide **44** (TMAO). The TEA oxide

exists, but it needs to be stabilized by the addition of another compound which could affect the reactivity. For this reason, we used similar but most stable compound TMAO. Both resulting solutions were kept in an NMR tube at room temperature with a capillary filled with C₆D₆. Two ³¹P-CPD NMR spectrum (400 MHz) has been made, one at t = 0 h and the second at t = 24 h. Both are shown in Figure 5-15.

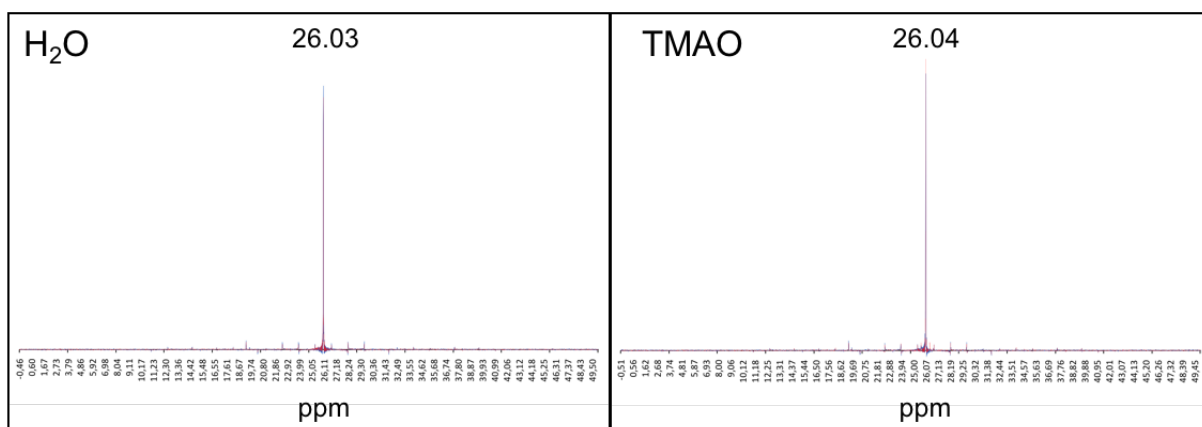


Figure 5-15: Comparison of 400MHz NMR ³¹P-CPD signals for EtHP diluted in nPrOH in presence of water (left) or trimethylamine oxide (right) at t = 0 h (blue) and t = 24 h (red); measurements were done with a capillary filled with C₆D₆ as reference.

We can see that both systems do not present any evolution after 24 h, whether for TMAO or H₂O. This means that there is no degradation nor alcohol exchange with *n*-propanol at room temperature. Thus, we can reasonably conclude that neither water nor TEA oxide is the mysterious catalyst.

5.4.6 Conclusion

We saw in this section that the addition of methanol onto phosphinous acid could not be model, even with the addition of TMA. This does not mean that it cannot happen, but we consequently decided not to take this possibility into account in our study.

The addition of TMA in mechanism F2-V1 has been shown to lower the transition Gibbs free energy, as was expected after experimental results. The lowest energetic addition, referred to the first AC step, appeared to be R_{EA} ($\Delta_r G^{0\ddagger} = 58 \text{ kJ}\cdot\text{mol}^{-1}$), followed R_{PD} ($\Delta_r G^{0\ddagger} = 88 \text{ kJ}\cdot\text{mol}^{-1}$). For mechanism R_{EPA}, for which the AC could not be modeled, we referred to the sum of reactants and obtained a $\Delta_r G^{0\ddagger} = 99 \text{ kJ}\cdot\text{mol}^{-1}$. Using the same reference for other addition mechanisms, R_{EPA} is still higher than R_{EA} and R_{PD} by respectively 21 kJ·mol⁻¹ and 11 kJ·mol⁻¹. It is important, though, to note that the reference is different than the previous comparison, and

the reliability of association energies has not been checked yet. It is thus too early to definitely conclude anything, but we can still use it to explore various theories.

Those DFT models are in good agreement with kinetic modeling which showed good fitting between measured and predicted $\Delta_r G^{0\ddagger}$ for R_{EA} and R_{EAX} to happen, but not R_{PD} nor R_{EPA} . However, we notice big differences between theoretical transition Gibbs free energies and measured ones. It could come from the fact that several reactions happen simultaneously in solution, or from differences between models and reality.

Another possibility was found while investigating the R_{DP} pathway, where we saw that the rotation of the hydroxyl group was actually 23 kJ.mol^{-1} higher than the addition ($\Delta_r G^{0\ddagger} = 111 \text{ kJ.mol}^{-1}$). We can conclude that, if the addition of methanol is catalyzed by the presence of TMA, this may not be the case of the subsequent steps which could be higher in energy. As a result, it is important to model the whole mechanism if we want to compare calculations to experimental measurements.

Finally, we tried to determine the nature of the X compound with modeling and NMR studies. DFT modeling showed that H_2O could lower the energy barrier of addition to 80 kJ.mol^{-1} , but NMR study with either H_2O or TMAO showed no catalytic effect. We thus conclude that none of those two compounds is our mysterious catalyst.

5.5 Conclusion

In this chapter, we experimentally monitored the racemization of EtHP in presence of TEA and showed that the apparent transition Gibbs free energy of enantiomerization was lowered with the increase of C_B/C_P ratio. Two sets of ten experiments have been studied while varying C_B/C_P ratio, one with C_B constant and the other with C_P constant. In basic conditions, we see that the highest $\Delta_r G_{app}^{0\ddagger}$ has been estimated at $121.5 \text{ kJ.mol}^{-1}$, 15 kJ.mol^{-1} lower than the lowest $\Delta_r G_{app}^{0\ddagger}$ in neutral conditions, which shows the catalytic effect of basic compound.

Kinetic modeling was used with seven different reactions: direct addition R_0 , activation of ethanol R_{EA} , activation of phosphinate R_{PA} , activation of both reactants R_{EPA} , deprotonation of phosphinate R_{PD} , and activation by X R_{EAX} and R_{PAX} . We observed that only R_{EA} and R_{EAX} fit with measured data for C_P constant, but only after $C_B/C_P > 1$, indicating that the activation by ethanol would be a part of the global mechanism. The behavior of R_{EPA} before 1 equivalent is interesting, but does not fit well with experimental data. This still suggests that activating both reactants could be a good lead for future studies.

One of our goal in this study was to compare kinetic modeling with mechanistic studies at DFT level (all values were calculated for 25 °C). We have first studied the new equilibrium in basic conditions with addition of TMA, and noticed that the phosphinous acid AC **33** was 12 kJ.mol⁻¹ favored over the MeHP AC **32**. However, we did not manage to model the addition of methanol on **33**, so we decided not to take this possibility into account in our following calculations.

We noticed that the deprotonation of MeHP by TMA was possible with a $\Delta_r G^{0\ddagger} = 56 \text{ kJ.mol}^{-1}$ referred to MeHP complex **32**, resulting on phosphonide complex **34** (48 KJ.mol⁻¹). Because of the difference of Gibbs free energy between **34** and **32**, we deduced that, if the deprotonation occurs, it would be as a first step, but **32** should not be present in solution.

The addition of methanol onto neutral AC **32** could not be achieved for R_{PA} nor R_{EPA} because of the system's flexibility. While we cannot assure that it does not happen in solution, the approach of methanol systematically pushed the TMA away up to 2.9 Å. We concluded that TMA coordinated to H-P does not act onto the addition mechanism, which could explain why kinetic models R_{PA} and R_{EPA} do not fit the overall experimental data, especially with an excess of base.

DFT modeling of R_{EA} worked well, showing a 56 kJ.mol⁻¹ transition Gibbs free energy referred to the first AC (78 kJ.mol⁻¹ to reactants), 57 kJ.mol⁻¹ lower than neutral addition. This shows that the coordination of TEA onto alcohol highly facilitate its addition, which is consistent with the good description of experimental data by R_{EA} kinetic model.

Whereas R_{PD} did not give good agreement with experimental data, we saw that deprotonation could occur according to our study of equilibrium, and determined the transition Gibbs Free energy for the addition of MeOH onto MeP⁻ at 88 kJ.mol⁻¹ referred to AC **8**. We also noted that the resulting intermediate **39**, where the hydrogen is borne by the oxygen atom, is 27 kJ.mol⁻¹ higher than the previously modeled intermediate **11**, where the hydrogen was borne by the phosphorus atom. This means that **39** could undergo prototropic equilibrium to stabilize, then not proceed to the elimination of methoxy group. This equilibrium could then explain why R_{PD} does not fit with experimental data despite a clear catalytic effect.

Another interesting fact is the modeling of OH rotation step for R_{PD} mechanism which showed a 111 kJ.mol⁻¹ transition Gibbs free energy, 23 kJ.mol⁻¹ higher than its addition step. This means that the addition-elimination step is no longer the highest step for R_{PD} mechanism, thus not its

determining step. This observation shows the importance of modeling the whole mechanism in future study to be sure that we modeled the determining step, which is of primary interest for comparison with experimental results.

We also have to remember that the prototropic equilibrium between P(III) and P(V) is inversed in presence of TMA according to our first calculations, but its participation is not visible through kinetic model. Calculations using acid as the less energetic step, maybe the first one, could be useful information for the comparison with experimental work in the future.

The study about the effect of basic conditions on enantiomerization is not finished yet. In the future, we can use the kinetic model adjustment with more simultaneous reactions to determine their relative participation. In order to compare theoretical work with experimental data, it will be necessary to model the whole transesterification mechanism for all reactions to identify their respective determining step.

Another study planed, using basic catalysis, is to determine the effect of the alkyl group borne by the phosphorus atom. We already started some simulations and experiments which are presented in the next chapter.

Chapter 6:

Effect of the hindrance on the enantioselectivity of alkyl *hydrogeno*-phenylphosphinates

RESUME EN FRANÇAIS

Au départ de cette thèse, nous avons projeté d'étudier l'effet de l'encombrement sur la réactivité des AlkHP. Dans le chapitre 4, nous avons déterminé un mécanisme générique d'inversion via S_N2, que nous avons nommé **F2-V1**, et qui va nous servir de base pour l'étude de l'encombrement stérique. Nous avons ainsi remplacé les groupements méthyles par d'autres plus encombrés : l'éthyle (**B**), l'*iso*-propyle (**C**), le menthyle (**D**), le *tert*-butyle (**E**) et l'adamantyle (**F**). Le changement de groupe s'est fait soit uniquement sur l'alcool (**I**), uniquement sur le phosphinate (**2**), ou uniquement sur le réactif (**3**).

Il été constaté que, si l'on réfère au premier AC du mécanisme simulé, la nature du groupement ne semble pas agir sur la barrière d'addition-élimination (**F2**: 106 kJ.mol⁻¹, **F2-V1**: 113 kJ.mol⁻¹, **D1** = **F1** = **B3**: 118 kJ.mol⁻¹, **E1**: 123 kJ.mol⁻¹, **C3**: 124 kJ.mol⁻¹, **E3**: 128 kJ.mol⁻¹). C'est notamment visible lorsqu'on compare l'addition sur le phosphinate de méthyle du 1-adamantanol (**F1** = 106 kJ.mol⁻¹), 7 kJ.mol⁻¹ plus basse que l'addition de méthanol (**F2-V1** = 113 kJ.mol⁻¹).

Si l'on se réfère à la somme des enthalpies libres des réactifs, en revanche, l'effet de l'encombrement se fait plus visible et on remarque une augmentation de la barrière avec le groupement, et qu'elle semble plus importante si positionnée sur l'alcool (**F2-V1**: 121 kJ.mol⁻¹, **D1-TS** = 138 kJ.mol⁻¹, **C1-TS**: 139 kJ.mol⁻¹, **E1-TS**: 146 kJ.mol⁻¹, **F1-TS**: 152 kJ.mol⁻¹) que

sur le phosphinate (**F2-V1-TS**: 121 kJ.mol⁻¹, **D2-TS** = 122 kJ.mol⁻¹, **F2-TS**: 129 kJ.mol⁻¹, **E2-TS**: 136 kJ.mol⁻¹).

En conclusion, si l'effet de l'encombrement de l'alcool est plus important que celui du phosphinate, on peut en déduire que le plus important sera l'élimination de l'alcool et non son addition. Si tel est le cas, on peut imaginer l'addition d'un alcool plus encombré que l'alkyle du phosphinate (exemple avec le 1-adamantanol **F** sur le phosphinate de *tert*-butyle **E**) qui résulterait sur l'éjection de l'alcool le moins encombré, soit le groupement alkyle initial (dans notre exemple, le *tert*-butanol). Cependant, il nous manque encore des données pour compléter cette étude et certifier cette hypothèse.

Concernant les essais expérimentaux, il a été observé lors du chapitre 4 que la racémisation du EtHP dans l'éthanol s'avère très longue à échelle humaine. Il semblait donc cohérent que l'utilisation de phosphinates plus encombrés que l'EtHP rallongerait d'autant plus la durée de la réaction. Dans le chapitre 5, nous avons constaté que l'ajout de TEA permettait d'accélérer l'échange d'alcool. Nous avons donc recouru à cette méthode pour accélérer les réactions et constater l'effet de l'encombrement stérique.

Malheureusement, les études ont montré une dégradation des produits phosphorés en acide *hydrogénophénylphosphinique*. Il est donc difficile de tirer des conclusions de ces premiers travaux car nous ne pouvons pas déterminer quel composé, entre le réactif ou le produit, est la molécule qui se dégrade. De plus, la présence de l'acide monopolise une partie de la TEA ce qui rend les expériences difficilement comparables. Néanmoins, nous avons pu observer que l'ajout d'*iso*-propanol sur l'EtHP (118 kJ.mol⁻¹) était plus lente que celle de l'éthanol (107 kJ.mol⁻¹), ce qui va dans le sens d'un effet ralentissant de l'encombrement. Cette hypothèse ne peut cependant pas être confirmée tant que des cinétiques plus contrôlées n'ont pas été réalisées.

En conclusion, il semble donc que la taille et la nature du groupement alkyle porté par l'alcool joue un rôle plus important dans la réaction d'échange que celui porté par le phosphinate. D'autres modèles DFT à l'avenir nous permettront d'approfondir cette observation. Les études cinétiques semblent aller dans le sens d'un effet stérique sur la cinétique d'échange, mais nous manquons de contrôle pour affirmer cette hypothèse. En somme, d'autres études devront être menées à l'avenir sur le sujet pour agrémenter les résultats et apporter des précisions sur ces premières observations.

6 Effect of the hindrance of the alkyl groups on the S_N2@P

6.1 Introduction

6.1.1 Context

At the beginning of the thesis, we presented the work of Buono et al. about the effect of hindrance borne by the alkoxy group on the reactivity of phosphinate. We observed in chapter 4 how EtHP was racemizing in solution, and identified, using DFT, the major mechanism of enantiomerization, which consists in a transesterification after *syn*-addition of methanol on the opposite side of the alkoxy group (Figure 4-12, p.69): the F2-V1 mechanism. In this chapter, we will present some DFT simulations to determine the effect of the hindrance and nature of the alkyl group on S_N2@P using the addition step of F2-V1 mechanism. To do so, we replaced the methyl groups by bigger ones such as ethyl, isopropyl, menthyl, *tert*-butyl and adamantyl, in order to get the effect of the hindrance and nature of alcohol.

We also want to do experimental study of this effect, but kinetic measurements of enantiomerization of EtHP in ethanol (section 4.4, p.76) showed that it was a very low process. It should then be expected that more hindered phosphinates and alcohols react even slower. In chapter 5, we showed that the use of TEA as basic catalyst allowed to accelerate the enantiomerization in a reasonable amount of time. Hence, we decided to perform kinetic measurements on various hindered phosphinates and alcohols using TEA as catalyst in order to perform those kinetics in a reasonable amount of time.

6.1.2 Methodology

Models have been made using the same level of theory as before, SMD(THF)//M06-2X/6-31++G**, in neutral conditions. Since we did not check the reliability of energies of association for these systems, and to remain coherent with our previous methodology, we will first present our results without considering the association energies between reactants, then we will consider this energy based on our good agreement showed in section 4.5 (p. 84).

The tested alkyl groups are methyl, isopropyl and *tert*-butyl to test the nature of the alcohol, then menthyl and adamantyl to study the influence of the hindrance. The modeling with ethanol done in section 4.5 (p.84) will also be considered. We chose our R group on the basis of previous works in our lab, and considered the steric effect as the cone formed by substituents and their chain length.

The mechanism used for DFT study is the determining addition-elimination step in neutral conditions that consists in the *syn*-addition of the hydroxide onto the P=O bond, previously presented in the mechanism F2-V1 in section 4.2.2.1 (p. 65). All reactants have been studied using their more stable conformer. Activated complexes and TBP intermediates presented in this study are the result of IRC calculation, meaning that more stable conformers of these intermediate could exist but have not been identified.

Kinetic studies have been made using ^{31}P -CPD NMR in basic conditions using 85% phosphoric acid as external reference for calibration. Experiments have been done on a Bruker Avance III 500 and a 600 NMR, respectively with *n*-propyl phosphinate in ethanol and ethyl phosphinate in *n*-propanol or *iso*-propanol. Kinetic studies were made at 50 °C in a NMR tube containing a capillar filled with C₆D₆ in order to lock the signal without having to use deuterated solvent for the reaction. A small portion of triphenylphosphine (TPP) was added in the capillar to determine the real quantity of phosphinate at the beginning of the reaction.

6.2 Influence of the alkyl group on SN2@P in neutral conditions

Starting with the effect of phosphinate's alkoxy groups, we modeled the addition of methanol onto *iso*-propyl (iPrHP, **45**), (*R*_P)-menthyl ((*R*_P)-MenHP, **46**), *tert*-butyl (*t*-BuHP, **47**) and adamantyl (AdHP, **48**) phosphinates. Then, we worked on the effect of hindrance from alcohol by modeling the addition of different alcohols on the MeHP **1**: *iso*-propanol (iPrOH, **49**), (-)-menthol ((-)MenOH, **50**), *tert*-butanol (*t*-BuOH, **51**) and 1-adamantanol (AdOH, **52**). All used reactants are presented in Figure 6-1.

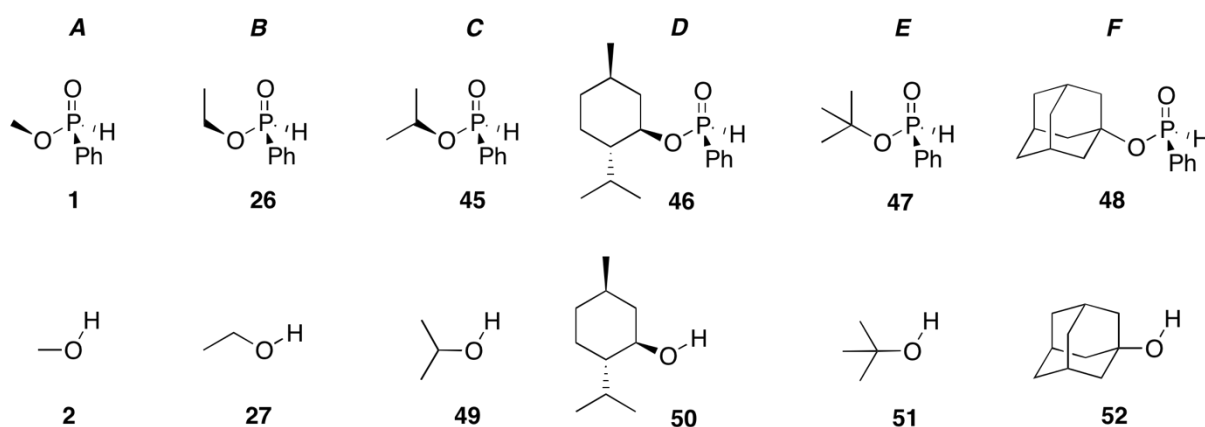


Figure 6-1: Different reactants used to study the influence of the hindrance in F2-V1 mechanism

We will here study the determining step of the F2-V1 mechanism, previously defined in section 4.3.1 (p. 68). First, we define systems depending on the specific alkyl group from **A** (methyl)

to **F** (adamantyl) with increasing hindrance. The first objective is to study the effect of hindrance in alcohol with the systems **1**, where we add every alcohol onto MeHP **1**. Then, in the systems **2**, we performed the addition of methanol **2** on every phosphinate. The last possibility is systems **3**, where alkyl groups borne by the phosphinate and the alcohol are the same. Gibbs free energies obtained from the first three steps from F2-V1 mechanism are shown in Figure 6-2, where **AC** is the associated complex, **TS** is the transition state of addition, and **TBP** the resulting pentacoordinated intermediate, are given in Table 6-1.

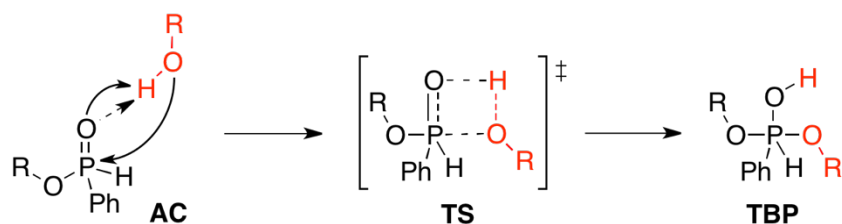


Figure 6-2: First three steps of the F2-V1 addition mechanism modeled at DFT level: activated complex **AC**, transition state **TS**, and reactional intermediate **TBP**.

		MeOH	EtOH	<i>i</i> PrOH	MenOH	<i>t</i> -BuOH	AdOH
MeHP	AC*						
	TS	F2-V1 113		C1 115	D1 115	E1 121	F1 106
	TBP	56		50	62	70	50
EtHP	AC*			9*			
	TS			B3 119			
	TBP			65			
<i>i</i> PrHP	AC*				8*		
	TS				C3 124		
	TBP				69		
MenHP	AC*	4*					
	TS	D2 118					
	TBP	61					
<i>t</i> -BuHP	AC*	13*				12*	
	TS	E2 123				E3 129	
	TBP	68				88	
AdHP	AC*	11*					

	TS	F2	118				
	TBP		58				

Table 6-1: Gibbs free energies in $\text{kJ}\cdot\text{mol}^{-1}$ of the first steps for the addition of ROH onto AlkHP using the F2-V1 mechanism at 25 °C. **AC**: associated complex, **TS**: transition state, **TBP**: pentacoordinated intermediate. The energetic reference noted with * for **AC** is the sum of the Gibbs free energies of the reactants at infinite distance, while **TS** and **TBP** are referred to **AC**.

While some systems have not been modeled yet (iPrHP with MeOH, AdHP with AdOH, and MenHP with MenOH), we can still compare the first results.

First, if we take our energetic referred as the first AC, we observe that all transition state's energies are relatively close to each other. Comparing the addition of methanol onto various phosphinates (systems **2**), the transition Gibbs free energy difference is only about 10 $\text{kJ}\cdot\text{mol}^{-1}$ (**F2-V1-TS**: 113 $\text{kJ}\cdot\text{mol}^{-1}$, **D2-TS** = **F2-TS**: 118 $\text{kJ}\cdot\text{mol}^{-1}$, **E2-TS**: 123 $\text{kJ}\cdot\text{mol}^{-1}$). For the addition of various alcohol onto MeHP (systems **1**), we see a variation of 20 $\text{kJ}\cdot\text{mol}^{-1}$ (**F1-TS**: 106 $\text{kJ}\cdot\text{mol}^{-1}$, **F2-V1**: 113 $\text{kJ}\cdot\text{mol}^{-1}$, **C1-TS** = **D1-TS**: 115 $\text{kJ}\cdot\text{mol}^{-1}$, **E1-TS**: 121 $\text{kJ}\cdot\text{mol}^{-1}$). Finally, while adding two reactants with the same alkyl groups (systems **3**), we observe a dependency of $\Delta_r G^{0\ddagger}$ on the hindrance with an increasing of 15 $\text{kJ}\cdot\text{mol}^{-1}$ (**F2-V1**: 113 $\text{kJ}\cdot\text{mol}^{-1}$, **B3**: 118 $\text{kJ}\cdot\text{mol}^{-1}$, **C3**: 124 $\text{kJ}\cdot\text{mol}^{-1}$, **E3**: 128 $\text{kJ}\cdot\text{mol}^{-1}$).

We can see that the adamantyl group shows a low difference with less hindered groups. It has the same transition Gibbs free energy as menthyl for the addition of methanol (**F2-TS** = **D2-TS** = 118 $\text{kJ}\cdot\text{mol}^{-1}$), and the lowest for AdOH addition onto MeHP (**F1-TS** = 106 $\text{kJ}\cdot\text{mol}^{-1}$, 7 $\text{kJ}\cdot\text{mol}^{-1}$ lower than MeOH). We also noticed that the addition of secondary alcohol onto MeHP, **C2-TS** and **D2-TS**, are only 2 $\text{kJ}\cdot\text{mol}^{-1}$ higher than MeOH addition, and that their $\Delta_r G^{0\ddagger}$ are equal despite bigger hindrance of MenOH over iPrOH (115 $\text{kJ}\cdot\text{mol}^{-1}$).

Now, if we use the sum of reactants at infinite distance as reference (a.k.a. by adding the Gibbs free energy value of **AC** to **TS** and **TBP**), we get the energetic values presented in Table 6-2. We should note that the reliability of our method has not been tested for isopropyl, menthyl, *tert*-butyl and adamantyl, but we have shown its reliability for methyl and ethyl in section 4.5 (p. 84). Even if the molecules are different, the core of the reaction, *syn*-addition of hydroxide onto P=O bond, is the same, and reactants have the same nature. Consequently, it is a reasonable assumption to consider our modeling as reliable. Because we consider the sum of reactants as

energetic reference, the AC step has no interest in the following results, so it will not appear in Table 6-2 for more visibility.

First, we can observe the effect of hindrance on alcohol (systems **I**) and see that the higher the hindrance, the higher the TS according to our modeling (**F2-V1**: 121 kJ.mol⁻¹, **D1-TS** = 138 kJ.mol⁻¹, **C1-TS**: 139 kJ.mol⁻¹, **E1-TS**: 146 kJ.mol⁻¹, **F1-TS**: 152 kJ.mol⁻¹). Second, when we add methanol on various phosphinate (systems **2**), we observe less dependency on the hindrance (**F2-V1-TS**: 121 kJ.mol⁻¹, **D2-TS** = 122 kJ.mol⁻¹, **F2-TS**: 129 kJ.mol⁻¹, **E2-TS**: 136 kJ.mol⁻¹). It is especially visible for MenHP **D2**, for which the addition transition energy is only 1 kJ.mol⁻¹ higher than MeHP **F2-V1** despite a higher hindrance. To end with, we can compare the variation on both reactants (systems **3**) and observe a clear dependency of the transition Gibbs free energy on the hindrance as for systems **I** (**F2-V1**: 121 kJ.mol⁻¹, **B3**: 128 kJ.mol⁻¹, **C3**: 132 kJ.mol⁻¹, **E3**: 142 kJ.mol⁻¹).

		MeOH	EtOH	<i>i</i> PrOH	MenOH	<i>t</i> -BuOH	AdOH
MeHP	TS	F2-V1 121		C1 139	D1 138	E1 146	F1 152
	TBP	64		74	85	95	96
EtHP	TS		B3 128				
	TBP		74				
<i>i</i> PrHP	TS			C3 132			
	TBP			77			
MenHP	TS	D2 122					
	TBP	65					
<i>t</i> -BuHP	TS	E2 136				E3 142	
	TBP	81				100	
AdHP	TS	F2 129					
	TBP	69					

Table 6-2: Gibbs free energies in kJ.mol⁻¹ of first steps for the addition of ROH onto AlkHP using the F2-V1 mechanism at 25 °C. TS: transition state, TBP: pentacoordinated intermediate. The energetic reference for all step is the sum of the Gibbs free energies of the reactants at infinite distance.

An interesting observation is that, while the hindrance of the alkyl groups borne by the phosphinate seems not to act directly as shown by the addition of MeOH onto MeHP **F2-V1**

and MenHP **D2** which are almost equal, we observe that the more hindered the alcohol, the higher the transition state. Consequently, the hindrance on phosphinate would matter less than the one on alcohol during the addition.

As a result, in the case of the addition of a small alcohol onto a big phosphinate, and since the elimination step is lower with the less hindered alcohol, we would keep the more hindered phosphinate and reform the less hindered alcohol. However, if we manage to do the addition of a hindered alcohol onto a less hindered phosphinate, the elimination step should still favor the formation of an alcohol bearing the less hindered alkyl group. As a result, this would lead to an alcohol exchange ending on a more hindered phosphinate with a less hindered alcohol. Consequently, a logical hypothesis is that, in a transesterification mechanism with different hindrance, the most important step is the elimination step more than the addition, because it is decided by the hindrance of the alkyl groups, while the addition step is less influenced.

As a conclusion, it seems that the reactivity of AlkHP is more complicated than a simple relation to the hindrance of alkyl groups. For now, our modeling showed that the influence of alcohol is more important than phosphinate, but we must remember that we are still in the early developments of this study. In addition, the reliability of the DFT model, even if previously tested, has not been confirmed yet. As a result, it is too early to draw a conclusion from those data.

6.3 Kinetic study in basic conditions using ^{31}P -CPD NMR

6.3.1 Choice of the system

For the first kinetic study on hindrance, we decided to test the length of the alkyl chain with *n*-propyl, and the nature of alcohol with isopropyl. While we were doing the measurements, it appeared that the volume of deuterated benzene in the capillary, where a known quantity of TPP had been put to be used as reference for measurement, was diminishing over time. Consequently, we could not use the concentration of TPP as reference along the reaction to determine the evolution of the quantity of EtHP over time, and had to find another way to determine k_{app} than from the equation $\ln \left(\frac{[A]}{[A]_0} \right) = -k_{\text{app}}t$. Besides, in the case of our reaction middle also evaporates, it is better use a method independent from the volume.

Since reactants are in the same volume, constant or not, we have $\ln \left(\frac{[A]}{[A]_0} \right) = \ln \left(\frac{n(t)}{n(0)} \right)$ with n being a reactant amount of substance. Since the percentage of each compound is defined as

$\frac{X}{100} = \frac{n}{\sum_i n_i}$ with X being the percentage of a given reactant in solution, and because $\sum_i n_i$ is constant over time since no external compound is added during the reaction, it means that we can replace n by X in the equation:

Eq. 6-1

$$\ln\left(\frac{n(t)}{n(0)}\right) = \ln\left(\frac{n(t)/\sum_i n_i(t)}{n(0)/\sum_i n_i(0)}\right) = \ln\left(\frac{n(t)/\sum_i n_i}{n(0)/\sum_i n_i}\right) = \ln\left(\frac{X(t)/100}{X(0)/100}\right) = \ln\left(\frac{X(t)}{X(0)}\right)$$

As a result, we can determine k_{app} from the evolution of the percentage of the compound over time. This methodology has been used for every following kinetic study except noticed otherwise. The question of the reliability of the proportionality of surface S can be noted, and a sampling could be done in future studies. But since we hereby study very close structural compounds and previous using of this methodology were reliable, we can use the following results as a beginning.

6.3.2 Observations

NMR studies have been performed with the help of R. Rosas and G. Herbette from the Spectropole of Marseille. The resulting curves that describe the conversion of phosphinates and their respective kinetic study are represented in Figure 6-3. We observed the presence of an impurity at the position 17.9 ppm or 17.4 ppm depending on the phosphinate and solvent used (green curve) which remains constant over time. We identify it as the unknown one presented in section 2.3 (p.28). Its effect should be checked in future study, but since its signal remains constant during the reaction, and we here study the activity of TEA, which quantity is always proportional to the one of phosphinate and its impurity, we do not consider its effect because it should be constant from an experiment to another.

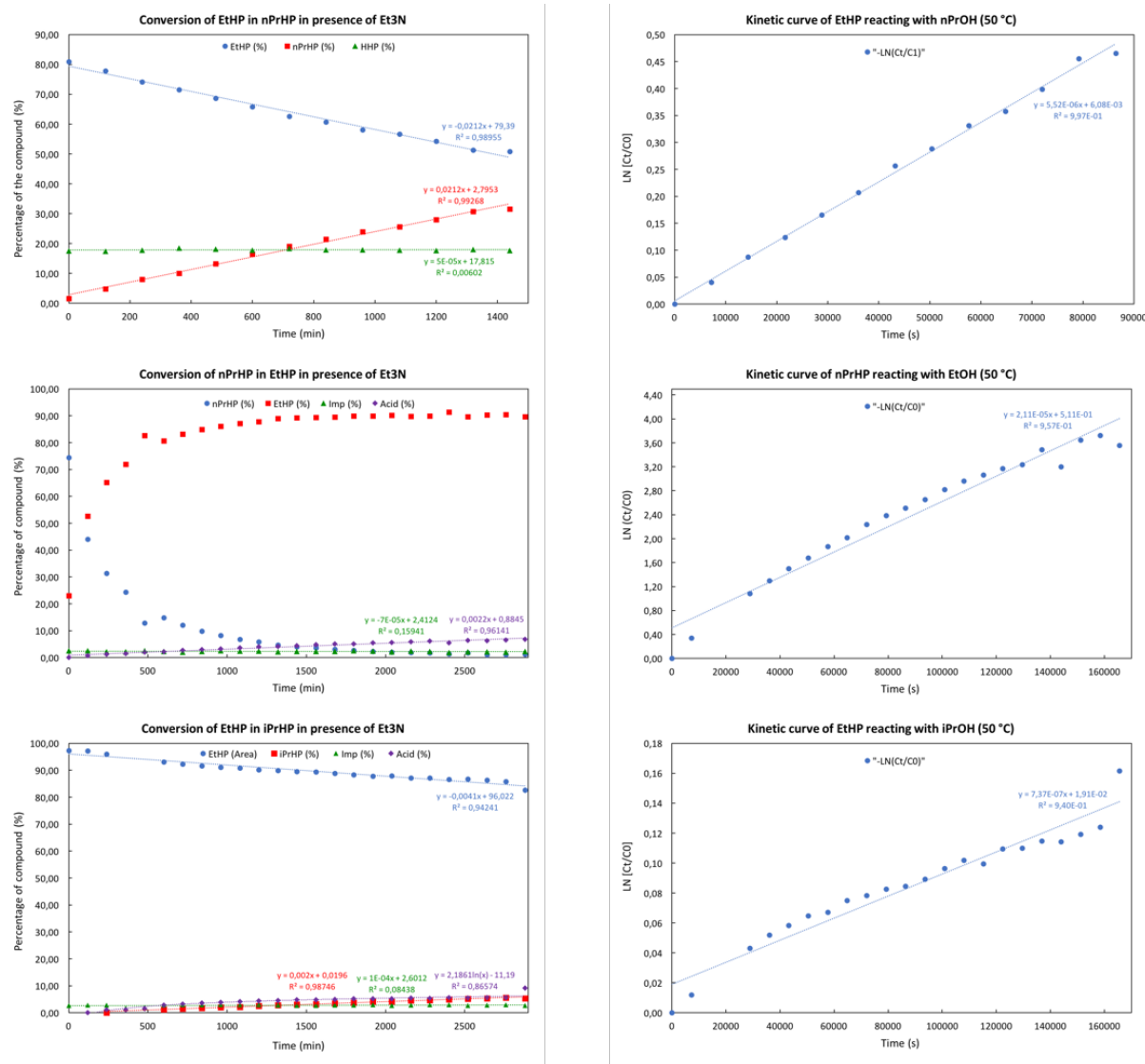


Figure 6-3: Kinetic study of the conversion of phosphinates diluted in alcohol with TEA as a basic catalyst, top: EtHP diluted in nPrOH, middle: nPrHP diluted in EtOH, bottom: EtHP diluted in iPrOH; right: evolution of the proportion of phosphorous compounds determined by ³¹P-CPD NMR 500 MHz for the first, 600 MHz for the two others; left: kinetic curves determined from the percentage of the phosphinate reactant.

Solutions with *n*-propyl *hydrogeno*-phenylphosphinate (*n*-PrHP) in EtOH and EtHP in iPrOH shows the presence of a side-product characterized by an NMR ³¹P-CPD signal around 13.9 ppm. In general, the side-product with phosphinate is *hydrogeno*-phenylphosphinic acid (HHP). To check this hypothesis, we did a ³¹P-CPD NMR spectrum of HHP in *n*-PrOH without TEA (Figure 6-4, red signal), and another after addition of TEA (Figure 6-4, turquoise signal), using a capillary filled with C₆D₆ as NMR solvent.

We can see that the signal of HHP goes from 18.23 ppm to 13.96 ppm with the addition of base, probably due to the interaction between HHP and TEA, maybe even its deprotonation. The

correspondence between this spectrum and the side-product shows that phosphinic acid is formed along the reaction despite the use of distilled compounds in dry vessels.

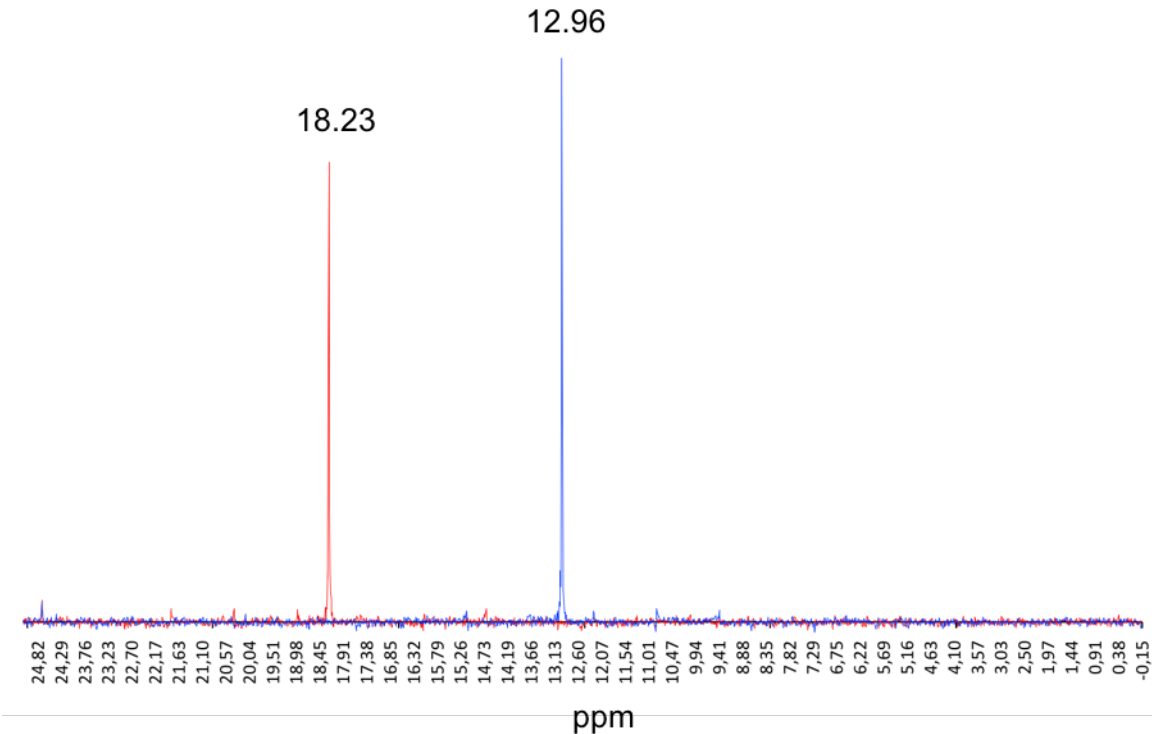


Figure 6-4: ³¹P-CPD NMR signal 400 MHz for *hydrogeno-phenylphosphinic acid* in *n*-propanol with a capillary of C₆D₆ with triphenylphosphine as a reference (-6 ppm). In blue: acid alone was diluted in *n*-propanol, in red: after the addition of TEA.

From Figure 6-3, we can determine that $k_{app} = 5.52 \cdot 10^{-6} \text{ s}^{-1}$ for *n*-PrOH addition on EtHP, which gives us a $\Delta_r G_{app}^{0\ddagger}$ of 118.8 kJ.mol⁻¹. This value is lower than the one determined for EtHP in EtOH without TEA which was around $\Delta_r G_{app}^{0\ddagger} = 135 \text{ kJ.mol}^{-1}$ (4.4, p.76), this despite a slightly higher hindrance with *n*-propyl instead of ethyl on the alcohol. From this, we can conclude there is an effect of the basic catalysis.

In other reactions, we determined $k_{app} = 2.11 \cdot 10^{-5} \text{ s}^{-1}$ for EtOH addition on iPrHP which gives us a $\Delta_r G_{app}^{0\ddagger}$ of 115.2 kJ.mol⁻¹, and $k_{app} = 7.37 \cdot 10^{-7} \text{ s}^{-1}$ for EtOH addition on *n*-PrHP which gives us a $\Delta_r G_{app}^{0\ddagger} = 124.2 \text{ kJ.mol}^{-1}$. This last value is 6 kJ.mol⁻¹ above the previous study of EtHP in *n*-PrOH, which can show the influence of the hindrance on the conversion of phosphinate. However, it is possible that the reactant is degrading into the acid throughout the reaction, which could explain the lower energy barrier. It must be noted that the degradation in

acid can partially come from the product, which means that this kinetic analysis could be incomplete.

6.4 Early conclusion

We are still in early stages of this study and a lot of work still need to be done. But if we look at the modeling study, it seems that, when we refer to the **AC** step, hindrance has no direct effect on the addition step (**F2-TS**: 106 kJ.mol⁻¹, **F2-V1-TS**: 113 kJ.mol⁻¹, **D1-TS = F1-TS = B3-TS**: 118 kJ.mol⁻¹, **E1-TS**: 123 kJ.mol⁻¹, **C3**: 124 kJ.mol⁻¹, **E3**: 128 kJ.mol⁻¹). It is especially true for AdOH added onto MeHP for which $\Delta_r G_{app}^{0\ddagger} = 106 \text{ kJ.mol}^{-1}$, 7 kJ.mol⁻¹ lower than MeOH onto MeHP.

However, using the sum of reactants at infinite distance as energetic reference, we showed that the more hindered the alcohol, the higher transition Gibbs free energies (**F2-V1-TS**: 121 kJ.mol⁻¹, **C2-TS**: 139 kJ.mol⁻¹, **D2-TS**: 138 kJ.mol⁻¹, **E2-TS**: 146 kJ.mol⁻¹, **F2-TS**: 152 kJ.mol⁻¹), while for the hindrance onto phosphinate, it appears that the energy of transition for some more hindered group is lower than less hindered (Menthyl over *iso*-propyl, adamantyl over *tert*-butyl). This observation implies that the most important would be the hindrance of the alcohol over phosphinate, but more calculation would be useful to get more information about the phenomenon before we confirm this hypothesis.

During kinetic studies, we encountered difficulties with the formation of HHP in solution. This side product prevents us to conclude anything onto the effect of hindrance, but we still find a $\Delta_r G_{app}^{0\ddagger} = 118 \text{ kJ.mol}^{-1}$ for *n*-PrOH reacting with EtHP, 11 kJ.mol⁻¹ higher than EtOH. We could conclude that the hindrance acts on the energy barrier, but we need to get the results from more controlled experiments to conclude on the matter.

As a conclusion for this chapter, we can only say that hindrance has an effect on S_N2@P mechanisms, but it seems to be more complex than a simple “the bigger, the higher”. More studies must be done using DFT simulations and kinetic measurements before we get to final conclusions.

General conclusion

Within the framework of constantly improving asymmetric catalysis, the use of SPO as preligands showed promising results. Our lab has contributed to the evolution of synthesis of such compounds in an enantioselective way from alkyl phenylphosphinates. It has been noticed that the alkyl group borne by the alkoxide of the phosphinate influenced both its enantiostability, and the resulting e.e. at the end of the synthesis of SPO. Our objective was here to understand how this alkyl group acts on the reactivity by using kinetic and theoretical studies.

The first chapter was a summary of previous researches about organophosphorous compounds. The tautomeric equilibrium has been showed to generally favor the P(V) form with a 240 kJ.mol^{-1} energy barrier and a lower Gibbs free energy by 12 kJ.mol^{-1} . Since we here work on the synthesis of SPO from AlkHP, which goes through a $\text{S}_{\text{N}}2@P$, we interested ourselves to the theoretical work of Bickelhaupt *et al.* who showed the importance to use a model close to the real system to obtain a good simulation of organophosphorous compounds. We also described the pseudorotations that could happen if the mechanism goes through a TBP intermediate, especially the most favored Berry pseudorotations.

The second chapter presented the various tools used during the thesis. We first presented DFT, its major concept, and the origin of exchange-correlation equation. Then, we described how to get closer from theoretical results to experimental ones with the consideration of solvent and temperature. In the end, we chose M06-2X/6-31++G** with SMD model of solvent as theoretical level, and the use of partition functions for the effect of temperature. We described the synthesis methodology of AlkHP, the separation of enantiomers using chiral HPLC, and their identification by NMR spectroscopy. To end with, we presented the kinetic equations used in the thesis and the concept of kinetic modeling, developed by R. Fortrie, that consists in determining reactions happening in solution by comparing their theoretical Gibbs free energies to experimental kinetic measurements.

The objective of the third chapter was to determine the system of interest for our study. We chose to work on the nucleophilic substitution between MeHP and MeOH, and showed that

the acidic form of MeHP should not be present in neutral conditions because of its higher 10 kJ.mol⁻¹ energy. Then, we determined the pKa of MeHP and MeOH as -9.8 for MeOH⁺/MeOH, 17.9 for MeHP/MeP⁻, -3.6 for MeH⁺/MeHP, and +29.0 for MeOH/MeO⁻.

If MeOH was deprotonated, despite the low probability for it to happen, the resulting alkoxide MeO⁻ would spontaneously react with a deprotonation of MeHP, 61 kJ.mol⁻¹ favored over the addition onto MeHP to form a TBP intermediate. As a conclusion, in neutral conditions, we should only find MeHP with MeOH in solution.

The transesterification mechanism between MeHP and MeOH has been studied in chapter 4. Several paths have been tested using PM6, then DFT level. We have shown that the most favored reactivity is the formation of TBP intermediate with a *syn*-addition of methanol onto the P=O bond of phosphinate. Then, the less energetic addition step is the one on the opposite side of the alkoxy group MeO, called mechanism F2-V1, with a 121 kJ.mol⁻¹ energy barrier. This addition results on the most stable TBP intermediate with both MeO groups in apical position.

From there, the TBP can evolve backward by eliminating the new MeO, or forward with a rotation of its hydroxyl group which allows the departure of the original MeO which involves an inversion of configuration. TBP intermediate can also evolve with pseudorotations, which highest transition Gibbs free energy (123 kJ.mol⁻¹) is actually competitive with the addition step. It means that, depending on the hindrance of the alkyl group, the addition of alcohol onto phosphinate can result in 5 possibilities: with or without addition of alcohol, backward with no changing in the conformation, forward with inversion of configuration, or via pseudorotations which would invert the configuration before the elimination.

With the help of Marion Jean and Nicolas Vanthuyne, we have performed an experimental measurement of the enantiomerization of EtHP in ethanol under reflux using chiral HPLC. The resulting transition Gibbs free energy, determined from the apparent 1st order kinetic, is around 135 kJ.mol⁻¹ which is in excellent agreement with our model (136 kJ.mol⁻¹). A dependency of this barrier with concentration of phosphinate has been observed, and kinetic modeling suggests that it is related to the formation of dimeric MeHP for which a second MeHP acts as a basic or acidic catalyst, lowering the enantiomerization barrier.

This catalytic phenomenon has been the subject of the 5th chapter, with the use of TEA as basic catalyst. We first have shown that the addition of TEA in the kinetic decreased the enantiomerization barrier even with a small quantity, and continue to decrease with the addition

of TEA from $121.5 \pm 0.9 \text{ kJ.mol}^{-1}$ to $98.4 \pm 0.2 \text{ kJ.mol}^{-1}$. We used kinetic modeling to test 7 possible reactions: neutral addition developed in chapter 4 (R_0), activation of ethanol or MeHP by TEA (R_{EA} and R_{PA}), activation by an impurity brought with TEA (R_{EAX} and R_{PAX}), activation of both reactants by TEA (R_{EPA}), and deprotonation of MeHP (R_{PD}). According to our results, only two mechanisms match: R_{EA} and R_{EAX} fit with measured data for C_P constant after $C_B/C_P > 1$. However, those mechanisms do not cover the overall experimental results, which means that they are not enough to explain the basic catalysis by their own, but might participate to it. Reaction R_{EPA} showed a good behavior for $C_B/C_P > 1$, but did not fit well with experimental results. It is possible that the activation of both reactants could be a good lead for future studies. The addition step from F2-V1 mechanism has been tested with addition of TMA, and showed a general decrease of the transition Gibbs free energy. The less energetic pathway is the one with activation of ethanol (56 kJ.mol^{-1} referred to AC) which is in good agreement with the effect fact that R_{EA} kinetic model fits well with experimental data.

With calculations of reaction R_{PD} , we have shown a 111 kJ.mol^{-1} energy barrier for the rotation of hydroxyl, which is 23 kJ.mol^{-1} higher than the addition step. As a result, if such a mechanism occurred, the determining step would not be the addition-elimination step anymore, as opposite to the neutral mechanism. This shows the importance to model the overall mechanism for future study.

In the last chapter, we presented the early work about the impact of hindrance on transesterification of phosphinate. By replacing the alkyl group of phosphinate's alkoxy part and alcohol, we have seen that the hindrance does not seem to have a big impact on the addition step in neutral conditions if calculations are referred to the AC. When referred to the sum of reactants, it appeared that the more hindered the alcohol, the higher the addition-elimination step, whereas it seemed less effective when the hindered group was borne by the phosphinate. We conclude that the more important for the transesterification mechanism was the hindrance of the leaving alcohol, since the one borne by the phosphorus atom at the beginning had less effect. But more calculation should be done to bring information to this hypothesis.

During NMR kinetic studies, we encountered difficulties with the formation of HHP in solution with *iso*-propyl and *n*-propyl phosphinates reacting with ethanol. This side product prevents us to conclude anything on the nature of the alkyl group, but we still find a $\Delta_r G_{app}^{0\ddagger} = 118 \text{ kJ.mol}^{-1}$ for *n*-PrOH reacting with EtHP, 11 kJ.mol^{-1} higher than EtOH in the same conditions. This

result shows that the hindrance acts on the energy barrier, but it is still too early to conclude how.

As a conclusion, we identified a general mechanism for transesterification mechanism ending on an inversion of configuration of phosphinate in presence of an alcohol. Then, we have shown that the presence of basic compounds increases the kinetic of the reaction, probably by the activation of the alcohol, maybe both reactants, which is showed by kinetic and computing modeling. Early studies on the effect of hindrance, have shown that it was more important onto the alcohol, but we need more data to conclude on this hypothesis.

In the future, more simulations should be done, especially modeling the whole enantiomerization mechanism to identify the determining step in basic conditions. Also, more researches should be made on the effect of nature of alkyl group by testing different nature and size of alcohol and phosphinates with kinetic measurements and DFT simulations. The understanding of such effect could help us to better understand the behavior of phosphinates and their derivative, making future studies about their enantioselectivity and reactivity easier. The multidisciplinary aspect of this study allowed a wide and comprehensive cover of the subject, and more collaboration and crossed researches should only benefit the understanding of chemical processes.

Bibliography

- 1: Anastas, P.; Warner, J. *Green Chemistry: Theory and Practice*; Oxford University Press: Oxford, New York, **2000**.
- 2: Noyori, R.; Ikeda, T.; Ohkuma, T.; Widhalm, M.; Kitamura, M.; Takaya, H.; Akutagawa, S.; Sayo, N.; Saito, T.; Taketomi, T.; Kumobayashi, H. *J. Am. Chem. Soc.* **1989**, *111* (25), 9134.
- 3: Mashima, K.; Matsumura, Y.; Kusano, K.; Kumobayashi, H.; Sayo, N.; Hori, Y.; Ishizaki, T.; Akutagawa, S.; Takaya, H. *J. Chem. Soc. Chem. Commun.* **1991**, *0* (9), 609.
- 4: Kumobayashi, H. *Recl. Trav. Chim. Pays-bas* **1996**, *115*, 381
- 5: Dobbs, D. A.; Vanhessche, K. P. M.; Brazi, E.; Rautenstrauch, V.; Lenoir, J.-Y.; Genêt, J.-P.; Wiles, J.; Bergens, S. H. *Angew. Chem. Int. Ed.* **2000**, *39* (11), 1992.
- 6: Togni, A. *Angew. Chem. Int. Ed. Engl.* **1996**, *35* (13-14), 1475.
- 7: Knowles, W. S.; Sabacky, M. J. *Chem. Commun. Lond.* **1968**, No. 22, 1445.
- 8: Knowles, W. S.; Sabacky, M. J.; Vineyard, B. D. *J. Chem. Soc. Chem. Commun.* **1972**, No. 1, 10.
- 9: Knowles, W. S. *Angew. Chem. Int. Ed.* **2002**, *41* (12), 1998.
- 10: Dang, T. P.; Kagan, H. B. *J. Chem. Soc. Chem. Commun.* **1971**, No. 10, 481.
- 11: Vineyard, B. D.; Knowles, W. S.; Sabacky, M. J.; Bachman, G. L.; Weinkauff, D. J. *J. Am. Chem. Soc.* **1977**, *99* (18), 5946.
- 12: Miyashita, A.; Yasuda, A.; Takaya, H.; Toriumi, K.; Ito, T.; Souchi, T.; Noyori, R. *J. Am. Chem. Soc.* **1980**, *102* (27), 7932.
- 13: *Asymmetric Catalysis on Industrial Scale: Challenges, Approaches and Solutions*, 2nd Edition, Wiley-VCH Verlag GmbH & Co.; Blaser, H.-U., Federsel, H.-J., Eds.; **2010**.
- 14: Börner, A. *Phosphorus Ligands in Asymmetric Catalysis*; Wiley-VCH Verlag GmbH & Co., **2008**.
- 15: Jiang, X.; Minnaard, A. J.; Hessen, B.; Feringa, B. L.; Duchateau, A. L. L.; Andrien, J. G. O.; Boogers, J. A. F.; de Vries, J. G. *Org. Lett.* **2003**, *5* (9), 1503.
- 16: Dutartre, M.; Bayardon, J.; Jugé, S. *Chem. Soc. Rev.* **2016**, *45* (20), 5771.
- 17: Shaikh, T. M.; Weng, C.-M.; Hong, F.-E. *Coord. Chem. Rev.* **2012**, *256* (9–10), 771.
- 18: Erre, G.; Enthalter, S.; Junge, K.; Gladiali, S.; Beller, M. *Coord. Chem. Rev.* **2008**, *252* (5–7), 471.
- 19: Ackermann, L. *Synthesis* **2006**, *2006* (10), 1557.
- 20: Hammond, P. R. *J. Chem. Soc. Resumed* **1962**, No. 0, 1365.
- 21: Wesolowski, S.; Brinkman, N.; Valeev, E.; Schaefer, H. *J. Chem. Phys.* **2001**, *116* (1), 112.
- 22: Wang, F.; Polavarapu, P. L.; Drabowicz, J.; Mikołajczyk, M. *J. Org. Chem.* **2000**, *65* (22), 7561.

- 23: Babin, Y. V.; Prisyazhnyuk, A. V.; Ustynyuk, Y. A. *Russ. J. Phys. Chem. A* **2008**, 82 (1), 94.
- 24: Mamaev, V. M.; Prisyajnuk, A. V.; Laikov, D. N.; Logutenko, L. S.; Babin, Y. V. *Mendeleev Commun.* **1999**, 9 (6), 240.
- 25: Janesko, B. G.; Fisher, H. C.; Bridle, M. J.; Montchamp, J.-L. *J. Org. Chem.* **2015**, 80 (20), 10025.
- 26: Tavakol, H.; Keshavarzipour, F. *Heteroat. Chem.* **2016**, 27 (4), 210.
- 27: Hoge, B.; Neufeind, S.; Hettel, S.; Wiebe, W.; Thösen, C. *J. Organomet. Chem.* **2005**, 690 (10), 2382.
- 28: Chatt, J.; Heaton, B. T. *J. Chem. Soc. Inorg. Phys. Theor.* **1968**, No. 0, 2745.
- 29: Roundhill, D. M.; Sperline, R. F.; Beaulieu, W. B. *Coord. Chem. Rev.* **1978**, 26 (3), 263.
- 30: Dubrovina, N. V.; Börner, A. *Angew. Chem. Int. Ed.* **2004**, 43 (44), 5883.
- 31: Williams, R. H.; Hamilton, L. A. *J. Am. Chem. Soc.* **1952**, 74 (21), 5418.
- 32: Williams, R. H.; Hamilton, L. A. *J. Am. Chem. Soc.* **1955**, 77 (12), 3411.
- 33: Korpiun, O.; Mislow, K. *J. Am. Chem. Soc.* **1967**, 89 (18), 4784.
- 34: Korpiun, O.; Lewis, R. A.; Chickos, J.; Mislow, K. *J. Am. Chem. Soc.* **1968**, 90 (18), 4842.
- 35: Leyris, A.; Bigeault, J.; Nuel, D.; Giordano, L.; Buono, G. *Tetrahedron Lett.* **2007**, 48 (30), 5247
- 36: Emmick, T. L.; Letsinger, R. L. *J. Am. Chem. Soc.* **1968**, 90 (13), 3459.
- 37: Gatineau, D.; Nguyen, D. H.; Héault, D.; Vanthuyne, N.; Leclaire, J.; Giordano, L.; Buono, G. *J. Org. Chem.* **2015**, 80 (8), 4132.
- 38: Xu, Q.; Zhao, C.-Q.; Han, L.-B. *J. Am. Chem. Soc.* **2008**, 130 (38), 12648.
- 39: Eymery, F.; Iorga, B.; Savignac, P. *Tetrahedron* **1999**, 55 (46), 13109.
- 40: Humbel, S.; Bertrand, C.; Darcel, C.; Bauduin, C.; Jugé, S. *Inorg. Chem.* **2003**, 42 (2), 420.
- 41: Sølling, T. I.; Pross, A.; Radoma, L. *Int. J. Mass Spectrom.* **2001**, 210–211, 1.
- 42: Corriu, R. J. P.; Lanneau, G. F.; Leclercq, D. *Tetrahedron* **1989**, 45 (7), 1959.
- 43 : Uchimaru, T.; Stec, W. J.; Tsuzuki, S.; Hirose, T.; Tanabe, K.; Taira, K. *Chem. Phys. Lett.* **1996**, 263 (5), 691.
- 44: Holmes, R. R. *Chem. Rev.* **1996**, 96 (3), 927.
- 45: Jennings, V. E.; Nikitin, K.; Ortin, Y.; Gilheany, G. D. *J. Am. Chem. Soc.* **2014**, 136, 16217.
- 46: van Bochove, M. A.; Swart, M.; Bickelhaupt, F. M. *J. Am. Chem. Soc.* **2006**, 128 (33), 10738.
- 47: van Bochove, M. A.; Swart, M.; Bickelhaupt, F. M. *ChemPhysChem* **2007**, 8 (17), 2452.
- 48: van Bochove, M. A.; Bickelhaupt, F. M. *Eur. J. Org. Chem.* **2008**, 2008 (4), 649.
- 49: Bochove, M. A. van; Swart, M.; Bickelhaupt, F. M. *Phys. Chem. Chem. Phys.* **2009**, 11 (2), 259.

- 50: Cahn, R. S.; Ingold, C.; Prelog, V. *Angew. Chem. Int. Ed. Engl.* **1966**, *5* (4), 385.
- 51: Wang, P.; Zhang, Y.; Glaser, R.; Reed, A. E.; Schleyer, P. v. R.; Streitwieser, A. *J. Am. Chem. Soc.* **1991**, *113* (1), 55.
- 52: Kobayashi, J.; Kawashima, T. *Comptes Rendus Chim.* **2010**, *13* (8–9), 1249.
- 53: Holmes, R. R. *J. Am. Chem. Soc.* **1978**, *100* (2), 433.
- 54: Berry, R. S. *J. Chem. Phys.* **1960**, *32* (3), 933.
- 55: Strich, A.; Veillard, A. *J. Am. Chem. Soc.* **1973**, *95* (17), 5574.
- 56: Daul, C.; Frioud, M.; Schafer, O.; Selloni, A. *Chem. Phys. Lett.* **1996**, *262* (1), 74.
- 57: Raynaud, C.; Maron, L.; Daudey, J.-P.; Jolibois, F. *ChemPhysChem* **2006**, *7* (2), 407.
- 58: DeBruin, K. E.; Naumann, K.; Zon, G.; Mislow, K. *J. Am. Chem. Soc.* **1969**, *91* (25), 7031.
- 59: Asymmetric Catalysis on Industrial Scale: Challenges, Approaches and Solutions, 2nd Edition, Wiley-VCH Verlag GmbH & Co.; Blaser, H.-U., Federsel, H.-J., Eds.; **2010**.
- 60: Tang, W.; Zhang, X. *Chem. Rev.* **2003**, *103* (8), 3029.
- 61: Noyori, R. *Angew. Chem. Int. Ed.* **2013**, *52* (1), 79.
- 62: Herault, D.; Buono, G.; Vanthuyne, N.; Roussel, C.; Giordano, L.; Moraleda, D.; Gatineau, D.; Leclaire, J.; Nuel, D. P-Stereogenic Chiral Precursor of Chiral Ligands and Use Thereof. WO/2014/108487, July 18, **2014**.
- 63: Montchamp, J.-L. *Acc. Chem. Res.* **2014**, *47* (1), 77.
- 64: Schrödinger, E. *Phys. Rev.* **1926**, *28* (6), 1049.
- 65: Koch, W.; Holthausen, M. C. *A Chemist's Guide to Density Functional Theory*; John Wiley & Sons, **2001**.
- 66: Kohn, W.; Sham, L. J. *Phys. Rev.* **1965**, *140* (4A), A1133.
- 67: Zhao, Y.; Truhlar, D. G. *Theor. Chem. Acc.* **2008**, *120* (1-3), 215.
- 68: Peverati, R.; Truhlar, D. G. *Phil Trans R Soc A* **2014**, *372* (2011), 20120476.
- 69: Levine, I. N. *Quantum Chemistry: International Edition*, 6th Edition, 6th ed.; Pearson International Edition, **2007**.
- 70: Klimeš, J.; Michaelides, A. *J. Chem. Phys.* **2012**, *137* (12), 120901.
- 71: Zhao, Y.; Schultz, N. E.; Truhlar, D. G. *J. Chem. Theory Comput.* **2006**, *2* (2), 364.
- 72: Tomasi, J.; Mennucci, B.; Cammi, R. *Chem. Rev.* **2005**, *105* (8), 2999.
- 73: Marenich, A. V.; Cramer, C. J.; Truhlar, D. G. *J. Phys. Chem. B* **2009**, *113* (18), 6378.
- 74: 74, P.; de Paula, J. *Chimie physique ed. 4*; de Boeck, **2013**.
- 75: Sun, J.; Remsing, R. C.; Zhang, Y.; Sun, Z.; Ruzsinszky, A.; Peng, H.; Yang, Z.; Paul, A.; Waghmare, U.; Wu, X.; Klein, M. L.; Perdew, J. P. *Nat. Chem.* **2016**, *8* (9), 831.
- 76: Beljers, H. G.; van der Kint, L.; van Wieringen, J. S. *Phys. Rev.* **1954**, *95* (6), 1683.
- 77: Overhauser, A. W. *Phys. Rev.* **1953**, *92* (2), 411.
- 78: Li, J.-N.; Liu, L.; Fu, Y.; Guo, Q.-X. *Tetrahedron* **2006**, *62* (18), 4453.
- 79: Zhang, S.; Baker, J.; Pulay, P. *J. Phys. Chem. A* **2010**, *114* (1), 425.

- 80: Lide, D. CRC *Handbook of Chemistry and Physics*, CRC, 1997.
- 81: Olmstead, W. N.; Margolin, Z.; Bordwell, F. G. *J. Org. Chem.* **1980**, *45* (16), 3295.
- 82: Kolthoff, I. M.; Chantoni, M. K.; Bhowmik, S. *J. Am. Chem. Soc.* **1968**, *90* (1), 23.
- 83: Crampton, M. R.; Robotham, I. A. *J. Chem. Res. Synop.* **1997**, No. 1, 22.
- 84: Bordwell, F. G.; Algrim, D. *J. Org. Chem.* **1976**, *41* (14), 2507.
- 85: Chmurzynski, L.; Warnke, Z. *Aust. J. Chem.* **1993**, *46* (2), 185.
- 86: Bordwell, F. G. *Acc. Chem. Res.* **1988**, *21* (12), 456.
- 87: Benoit, R. L.; Lefebvre, D.; Fréchette, M. *Can. J. Chem.* **1987**, *65* (5), 996.
- 88: Stewart, J. J. P. *J. Mol. Model.* **2007**, *13* (12), 1173.
- 89: Frisch MJ, Trucks GW, Schlegel HB, Scuseria GE, Robb MA, Cheeseman JR, Scalmani G, Barone V, Mennucci B, Petersson GA, Nakatsuji H, Caricato M, Li X, Hratchian HP, Izmaylov AF, Bloino J, Zheng G, Sonnenberg JL, Hada M, Ehara M, Toyota K, Fukuda R, Hasegawa J, Ishida M, Nakajima T, Honda Y, Kitao O, Nakai H, Vreven T, Montgomery Jr JA, Peralta JE, Ogliaro F, Bearpark M, Heyd JJ, Brothers E, Kudin KN, Staroverov VN, Kobayashi R, Normand J, Raghavachari K, Rendell A, Burant JC, Iyengar SS, Tomasi J, Cossi M, Rega N, Millam JM, Klene M, Knox JE, Cross JB, Bakken V, Adamo C, Jaramillo J, Gomperts R, Stratmann RE, Yazyev O, Austin AJ, Cammi R, Pomelli C, Ochterski JW, Martin RL, Morokuma K, Zakrzewski VG, Voth GA, Salvador P, Dannenberg JJ, Dapprich S, Daniels AD, Farkas Ö, Foresman JB, Ortiz JV, Ciosowski J, Fox DJ (2009) Gaussian09, revision D.01. Gaussian Inc., Wallingford
- 90: Muetterties, E. L.; Mahler, W.; Packer, K. J.; Schmutzler, R. *Inorg. Chem.* **1964**, *3* (9), 1298.
- 91: Barone, V.; Cossi, M. *J. Phys. Chem. A* **1998**, *102* (11), 1995.
- 92: Cossi, M.; Rega, N.; Scalmani, G.; Barone, V. *J. Comput. Chem.* **2003**, *24* (6), 669.
- 93: Farnham, W. B.; Murray, R. K.; Mislow, K. *J. Am. Chem. Soc.* **1970**, *92* (19), 5809.
- 94: Leyris, A. « *Nouvelles méthodes en synthèse asymétrique d'oxydes de phosphines secondaires* », thesis for a PhD in organic chemistry under the supervision of Buono G. **2008**, 151
- 95: Javierre, G.; Fortrie, R.; Jean, M.; Moraleda, D.; Naubron, J.-V.; Fotiadu, F. *J Mol Model* **2017**, *23*, 168

Annexes

1. EXPERIMENTAL SECTION	140
1.1. SYNTHESIS METHODOLOGIES	140
1.1.1. <i>General informations</i>	140
1.1.2. <i>Ethyl hydrogено-phenylphosphinate</i> ⁹⁴	140
1.1.3. <i>N-propyl hydrogено-phenylphosphinate</i>	141
1.1.4. <i>Adamantyl hydrogено-phenylphosphinate</i> ³⁷	141
1.1.5. <i>Methyl hydrogено-phenylphosphinate</i>	141
1.2. KINETIC PROTOCOLE.....	142
1.2.1. <i>Chiral HPLC</i>	142
1.2.2. <i>Experimental procedure</i>	144
1.3. KINETIC MODELING	145
1.3.1. <i>Relative concentration</i>	145
2. THEORETICAL DATA.....	146
2.1. ENERGETIC DATA	146
2.2. SYMMETRY DATA.....	151
2.3. FREQUENCIES.....	154
2.4. MOLECULAR MATRIX.....	160
2.4.1. <i>Methyl hydrogено-phenylphosphinate 1</i>	160
2.4.2. <i>Methanol 2</i>	160
2.4.3. <i>Hydrogено-phenylphosphinous acid 3</i>	161
2.4.4. <i>Methyl hydrogено-hydroxyphenylphosphonium 4</i>	161
2.4.5. <i>Methanolic acid 5</i>	162
2.4.6. <i>Methyl phenylphosphonide 6</i>	162
2.4.7. <i>Methoxide 7</i>	163
2.4.8. <i>Structure 8</i>	163
2.4.9. <i>Anionic TBP 10</i>	164
2.4.10. <i>Anionic TBP 11</i>	164
2.4.11. <i>Anionic TBP 12</i>	165
2.4.12. <i>Anionic TBP 13</i>	165
2.4.13. <i>Structure 14</i>	166
2.4.14. <i>Structure 14-IRC1-R</i>	167
2.4.15. <i>Structure 14-IRC1-P</i>	168
2.4.16. <i>Structure 14-IRC2-R</i>	168
2.4.17. <i>Structures 14-IRC2-P</i>	169
2.4.18. <i>Structure 14-IRC5</i>	169
2.4.19. <i>Structure 14-IRC6</i>	170
2.4.20. <i>Structure 15</i>	170
2.4.21. <i>Structure 15-IRC10</i>	172
2.4.22. <i>Structure 15-IRC16</i>	172
2.4.23. <i>Structure 15-IRC17</i>	173
2.4.24. <i>Structure 16</i>	173
2.4.25. <i>Structure 17</i>	174
2.4.26. <i>Structure 18</i>	174
2.4.27. <i>Structure 19</i>	175
2.4.28. <i>Structure 20</i>	176

2.4.29.	<i>Structure 20-IRC18</i>	176
2.4.30.	<i>Structure 21-IRC11</i>	177
2.4.31.	<i>Structure 22</i>	177
2.4.32.	<i>Structure 22-IRC17</i>	178
2.4.33.	<i>Structure 23</i>	178
2.4.34.	<i>Structure 23-IRC16</i>	179
2.4.35.	<i>Structure 24</i>	179
2.4.36.	<i>Structure 24-IRC14</i>	180
2.4.37.	<i>Structure 25</i>	180
2.4.38.	<i>Structure 25-IRC12</i>	181
2.4.39.	<i>Structure 25-IRC13</i>	181
2.4.40.	<i>Structure 26</i>	182
2.4.41.	<i>Structure 27</i>	182
2.4.42.	<i>Structure 28</i>	183
2.4.43.	<i>Structure 29</i>	184
2.4.44.	<i>B1: Triethylamine 30</i>	185
2.4.45.	<i>Trimethylamine 31</i>	185
2.4.46.	<i>Structure 32</i>	186
2.4.47.	<i>Structure 33</i>	186
2.4.48.	<i>Structure 34</i>	187
2.4.49.	<i>Structure 35</i>	187
2.4.50.	<i>Structure 36</i>	188
2.4.51.	<i>Structure 38</i>	188
2.4.52.	<i>Structure 39</i>	189
2.4.53.	<i>Structure 40</i>	189
2.4.54.	<i>Water 41</i>	190
2.4.55.	<i>Structure 42</i>	190
2.4.56.	<i>Structure 43</i>	191
2.4.57.	<i>Iso-propyl hydrogeno-phenylphosphinate 45</i>	191
2.4.58.	<i>Menthyl hydrogeno-phenylphosphinate 46</i>	192
2.4.59.	<i>tert-butyl hydrogeno-phenylphosphinate 47</i>	192
2.4.60.	<i>Adamantyl hydrogeno-phenylphosphinate 48</i>	193
2.4.61.	<i>Iso-propanol 49</i>	193
2.4.62.	<i>Menthol 50</i>	194
2.4.63.	<i>tert-butanol 51</i>	194
2.4.64.	<i>1-adamantanol 52</i>	195
2.4.65.	<i>Structure TS1</i>	195
2.4.66.	<i>Structure TS2</i>	196
2.4.67.	<i>Structure TS3</i>	197
2.4.68.	<i>Structure TS4</i>	198
2.4.69.	<i>Structure TS5</i>	198
2.4.70.	<i>Structure TS6</i>	199
2.4.71.	<i>Structure TS7</i>	199
2.4.72.	<i>Structure TS8</i>	200
2.4.73.	<i>Structure TS9</i>	201
2.4.74.	<i>Structure TS10</i>	201
2.4.75.	<i>Structure TS10b</i>	202
2.4.76.	<i>Structure TS11</i>	203
2.4.77.	<i>Structure TS12</i>	203
2.4.78.	<i>Structure TS13</i>	204
2.4.79.	<i>Structure TS14</i>	204
2.4.80.	<i>Structure TS15</i>	205

2.4.81.	<i>Structure TS16</i>	205
2.4.82.	<i>Structure TS17</i>	206
2.4.83.	<i>Structure TS18</i>	206
2.4.84.	<i>Structure TS19</i>	207
2.4.85.	<i>Structure TS20</i>	207
2.4.86.	<i>Structure TS21</i>	208
2.4.87.	<i>Structure TS22</i>	209
2.4.88.	<i>Structure TS24</i>	209
2.4.89.	<i>Structure TS25</i>	210
2.4.90.	<i>Structure TS26</i>	210
2.4.91.	<i>A1: Triethylammonium</i>	211
2.4.92.	<i>A2: Acetic acid</i>	211
2.4.93.	<i>B2: Acetate</i>	212
2.4.94.	<i>A3: Oxypyridinic acid</i>	212
2.4.95.	<i>B3: Oxypyridine</i>	213
2.4.96.	<i>A4: Protonated quinuclidine</i>	213
2.4.97.	<i>B4: Quinuclidine</i>	214
2.4.98.	<i>A5: Oxime</i>	214
2.4.99.	<i>B5: Deprotonated oxime</i>	215
2.4.100.	<i>C1-AC</i>	215
2.4.101.	<i>C1-TS</i>	216
2.4.102.	<i>C1-TBP</i>	216
2.4.103.	<i>C3-AC</i>	217
2.4.104.	<i>C3-TS</i>	217
2.4.105.	<i>C3-TBP</i>	218
2.4.106.	<i>D1-AC</i>	218
2.4.107.	<i>D1-TS</i>	219
2.4.108.	<i>D1-TBP</i>	219
2.4.109.	<i>D2-AC</i>	220
2.4.110.	<i>D2-TS</i>	220
2.4.111.	<i>D2-TBP</i>	221
2.4.112.	<i>E1-AC</i>	221
2.4.113.	<i>E1-TS</i>	222
2.4.114.	<i>E1-TBP</i>	222
2.4.115.	<i>E2-AC</i>	223
2.4.116.	<i>E2-TS</i>	223
2.4.117.	<i>E2-TBP</i>	224
2.4.118.	<i>E3-AC</i>	224
2.4.119.	<i>E3-TS</i>	225
2.4.120.	<i>E3-TBP</i>	225
2.4.121.	<i>F1-AC</i>	226
2.4.122.	<i>F1-TS</i>	226
2.4.123.	<i>F1-TBP</i>	227
2.4.124.	<i>F2-AC</i>	227
2.4.125.	<i>F2-TS</i>	228
2.4.126.	<i>F2-TBP</i>	228

1. Experimental section

1.1. Synthesis methodologies

During the thesis, other compounds than ethyl *hydrogeno*-phosphinate have been synthetized. Most of these are not presented in the manuscript because they did not bring interesting data to our study. Nevertheless, in order to describe the complete three year study, we here present these compounds and their synthesis.

1.1.1. General informations

- Reagents and solvents

All reagents were obtained from commercial sources and used as received unless specified otherwise. Solvents THF and dichloromethane were purified and dried over Braun solvent purification system (MB-SPS-800).

- Nuclear Magnetic Resonance (NMR)

^1H and ^{31}P NMR spectra were recorded in CDCl_3 at ambient temperature on Bruker Avance III 400 spectrometers operating at 400 MHz for ^1H . ^{31}P nuclei were observed with ^1H decoupling using 85% phosphoric acid as external reference. Solvent residual signals were used as internal standard. Chemical shifts (δ) and coupling constants (J) are given in ppm and Hz respectively. The peaks patterns are indicated as the following format multiplicity (s: singlet; d: doublet; t: triplet; m: multiplet). The prefix “b” indicates a broadened signal.

- Chiral High-Performance Chromatography

Solvents for chiral chromatography (n-hexane, EtOH) were HPLC grade, degassed and filtered on 0.45 μm membranes before use. The sign given by the chiroptical detector is the sign of the enantiomer in the mobile phase used, at the specified wavelength.

1.1.2. Ethyl *hydrogeno*-phenylphosphinate⁹⁴

- Procedure

A volume of 100 mL of dry THF is put in a dry bicol flask under nitrogen. THF is cooled to 0 °C before 65 mmol of PhPCl_2 are added. Then, 40 mL of ethanol is added dropwise at 0 °C while stirring. The stirring is maintained for 20 hours at room temperature. Then, the solvent is evaporated under reduced pressure to get the ethyl *hydrogeno*-phenylphosphinate with a 95.3% yield.

- NMR data

NMR ^1H (CDCl_3 , 400 MHz): δ 1.10 (t, $^4J = 6.6$ Hz, 3H), 3.88 (m, 2H), 7.32 (d, $^1J_{\text{P-H}} = 563.88$ Hz, 1H), 7.24–7.55 (m, 5H_{arom}). RMN ^{31}P { ^1H } (CDCl_3 , 400 MHz): δ 24.5 (s).

1.1.3. *N*-propyl *hydrogeno*-phenylphosphinate

- Procedure

The same procedure as ethyl *hydrogeno*-phenylphosphinate has been used for the synthesis of *n*-propylphosphinate but using *n*-propanol instead of ethanol.

- NMR data

NMR ^1H (CDCl_3 , 400 MHz): δ 0.9 (t, $^4J = 6.6$ Hz, 3H), 1.7 (m, 2H), 4.00 (m, 2H), 7.55 (d, $^1J_{\text{P-H}} = 562.99$ Hz, 1H), 7.47–7.77 (m, 5H_{arom}). RMN ^{31}P { ^1H } (CDCl_3 , 400 MHz): δ 24.9 (s).

1.1.4. Adamantyl *hydrogeno*-phenylphosphinate³⁷

This compound has been synthetized to test the addition of alcohol in neutral conditions. Since no reaction was noted and because the use of chiral HPLC gave us good results, we decided not to use it afterward.

- Procedure

A solution of 1-adamantanol (56 mmol) and pyridine (56 mmol) in dichloromethane (100 mL) was added dropwise at 0 °C to a solution of dichlorophenylphosphine (56 mmol) in dichloromethane (20 mL) under nitrogen while stirring. After 15 h at room temperature, water (40 mL) was added slowly at 0 °C. The two layers were separated and the aqueous phase was extracted with hexane (3 x 20 mL). The organic layers were collected and concentrated under reduced pressure. Hexane (100mL) was added to the resulting crude product and the organic phase was washed with 10% aqueous sodium bicarbonate solution (100 mL). The aqueous phase was extracted with hexane (3 x 30 mL). The organic layers were collected, dried over MgSO₄, filtered, and concentrated under reduced pressure to get adamantyl *hydrogeno*-phenylphosphinate with a 90% yield.

Both enantiomers can then be separated by chiral HPLC (Lux Cellulose-2 in hexane/ethanol (1/1) at 1 mL/min) to give an access to enantiopure (*R*_P)-AdHP and (*S*_P)-AdHP.

- NMR data

NMR ^1H (CDCl_3 , 400 MHz): δ 1.67 (bs, 6H), 2.15 (bs, 6H), 2.23 (bs, 3H), 7.79 (d, $^1J_{\text{P-H}} = 563.88$ Hz, 1H), 7.71–7.82 (m, 5H_{arom}). RMN ^{31}P { ^1H } (CDCl_3 , 400 MHz): δ 14.2 (s).

1.1.5. Methyl *hydrogeno*-phenylphosphinate^A

^A Wilkening, I.; Signore, G.; Hackenberger, C. *Chem. Commun.* **2011**, 47 (1), 349; Supplementary files: General synthetic procedures, synthesis and characterisation of compounds (p. 7).

Since the DFT models were made onto methyl *hydrogeno*-phenylphosphinate, we wanted to do experimental works on the same compound.

- Procedure

Phenylphosphinic acid (48 mmol) was dissolved in 80 mL dichloromethane and one equivalent formate (48 mmol) was added to the solution followed by one equivalent of pyridine (48 mmol). When the evanescent had stopped, the reaction mixture was refluxed for 15 min. and cooled to room temperature. The reaction mixture was poured into hydrochloric acid (0.1 M, 30 mL) and the organic layer was washed with water (50 mL) and dried over MgSO_4 . The solvent was removed under reduced pressure and the pure methyl *hydrogeno*-phenylphosphinate was obtained without further purification with a 75.2% yield.

After only one night, the whole compound degraded despite the conservation under controlled atmosphere at 4 °C. Consequently, we chose not to work on this compound.

- NMR data

NMR ^1H (CDCl_3 , 400 MHz): 3.29 (d, 3H), 7.03 (d, $^1J_{\text{P-H}} = 568.59$ Hz, 1H), 7.03–7.33 (m, 5H_{arom}). RMN ^{31}P { ^1H } (CDCl_3 , 400 MHz): δ 26.6 (s).

1.2. Kinetic protocole

1.2.1. Chiral HPLC

In the figure below is presented the separation signal of a racemic sample of ethyl *hydrogeno*-phenylphosphinate using Lux-Cellulose-2 chiral HPLC, hexane/ethanol 50/50, 1 mL/min.

Enantiomer	Retention	Time Area	Area %	Capacity factor	Relative RT	Resolution (USP)
(+)	5.28	3750540	49.55	0.76	1.00	0.00
(-)	6.38	3819340	50.45	1.13	1.48	4.90

Table 6-3: Characteristics of separation of racemic ethyl *hydrogeno*-phenylphosphinate on Lux-Cellulose-2 column, hexane/ethanol 50/50, 1 mL/min, UV 254nm and polarimeter. Performed by Nicolas Vanthuyne and

Marion Jean

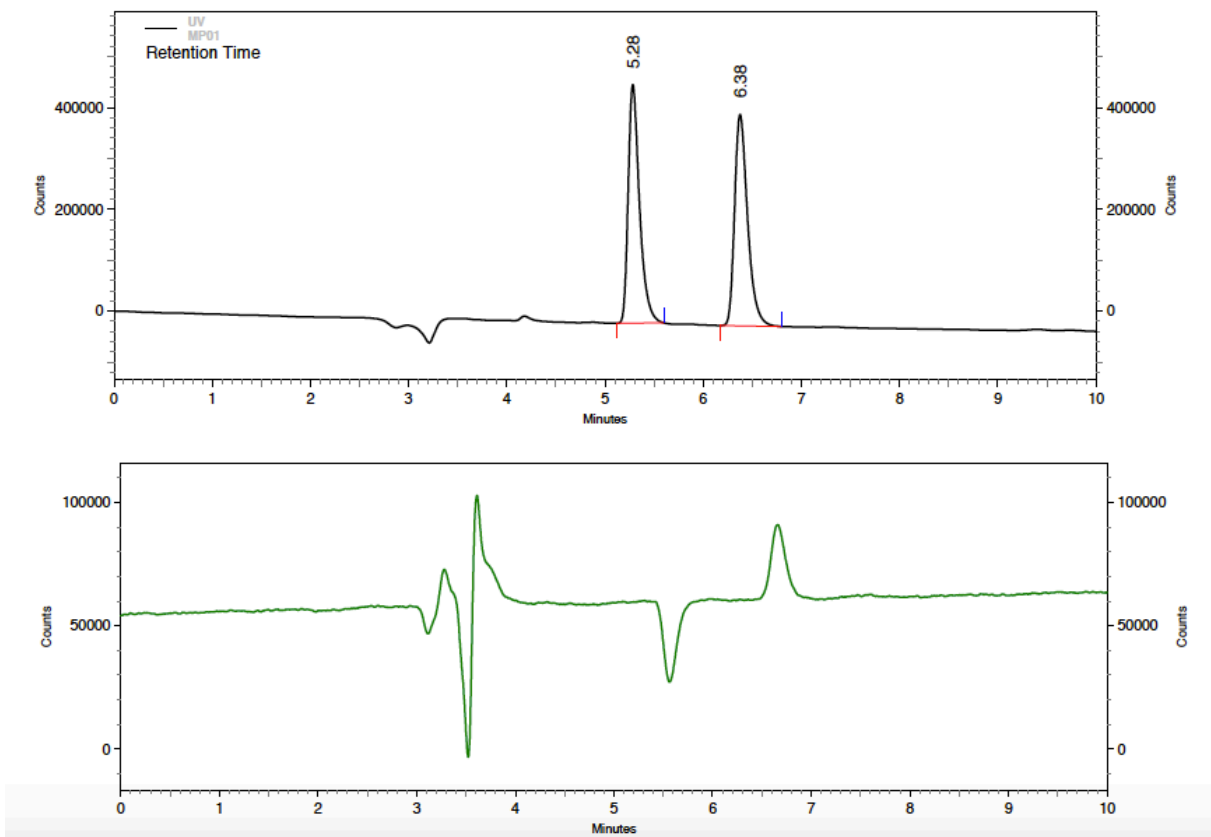


Figure 6-5 : UV spectrum and polarimeter signal for the enantiomeric separation of racemic ethyl *hydrogено*-phosphinate on Lux-Cellulose-2 column, hexane/ethanol 50/50, 1 mL/min, UV 254nm and polarimeter.
Performed by Nicolas Vanthuyne and Marion Jean.

Giving the good results for separation, this column has been used for kinetic studies with the following characteristics: Lux-Cellulose-2, $250 \text{ \AA} \sim 4.6 \text{ mm}$, Cellulose tris(3-chloro-4-methylphenylcarbamate), heptane/ethanol 80/20, 1 mL/min, UV detection at 220 nm, Retention times: 8.2 and 10.8 min.

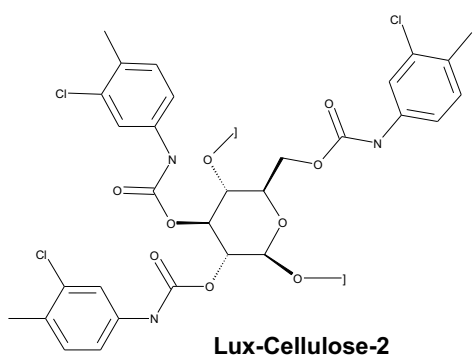


Figure 6-6: Stationary phase of Lux-Cellulose-2 column.

1.2.2. Experimental procedure

1.2.2.1. Neutral conditions

Various concentrations of enantio-enriched ethyl *hydrogeno*-phenylphosphinate was refluxed in 30 mL of ethanol ($C_P = 1.31 \cdot 10^{-2}, 2.60 \cdot 10^{-4}, 1.30 \cdot 10^{-4} \text{ mol.L}^{-1}$) in a bicol flask heated in a oil bath under air. Aliquots of this solution were injected using a syringe on the previously described column to monitor the enantiomeric excess over time.

1.2.2.2. Basic conditions

Solutions S_0 and S_B was prepared by diluting respectively ethyl *hydrogeno*-phenylphosphinate or triethylamine in pure ethanol. The procedure was the same as neutral conditions.

Two solutions were made: S_1 with ethyl *hydrogeno*-phenylphosphinate (86.1 mg) diluted in pure ethanol (5.1 mL), S_{B1} with trimethylamine (0.15 mL) diluted in pure ethanol (5.0 mL). The solutions S_n and S_{Bn} , with n going from 2 to 10, were made by successive dilution of respectively S_1 and S_{B1} respecting volumes presented in Table 6-4:

Solution S_n	Volume of solution S_{n-1} used	Additional volume of ethanol
S_2	$3.00 \text{ mL} \pm 3.0 \cdot 10^{-2}$	$3.00 \text{ mL} \pm 3.0 \cdot 10^{-2}$
S_3	$3.50 \text{ mL} \pm 3.5 \cdot 10^{-2}$	$3.50 \text{ mL} \pm 3.5 \cdot 10^{-2}$
S_4	$4.50 \text{ mL} \pm 4.5 \cdot 10^{-2}$	$4.50 \text{ mL} \pm 4.5 \cdot 10^{-2}$
S_5	$6.50 \text{ mL} \pm 6.5 \cdot 10^{-2}$	$6.50 \text{ mL} \pm 6.5 \cdot 10^{-2}$
S_6	$1.50 \text{ mL} \pm 1.5 \cdot 10^{-2}$	$1.50 \text{ mL} \pm 1.5 \cdot 10^{-2}$
S_7	$1.50 \text{ mL} \pm 1.5 \cdot 10^{-2}$	$1.50 \text{ mL} \pm 1.5 \cdot 10^{-2}$
S_8	$1.50 \text{ mL} \pm 1.5 \cdot 10^{-2}$	$1.50 \text{ mL} \pm 1.5 \cdot 10^{-2}$
S_9	$1.50 \text{ mL} \pm 1.5 \cdot 10^{-2}$	$1.50 \text{ mL} \pm 1.5 \cdot 10^{-2}$
S_{10}	$1.00 \text{ mL} \pm 1.0 \cdot 10^{-2}$	$1.00 \text{ mL} \pm 1.0 \cdot 10^{-2}$
S_{B2}	$2.50 \text{ mL} \pm 1.0 \cdot 10^{-2}$	$2.50 \text{ mL} \pm 1.0 \cdot 10^{-2}$
S_{B3}	$3.00 \text{ mL} \pm 3.0 \cdot 10^{-2}$	$3.00 \text{ mL} \pm 3.0 \cdot 10^{-2}$
S_{B4}	$3.50 \text{ mL} \pm 3.5 \cdot 10^{-2}$	$3.50 \text{ mL} \pm 3.5 \cdot 10^{-2}$
S_{B5}	$4.50 \text{ mL} \pm 4.5 \cdot 10^{-2}$	$4.50 \text{ mL} \pm 4.5 \cdot 10^{-2}$
S_{B6}	$6.50 \text{ mL} \pm 6.5 \cdot 10^{-2}$	$6.50 \text{ mL} \pm 6.5 \cdot 10^{-2}$
S_{B7}	$1.50 \text{ mL} \pm 1.5 \cdot 10^{-2}$	$1.50 \text{ mL} \pm 1.5 \cdot 10^{-2}$
S_{B8}	$1.50 \text{ mL} \pm 1.5 \cdot 10^{-2}$	$1.50 \text{ mL} \pm 1.5 \cdot 10^{-2}$

S_{B9}	$1.50 \text{ mL} \pm 1.5 \cdot 10^{-2}$	$1.50 \text{ mL} \pm 1.5 \cdot 10^{-2}$
S_{B10}	$1.00 \text{ mL} \pm 1.0 \cdot 10^{-2}$	$1.00 \text{ mL} \pm 1.0 \cdot 10^{-2}$

Table 6-4: Volume used for making solutions S_n and S_{Bn} by successive dilution from respectively S_1 and S_{B1}

Then, two sets of solutions M_n were made by mixing 0.5 mL of S_n with 0.5 mL of S_{Bn} . M_1 to M_{10} contains a mix of S_{B6} with S_1 to S_{10} to keep the concentration of triethylamine constant; M_{11} to M_{20} contains a mix of S_5 with S_{B1} to S_{B10} to keep the concentration of ethyl *hydrogeno*-phenylphosphinate constant. Aliquots of M_n solutions were injected on the previously described column to monitor the enantiomeric excess over time.

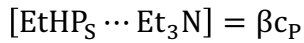
1.2.2.3. Alcohol exchange

A volume of 5 mL of alcohol was added to $0.3 \cdot 10^{-3}$ mol of phosphinate in a flask at room temperature under air. To this solution, 1 equivalent ($0.3 \cdot 10^{-3}$ mol) of TEA, TEAO or H_2O was added. 0.3 mL of the resulting solution was taken and put in a NMR tube. A capillary containing $0.05 \cdot 10^{-3}$ mol of triphenylphosphine diluted in 1 mL of deuterated benzene was put inside the tube to serve as reference. The resulting tube was kept as long as necessary inside the NMR device at 20°C under air to perform the kinetic measurements.

1.3. Kinetic modeling

1.3.1. Relative concentration

- Concentration of ethanol C_E :
 - Ethanol coordinated to TEA: $[\text{EtOH} \cdots \text{Et}_3\text{N}] = \varepsilon c_E$
 - Ethanol coordinated to X: $[\text{EtOH} \cdots \text{X}] = \varepsilon_X c_E$
 - Ethanol not coordinated: $[\text{EtOH}] = (1 - \varepsilon - \varepsilon_X)c_E$
- Concentration of phosphinate C_P :
 - Phosphinate coordinated to TEA: $[\text{EtHP}_R \cdots \text{Et}_3\text{N}] + [\text{EtHP}_S \cdots \text{Et}_3\text{N}] = \beta c_P$
 - Phosphinate coordinated to X: $[\text{EtHP}_R \cdots \text{X}] + [\text{EtHP}_S \cdots \text{X}] = \beta_X c_P$
 - Deprotonated phosphinate: $[\text{EtP}_R^-] + [\text{EtP}_S^-] = \delta c_P$
 - Phosphinate not coordinated: $[\text{EtHP}_R] + [\text{EtHP}_S] = (1 - \beta - \beta_X - \delta)c_P$
- Concentration of triethylamine C_B :
 - Triethylamine coordinated to ethanol: $[\text{EtOH} \cdots \text{Et}_3\text{N}] = \varepsilon c_E$
 - Triethylamine coordinated to phosphinate: $[\text{EtHP}_R \cdots \text{Et}_3\text{N}] +$



- Protonated trimethylamine: $[\text{Et}_3\text{NH}^+] = \tau(1 - y)c_B - \varepsilon c_E - \beta c_P$
- Triethylamine not coordinated: $[\text{Et}_3\text{N}] = (1 - \tau)(1 - y)c_B$
- Concentration of unknown catalyst C_X :
 - X coordinated to ethanol: $[\text{EtOH} \cdots X] = \varepsilon_X c_E$
 - X coordinated to phosphinate: $[\text{EtHP}_R \cdots X] + [\text{EtHP}_S \cdots X] = \beta_X c_P$
 - Protonated X: $[\text{XH}^+] = \tau_X x c_B - \varepsilon_X c_E - \beta_X c_P$
 - X not coordinated: $[X] = (1 - \tau_X) x c_B$

Total k_{app} is then the sum of k for each mechanism weighted by the concentrations of their respective reactants, such as:

$$\begin{aligned} k_{app} = & \frac{c_E}{c^\circ} [(1 - \varepsilon - \varepsilon_X)(1 - \beta - \beta_X - \delta)k_{R0} + (1 - \varepsilon - \varepsilon_X)\delta k_{RPD} \\ & + \varepsilon(1 - \beta - \beta_X - \delta)k_{REA} + \varepsilon_X(1 - \beta - \beta_X - \delta)k_{REAX} \\ & + (1 - \varepsilon - \varepsilon_X)\beta k_{RPA} + (1 - \varepsilon - \varepsilon_X)\beta_X k_{RPAX} + \varepsilon\beta k_{REPA} + \varepsilon_X\beta k_{REXPAX} \\ & + \varepsilon\beta_X k_{REPAX} + \varepsilon_X\beta_X k_{REXPAX}] \end{aligned}$$

In this model, experimental data are T , c_E , c_P , c_B , and k_{app} ; whereas parameters are x , y , $\Delta_r G_{PD}^\circ$, $\Delta_r G_{PDX}^\circ$, $\Delta_r G_{EA}^\circ$, $\Delta_r G_{EAX}^\circ$, $\Delta_r G_{PA}^\circ$, $\Delta_r G_{PAX}^\circ$, $\Delta_r G_{R0}^{0\dagger}$, $\Delta_r G_{RPD}^{0\dagger}$, $\Delta_r G_{REA}^{0\dagger}$, $\Delta_r G_{REAX}^{0\dagger}$, $\Delta_r G_{RPA}^{0\dagger}$, $\Delta_r G_{RPAX}^{0\dagger}$, $\Delta_r G_{REPA}^{0\dagger}$, $\Delta_r G_{REXPAX}^{0\dagger}$, $\Delta_r G_{REPAX}^{0\dagger}$, and $\Delta_r G_{REXPAX}^{0\dagger}$.

Reaction standard molar Gibbs free energies are transformed into equilibrium constants using the following expression.

$$k = \frac{k_B T}{h} \exp\left(-\frac{\Delta_r G^{0\dagger}}{RT}\right)$$

2. Theoretical data

2.1. Energetic data

Units used for describing molecular structures are Ångströms.

Table 6-5. Electronic energies of all calculated molecular structures at various theoretical levels

Acronym	Theory	Solvation model	Description
PM6	Semi-empirical	none	PM6

M+SMD(D)	DFT	SMD(DMSO)	M06-2X/6-31++G(d,p)
M+SMD	DFT	SMD(THF)	M06-2X/6-31++G(d,p)
M+CPCM	DFT	CPCM(THF)	M06-2X/6-31++G(d,p)
B+ SMD	DFT	SMD(THF)	B3LYP/6-31++G(d,p)
B+CPCM	DFT	CPCM(THF)	B3LYP/6-31++G(d,p)

Table 6-6. Electronic energies of all calculated molecular structures at various theoretical levels (part 2).

Structure	Energy (kJ.mol ⁻¹)	Energy (Hartree)				
	PM6	M+SMD(D)	M+SMD	M+CPCM	B+SMD	B+CPCM
1		- 763.802949467	-763.802463471			
2		- 115.676283850	-115.675985552			
3			-764.219988952			
4		- 763.314203133	-763.305672150			
5		- 116.078981086	-116.066787315			
6		- 764.227802710	-764.219988952			
7		- 115.149678512	-115.138144541			
8			-879.001102388			
10			-878.955593085			
11			-878.980561818			
12			-878.970136267			
13			-878.967784124			
14	-612.73		-879.491486654	- 879.486349124	- 879.776116529	- 879.770924716
14-IRC5-R	-589.14		-879.467005800			
14-IRC5-P	-575.39		-879.468409875			
14-IRC6-R	-599,95		-879.487184889			
14-IRC6-P	-576.20		-879.488255990			
14-IRC3	-604.06		-879.490822837			
14-IRC4	-591.16		-879.491269350			
15	-588.86		-879.477474552	- 879.472925024	- 879.747781588	- 879.743363069
15-IRC11			-879.471199636			
15-IRC17			-879.468902745			
15-IRC18			-879.473162730			

Structure	Energy (kJ.mol ⁻¹)	Energy (Hartree)				
		PM6	M+SMD(D)	M+SMD	M+CPCM	B+SMD
16	-561.04		-879.461164677			
17	-586.29		-879.466853373			
18			-879.475107955	<i>leads to 19</i>	- 879.746721574	<i>leads to 13</i>
19			-879.471553655	- 879.467250804	- 879.743812907	- 879.739395338
20			-879.467630596			
20-IRC18			-879.463389330			
21			-879.457761877			
21-IRC11			-879.457211775			
22			-879.464378525			
22-IRC17			-879.464320259			
23			-879.470946563			
23-IRC16			-879.468646094			
24			-879.468341476			
24-IRC14			-879.461163473			
25			-879.468341270			
25-IRC12			-879.464378525			
25-IRC13			-879.464763337			
26			-803.104708584		- 803.352763658	
27			-154.977643306		- 155.062236055	
28			-958.094035625		- 958.423397118	
29			-958.078920240		- 958.393851369	
B1 / 30	- 292.280021589	-292.282016161				
31			-174.393105504			
32			-938.207259832			
33			-938.21214815			
34			-938.189127821			
35			-1053.89551299			
36			-1053.89006527			
38			-1228.28843895			
39			-878.967182611			
40 & 40'			-878.967848066			
41			-76.4019778027			
42			-955.90805995			
43			-955.893134757			

Structure	Energy (kJ.mol ⁻¹)	Energy (Hartree)				
	PM6	M+SMD(D)	M+SMD	M+CPCM	B+SMD	B+CPCM
45			-842.404496637			
46			-1115.05640300			
47			-881.706436887			
48			-1113.90117811			
49			-194.279445044			
50			-466.928166250			
51			-233.581189674			
52			-465.779028662			
TS1			-763.217044503			
TS2	-564.87		-879.449366772	879.444200163	879.726537565	879.721360563
TS3	-539.81		-879.440138072			
TS4	-538.20		-879.443498270			
TS5	-479.21		-879.389507857			
TS6	-491.98		-879.413000547			
TS7			-879.412986784			
TS8			-879.469021897	879.459147446	879.740882987	879.731214833
TS9			-879.471034336	<i>Does not exist</i>	879.742921402	<i>Does not exist</i>
TS10			-879.468308863	879.468309678	879.733776469	879.738272977
TS10b			-879.453793898			
TS11			-879.450396161			
TS12			-879.455039416			
TS13			-879.454949028			
TS14			-879.450591696			
TS15			-879.451946329			
TS16			-879.464022554			
TS17			-879.463751809			
TS18			-879.457749217			
TS19			-879.461077979			
TS20			-958.051544490		958.373484444	
TS21			-938.185564476			
TS22			-1053.88054330			
TS24			-878.965411514			
TS25			-878.957012350			
TS26			-955.878174189			
C1-AC			-958.09467721			

Structure	Energy (kJ.mol ⁻¹)	Energy (Hartree)				
		PM6	M+SMD(D)	M+SMD	M+CPCM	B+SMD
C1-TS			-958.051781526			
C1-TBP			-958.078578255			
C3-AC			-1036.69464363			
C3- TS			-1036.65087646			
C3- TBP			-1036.67476400			
D1-AC			-1230.74786609			
D1- TS			-1230.70553330			
D1- TBP			-1230.72860110			
D2-AC			-1230.74450886			
D2- TS			-1230.70065283			
D2- TBP			-1230.72866910			
E1-AC			-997.395178880			
E1- TS			-997.351322972			
E1- TBP			-997.374779499			
E2-AC			-997.394982861			
E2- TS			-997.350449391			
E2- TBP			-997.374629247			
E3-AC			-1115.29856315			
E3- TS			-1115.25230529			
E3- TBP			-1115.27190182			
F1-AC			-1229.58679073			
F1-TS			-1229.54676483			
F1- TBP			-1229.57381380			
F2-AC			-1229.59028568			
F2- TS			-1229.54681742			
F2- TBP			-1229.57308630			
A1	-292.753952264		-292.745294126			
A2	-229.010521102		-229.009669463			
B2	-228.530228677		-228.519366644			
A3	-323.776546749		-323.768035574			
B3	-323.333813277		-323.334223253			
A4	-329.654968937					
B4	-329.179812030					

Structure	Energy (kJ.mol ⁻¹)	Energy (Hartree)					
		PM6	M+SMD(D)	M+SMD	M+CPCM	B+SMD	B+CPCM
A5		-	631.702186014				
B5		-	631.207718600				

2.2. Symmetry data

Table 6-7. Static and dynamic symmetry groups used for all calculated molecular structures. Static groups are those to which static molecular structures belong. Dynamic groups are those to which belong the molecular structures averaged over their conformational degrees of freedom. Dynamic groups are those that express while molecules are rotating and are used for calculating rotational partition functions, and, consequently, Gibbs free energies.

Structure	Symmetry		Number of rotation operations		Symmetry rotational Gibbs free energy		Gibbs free energy correction
	Static	Dynamic	Static	Dynamic	Static	Dynamic	
1	C ₁	C ₁	1	1	0	0	0
2	C _S	C _S	1	1	0	0	0
3	C ₁	C ₁	1	1	0	0	0
4	C ₁	C ₁	1	1	0	0	0
5	C _S	C _S	1	1	0	0	0
6	C ₁	C ₁	1	1	0	0	0
7	C _{3v}	C _{3v}	3	3	+RTln(3)	+RTln(3)	0
8	C ₁	C ₁	1	1	0	0	0
10	C ₁	C ₁	1	1	0	0	0
11	C ₁	C ₁	1	1	0	0	0
12	C ₁	C ₁	1	1	0	0	0
13	C ₁	C ₁	1	1	0	0	0
14	C ₁	C ₁	1	1	0	0	0
14-IRC5-R	C ₁	C ₁	1	1	0	0	0
14-IRC5-P	C ₁	C ₁	1	1	0	0	0
14-IRC6-R	C ₁	C ₁	1	1	0	0	0
14-IRC6-P	C ₁	C ₁	1	1	0	0	0
14-IRC3	C ₁	C ₁	1	1	0	0	0
14-IRC4	C ₁	C ₁	1	1	0	0	0
15	C ₁	C ₁	1	1	0	0	0
15-IRC11	C ₁	C ₁	1	1	0	0	0
15-IRC17	C ₁	C ₁	1	1	0	0	0
15-IRC18	C ₁	C ₁	1	1	0	0	0
16	C ₁	C ₁	1	1	0	0	0
17	C ₁	C ₁	1	1	0	0	0

Structure	Symmetry		Number of rotation operations		Symmetry rotational Gibbs free energy		Gibbs free energy correction
	Static	Dynamic	Static	Dynamic	Static	Dynamic	
18	C ₁	C ₁	1	1	0	0	0
19	C ₁	C ₁	1	1	0	0	0
20	C ₁	C ₁	1	1	0	0	0
20-IRC19	C ₁	C ₁	1	1	0	0	0
21-IRC12	C ₁	C ₁	1	1	0	0	0
21	C ₁	C ₁	1	1	0	0	0
22	C ₁	C ₁	1	1	0	0	0
22-IRC18	C ₁	C ₁	1	1	0	0	0
23	C ₁	C ₁	1	1	0	0	0
23-IRC17	C ₁	C ₁	1	1	0	0	0
24	C ₁	C ₁	1	1	0	0	0
24-IRC15	C ₁	C ₁	1	1	0	0	0
25	C ₁	C ₁	1	1	0	0	0
25-IRC13	C ₁	C ₁	1	1	0	0	0
25-IRC14	C ₁	C ₁	1	1	0	0	0
26	C ₁	C ₁	1	1	0	0	0
27	C _S	C _S	1	1	0	0	0
28	C ₁	C ₁	1	1	0	0	0
29	C ₁	C ₁	1	1	0	0	0
B1 / 30	C ₃	C _{3v}	3	3	+RTln(3)	+RTln(3)	0
31	C ₃	C _{3v}	3	3	+RTln(3)	+RTln(3)	0
32	C ₁	C _S	1	1	0	0	0
33	C ₁	C _S	1	1	0	0	0
34	C ₁	C _S	1	1	0	0	0
35	C ₁	C _S	1	1	0	0	0
36	C ₁	C _S	1	1	0	0	0
37	C ₁	C _S	1	1	0	0	0
38	C ₁	C _S	1	1	0	0	0
39	C ₁	C _S	1	1	0	0	0
40 & 40'	C ₁	C _S	1	1	0	0	0
41	C ₁	C _S	1	1	0	0	0
42	C _{2v}	C _{2v}	2	2	+RTln(2)	+RTln(2)	0
TS26	C ₁	C _S	1	1	0	0	0
43	C ₁	C _S	1	1	0	0	0
45	C ₃	C _{3v}	3	3	+RTln(3)	+RTln(3)	0
46	C ₁	C _S	1	1	0	0	0
47	C ₁	C _S	1	1	0	0	0
48	C ₁	C _S	1	1	0	0	0

Structure	Symmetry		Number of rotation operations		Symmetry rotational Gibbs free energy		Gibbs free energy correction
	Static	Dynamic	Static	Dynamic	Static	Dynamic	
49	C ₁	C _S	1	1	0	0	0
50	C ₁	C _S	1	1	0	0	0
51	C ₁	C _S	1	1	0	0	0
52	C ₁	C _S	1	1	0	0	0
TS1	C ₁	C ₁	1	1	0	0	0
TS2	C ₁	C ₁	1	1	0	0	0
TS3	C ₁	C ₁	1	1	0	0	0
TS4	C ₁	C ₁	1	1	0	0	0
TS5	C ₁	C ₁	1	1	0	0	0
TS6	C ₁	C ₁	1	1	0	0	0
TS7	C ₁	C ₁	1	1	0	0	0
TS8	C ₁	C ₁	1	1	0	0	0
TS9	C ₁	C ₁	1	1	0	0	0
TS10	C ₁	C ₁	1	1	0	0	0
TS10b	C ₁	C ₁	1	1	0	0	0
TS11	C ₁	C ₁	1	1	0	0	0
TS12	C ₁	C ₁	1	1	0	0	0
TS13	C ₁	C ₁	1	1	0	0	0
TS14	C ₁	C ₁	1	1	0	0	0
TS15	C ₁	C ₁	1	1	0	0	0
TS16	C ₁	C ₁	1	1	0	0	0
TS17	C ₁	C ₁	1	1	0	0	0
TS18	C ₁	C ₁	1	1	0	0	0
TS19	C ₁	C ₁	1	1	0	0	0
TS20	C ₁	C ₁	1	1	0	0	0
TS21	C ₁	C _S	1	1	0	0	0
TS22	C ₁	C _S	1	1	0	0	0
TS24	C ₁	C _S	1	1	0	0	0
TS25	C ₁	C _S	1	1	0	0	0
TS26	C ₁	C _S	1	1	0	0	0
C1-AC	C ₁	C _S	1	1	0	0	0
C1-TS	C ₁	C _S	1	1	0	0	0
C1-TBP	C ₁	C _S	1	1	0	0	0
C3-AC	C ₁	C _S	1	1	0	0	0
C3- TS	C ₁	C _S	1	1	0	0	0
C3- TBP	C ₁	C _S	1	1	0	0	0
D1-AC	C ₁	C _S	1	1	0	0	0
D1- TS	C ₁	C _S	1	1	0	0	0

Structure	Symmetry		Number of rotation operations		Symmetry rotational Gibbs free energy		Gibbs free energy correction
	Static	Dynamic	Static	Dynamic	Static	Dynamic	
D1- TBP	C ₁	C _S	1	1	0	0	0
D2-AC	C ₁	C _S	1	1	0	0	0
D2- TS	C ₁	C _S	1	1	0	0	0
D2- TBP	C ₁	C _S	1	1	0	0	0
E1-AC	C ₁	C _S	1	1	0	0	0
E1- TS	C ₁	C _S	1	1	0	0	0
E1- TBP	C ₁	C _S	1	1	0	0	0
E2-AC	C ₁	C _S	1	1	0	0	0
E2- TS	C ₁	C _S	1	1	0	0	0
E2- TBP	C ₁	C _S	1	1	0	0	0
E3-AC	C ₁	C _S	1	1	0	0	0
E3- TS	C ₁	C _S	1	1	0	0	0
E3- TBP	C ₁	C _S	1	1	0	0	0
F1-AC	C ₁	C _S	1	1	0	0	0
F1- TS	C ₁	C _S	1	1	0	0	0
F1- TBP	C ₁	C _S	1	1	0	0	0
F2-AC	C ₁	C _S	1	1	0	0	0
F2- TS	C ₁	C _S	1	1	0	0	0
F2- TBP	C ₁	C _S	1	1	0	0	0
A1	C ₁	C _S	1	1	0	0	0
A2	C ₁	C _{3v}	3	3	0	+RTln(3)	+RTln(3)
B2	C _S	C _S	1	1	0	0	0
A3	C _S	C _S	1	1	0	0	0
B3	C _S	C _S	1	1	0	0	0
A4	C _{2v}	C _{2v}	2	2	+RTln(2)	+RTln(2)	0
B4	C _{3v}	C _{3v}	3	3	+RTln(3)	+RTln(3)	0
A5	C _{3v}	C _{3v}	3	3	+RTln(3)	+RTln(3)	0
B5	C ₁	C _S	1	1	0	0	0

2.3. Frequencies

Table 6-8. First vibrational frequencies for all calculated molecular structures (part 2).

Structure	First vibrational frequencies (cm ⁻¹)					
	PM6	M+SMD(D)	M+SMD	M+CPCM	B+SMD	B+CPCM
1		31, 75, 129	39, 97, 98			
2		374, 1073, 1102	382, 1073, 1101			
3			25, 103, 152			
4		43, 63, 97	37, 73, 97			
5		294, 762, 896	300, 755, 892			

Structure	First vibrational frequencies (cm ⁻¹)					
	PM6	M+SMD(D)	M+SMD	M+CPCM	B+SMD	B+CPCM
6		25, 101, 140	25, 103, 152			
7		1172, 1192, 1193	1181, 1185, 1191			
8			39, 44, 54			
10			34, 70, 99			
11			36, 84, 107			
12			49, 68, 96			
13			52, 69, 82			
14	24, 52, 59		36, 44, 67	14, 36, 66	2, 33, 51	13, 20 26
15	33, 68, 83		48, 62, 95	52, 87, 111	43, 80, 105	44, 79, 99
16	25, 48, 63		24, 59, 79			
17	28, 58, 89		53, 67, 104			
18			51, 67, 100	<i>leads to 13</i>	47, 84, 98	<i>leads to 13</i>
19			27, 73, 86	28, 75, 82	36, 59, 75	22, 34, 60
14			23, 70, 86			
14- IRC17			37, 86, 100			
15			48, 74, 88			
15- IRC10			22, 67, 84			
16			15, 50, 56			
16- IRC16			41, 47, 59			
17			11, 71, 80			
17- IRC15			46, 85, 130			
18			44, 68, 119			
18- IRC13			57, 77, 84			
19			45, 68, 119			
19- IRC11			15, 50, 56			
19- IRC12			45, 72, 87			
26			40, 40, 65		24, 42, 63	
27			245, 292, 417		251, 294, 410	
28			24, 26, 37		18, 31, 40	
29			46, 61, 72		36, 48, 61	
B1 / 30		84, 118, 122	70, 111, 117			
31			251, 293, 304			
32			17, 29, 32			
33			21, 25, 40			

Structure	First vibrational frequencies (cm ⁻¹)					
	PM6	M+SMD(D)	M+SMD	M+CPCM	B+SMD	B+CPCM
34			17, 29, 32			
35			21, 34, 40			
36			16, 30, 39			
38			22, 34, 41			
39			19, 44, 81			
40 & 40'			55, 85, 91			
41			1585, 3842, 3948			
42			38, 59, 62			
43			30, 44, 67			
45			41, 50, 71			
46			21, 38, 58			
47			34, 40, 50			
48			29, 41, 44			
49			231, 279, 314			
50			90, 102, 143			
51			188, 235, 269			
52			261, 268, 293			
TS1			-580, 48, 100			
TS2	-561, 34, 71		-1178, 34, 77	-1216, 30, 67	-873, 32, 66	-906, 21, 67
TS3	-571, 28, 59		-772, 39, 52			
TS4	-541, 37, 59		-589, 41, 73			
TS5	-497, 27, 39		-892, 26, 44			
TS6	-557, 20, 38		-420, 28, 53			
TS7			-412, 52, 62			
TS8			-139, 27, 64	-149, 38, 75	-140, 40, 86	-144, 41, 71
TS9			-57, 55, 92	<i>does not exist</i>	-51, 48, 96	<i>does not exist</i>
TS10			-97, 27, 58	-100, 27, 58	-310, 38, 68	-107, 33, 53
TS10b			-591, 30, 80			
TS11			-102, 24, 86			
TS12			-82, 48, 92			
TS13			-75, 40, 88			
TS14			-118, 35, 102			
TS15			-141, 33, 64			
TS16			-32, 61, 87			
TS17			-65, 42, 55			

Structure	First vibrational frequencies (cm ⁻¹)					
	PM6	M+SMD(D)	M+SMD	M+CPCM	B+SMD	B+CPCM
TS18			-117, 58, 87			
TS19			-84, 38, 70			
TS20			-1125, 43, 54		-830, 38, 47	
TS21			-1043, 29, 35			
TS22			-64, 39, 41			
TS24			-183, 36, 45			
TS25			-366, 26, 78			
TS26			-1244, 37, 62			
C1-AC			31, 33, 52			
C1-TS			-1209, 31, 42			
C1-TBP			31, 38, 56			
C3-AC			14, 19, 30			
C3- TS			-1077, 38, 47			
C3- TBP			37, 51, 58			
D1-AC			19, 32, 35			
D1- TS			-846, 16, 34			
D1- TBP			24, 39, 56			
D2-AC			15, 23, 28			
D2- TS			-786, 10, 23			
D2- TBP			31, 34, 55			
E1-AC			19, 22, 44			
E1- TS			-1101, 37, 46			
E1- TBP			35, 61, 64			
E2-AC			22, 32, 39			
E2- TS			-901, 48, 57			
E2- TBP			39, 54, 68			
E3-AC			13, 22, 29			
E3- TS			-822, 31, 39			
E3- TBP			41, 49, 53			
F1-AC			16, 28, 38			
F1-TS			-1224, 16, 38			
F1- TBP			42, 62, 67			
F2-AC			31, 38, 47			
F2- TS			-1063, 30, 38			
F2- TBP			35, 57, 64			
A1	67, 110, 121	62, 117, 133				
A2	58, 444, 550	79, 443, 550				
B2	41, 447, 629	19, 450, 626				
A3	191, 219, 412	206, 219, 406				

Structure	First vibrational frequencies (cm ⁻¹)					
	PM6	M+SMD(D)	M+SMD	M+CPCM	B+SMD	B+CPCM
B3		226, 421, 483	225, 420, 486			
A4		143, 296, 298				
B4		85, 295, 298				
A5		25, 63, 74				
B5		45, 70, 84				

2.4. Molecular matrix

2.4.1. Methyl *hydrogeno-phenylphosphinate* **1**

2.4.1.1. SMD(DMSO)//M06-2X/6-31++G(d,p)

```

P  1.38286200  0.41883700 -0.60156500
H  1.57847800  0.26955200 -1.97880500
O  1.90546900  1.68799800 -0.01252000
C  -0.37407200  0.16591500 -0.27233800
C  -1.00217900 -1.02589800 -0.65378300
C  -1.10534600  1.17560500  0.35850200
C  -2.36035800 -1.20318500 -0.40116300
H  -0.43477200 -1.81417200 -1.14306800
C  -2.46484000  0.99332200  0.61195200
H  -0.60647000  2.09531100  0.65139800
C  -3.09013300 -0.19373600  0.23119700
H  -2.85023500 -2.12661700 -0.69485900
H  -3.03298700  1.77648400  1.10457000
H  -4.14885600 -0.33550800  0.42760200
O  2.10600700 -0.94498600 -0.12750300
C  2.11259900 -1.25418700  1.27614500
H  1.09013400 -1.33819100  1.65912000
H  2.61932100 -2.21318500  1.38112500
H  2.65662000 -0.48733000  1.83350300

```

2.4.1.2. SMD(THF)//M06-2X/6-31++G(d,p)

```

P  -1.23662     0.39689    0.39185
H  -1.55563     0.03048    1.71339
O  -1.67442     1.78198    0.05214
C   0.51739     0.08505    0.15134
C   1.05578    -1.19714    0.31137
C   1.34542     1.16404   -0.16780
C   2.42385    -1.39580    0.14454
H   0.41033    -2.03547    0.56022
C   2.71433     0.95923   -0.33722
H   0.91381     2.15391   -0.28664
C   3.25104    -0.31821   -0.18042
H   2.84580    -2.38882    0.26463
H   3.35881     1.79529   -0.59046
H   4.31738    -0.47736   -0.31126
O  -1.89806    -0.80484   -0.45983
C  -3.32612    -0.94269   -0.39203
H  -3.81497    -0.11456   -0.91112
H  -3.57425    -1.88282   -0.88418
H  -3.66239    -0.97806    0.65046

```

2.4.2. Methanol **2**

2.4.2.1. SMD(DMSO)//M06-2X/6-31++G(d,p)

```

C  0.66571000  -0.01998000  0.00002100
H  1.09103700   0.98569700 -0.00106400
H  1.01984700  -0.55012300 -0.89204100
H  1.01996200  -0.54834000  0.89309900
O  -0.74784200   0.12371500 -0.00002200
H  -1.14236600  -0.75707500  0.00006100

```

2.4.2.2. SMD(THF)//M06-2X/6-31++G(d,p)

```

C   0.66566      -0.02016     0.00001
H   1.09010      0.98589   -0.00112
H   1.01978      -0.54991   -0.89257
H   1.01995      -0.54809     0.89360
O   -0.74746      0.12360     0.00001
H   -1.14412     -0.75576   -0.00005

```

2.4.3. Hydrogeno-phenylphophinous acid **3**

2.4.3.1. SMD(THF)//M06-2X/6-

31++G(d,p)

P	-1.31477	0.38396	-0.59999
H	-1.63198	0.52379	-1.94647
O	-2.17319	-0.86568	-0.18673
C	-2.13479	-1.42244	1.16023
H	-2.57322	-0.70883	1.85910
H	-2.73542	-2.32811	1.11444
H	-1.10662	-1.66121	1.43888
O	-1.71708	1.69943	0.18562
C	0.40478	0.15970	-0.25461
C	1.16139	1.20079	0.29612
C	0.98738	-1.07463	-0.57697
C	2.51715	0.99464	0.53389
H	0.69900	2.15172	0.54017
C	2.34341	-1.26328	-0.33534
H	0.39361	-1.87865	-1.00532
C	3.10343	-0.23074	0.21789
H	3.11382	1.79163	0.96503
H	2.80709	-2.21415	-0.57592
H	4.16149	-0.38507	0.40586
H	-2.58057	2.09526	-0.03423

2.4.4. Methyl hydrogeno-

hydroxyphenylphosphonium **4**

2.4.4.1. SMD(DMSO)//M06-2X/6-

31++G(d,p)

P	1.32996100	0.35164600	-0.61781700
H	1.66504400	0.42966600	-1.96495600
O	1.74755800	1.68581200	0.12763100
C	-0.39717600	0.16572100	-0.27847700
C	-1.00457600	-1.04691900	-0.63351800
C	-1.12720600	1.19618100	0.32409800
C	-2.35963900	-1.22337900	-0.37665200
H	-0.43158200	-1.84425500	-1.10026600
C	-2.48209500	1.00202200	0.57926600
H	-0.64598000	2.13006300	0.59608800
C	-3.09390500	-0.20137000	0.22859100
H	-2.84173800	-2.15746000	-0.64571400
H	-3.05723200	1.79121900	1.05217300
H	-4.15081600	-0.34694300	0.43023600
O	2.14770500	-0.90302300	-0.13788800
C	2.06087900	-1.39542100	1.23080400
H	1.02250800	-1.40189200	1.56816000
H	2.45375000	-2.40926900	1.20010100
H	2.67617400	-0.76473300	1.87312200
H	2.62065500	2.05559300	-0.10430300

2.4.4.2. SMD(THF)//M06-2X/6-

31++G(d,p)

P	-1.31477	0.38396	-0.59999
H	-1.63198	0.52379	-1.94647
O	-2.17319	-0.86568	-0.18673
C	-2.13479	-1.42244	1.16023
H	-2.57322	-0.70883	1.85910
H	-2.73542	-2.32811	1.11444
H	-1.10662	-1.66121	1.43888
O	-1.71708	1.69943	0.18562
C	0.40478	0.15970	-0.25461
C	1.16139	1.20079	0.29612
C	0.98738	-1.07463	-0.57697
C	2.51715	0.99464	0.53389
H	0.69900	2.15172	0.54017
C	2.34341	-1.26328	-0.33534
H	0.39361	-1.87865	-1.00532
C	3.10343	-0.23074	0.21789
H	3.11382	1.79163	0.96503
H	2.80709	-2.21415	-0.57592
H	4.16149	-0.38507	0.40586
H	-2.58057	2.09526	-0.03423

2.4.5. Methanolic acid **5**

2.4.5.1. SMD(DMSO)//M06-2X/6-

31++G(d,p)

C	0.77901600	0.00000200	0.01850200
H	1.10257600	0.90068300	-0.49605800
H	1.10268700	-0.90021100	-0.49680300
H	1.04003500	-0.00043400	1.07430100
O	-0.71005900	0.00000100	-0.09907100
H	-1.11943300	-0.80129600	0.30002700
H	-1.11948600	0.80123500	0.30008700

2.4.5.2. SMD(THF)//M06-2X/6-

31++G(d,p)

C	0.780193	-0.000088	0.018560
H	1.101837	0.900545	-0.497601
H	1.102563	-0.899319	-0.499528
H	1.044025	-0.000446	1.073660
O	-0.709698	-0.000096	-0.096187
H	-1.126136	-0.801913	0.291335
H	-1.125868	0.802429	0.290265

2.4.6. Methyl phenylphosphonide **6**

2.4.6.1. SMD(DMSO)//M06-2X/6-

31++G(d,p)

P	1.51018500	0.22654400	-0.85807800
O	1.96960600	1.54764800	-0.20606000
C	-0.30678300	0.10694000	-0.37342600
C	-1.07463500	-1.00077500	-0.75453900
C	-0.93161700	1.14229000	0.32769900
C	-2.42906500	-1.08341500	-0.42861900
H	-0.60606800	-1.81271900	-1.31084300
C	-2.28822200	1.07066300	0.65640100
H	-0.33168500	2.00339900	0.61645900
C	-3.03929500	-0.04390000	0.27906400
H	-3.01063100	-1.95239800	-0.72559800
H	-2.76192500	1.88163800	1.20415500
H	-4.09498800	-0.10122400	0.52968000
O	2.04778400	-1.05787000	0.13307600
C	1.84151700	-0.94872300	1.53026700
H	0.79375700	-1.14718800	1.79639800
H	2.47167700	-1.69391400	2.02595800
H	2.11656900	0.04753300	1.89775900

2.4.6.2. SMD(THF)//M06-2X/6-

31++G(d,p)

P	-1.51118	0.23201	-0.86109
O	-1.96456	1.54527	-0.19171
O	-2.04250	-1.06296	0.12650
C	-1.85647	-0.94406	1.52358
H	-2.16235	0.04616	1.88346
H	-2.47156	-1.70530	2.01504
H	-0.80636	-1.11129	1.80391
C	0.30883	0.10557	-0.37333
C	1.07469	-1.00652	-0.74480
C	0.93604	1.14483	0.31932
C	2.42868	-1.08992	-0.41791
H	0.60204	-1.82101	-1.29383
C	2.29244	1.07320	0.64829
H	0.33471	2.00758	0.60063
C	3.04156	-0.04582	0.28064
H	3.00836	-1.96288	-0.70748
H	2.76760	1.88792	1.18952
H	4.09721	-0.10346	0.53208

2.4.7. Methoxide **7**

2.4.7.1. SMD(DMSO)//M06-2X/6- 31++G(d,p)

```
C -0.55301000 -0.00003100 0.00007300
H -1.02724300 -1.00549200 0.17206300
H -1.02806300 0.35349200 -0.95626300
H -1.02779700 0.65178100 0.78406700
O 0.80014500 0.00005100 -0.00003800
```

2.4.7.2. SMD(THF)//M06-2X/6- 31++G(d,p)

```
C -0.55072300 -0.00008400 0.00004500
H -1.02914500 -1.01396600 0.11234000
H -1.02866600 0.40980100 -0.93417700
H -1.02899000 0.60469600 0.82146300
O 0.79889300 -0.00000300 0.00001300
```

2.4.8. Structure **8**

2.4.8.1. SMD(THF)//M06-2X/6- 31++G(d,p)

```
C -3.36935900 -0.11731900 -0.94331400
C -3.67214200 -1.02253600 0.07737100
C -2.65628300 -1.48748100 0.91370800
C -1.34345700 -1.04580300 0.73054900
C -1.02923300 -0.13530600 -0.28163200
C -2.05496000 0.31498900 -1.12165900
P 0.74059000 0.43406700 -0.54713000
O 0.48373900 2.06302200 -0.13599800
C -0.03852900 2.35146300 1.15052000
O 1.47265100 -0.21943200 0.66175700
O 3.92445700 -1.08411900 0.55033200
C 4.23995600 -0.96654400 -0.81215500
H 2.98438500 -0.75367000 0.65229400
H 0.42334600 1.71689800 1.91663500
H 0.18134100 3.39943700 1.37662000
H -1.12717700 2.20564800 1.17779500
H -0.53866900 -1.39184800 1.37615500
H -1.82379600 1.01802300 -1.92161100
H -2.88821000 -2.19320300 1.70761900
H -4.15667100 0.24633300 -1.59866100
H -4.69385400 -1.36540500 0.21613500
H 4.19589400 0.07579400 -1.16504600
H 3.56993200 -1.56351100 -1.45038200
H 5.26188200 -1.33003700 -0.96966800
```

2.4.9. Anionic TBP **10**

2.4.9.1. SMD(THF)//M06-2X/6- 31++G(d,p)

```

C  3.58817200   0.07128200  -0.33236300
C  2.93307200  -1.13210700  -0.07154400
C  1.56623100  -1.13837900   0.20987700
C  0.81122500   0.04482300   0.20876100
C  1.48685000   1.24573500  -0.05806000
C  2.85939700   1.26031500  -0.31564200
P  -1.02127800  -0.13862000   0.57559200
O  -1.14603500   1.59325200  -0.05644600
C  -2.41233000   2.15407100  -0.02039500
O  -1.93092700  -0.47174400  -0.79891700
C  -2.26607900  -1.81266900  -1.10497400
O  -0.98030700  -1.54578800   1.22411000
H  -1.68033000   0.49399100   1.67341200
H  -2.70476700  -2.33186600  -0.24977300
H  -2.98908700  -1.77126700  -1.92677800
H  -1.38848100  -2.38148000  -1.43635100
H  1.05217100  -2.06249600   0.45390700
H  0.92485600   2.17052000  -0.06396000
H  3.48822000  -2.06664400  -0.07552500
H  3.35906000   2.20650800  -0.50778600
H  4.65465900   0.08331000  -0.54122300
H  -3.03386300   1.84785600  -0.87694500
H  -2.33584800   3.25129600  -0.02620400
H  -2.96849200   1.87538200   0.89940300

```

2.4.10. Anionic TBP **11**

2.4.10.1. SMD(THF)//M06-2X/6- 31++G(d,p)

```

P   1.10109800   0.00092500  -0.00155200
H   1.85960900   0.21596100  -1.19080500
O   1.01667000   1.77592700   0.08566600
C   2.26330100   2.39651300   0.16833300
H   2.97779300   1.99032500  -0.57391200
H   2.14975000   3.46837900  -0.03776500
H   2.71945100   2.27469200   1.16096600
O   1.85254300  -0.27880500   1.29229800
C   -0.74305400   0.03012900  -0.01681100
C   -1.43211300  -0.83651000   0.83747100
C   -1.47681500   0.88394200  -0.84519900
C   -2.82642300  -0.84188800   0.87466400
H   -0.86563300  -1.50901800   1.47603400
C   -2.87271000   0.86289300  -0.83106200
H   -0.95177700   1.57530700  -1.49718900
C   -3.55159000   0.00478500   0.03410400
H   -3.34779200  -1.51127200   1.55388500
H   -3.43051100   1.52544500  -1.48768900
H   -4.63788600  -0.00368900   0.05507600
C   2.15199800  -2.33939900  -0.75785100
H   2.90977100  -1.70504100  -1.25861600
H   2.00120800  -3.22776800  -1.38465200
H   2.57809800  -2.65622900   0.20500000
O   0.93652300  -1.67384200  -0.60033200

```

2.4.11. Anionic TBP **12**

2.4.11.1. SMD(THF)//M06-2X/6- 31++G(d,p)

```
P -1.10746800  0.00153600  0.63360100
H -1.03442300  1.41772800  1.00944600
O -2.16410200  0.48361000  -0.60125600
C -2.61492400  1.81851100  -0.66709200
H -1.80899300  2.51758700  -0.92572800
H -3.37416100  1.85918900  -1.45446300
H -3.07114200  2.14995100  0.27411300
O -1.55578500  -0.52318700  1.99249000
C 0.72690100   0.10817200  0.23721900
C 1.55965000   -1.02014100  0.25026200
C 1.31519800   1.35495100  0.00823100
C 2.93403000   -0.90254200  0.04756700
H 1.11233200   -1.99515400  0.42073100
C 2.68625900   1.47961100  -0.23052300
H 0.69204400   2.24736300  0.02348300
C 3.50163200   0.34907500  -0.20353100
H 3.56377000   -1.78784000  0.07926600
H 3.11801200   2.45825300  -0.42343800
H 4.57105900   0.44128300  -0.37229200
C -0.98171000  -1.70809600  -1.51600000
H -1.92749000  -1.60995800  -2.06839500
H -0.56160500  -2.70358100  -1.72170200
H -0.28282700  -0.96436900  -1.93165400
O -1.17346000  -1.57676600  -0.13750700
```

2.4.12. Anionic TBP **13**

2.4.12.1. SMD(THF)//M06-2X/6- 31++G(d,p)

```
P 1.09142800  0.33636700  -0.35545800
O 1.34440200  -0.32041000  1.16245400
C 0.44837200  -0.10698500  2.23626700
H -0.41210800  -0.78498200  2.19696500
H 1.00885000  -0.30163800  3.15577000
H 0.08185300  0.92572200  2.26581300
O 1.05933600  1.84013400  -0.56096700
C 3.40705900  -1.06344200  -0.51382500
H 3.60138900  -1.36894600  0.52629300
H 4.35787900  -1.08380500  -1.06344000
H 2.75602600  -1.83882700  -0.96558000
O 2.85030600  0.20868400  -0.59532500
C -0.82876200  0.07982000  -0.25494600
C -1.73642300  1.12831700  -0.06274400
C -1.35808500  -1.20248300  -0.44297900
C -3.11586600  0.90564700  -0.04115400
H -1.33961100  2.13353700  0.05934900
C -2.73372900  -1.44500300  -0.41835800
H -0.67574900  -2.03745500  -0.61707100
C -3.62001900  -0.38521700  -0.21521800
H -3.80071500  1.73785000  0.10532700
H -3.11613500  -2.45267200  -0.56354200
H -4.69213400  -0.56239500  -0.20166500
H 1.05139300  -0.70309200  -1.33791600
```

2.4.13. Structure 14

2.4.13.1. PM6

P	0.00000000	0.00000000	0.00000000
H	1.44479600	0.00000000	0.00000000
O	-0.76866961	1.30808925	0.00000000
C	-0.53465859	-1.30600255	-1.19391273
C	-0.51420594	-2.63828368	-0.78100667
C	-0.95622848	-0.94895956	-2.47167324
C	-0.92025397	-3.63663761	-1.67297160
H	-0.19535028	-2.91779697	0.22806280
C	-1.36194610	-1.95247748	-3.36241713
H	-0.96868304	0.09812783	-2.79764991
C	-1.34309309	-3.29126404	-2.96214182
H	-0.90952451	-4.67983113	-1.36505148
H	-1.69304259	-1.68683585	-4.36412070
H	-1.65976292	-4.07015714	-3.65500570
O	-0.19362935	-0.77272343	1.49559267
C	-1.49213451	-0.59128460	2.09310798
H	-1.31870126	-0.84988043	3.14628318
H	-1.84557599	0.44840298	2.01277632
H	-2.20730171	-1.28831329	1.64028398
O	0.59907003	1.33626999	-1.84334607
C	1.86980380	1.82558366	-2.28944528
H	2.39902973	0.93612125	-2.65100109
H	1.72152567	2.53866878	-3.10695264
H	2.41029246	2.29154789	-1.45922068
H	0.01388937	2.09870199	-1.48766810

2.4.13.2. SMD(THF)//M06-2X/6-

31++G(d,p)

P	-0.57689	1.15306	-0.47805
H	-0.82764	1.19332	-1.85377
O	-1.78791	0.94743	0.38025
C	0.70372	-0.08303	-0.18916
C	0.41118	-1.21433	0.57847
C	1.97724	0.08145	-0.74841
C	1.39456	-2.18154	0.78565
H	-0.58055	-1.33971	1.00690
C	2.95479	-0.88797	-0.53898
H	2.20656	0.96399	-1.34091
C	2.66208	-2.01836	0.22731
H	1.16854	-3.06071	1.38097
H	3.94283	-0.76246	-0.97086
H	3.42565	-2.77359	0.38792
O	0.14597	2.58231	-0.32700
C	0.56282	2.99401	0.98768
H	1.25577	2.26502	1.42032
H	1.06918	3.95071	0.86386
H	-0.30640	3.11615	1.63827
O	-3.05896	-1.49789	0.60834
C	-2.93882	-1.81569	-0.76249
H	-1.89383	-1.78433	-1.10711
H	-3.30914	-2.83434	-0.90543
H	-3.53299	-1.14194	-1.39448
H	-2.72280	-0.58998	0.71194

2.4.13.3. CPCM(THF)//M06-2X/6-

31++G(d,p)

P	-0.28461	1.27499	-0.61053
H	-0.29867	1.48259	-1.99268
O	-1.63999	1.18284	0.02217
C	0.74947	-0.15837	-0.26533
C	0.19145	-1.28768	0.34078
C	2.10523	-0.13999	-0.61653
C	0.99345	-2.40043	0.59362

H	-0.85911	-1.29282	0.62123
C	2.90013	-1.25412	-0.36208
H	2.53775	0.74338	-1.07963
C	2.34257	-2.38330	0.24174
H	0.56441	-3.27806	1.06605
H	3.95137	-1.24236	-0.63081
H	2.96379	-3.25093	0.44111
O	0.59357	2.55784	-0.19590
C	0.89093	2.76505	1.19627
H	1.44601	1.91212	1.59861
H	1.50590	3.66147	1.24707
H	-0.03264	2.91261	1.76007
O	-3.23240	-0.95580	0.75048
C	-3.48454	-1.47858	-0.54020
H	-2.55352	-1.65199	-1.09787
H	-3.99508	-2.43625	-0.41849
H	-4.12516	-0.81369	-1.13205
H	-2.73746	-0.12527	0.63170

2.4.13.4. SMD(THF)//B3LYP/6-

31++G(d,p)

P	-0.35847	0.90390	-0.59574
H	-0.39391	1.12166	-1.98258
O	-1.62535	0.33656	-0.00933
C	1.09870	-0.11529	-0.24500
C	0.95368	-1.31451	0.46882
C	2.36744	0.27639	-0.70627
C	2.07262	-2.11028	0.73074
H	-0.02845	-1.61934	0.81693
C	3.48160	-0.52319	-0.44391
H	2.48860	1.20100	-1.26488
C	3.33433	-1.71550	0.27516
H	1.95727	-3.03690	1.28575
H	4.46161	-0.21804	-0.79959
H	4.20307	-2.33569	0.47818
O	0.00406	2.42308	-0.15515
C	0.15596	2.76178	1.24585
H	0.90950	2.12610	1.72179
H	0.48647	3.80092	1.27062
H	-0.80030	2.66516	1.76686
O	-3.64777	-1.52239	-0.50552
C	-4.74368	-1.12419	0.30838
H	-5.11833	-0.12551	0.03800
H	-5.55294	-1.84535	0.15472
H	-4.48574	-1.11990	1.37806
H	-2.92120	-0.88196	-0.37035

2.4.13.5. CPCM(THF)//B3LYP/6-

31++G(d,p)

P	-0.40127	0.81040	-0.54219
H	-0.53743	0.94838	-1.93297
O	-1.60314	0.22364	0.15336
C	1.11646	-0.12417	-0.22538
C	1.04989	-1.33309	0.48413
C	2.35214	0.33739	-0.71086
C	2.21411	-2.07151	0.71364
H	0.09249	-1.68630	0.85378
C	3.51175	-0.40534	-0.48104
H	2.41103	1.27220	-1.26150
C	3.44243	-1.60900	0.23083
H	2.16125	-3.00520	1.26538
H	4.46602	-0.04721	-0.85538
H	4.34595	-2.18506	0.40811
O	-0.08132	2.36518	-0.21058
C	0.11902	2.79956	1.15715
H	0.96056	2.26798	1.61081
H	0.34231	3.86473	1.10369

H	-0.78913	2.63781	1.74248
O	-3.65210	-1.58727	-0.37021
C	-4.85090	-1.02760	0.15662
H	-5.11666	-0.08399	-0.34032
H	-5.65581	-1.74710	-0.01775
H	-4.77811	-0.84492	1.23788
H	-2.92036	-0.95721	-0.21252

2.4.14. Structure **14-IRC1-R**

2.4.14.1. PM6

P	0.00000000	0.00000000	0.00000000
H	1.44292587	0.00000000	0.00000000
O	-0.65177498	1.36159998	0.00000000
C	-0.58336618	-1.05086197	1.40597124
C	-1.75133044	-0.63027548	2.04305217
C	0.09975045	-2.18906352	1.82581937
C	-2.25125119	-1.37365504	3.11883514
H	-2.27749089	0.27811613	1.72469353
C	-0.40380606	-2.93071610	2.90197486
H	1.02080557	-2.52272115	1.33334336
C	-1.57726473	-2.52293152	3.54476157
H	-3.16029697	-1.05506644	3.62474431
H	0.11911644	-3.82302054	3.23879369
H	-1.96634285	-3.10105861	4.38231305
O	-0.44229808	-0.81890482	-1.41831607
C	-1.77318715	-0.49337196	-1.87620688
H	-1.73660224	-0.74264610	-2.94418935
H	-2.49989702	-1.12654527	-1.35462915
H	-2.01165551	0.57584864	-1.74697772
O	1.34168370	-2.00533219	-0.66186545
C	2.58234416	-2.00223989	-1.39307769
H	2.86646741	-3.02939281	-1.64118501
H	2.48274271	-1.39061159	-2.29641698
H	3.30794578	-1.56041190	-0.70036923
H	0.62878286	-2.42498172	-1.23140061

2.4.14.2. SMD(THF)//M06-2X/6-

31++G(d,p)

P	0.43270	-1.15613	-0.59181
H	1.14646	-0.56295	-1.64069
O	0.11746	-2.60416	-0.74368
C	-1.01584	-0.13057	-0.28103
C	-2.28193	-0.72077	-0.26156
C	-0.87227	1.24693	-0.07507
C	-3.40814	0.06781	-0.02788
H	-2.37844	-1.79087	-0.42563
C	-2.00036	2.03014	0.15614
H	0.11460	1.70745	-0.09697
C	-3.26599	1.43964	0.17996
H	-4.39401	-0.38754	-0.00884
H	-1.89322	3.09896	0.31668
H	-4.14437	2.05278	0.36173
O	1.47585	-0.77998	0.59957
C	1.15016	-1.19493	1.93977
H	1.91414	-0.76905	2.59072
H	0.16557	-0.81463	2.23197
H	1.16932	-2.28500	2.00835
O	2.70670	1.75372	0.15097
C	3.81648	1.44287	-0.67544
H	4.60336	0.91634	-0.12007
H	3.52508	0.83100	-1.53973
H	4.22403	2.38741	-1.04350
H	2.32431	0.91471	0.45888

2.4.15. Structure **14**-IRC1-P

2.4.15.1. PM6

P	0.00000000	0.00000000	0.00000000
H	1.45424794	0.00000000	0.00000000
O	-0.58488927	1.38508600	0.00000000
C	-0.36733447	-1.12139462	1.43035177
C	-0.78548570	-0.55706825	2.63296959
C	-0.21840896	-2.49895462	1.28323319
C	-1.04991823	-1.39644969	3.72319380
H	-0.91529650	0.52350924	2.74408090
C	-0.48754636	-3.33349021	2.37468684
H	0.09607095	-2.94118331	0.33374283
C	-0.89969417	-2.78058209	3.59226294
H	-1.37214713	-0.97064328	4.67138926
H	-0.37496020	-4.41131696	2.27678694
H	-1.10476176	-3.43146370	4.44147996
O	-2.30921306	-0.40425148	-0.33888252
C	-3.27399518	0.43523477	0.32746654
H	-4.22841374	0.37744557	-0.19942726
H	-3.36783985	0.14591683	1.37671079
H	-2.82921782	1.44468053	0.24054310
O	-0.25050445	-1.00462086	-1.33791665
C	-0.68603623	-0.30135007	-2.52239860
H	-1.01018183	-1.11680966	-3.18189992
H	-1.53054758	0.37371988	-2.31061509
H	0.15716330	0.23897814	-2.96725760
H	-2.57484603	-1.34777177	-0.27558409

2.4.15.2. SMD(THF)//M06-2X/6-

31++G(d,p)

P	1.27223	1.12688	0.13926
H	1.59305	1.80439	1.32731
O	1.78746	1.79236	-1.08982
C	-0.49301	0.79961	0.16459
C	-1.24098	1.03615	-0.99163
C	-1.11133	0.32037	1.32494
C	-2.61209	0.78162	-0.98923
H	-0.74971	1.41659	-1.88354
C	-2.48156	0.07218	1.32329
H	-0.52767	0.13739	2.22493
C	-3.22922	0.30112	0.16602
H	-3.19654	0.96208	-1.88669
H	-2.96535	-0.30158	2.22105
H	-4.29795	0.10566	0.16676
O	0.59171	-2.60917	-0.86837
C	-0.71023	-2.75318	-0.32930
H	-0.69527	-2.80528	0.76782
H	-1.37524	-1.93506	-0.63761
H	-1.11826	-3.69259	-0.71192
O	1.85719	-0.36078	0.43613
C	3.28594	-0.50537	0.53994
H	3.46981	-1.51930	0.89562
H	3.75157	-0.36137	-0.43776
H	3.69007	0.21460	1.25973
H	1.00206	-1.82297	-0.46979

2.4.16. Structure **14**-IRC2-R

2.4.16.1. PM6

P	0.00000000	0.00000000	0.00000000
H	1.44577300	0.00000000	0.00000000
O	-0.78869525	1.28087964	0.00000000
C	-0.41473599	-1.05156772	1.48226992
C	0.15534449	-2.31214709	1.64484401
C	-1.30918797	-0.53444055	2.41515188
C	-0.17547476	-3.07181211	2.77298679
H	0.84906702	-2.72732927	0.91129932
C	-1.63764018	-1.29600047	3.54506758
H	-1.75968078	0.45621412	2.28106019
C	-1.06997606	-2.56101907	3.72116061
H	0.26177755	-4.05776922	2.91402772
H	-2.33319120	-0.90186391	4.28304839
H	-1.32399568	-3.15302761	4.59979674
O	-0.35230714	-1.05014426	-1.28727310
C	-1.76425845	-1.28983183	-1.45715871
H	-2.33428559	-0.35208383	-1.51810247
H	-1.81122279	-1.82513911	-2.41511554
H	-2.14128942	-1.93239844	-0.65081727
O	0.98101136	0.76430979	-1.99656537
C	0.77528927	2.16016245	-2.31177021
H	1.52414472	2.68283945	-1.70551714
H	0.94232887	2.33191668	-3.37587581
H	-0.23615600	2.45789865	-1.99484381
H	0.48771459	0.19635998	-2.65300868

2.4.16.2. SMD(THF)//M06-2X/6-

31++G(d,p)

P	-0.39880	0.66414	-0.57169
H	-0.71897	0.34639	-1.89812
O	-0.67664	2.06692	-0.15184
C	1.30676	0.15722	-0.28084
C	1.70207	-1.16515	-0.51432
C	2.23081	1.10020	0.17634
C	3.02353	-1.54119	-0.28803
H	0.98153	-1.89828	-0.86959
C	3.55276	0.71841	0.40344
H	1.91008	2.12278	0.35538
C	3.94672	-0.59893	0.17107
H	3.33323	-2.56622	-0.46738
H	4.27260	1.44756	0.76227
H	4.97685	-0.89398	0.34830
O	-1.30090	-0.48586	0.14048
C	-1.28986	-0.55788	1.57916
H	-1.71586	0.35246	2.00788
H	-1.89527	-1.42189	1.85396
H	-0.26796	-0.70114	1.94482
O	-4.01783	-1.03098	-0.60116
C	-4.47583	0.04123	0.20444
H	-4.36885	-0.17491	1.27598
H	-3.95122	0.97821	-0.02198
H	-5.53802	0.18383	-0.00929
H	-3.05490	-1.06102	-0.51438

2.4.17. Structures **14**-IRC2-P

2.4.17.1. PM6

P	0.00000000	0.00000000	0.00000000
H	1.45596000	0.00000000	0.00000000
O	-0.56364885	1.39462676	0.00000000
C	-0.36740791	-1.17126247	1.37588657
C	-0.16729416	-2.53880489	1.19529320
C	-0.84063418	-0.65445894	2.58055373
C	-0.42871132	-3.41046043	2.25936035
H	0.17502264	-2.94645814	0.24114109
C	-1.09510833	-1.53155508	3.64271205
H	-1.02388661	0.41546262	2.71352058
C	-0.88793906	-2.90508664	3.48055713
H	-0.28009435	-4.48091276	2.13475016
H	-1.46026954	-1.14402644	4.59154719
H	-1.08943287	-3.58532517	4.30716380
O	-2.26899482	-0.60453638	-0.24136630
C	-3.23902327	0.44961067	-0.05345122
H	-2.84612608	1.38600789	-0.47671576
H	-4.19334371	0.16079346	-0.49491014
H	-3.31735528	0.54155975	1.03632996
O	-0.26497176	-0.90349316	-1.42674694
C	0.06350315	-0.15652185	-2.61364338
H	1.15170478	-0.07899632	-2.72918488
H	-0.34965982	-0.77712729	-3.42135699
H	-0.41079537	0.83581156	-2.62416591
H	-2.27335954	-0.90150235	-1.19136528

2.4.17.2. SMD(THF)//M06-2X/6-

31++G(d,p)

P	1.44295	-0.92266	-0.61036
H	1.57964	-0.82733	-2.00118
O	2.14661	-2.04587	0.07048
C	-0.32715	-0.84565	-0.28978
C	-1.17373	-0.24930	-1.22992
C	-0.84073	-1.32987	0.91847
C	-2.53354	-0.12304	-0.95397
H	-0.77456	0.12387	-2.17041
C	-2.20046	-1.19539	1.19251
H	-0.17894	-1.81079	1.63404
C	-3.04336	-0.59098	0.25802
H	-3.19378	0.33878	-1.68155
H	-2.60258	-1.56647	2.13016
H	-4.10316	-0.48988	0.47278
O	0.10109	2.76549	-0.60107
C	-0.64649	2.67665	0.59982
H	-1.00235	1.65565	0.79402
H	-0.06959	3.02340	1.46779
H	-1.51949	3.32508	0.48862
O	2.00628	0.55688	-0.22088
C	2.20410	0.83098	1.18076
H	2.97062	0.16849	1.58802
H	2.53806	1.86655	1.25067
H	1.26794	0.70379	1.73582
H	0.78026	2.07634	-0.59721

2.4.18. Structure **14**-IRC5

2.4.18.1. PM6

P	0.00000000	0.00000000	0.00000000
H	1.44417000	0.00000000	0.00000000
O	-0.78756489	1.29479025	0.00000000
C	-0.43023684	-1.02992112	1.48882052
C	0.09177360	-2.31247790	1.64203886
C	-1.28762414	-0.47752898	2.43643372
C	-0.24837569	-3.05750885	2.77707342
H	0.75343945	-2.75587241	0.89539705
C	-1.62459817	-1.22454902	3.57341391
H	-1.70319196	0.52907193	2.30780370
C	-1.10402227	-2.51081534	3.74099959
H	0.15076951	-4.06049639	2.91094243
H	-2.29072293	-0.80279948	4.32328153
H	-1.36528806	-3.09180515	4.62491714
O	-0.33534331	-1.04342827	-1.27957792
C	-1.74466533	-1.15127761	-1.57083902
H	-2.22594939	-0.16726213	-1.66168987
H	-1.75298658	-1.66761811	-2.54069404
H	-2.24155167	-1.76838510	-0.81111296
O	0.85851976	1.43380399	-1.65564819
C	0.93522817	1.16598543	-3.06371331
H	-0.00298701	0.72116831	-3.41251085
H	1.16552986	2.08862290	-3.60362913
H	1.75591793	0.44508426	-3.15912817
H	0.13881816	2.12551172	-1.46434126

2.4.18.2. SMD(THF)//M06-2X/6-

31++G(d,p)

P	0.47713	0.00752	-0.80522
H	0.51832	0.20286	-2.18896
O	1.30118	-1.13890	-0.30247
C	-1.24834	-0.12670	-0.30671
C	-2.12960	0.93960	-0.52431
C	-1.70019	-1.30533	0.29241
C	-3.46229	0.82286	-0.13892
H	-1.77537	1.85811	-0.98702
C	-3.03572	-1.41670	0.67785
H	-1.00459	-2.12323	0.45769
C	-3.91339	-0.35488	0.46139
H	-4.14886	1.64740	-0.30394
H	-3.38999	-2.33039	1.14505
H	-4.95329	-0.44259	0.76199
O	0.95381	1.47662	-0.34983
C	0.96880	1.78650	1.05518
H	1.44339	0.98390	1.62645
H	1.54601	2.70456	1.16343
H	-0.0521	1.94635	1.41490
O	4.08176	-1.14479	-0.14018
C	4.20049	0.01882	0.65050
H	3.73729	0.89228	0.16978
H	3.75448	-0.11301	1.64612
H	5.26584	0.22860	0.78155
H	3.12932	-1.29606	-0.27329

2.4.19. Structure 14-IRC6

2.4.19.1. PM6

P	0.00000000	0.00000000	0.00000000
H	1.45318000	0.00000000	0.00000000
O	-0.58313500	1.39897000	0.00000000
C	-0.35692000	-1.11160200	1.43802900
C	-0.47773700	-0.55350800	2.70895300
C	-0.48206500	-2.48267500	1.22794000
C	-0.72313000	-1.39574300	3.80071200
H	-0.39344700	0.52343100	2.87506100
C	-0.72978900	-3.31994100	2.32315400
H	-0.39698300	-2.91605300	0.22681000
C	-0.84756500	-2.77556100	3.60607700
H	-0.81806600	-0.97643800	4.80041900
H	-0.82992800	-4.39340000	2.17552600
H	-1.03742500	-3.42840100	4.45734300
O	-0.16560300	-0.92840700	-1.38459300
C	-1.33696900	-0.69905500	-2.19582500
H	-1.52430200	0.36971000	-2.35866500
H	-1.06953500	-1.19418900	-3.13853600
H	-2.21219000	-1.17743000	-1.73241300
O	-2.42915900	0.03904400	0.05521100
C	-3.40880300	-0.47294200	0.96609400
H	-4.40210400	-0.12497800	0.66710400
H	-3.33241100	-1.56257200	0.87200300
H	-3.17404500	-0.16493200	1.99034400
H	-2.35470200	1.05680000	0.13536600

2.4.19.2. SMD(THF)//M06-2X/6-

31++G(d,p)

P	0.29366	1.27654	-0.62653
H	0.27172	1.49841	-2.00676
O	1.66450	1.14635	-0.03664
C	-0.76005	-0.14288	-0.27285
C	-0.21598	-1.27794	0.33473
C	-2.11666	-0.10749	-0.61920
C	-1.03213	-2.37878	0.59548
H	0.83589	-1.29819	0.61072
C	-2.92607	-1.20973	-0.35733
H	-2.54009	0.77902	-1.08568
C	-2.38224	-2.34436	0.24893
H	-0.61229	-3.26061	1.06954
H	-3.97839	-1.18460	-0.62300
H	-3.01475	-3.20304	0.45426
O	-0.54690	2.57100	-0.17024
C	-0.81287	2.75219	1.23214
H	0.12222	2.88600	1.78151
H	-1.42085	3.65239	1.31566
H	-1.36509	1.89681	1.63468
O	3.23052	-0.98430	0.75646
C	3.44969	-1.54130	-0.52366
H	4.07818	-0.89489	-1.15042
H	3.96367	-2.49713	-0.39107
H	2.50803	-1.73101	-1.05970
H	2.73971	-0.15384	0.62218

2.4.20. Structure 15

2.4.20.1. PM6

P	0.00000000	0.00000000	0.00000000
H	1.45068000	0.00000000	0.00000000
O	-1.01243300	1.34425848	0.00000000
C	-0.73890554	-1.69506277	-0.08153927
C	-0.39949110	-2.62610507	0.90021609
C	-1.63218933	-2.01178544	-1.10280703
C	-0.95826365	-3.90813277	0.84857801
H	0.28366265	-2.36975431	1.71651716
C	-2.19408923	-3.29422275	-1.14694018
H	-1.89328317	-1.27926749	-1.87503234
C	-1.85459110	-4.23911711	-0.1739247
H	-0.69937222	-4.64562346	1.60550305
H	-2.89420129	-3.55364602	-1.93843292
H	-2.29054390	-5.23712943	-0.21061027
O	0.09244089	0.13560590	1.71457340
C	-1.09797033	0.34619362	2.48041063
H	-0.73797256	0.33315542	3.51782613
H	-1.53745284	1.32547009	2.24849648
H	-1.82314413	-0.45893468	2.32090504
O	-0.09094106	0.29734520	-1.76405559
C	0.88063999	-0.28062900	-2.61867554
H	0.81802936	-1.37579008	-2.60537367
H	0.61506674	0.08754482	-3.62045741
H	1.89234246	0.06008686	-2.36717346
H	-1.20434341	1.70889133	-0.92216922

2.4.20.2. SMD(THF)//M06-2X/6-

31++G(d,p)

P	1.28264	0.03423	-0.20853
H	1.78641	0.25962	-1.50040
O	2.08411	-0.18071	1.20089
C	-0.53914	0.00671	-0.06482
C	-1.19196	0.87119	0.82130
C	-1.29481	-0.88456	-0.83496
C	-2.57897	0.83045	0.95062
H	-0.61071	1.57820	1.40659
C	-2.68478	-0.90535	-0.72567
H	-0.79226	-1.56565	-1.51538
C	-3.32726	-0.05399	0.17250
H	-3.07518	1.49481	1.65187
H	-3.26420	-1.59194	-1.3356
H	-4.40906	-0.07767	0.26588
O	1.46232	-1.60045	-0.58403
C	1.18003	-2.61471	0.36625
H	0.32473	-2.35872	1.00498
H	0.93913	-3.52819	-0.18550
H	2.04937	-2.79871	1.00546
O	1.42725	1.73715	0.08974
C	0.97435	2.61244	-0.91547
H	1.49815	3.56576	-0.80563
H	1.18625	2.21917	-1.92262
H	-0.10700	2.78994	-0.84010
H	2.22069	0.67895	1.62721

2.4.20.3. CPCM(THF)//M06-2X/6-

31++G(d,p)

P	-1.28018	-0.02989	-0.20630
H	-1.79123	-0.25128	-1.49657
O	-2.07430	0.19378	1.20502
C	0.54058	-0.00956	-0.06628
C	1.19055	-0.88134	0.81478
C	1.29847	0.88333	-0.83211
C	2.57763	-0.84591	0.94334

H	0.60581	-1.58836	1.39580	H	-2.06919	2.76122	1.05577
C	2.68835	0.89942	-0.72303	O	-1.43816	-1.74735	0.10269
H	0.79578	1.56949	-1.50676	C	-1.11222	-2.65470	-0.93709
C	3.32824	0.04066	0.16990	H	-1.46057	-2.2899	-1.91656
H	3.07199	-1.51553	1.64009	H	-0.02927	-2.82805	-0.99679
H	3.26960	1.58747	-1.32866	H	-1.61381	-3.60362	-0.72747
H	4.40969	0.06048	0.26299	H	-2.20244	-0.68189	1.64737
O	-1.45525	1.60699	-0.58456				
C	-1.16608	2.62190	0.36456				
H	-0.28789	2.37112	0.97243				
H	-0.95818	3.54117	-0.18852				
H	-2.01944	2.78073	1.03005				
O	-1.43404	-1.73015	0.09348				
C	-1.00455	-2.61397	-0.91639				
H	-1.27897	-2.24584	-1.91695				
H	0.08379	-2.75489	-0.88765				
H	-1.49431	-3.57731	-0.76000				
H	-2.21443	-0.66106	1.63821				

2.4.20.4. SMD(THF)//B3LYP/6-

31++G(d,p)

P	1.26540	0.02754	-0.19577
H	1.75394	0.25173	-1.49887
O	2.06514	-0.18338	1.23347
C	-0.56492	0.00429	-0.05072
C	-1.22191	0.83520	0.87192
C	-1.32915	-0.84042	-0.87213
C	-2.61416	0.80570	0.98498
H	-0.64499	1.50792	1.49845
C	-2.72413	-0.84947	-0.77698
H	-0.83302	-1.49357	-1.58269
C	-3.36867	-0.03226	0.15643
H	-3.10908	1.44318	1.71260
H	-3.30382	-1.49975	-1.42648
H	-4.45226	-0.04589	0.23704
O	1.47222	-1.61715	-0.58539
C	1.23194	-2.67871	0.33989
H	1.08990	-3.59306	-0.24547
H	2.08804	-2.81334	1.01006
H	0.33321	-2.50930	0.94640
O	1.43915	1.74831	0.101780
C	1.09613	2.64913	-0.93727
H	1.41183	2.27329	-1.92456
H	0.01432	2.84026	-0.97043
H	1.61583	3.59511	-0.75369
H	2.21240	0.68731	1.63857

2.4.20.5. CPCM(THF)//B3LYP/6-

31++G(d,p)

P	-1.26098	-0.02838	-0.19408
H	-1.75160	-0.24946	-1.49742
O	-2.05388	0.18553	1.23757
C	0.56804	-0.00416	-0.05232
C	1.22643	-0.85328	0.85277
C	1.33057	0.85773	-0.85734
C	2.61854	-0.82418	0.96577
H	0.64866	-1.53913	1.46340
C	2.72543	0.86750	-0.76180
H	0.83167	1.52214	-1.55480
C	3.37129	0.03232	0.15465
H	3.11481	-1.47607	1.67894
H	3.30394	1.53135	-1.39773
H	4.45448	0.04608	0.23525
O	-1.47323	1.61755	-0.58485
C	-1.24487	2.68344	0.34011
H	-0.30605	2.55229	0.89230
H	-1.18310	3.60686	-0.24276

2.4.21. Structure **15**-IRC10

2.4.21.1. SMD(THF)//M06-2X/6-

31++G(d,p)

P	-1.02435	0.03792	-0.08747
H	-1.8071	0.19648	-1.25141
O	-1.83181	-0.15038	1.32609
C	0.80054	0.01927	-0.04843
C	1.53780	1.06475	-0.61556
C	1.47866	-1.04408	0.56123
C	2.93189	1.03825	-0.58862
H	1.02188	1.89931	-1.07626
C	2.87068	-1.05175	0.61464
H	0.91902	-1.8675	0.99153
C	3.60069	-0.01514	0.03266
H	3.49234	1.84760	-1.04705
H	3.38461	-1.87348	1.10421
H	4.68629	-0.02938	0.06331
O	-1.02739	-1.66446	-0.38975
C	-2.23097	-2.25367	-0.83093
H	-2.72446	-1.64064	-1.60126
H	-1.99361	-3.22618	-1.26939
H	-2.94667	-2.41207	-0.01114
O	-1.02982	1.71849	0.11991
C	-2.28338	2.36654	0.08029
H	-2.11020	3.42810	-0.11396
H	-2.91981	1.96804	-0.72659
H	-2.81649	2.25559	1.03101
H	-1.94384	-1.08881	1.53726

2.4.22. Structure **15**-IRC16

2.4.22.1. SMD(THF)//M06-2X/6-

31++G(d,p)

P	1.26199	0.08409	-0.46448
H	1.72387	0.26907	-1.76858
O	2.10872	-0.06855	0.92970
C	-0.53052	-0.01097	-0.18103
C	-1.04331	-0.45323	1.04173
C	-1.40678	0.36947	-1.20273
C	-2.42381	-0.51721	1.23885
H	-0.36868	-0.73746	1.84541
C	-2.78445	0.29634	-1.00628
H	-1.01616	0.72912	-2.15151
C	-3.29441	-0.14667	0.21530
H	-2.81566	-0.85724	2.19281
H	-3.45893	0.59071	-1.80479
H	-4.36808	-0.19852	0.36950
O	1.32557	1.80934	-0.42542
C	0.88660	2.57866	0.67697
H	1.68136	2.70705	1.42757
H	0.00569	2.14456	1.16835
H	0.61884	3.57412	0.31226
O	1.49249	-1.56240	-0.79934
C	1.23381	-2.61203	0.11345
H	1.60189	-3.53616	-0.34068
H	0.15783	-2.72595	0.29901
H	1.75125	-2.45807	1.06619
H	2.32006	0.78418	1.33457

2.4.23. Structure **15**-IRC17

2.4.23.1. SMD(THF)//M06-2X/6-

31++G(d,p)

P	1.14263	0.18739	-0.25121
H	1.79437	0.23483	-1.49284
O	1.92228	0.40986	1.17614
C	-0.65059	-0.13869	-0.12696
C	-1.13947	-1.15141	0.70686
C	-1.55248	0.64136	-0.85846
C	-2.51106	-1.37115	0.81475
H	-0.44701	-1.77042	1.26774
C	-2.92361	0.40100	-0.77153
H	-1.18154	1.44042	-1.49300
C	-3.40499	-0.60063	0.07009
H	-2.88142	-2.14902	1.47575
H	-3.61327	1.00299	-1.35559
H	-4.47327	-0.78116	0.14654
O	0.99002	1.86037	-0.44181
C	0.48457	2.67966	0.59904
H	1.28993	2.98138	1.27666
H	-0.29361	2.17374	1.18495
H	0.04713	3.57197	0.14116
O	1.45956	-1.51420	-0.20354
C	2.74246	-1.94304	-0.60815
H	2.70324	-3.02187	-0.77852
H	3.51055	-1.7402	0.15158
H	3.05274	-1.45857	-1.54685
H	2.10883	-0.44577	1.59029

2.4.24. Structure **16**

2.4.24.1. PM6

P	0.00000000	0.00000000	0.00000000
H	1.44649233	0.00000000	0.00000000
O	-0.74724913	1.52801146	0.00000000
C	-0.28163706	-0.09438921	1.87850816
C	0.47117974	-1.02772351	2.59085718
C	-1.17494751	0.74983897	2.52924111
C	0.32312454	-1.11849431	3.97937540
H	1.17189056	-1.70195547	2.09493291
C	-1.32205936	0.65942496	3.92116245
H	-1.75833142	1.49386393	1.97712934
C	-0.57398730	-0.27334514	4.64321216
H	0.90536209	-1.84348671	4.54352023
H	-2.01565474	1.31956782	4.43715252
H	-0.68625393	-0.34309094	5.72408309
O	-0.59466452	-1.55661639	-0.31617848
C	-1.88686899	-1.88823164	0.21452313
H	-2.65809647	-1.18565431	-0.11902018
H	-2.07243596	-2.88167894	-0.22156378
H	-1.86407549	-1.96586263	1.30995955
O	0.04266033	0.24849298	-1.74040143
C	-0.94727558	-0.25873971	-2.62648913
H	-1.94420814	0.11353945	-2.37153415
H	-0.63956729	0.12656775	-3.60858154
H	-0.92898874	-1.35638780	-2.63417754
H	-0.74768826	1.96674050	-0.90282673

2.4.24.2. SMD(THF)//M06-2X/6-

31++G(d,p)

P	1.00398	-0.30517	-0.38626
H	0.82553	-0.57774	-1.75535
O	1.10607	-1.49877	0.73336
C	-0.86130	-0.25425	-0.15551
C	-1.62135	0.09623	-1.27490
C	-1.53082	-0.52713	1.04470
C	-3.01299	0.19505	-1.20330
H	-1.12454	0.29509	-2.22456
C	-2.91978	-0.43758	1.12293
H	-0.96252	-0.81608	1.92441
C	-3.66462	-0.07184	-0.00098
H	-3.58473	0.46936	-2.08527
H	-3.42458	-0.65614	2.05992
H	-4.74700	-0.00394	0.06044
O	1.29154	1.22869	0.09167
C	0.39971	2.07785	0.81531
H	0.13276	1.64102	1.78131
H	0.95100	3.00533	0.98151
H	-0.50721	2.29370	0.24536
O	2.66961	-0.45495	-0.77716
C	3.69500	-0.02124	0.09959
H	3.47907	-0.25314	1.15224
H	4.61645	-0.53848	-0.18384
H	3.85018	1.05940	0.01658
H	1.99507	-1.88316	0.75115

2.4.25. Structure 17

2.4.25.1. PM6

P	0.00000000	0.00000000	0.00000000
H	1.44858000	0.00000000	0.00000000
O	0.08700600	1.75673700	0.00000000
C	-0.78845100	-0.16421700	1.65947400
C	-0.83147000	0.95778400	2.48850800
C	-1.32195500	-1.38652800	2.06839300
C	-1.42316000	0.85273300	3.75252900
H	-0.41287200	1.92030000	2.16464600
C	-1.91549700	-1.48484000	3.33282900
H	-1.27908300	-2.27361700	1.42323800
C	-1.96452600	-0.36701400	4.17171100
H	-1.46066800	1.72017000	4.40819000
H	-2.33480200	-2.43279400	3.66302200
H	-2.42463800	-0.44674900	5.15624000
O	-0.09398900	-1.73790100	-0.28899000
C	0.66995100	-2.24081900	-1.38087500
H	1.74537600	-2.14268300	-1.18841000
H	0.40467200	-3.30703300	-1.41924900
H	0.38993500	-1.75844000	-2.32642600
O	-0.93995000	0.26044300	-1.38628600
C	-2.19114400	-0.44748000	-1.46398300
H	-2.53300300	-0.21963100	-2.48317600
H	-2.06149300	-1.53180000	-1.34195500
H	-2.89907800	-0.04656200	-0.72939600
H	-0.56430000	2.22028300	-0.55297600

2.4.25.2. SMD(THF)//M06-2X/6-

31++G(d,p)

P	0.97015	0.23247	-0.71164
H	0.74509	1.36881	-1.53801
O	1.43910	-0.58076	-2.05206
C	-0.80326	0.14867	-0.24113
C	-1.49902	-1.06267	-0.17166
C	-1.49168	1.34861	-0.04460
C	-2.86721	-1.07109	0.09524
H	-0.97261	-1.99949	-0.33420
C	-2.85240	1.33994	0.26093
H	-0.96318	2.29626	-0.13034
C	-3.54183	0.12901	0.32490
H	-3.4057	-2.01362	0.12947
H	-3.37513	2.27589	0.43415
H	-4.60502	0.12048	0.54654
O	1.97157	1.21627	0.13707
C	2.93215	0.87897	1.13750
H	3.35162	-0.11531	0.97634
H	3.72643	1.62444	1.05795
H	2.48665	0.94221	2.13405
O	1.39292	-1.18506	0.17760
C	1.04102	-1.35470	1.53889
H	1.93737	-1.60983	2.11386
H	0.59148	-0.45456	1.97664
H	0.31803	-2.17222	1.63614
H	1.67749	-1.49408	-1.82931

2.4.26. Structure 18

2.4.26.1. SMD(THF)//M06-2X/6-

31++G(d,p)

P	-1.14479	0.14621	0.02842
H	-1.80304	0.23289	1.27388
O	-1.93610	0.33184	-1.38655
C	0.65794	-0.13590	-0.01620
C	1.23569	-1.24676	0.60965
C	1.47894	0.77263	-0.69555
C	2.61603	-1.43882	0.56400
H	0.60369	-1.96073	1.12578
C	2.85426	0.56113	-0.76706
H	1.03817	1.64673	-1.16532
C	3.42564	-0.54093	-0.13059
H	3.05732	-2.29656	1.06270
H	3.47955	1.26217	-1.31183
H	4.49929	-0.69884	-0.17539
O	-0.99813	1.87815	0.06122
C	-0.50595	2.46860	1.24049
H	-0.89585	1.96675	2.14074
H	-0.83333	3.51139	1.26440
H	0.59146	2.44032	1.28240
O	-1.44162	-1.51898	-0.00302
C	-2.78456	-1.93071	0.14762
H	-3.35109	-1.7827	-0.77856
H	-3.28757	-1.38112	0.95942
H	-2.78513	-2.99347	0.40279
H	-2.00282	1.27646	-1.59463

2.4.26.2. SMD(THF)//B3LYP/6-

31++G(d,p)

P	1.13868	0.12363	-0.00804
H	1.81195	0.19435	-1.25215
O	1.90952	0.30139	1.43667
C	-0.67908	-0.12433	0.01837
C	-1.49598	0.78770	0.70807
C	-1.27663	-1.21536	-0.63497
C	-2.87920	0.59902	0.76292
H	-1.04961	1.64513	1.20009
C	-2.66393	-1.38495	-0.60381
H	-0.65744	-1.93230	-1.16108
C	-3.46732	-0.48403	0.10152
H	-3.49626	1.30301	1.31457
H	-3.11380	-2.22693	-1.12288
H	-4.54447	-0.62389	0.13465
O	1.41167	-1.56116	0.03031
C	2.74059	-2.02601	-0.16845
H	2.68949	-3.09332	-0.40520
H	3.23178	-1.50918	-1.00965
H	3.35272	-1.88957	0.73147
O	1.04486	1.88006	-0.04592
C	0.70576	2.51117	-1.26845
H	1.22098	2.04560	-2.12513
H	-0.37642	2.48284	-1.45977
H	1.02402	3.55700	-1.21060
H	1.99325	1.25122	1.62658

2.4.27. Structure 19

2.4.27.1. SMD(THF)//M06-2X/6- 31++G(d,p)

P	-1.26873	0.05642	0.09021
H	-1.75394	-0.0528	-1.23754
O	-1.90608	0.18102	1.58434
C	0.54232	0.00723	0.08873
C	1.24182	-0.21004	-1.10228
C	1.24487	0.20000	1.28229
C	2.63691	-0.24407	-1.09749
H	0.70350	-0.34847	-2.03770
C	2.63810	0.16206	1.28380
H	0.70524	0.38380	2.20772
C	3.33495	-0.06132	0.09534
H	3.17506	-0.41231	-2.02559
H	3.17938	0.31032	2.21352
H	4.42055	-0.08893	0.09907
O	-1.52045	-1.65018	0.24314
C	-1.23660	-2.48005	-0.85756
H	-1.57099	-2.02816	-1.80495
H	-1.77570	-3.42138	-0.72203
H	-0.16284	-2.69583	-0.93404
O	-1.45682	1.73907	-0.00448
C	-1.05170	2.36321	-1.20057
H	-1.37073	1.79835	-2.09122
H	0.03837	2.48947	-1.24223
H	-1.52139	3.34919	-1.23973
H	-2.07289	-0.71097	1.92417

2.4.27.2. CPCM(THF)//M06-2X/6-

31++G(d,p)

P	1.26617	0.04910	-0.09332
H	1.75636	-0.03861	1.23509
O	1.88922	0.15754	-1.59459
C	-0.54377	0.00472	-0.08450
C	-1.24433	0.16488	-1.28408
C	-1.24492	-0.17672	1.11127
C	-2.63751	0.13383	-1.28584
H	-0.70110	0.31678	-2.21276
C	-2.64008	-0.20421	1.10619
H	-0.70974	-0.29302	2.05124
C	-3.33611	-0.05140	-0.09184
H	-3.17737	0.25690	-2.21942
H	-3.1792	-0.34432	2.03769
H	-4.42127	-0.07372	-0.09566
O	1.45870	1.73435	-0.02384
C	1.08004	2.37815	1.17276
H	1.51239	3.38033	1.16212
H	-0.01108	2.45916	1.25777
H	1.45945	1.84695	2.05919
O	1.51763	-1.65575	-0.22314
C	1.23370	-2.46853	0.89239
H	1.60714	-2.01756	1.82449
H	0.15513	-2.64056	0.99739
H	1.73570	-3.42729	0.74933
H	2.05444	-0.73492	-1.93212

2.4.27.3. SMD(THF)//B3LYP/6-

31++G(d,p)

P	-1.22339	0.05958	0.12269
H	-1.67727	-0.06598	-1.22335
O	-1.76755	0.20113	1.67408
C	0.59673	0.00819	0.08833
C	1.34362	0.23129	1.25584

C	1.26553	-0.24484	-1.11951
C	2.73958	0.19101	1.21486
H	0.83646	0.43848	2.19343
C	2.66364	-0.28165	-1.15767
H	0.70213	-0.41135	-2.03406
C	3.40224	-0.06585	0.00926
H	3.30915	0.36309	2.12418
H	3.17208	-0.47700	-2.09794
H	4.48807	-0.09467	-0.02001
O	-1.48596	1.74451	0.01595
C	-1.26493	2.37604	-1.23589
H	-1.77507	3.34342	-1.21106
H	-0.19587	2.54418	-1.42454
H	-1.67855	1.79034	-2.07255
O	-1.54651	-1.64920	0.29856
C	-1.44763	-2.50721	-0.82624
H	-1.83632	-2.0302	-1.74017
H	-0.40950	-2.81587	-1.00876
H	-2.05024	-3.39829	-0.62436
H	-1.92693	-0.69332	2.01638

2.4.27.4. CPCM(THF)//B3LYP/6-

31++G(d,p)

P	-1.11898	0.04297	0.16111
H	-1.37210	-0.08769	-1.24683
O	-1.35766	0.20311	1.81794
C	0.70688	0.00768	0.06980
C	1.51623	0.21251	1.20023
C	1.31829	-0.22276	-1.17332
C	2.90830	0.18026	1.08692
H	1.05117	0.39704	2.16229
C	2.71165	-0.25801	-1.28592
H	0.70849	-0.37561	-2.05993
C	3.50850	-0.05650	-0.15504
H	3.52417	0.34068	1.96724
H	3.17124	-0.44049	-2.25298
H	4.59110	-0.08209	-0.24048
O	-1.66064	1.63477	0.07727
C	-1.68803	2.31303	-1.17861
H	-2.08527	1.67516	-1.97857
H	-2.34341	3.17815	-1.05602
H	-0.68637	2.65634	-1.46276
O	-1.71051	-1.54674	0.34598
C	-1.80528	-2.43308	-0.76861
H	-2.14824	-1.91097	-1.67089
H	-0.83719	-2.90306	-0.97638
H	-2.53332	-3.20409	-0.50624
H	-1.48433	-0.67580	2.20273

2.4.28. Structure **20**

2.4.28.1. SMD(THF)//M06-2X/6-

31++G(d,p)

P	1.07757	0.01337	0.33124
H	2.46965	0.04438	0.64422
O	0.84665	0.10615	1.97160
C	-0.77175	-0.01519	0.00543
C	-1.48358	-1.21631	-0.11709
C	-1.49907	1.18496	0.00399
C	-2.87337	-1.21815	-0.25149
H	-0.94852	-2.15958	-0.11761
C	-2.88777	1.18595	-0.12819
H	-0.97448	2.13087	0.09724
C	-3.58052	-0.01729	-0.25872
H	-3.40085	-2.16247	-0.35339
H	-3.42707	2.12902	-0.13295
H	-4.66141	-0.01828	-0.36567
O	1.24709	-1.44295	-0.41435
C	2.52928	-2.06574	-0.48079
H	3.22057	-1.47938	-1.09395
H	2.95661	-2.20975	0.51631
H	2.37628	-3.03982	-0.94853
O	1.21676	1.38594	-0.56758
C	2.47614	2.05247	-0.65430
H	3.23602	1.41073	-1.11091
H	2.31907	2.92693	-1.28776
H	2.82080	2.38076	0.33136
H	-0.09032	0.10877	2.22275

2.4.29. Structure **20-IRC18**

2.4.29.1. SMD(THF)//M06-2X/6-

31++G(d,p)

P	1.24068	0.27760	0.39647
H	2.58579	0.62787	0.67556
O	1.01759	0.41925	2.03724
C	-0.58627	-0.11812	0.14773
C	-1.52522	0.81561	0.61805
C	-1.06796	-1.28839	-0.44884
C	-2.89520	0.59129	0.49726
H	-1.18637	1.74500	1.07468
C	-2.44072	-1.51815	-0.57141
H	-0.36766	-2.0273	-0.82053
C	-3.35818	-0.58163	-0.09989
H	-3.59841	1.33103	0.86883
H	-2.79115	-2.43596	-1.03537
H	-4.42471	-0.76375	-0.19461
O	1.25103	1.57871	-0.62202
C	0.32106	1.86466	-1.66819
H	-0.54874	2.40643	-1.28764
H	-0.01268	0.95487	-2.17540
H	0.85481	2.49575	-2.38205
O	1.67169	-1.17104	-0.24579
C	3.05488	-1.50895	-0.34519
H	3.10452	-2.46144	-0.87522
H	3.50323	-1.62419	0.64638
H	3.60892	-0.75383	-0.91150
H	0.12537	0.18813	2.33731

2.4.30. Structure **21**-IRC11

2.4.30.1. SMD(THF)//M06-2X/6-

31++G(d,p)

P	-0.9368	0.04882	0.47904
H	-0.69197	0.26119	1.85990
O	-2.61099	0.00457	0.84532
C	0.91248	0.00730	0.17127
C	1.77285	0.18026	1.25408
C	1.46811	-0.17952	-1.10257
C	3.16156	0.16847	1.08257
H	1.36398	0.32500	2.25372
C	2.84808	-0.19084	-1.28276
H	0.81222	-0.31789	-1.95860
C	3.70047	-0.01702	-0.18709
H	3.81615	0.30335	1.93916
H	3.26514	-0.33502	-2.27572
H	4.77742	-0.02713	-0.32810
O	-1.04249	1.37023	-0.47575
C	-2.24183	2.08797	-0.77646
H	-2.65294	2.56459	0.11789
H	-1.95096	2.86101	-1.49017
H	-2.99458	1.43655	-1.22289
O	-1.04903	-1.41777	-0.21982
C	-2.23514	-2.19684	-0.40359
H	-1.91071	-3.10181	-0.92112
H	-2.68538	-2.45706	0.55548
H	-2.96575	-1.66444	-1.01560
H	-2.82988	0.60435	1.56978

2.4.31. Structure **22**

2.4.31.1. SMD(THF)//M06-2X/6-

31++G(d,p)

H	0.81850	0.00017	-1.86250
O	1.33845	-0.00014	1.20510
C	-0.81527	0.00018	-0.12276
C	-1.65983	0.00034	-1.23929
C	-1.38777	-0.00009	1.15803
C	-3.04571	0.00020	-1.08826
H	-1.23333	0.00061	-2.23935
C	-2.77321	-0.00022	1.30956
H	-0.74619	-0.00017	2.03083
C	-3.60458	-0.00010	0.18863
H	-3.68513	0.00027	-1.96577
H	-3.20446	-0.00053	2.30638
H	-4.68369	-0.00029	0.31170
O	1.71301	1.46720	-0.69901
C	2.03761	2.41582	0.31570
H	2.92004	2.11075	0.88651
H	2.26555	3.34862	-0.20449
H	1.19887	2.57529	0.99835
O	1.71272	-1.46726	-0.69928
C	2.03761	-2.41593	0.31532
H	1.19908	-2.57531	0.99827
H	2.26524	-3.34872	-0.20500
H	2.92025	-2.11096	0.88586
H	2.28356	-0.00002	1.40964

2.4.32. Structure **22**-IRC17

2.4.32.1. SMD(THF)//M06-2X/6-

31++G(d,p)

P	0.98180	0.10600	-0.44551
H	0.81075	0.42398	-1.81807
O	1.42787	-0.31250	1.13906
C	-0.82728	0.00196	-0.14083
C	-1.39339	-0.72294	0.91605
C	-1.67196	0.66213	-1.04019
C	-2.77835	-0.78088	1.06870
H	-0.75282	-1.25222	1.61449
C	-3.05531	0.62512	-0.87542
H	-1.24335	1.21242	-1.87515
C	-3.60989	-0.10169	0.17840
H	-3.20826	-1.35572	1.88379
H	-3.69881	1.15422	-1.57205
H	-4.68803	-0.14184	0.30332
O	1.61143	1.63197	-0.33671
C	2.01522	2.30049	0.85466
H	2.83141	1.77423	1.35459
H	1.17265	2.43037	1.54531
H	2.35993	3.28973	0.54742
O	1.73969	-1.24315	-0.99313
C	2.21793	-2.33784	-0.21040
H	2.56498	-3.08489	-0.92769
H	1.41972	-2.76319	0.40350
H	3.04552	-2.03253	0.43217
H	1.04552	0.26676	1.81137

2.4.33. Structure **23**

2.4.33.1. SMD(THF)//M06-2X/6-

31++G(d,p)

P	1.07921	-0.49312	-0.43393
H	1.40731	-0.52017	-1.80716
O	0.98552	-2.17446	-0.60827
C	-0.69302	-0.15857	-0.13444
C	-1.66077	-1.12466	-0.43693
C	-1.10278	1.06354	0.41775
C	-3.01067	-0.87673	-0.18880
H	-1.35313	-2.07071	-0.86932
C	-2.45042	1.30394	0.67962
H	-0.36490	1.82921	0.63665
C	-3.40690	0.33562	0.37398
H	-3.75097	-1.63246	-0.43423
H	-2.75442	2.25134	1.11492
H	-4.45761	0.52796	0.57081
O	1.60532	1.13276	-0.41206
C	1.37632	1.89860	-1.57362
H	0.30564	2.07846	-1.74478
H	1.87696	2.86101	-1.44108
H	1.79128	1.41247	-2.46870
O	1.86810	-0.75701	0.98712
C	2.21189	0.25676	1.93106
H	1.34525	0.87113	2.19166
H	2.55466	-0.27595	2.82081
H	3.00973	0.89548	1.55006
H	0.94870	-2.63230	0.24334

2.4.34. Structure **23**-IRC16

2.4.34.1. SMD(THF)//M06-2X/6-

31++G(d,p)

P	-0.95255	0.60384	-0.32861
H	-1.47242	1.00547	-1.57313
O	-0.72059	2.27098	-0.09275
C	0.80531	0.11797	-0.17712
C	1.81249	1.08458	-0.29951
C	1.17329	-1.21164	0.08286
C	3.15505	0.73319	-0.16049
H	1.54489	2.11321	-0.51207
C	2.51358	-1.55521	0.24469
H	0.40946	-1.97711	0.15017
C	3.50851	-0.58497	0.11968
H	3.92264	1.49314	-0.27195
H	2.78050	-2.58578	0.45949
H	4.55370	-0.85731	0.23488
O	-1.41374	-0.99823	-0.73978
C	-2.68641	-1.13970	-1.33301
H	-2.74863	-0.58597	-2.28178
H	-2.84641	-2.20048	-1.54211
H	-3.49654	-0.78664	-0.67820
O	-1.76525	0.57218	1.10555
C	-2.01037	-0.63536	1.82727
H	-2.38475	-0.32222	2.80380
H	-2.75858	-1.25951	1.33437
H	-1.09021	-1.21112	1.96305
H	-0.55740	2.50407	0.83220

2.4.35. Structure **24**

2.4.35.1. SMD(THF)//M06-2X/6-

31++G(d,p)

P	1.00956	-0.64314	-0.19329
H	0.74794	-1.77137	-1.03640
O	1.57814	-1.67341	0.97355
C	-0.77221	-0.20503	-0.11536
C	-1.22028	1.09045	0.17360
C	-1.71141	-1.19733	-0.41257
C	-2.58301	1.38306	0.16567
H	-0.49954	1.86910	0.40363
C	-3.07660	-0.91347	-0.39624
H	-1.37601	-2.20243	-0.66068
C	-3.51291	0.38016	-0.11186
H	-2.91884	2.39331	0.38052
H	-3.79621	-1.69712	-0.61366
H	-4.57494	0.60775	-0.10940
O	1.52935	0.65047	0.75187
C	1.26059	0.69107	2.14214
H	0.28780	0.24955	2.39249
H	2.03731	0.15855	2.69940
H	1.25492	1.74252	2.44532
O	1.84227	-0.05678	-1.47435
C	2.42909	1.24221	-1.58101
H	3.24903	1.36426	-0.87194
H	2.80893	1.31142	-2.60270
H	1.68489	2.02537	-1.41430
H	1.47369	-2.59281	0.69231

2.4.36. Structure **24**-IRC14

2.4.36.1. SMD(THF)//M06-2X/6-

31++G(d,p)

P	1.00422	-0.30422	-0.38633
H	0.82471	-0.57387	-1.75590
O	1.10549	-1.49990	0.73071
C	-0.86143	-0.25279	-0.15558
C	-1.62077	0.10147	-1.27426
C	-1.53212	-0.53033	1.04300
C	-3.01253	0.19947	-1.20352
H	-1.12332	0.30373	-2.22290
C	-2.92113	-0.44142	1.12045
H	-0.96458	-0.82286	1.92202
C	-3.66513	-0.07184	-0.00274
H	-3.58355	0.47684	-2.08501
H	-3.42657	-0.66366	2.05624
H	-4.74758	-0.00457	0.05796
O	1.29271	1.22825	0.09585
C	0.39978	2.07396	0.82229
H	0.10695	1.62081	1.77293
H	0.96143	2.98888	1.02016
H	-0.49237	2.31524	0.23926
O	2.66942	-0.45398	-0.77846
C	3.69599	-0.02107	0.09694
H	3.48342	-0.25687	1.14945
H	4.61764	-0.53569	-0.19058
H	3.84916	1.06013	0.01735
H	1.99441	-1.88444	0.74958

2.4.37. Structure **25**

2.4.37.1. SMD(THF)//M06-2X/6-

31++G(d,p)

P	1.00951	-0.64356	-0.19171
H	0.74770	-1.77367	-1.03218
O	1.57928	-1.67071	0.97704
C	-0.77230	-0.20523	-0.11509
C	-1.22044	1.09090	0.17071
C	-1.71132	-1.19843	-0.40995
C	-2.58319	1.38331	0.16194
H	-0.49974	1.87012	0.39897
C	-3.07654	-0.91474	-0.39428
H	-1.37564	-2.20402	-0.65572
C	-3.51296	0.37958	-0.11308
H	-2.91933	2.39401	0.37417
H	-3.79615	-1.69896	-0.60963
H	-4.57500	0.60708	-0.11112
O	1.52869	0.65268	0.75071
C	1.25903	0.69626	2.14060
H	0.28638	0.25469	2.39147
H	2.03566	0.16547	2.69971
H	1.25246	1.74837	2.44154
O	1.84318	-0.06046	-1.47355
C	2.42987	1.23835	-1.58339
H	3.24960	1.36229	-0.87443
H	2.80981	1.30498	-2.60521
H	1.68553	2.02185	-1.41896
H	1.47405	-2.59086	0.69861

2.4.38. Structure **25**-IRC12

2.4.38.1. SMD(THF)//M06-2X/6-

31++G(d,p)

P	0.98901	0.00005	-0.45510
H	0.81850	0.00017	-1.86250
O	1.33845	-0.00014	1.20510
C	-0.81527	0.00018	-0.12276
C	-1.65983	0.00034	-1.23929
C	-1.38777	-0.00009	1.15803
C	-3.04571	0.00020	-1.08826
H	-1.23333	0.00061	-2.23935
C	-2.77321	-0.00022	1.30956
H	-0.74619	-0.00017	2.03083
C	-3.60458	-0.00010	0.18863
H	-3.68513	0.00027	-1.96577
H	-3.20446	-0.00053	2.30638
H	-4.68369	-0.00029	0.31170
O	1.71301	1.46720	-0.69901
C	2.03761	2.41582	0.31570
H	2.92004	2.11075	0.88651
H	2.26555	3.34862	-0.20449
H	1.19887	2.57529	0.99835
O	1.71272	-1.46726	-0.69928
C	2.03761	-2.41593	0.31532
H	1.19908	-2.57531	0.99827
H	2.26524	-3.34872	-0.20500
H	2.92025	-2.11096	0.88586
H	2.28356	-0.00002	1.40964

2.4.39. Structure **25**-IRC13

2.4.39.1. SMD(THF)//M06-2X/6-

31++G(d,p)

P	-1.04807	-0.28694	0.21666
H	-1.07862	0.27345	1.51785
O	-0.95381	-1.87455	-0.15553
C	0.82518	-0.18519	0.21496
C	1.42565	0.67113	1.14053
C	1.64884	-0.89621	-0.66880
C	2.81296	0.83333	1.18163
H	0.80728	1.22477	1.84698
C	3.03321	-0.74174	-0.63287
H	1.20334	-1.57916	-1.38689
C	3.61896	0.12655	0.29211
H	3.25966	1.50473	1.90945
H	3.65828	-1.30273	-1.32210
H	4.69832	0.24442	0.32154
O	-1.33200	0.79343	-0.97097
C	-0.35431	1.51290	-1.72523
H	0.25783	0.83900	-2.32910
H	-0.92335	2.16997	-2.38520
H	0.28951	2.11752	-1.08151
O	-2.74859	-0.53082	0.36156
C	-3.52702	0.57309	0.75639
H	-3.75596	1.22337	-0.09569
H	-4.46002	0.19961	1.18734
H	-3.01433	1.17451	1.52518
H	-1.84641	-2.25294	-0.19057

2.4.40. Structure **26**

2.4.40.1. SMD(THF)//M06-2X/6-

31++G(d,p)

P	0.88244	0.84346	-0.71511
H	0.89472	1.08262	-2.09458
O	1.34191	1.98173	0.13328
C	-0.77530	0.27372	-0.27680
C	-1.27349	-0.92684	-0.79743
C	-1.55949	1.04453	0.58546
C	-2.55375	-1.35322	-0.45293
H	-0.66004	-1.52907	-1.46344
C	-2.84004	0.61300	0.93029
H	-1.16032	1.97171	0.98714
C	-3.33546	-0.58287	0.41084
H	-2.94085	-2.28510	-0.85350
H	-3.44963	1.20882	1.60267
H	-4.33282	-0.91746	0.68070
O	1.79073	-0.48815	-0.71491
C	2.02286	-1.17637	0.53628
H	1.30880	-0.83016	1.29304
H	1.82380	-2.23296	0.33988
C	3.44844	-0.95298	0.99103
H	3.63179	-1.50900	1.91564
H	4.15344	-1.30215	0.23146
H	3.63071	0.10830	1.18030

2.4.40.2. SMD(THF)//B3LYP/6-

31++G(d,p)

P	0.83471	1.07103	-0.60284
H	0.89530	1.24005	-1.99780
O	1.08578	2.31271	0.20449
C	-0.77292	0.30160	-0.24661
C	-1.18327	-0.84934	-0.94070
C	-1.62359	0.87998	0.70723
C	-2.42996	-1.41934	-0.67388
H	-0.53475	-1.30158	-1.68677
C	-2.86975	0.30474	0.97391
H	-1.30721	1.77466	1.23504
C	-3.27255	-0.84330	0.28445
H	-2.74376	-2.30923	-1.21223
H	-3.52485	0.75417	1.71494
H	-4.24223	-1.28830	0.49030
O	1.94853	-0.10997	-0.50002
C	2.29087	-0.69432	0.79102
H	2.77333	0.07403	1.40337
H	1.37136	-1.01734	1.29280
C	3.21961	-1.86674	0.54970
H	3.49878	-2.31146	1.51156
H	2.73357	-2.63765	-0.05736
H	4.13479	-1.54433	0.04221

2.4.41. Structure **27**

2.4.41.1. SMD(THF)//M06-2X/6-

31++G(d,p)

C	-0.08266	0.54767	-0.00003
H	-0.14312	1.19093	0.88830
H	-0.14305	1.19090	-0.88840
O	-1.14988	-0.39604	-0.00007
H	-1.98884	0.08057	0.00048
C	1.22012	-0.22213	0.00003
H	2.06952	0.46752	-0.00004
H	1.28989	-0.85734	0.88842
H	1.28988	-0.85748	-0.88825

2.4.41.2. SMD(THF)//B3LYP/6-

31++G(d,p)

C	-0.07876	0.54730	-0.00001
H	-0.14046	1.19152	0.88905
H	-0.14042	1.19151	-0.88909
O	-1.16313	-0.39679	-0.00003
H	-1.99713	0.09377	0.00023
C	1.22790	-0.22359	0.00002
H	2.07392	0.47316	-0.00003
H	1.30718	-0.85890	0.88925
H	1.30717	-0.85898	-0.88916

2.4.42.	Structure 28	H	4.20094	0.02475	1.59209
		H	5.93425	-0.05151	1.21875
2.4.42.1.	SMD(THF)//M06-2X/6-	H	5.15963	1.51892	1.52547

31++G(d,p)

P	0.20625	0.80207	-1.15935
H	0.61689	1.38397	-2.36198
O	-0.98594	-0.09900	-1.28100
C	1.62627	-0.03781	-0.43169
C	1.56210	-1.41228	-0.18796
C	2.78650	0.68190	-0.12092
C	2.65911	-2.06679	0.37164
H	0.65611	-1.96111	-0.42989
C	3.88079	0.02303	0.43283
H	2.83438	1.75211	-0.30797
C	3.81521	-1.35031	0.67918
H	2.61024	-3.13341	0.56754
H	4.78161	0.57823	0.67525
H	4.66870	-1.86147	1.11479
O	0.00299	2.14530	-0.30117
C	-0.41308	2.03358	1.08319
H	-0.09360	1.06608	1.48971
H	0.12931	2.81911	1.61375
O	-2.26134	-1.55728	0.72996
C	-3.49118	-1.94690	0.14373
H	-3.31463	-2.47583	-0.80474
H	-3.95119	-2.66230	0.83368
H	-1.78020	-1.02295	0.07102
C	-1.91073	2.21363	1.19973
H	-2.43932	1.41775	0.66769
H	-2.20134	2.17668	2.25427
H	-2.21462	3.18052	0.78876
C	-4.42450	-0.76906	-0.08911
H	-3.97627	-0.05326	-0.78671
H	-5.37534	-1.10911	-0.5141
H	-4.63316	-0.25208	0.85308

2.4.42.2. SMD(THF)//B3LYP/6-

31++G(d,p)

P	-0.01679	-0.43769	-0.74251
H	0.03340	-0.42792	-2.14654
O	1.25728	-0.01173	-0.05883
C	-1.44356	0.56944	-0.25509
C	-1.28690	1.58843	0.69618
C	-2.69790	0.35357	-0.85093
C	-2.38226	2.37736	1.05950
H	-0.31364	1.75918	1.14616
C	-3.78797	1.14712	-0.48824
H	-2.82559	-0.42863	-1.59500
C	-3.63019	2.15774	0.46787
H	-2.25962	3.16423	1.79832
H	-4.75648	0.97955	-0.95087
H	-4.47943	2.77495	0.74800
O	-0.43704	-1.99253	-0.55530
C	-0.62487	-2.55536	0.77932
H	0.33755	-2.53855	1.29972
H	-1.33554	-1.93004	1.33142
O	3.56184	1.46604	-0.69120
C	4.71495	0.66898	-0.42303
H	4.60486	-0.32878	-0.87575
H	5.55187	1.16348	-0.93013
H	2.76370	0.95381	-0.45106
C	-1.14481	-3.96995	0.62656
H	-0.43583	-4.59154	0.06994
H	-1.28310	-4.41225	1.61959
H	-2.10807	-3.98322	0.10615
C	5.01791	0.53343	1.06687

2.4.43.	Structure 29	H	4.26865	-1.92732	-0.57536
2.4.43.1.	SMD(THF)//M06-2X/6-	H	4.88566	-0.43071	-1.31058
		H	4.60227	-0.50793	0.44005

31++G(d,p)

P	0.19965	0.96569	-0.22565
H	-0.07636	1.53942	-1.47684
O	0.77293	1.68058	1.13053
C	-0.15576	-0.81979	-0.06315
C	-1.00208	-1.28502	0.94994
C	0.42234	-1.73654	-0.94838
C	-1.24867	-2.64955	1.08889
H	-1.46876	-0.57569	1.62783
C	0.15188	-3.09916	-0.82718
H	1.08674	-1.38066	-1.73025
C	-0.67667	-3.55750	0.19651
H	-1.89416	-3.00279	1.88750
H	0.59401	-3.80193	-1.52703
H	-0.87885	-4.61978	0.29844
O	1.76857	0.78292	-0.82048
C	2.81187	0.20957	-0.03744
H	2.40462	-0.27416	0.86012
H	3.28161	-0.57367	-0.64616
O	-1.37497	1.47163	0.30063
C	-2.47146	1.23345	-0.55673
H	-2.14511	1.26304	-1.61032
H	-2.87649	0.22692	-0.37511
H	0.02705	1.98576	1.66937
C	3.83567	1.26091	0.34748
H	3.37215	2.03173	0.96858
H	4.65801	0.80252	0.90702
H	4.25066	1.73399	-0.54792
C	-3.53946	2.28350	-0.32048
H	-3.15065	3.28238	-0.53999
H	-4.40457	2.09516	-0.96412
H	-3.87289	2.26222	0.72142

2.4.43.2. SMD(THF)//B3LYP/6-

31++G(d,p)

P	0.23643	-1.02573	-0.06045
H	0.58206	-1.50466	-1.33995
O	0.15614	-1.78584	1.40325
C	-0.15075	0.76674	0.00394
C	0.41989	1.58645	0.99099
C	-1.01098	1.33916	-0.94626
C	0.11817	2.94983	1.03921
H	1.10326	1.16114	1.71934
C	-1.29089	2.70901	-0.91369
H	-1.46413	0.71525	-1.71002
C	-0.73337	3.51507	0.08334
H	0.55459	3.57103	1.81667
H	-1.94948	3.14193	-1.66177
H	-0.95885	4.57761	0.11496
O	-1.32281	-1.57784	-0.46499
C	-2.45263	-1.50130	0.41650
H	-2.32690	-2.22211	1.23254
H	-2.51880	-0.49935	0.86353
O	1.95139	-0.84178	0.26969
C	2.80058	-0.34018	-0.75549
H	2.43920	-0.67370	-1.74377
H	2.77370	0.75977	-0.75673
H	1.03041	-1.73877	1.82435
C	-3.71277	-1.81112	-0.37574
H	-3.65946	-2.81390	-0.81430
H	-4.58826	-1.77235	0.28340
H	-3.86109	-1.08797	-1.18526
C	4.22324	-0.83342	-0.53511

2.4.44. B1: Triethylamine **30**

2.4.44.1. SMD(DMSO)//M06-2X/6- 31++G(d,p)

```

N  0.00017700  0.00043000 -0.18998400
C -1.14024100  0.79899000  0.26872000
H -2.05121900  0.32031400 -0.09875100
H -1.19449900  0.78880400  1.37614400
C -1.13033800  2.23995400 -0.22872800
H -0.94265600  2.27448000 -1.30766800
H -2.10787600  2.69447600 -0.04129700
H -0.38079600  2.85772800  0.27230000
C  1.26223000  0.58790100  0.26932800
H  1.30428000  1.61666000 -0.09649300
H  1.27968300  0.63783800  1.37690200
C  2.50514800 -0.14136900 -0.22894700
H  2.44325000 -0.31458800 -1.30904200
H  3.38924700  0.47352900 -0.03501300
H  2.66187900 -1.10285300  0.26663900
C -0.12216100 -1.38633600  0.26874300
H  0.74792800 -1.93609900 -0.09860600
H -0.08535200 -1.42700400  1.37619700
C -1.37489900 -2.09907800 -0.22860200
H -1.28337000 -3.17150300 -0.03183000
H -2.28618500 -1.75369900  0.26632300
H -1.49399300 -1.96146700 -1.30900200

```

2.4.44.2. SMD(THF)//M06-2X/6- 31++G(d,p)

```

N -0.00001100  0.00010600 -0.18006400
C  1.28126500  0.54546700  0.27479500
H  1.35175800  1.57370500 -0.08815700
H  1.30837000  0.59166100  1.38264100
C  2.49764600 -0.21898500 -0.23594700
H  2.41893500 -0.38847400 -1.31527700
H  3.40093100  0.36941900 -0.04912900
H  2.63106100 -1.18516500  0.25726500
C -0.16805800 -1.38223300  0.27441500
H  0.68687800 -1.95742800 -0.08902100
H -0.14144000 -1.42918800  1.38223600
C -1.43880100 -2.05287700 -0.23590500
H -1.54931000 -1.89442900 -1.31410000
H -1.37868300 -3.13027400 -0.05518300
H -2.34123500 -1.68892300  0.26171500
C -1.11262100  0.83670500  0.27570100
H -2.03864700  0.38308500 -0.08565700
H -1.16443900  0.83805300  1.38357300
C -1.05946300  2.27180400 -0.23642300
H -2.02090800  2.75975200 -0.05024400
H -0.28944800  2.87126300  0.25574000
H -0.87355000  2.28692200 -1.31576800

```

2.4.45. Trimethylamine **31**

2.4.45.1. SMD(DMSO)//M06-2X/6- 31++G(d,p)

```

C -1.03725200  0.90909400  0.06352900
H -2.01098900  0.58355500 -0.31452400
H -1.09169600  0.95284700  1.16814100
C  1.30627800  0.44332200  0.06366700
H  1.51204200  1.44927000 -0.31434400
H  1.37147500  0.46777400  1.16830200
C -0.26902000 -1.35235300  0.06342500
H  0.49910600 -2.03409500 -0.31365200
H -0.28077800 -1.42096600  1.16814000
H  2.08115500 -0.23226500 -0.31071600
H -1.24122000 -1.68712400 -0.31060400
H -0.84095000  1.91846700 -0.31021500

```

2.4.46. Structure **32**

2.4.46.1. SMD(THF)//M06-2X/6- 31++G(d,p)

```
P -0.13037800 1.40628700 -0.12944600
H 0.75472800 1.45247600 -1.20867200
O -1.30723700 2.29098200 -0.82408700
C -2.48006300 2.57188000 -0.05276600
H -2.22655800 3.15974100 0.83365200
H -3.14787300 3.14851600 -0.69360000
H -2.98053100 1.64455600 0.24969200
O 0.32094100 1.93922600 1.19076200
C -0.81481600 -0.26296100 -0.04243200
C -1.15616000 -0.80341700 1.19912000
C -1.00723200 -1.00842000 -1.20938000
C -1.69124400 -2.08966500 1.27325800
H -0.98838600 -0.21994300 2.10086200
C -1.52998800 -2.29800300 -1.13205000
H -0.74075900 -0.58824600 -2.17740500
C -1.87315200 -2.83714100 0.10963800
H -1.95855200 -2.51023200 2.23820800
H -1.67201100 -2.88014400 -2.03775300
H -2.28185500 -3.84159200 0.16932000
N 2.25802000 -0.24850400 -0.06153800
C 3.20696200 0.78289100 0.32111000
H 2.90692100 1.21537700 1.27919100
H 4.23692500 0.38990600 0.40691900
C 2.57409100 -0.79585100 -1.36798900
H 2.55909400 0.00182900 -2.11954700
H 3.57160100 -1.27265000 -1.39409100
C 2.18675300 -1.29531600 0.94163000
H 1.44223900 -2.04179200 0.64373100
H 3.15800500 -1.80563400 1.08089200
H 1.82801900 -1.54828200 -1.64470400
H 1.88027300 -0.86572700 1.90091500
H 3.20771100 1.58142200 -0.42940700
```

2.4.47. Structure **33**

2.4.47.1. SMD(THF)//M06-2X/6- 31++G(d,p)

```
P 0.00047200 0.53353000 -0.60980100
H 1.78907000 -0.34512000 0.35537200
O -0.18188200 2.08271000 -0.04299700
C -0.72054900 2.31254200 1.25882300
H -0.24453200 1.66312900 2.00083000
H -0.51896500 3.35608200 1.50975700
H -1.80276100 2.14145600 1.26754100
O 0.78548100 -0.23889000 0.58862700
C -1.68907200 -0.12959000 -0.27773000
C -1.91647200 -1.20575400 0.58421000
C -2.77328100 0.44563600 -0.95337400
C -3.21131500 -1.69105300 0.77956600
H -1.07614200 -1.65497200 1.10554800
C -4.06686800 -0.03278900 -0.75452900
H -2.60640600 1.27866200 -1.63439500
C -4.28700200 -1.10460100 0.11358600
H -3.38010100 -2.52569500 1.45432800
H -4.90152600 0.42645100 -1.27637000
H -5.29367800 -1.48298300 0.26606100
N 3.30754400 -0.47560100 -0.04352000
C 3.41762300 -1.45430000 -1.12435600
H 2.82791200 -1.11881600 -1.98206400
H 4.46406300 -1.58659900 -1.44166100
C 4.04519200 -0.91758100 1.13885600
H 3.65198500 -1.87991500 1.47783500
H 5.11952300 -1.02904900 0.92339900
C 3.76739700 0.84161800 -0.48301500
H 3.60973200 1.57002100 0.31739800
H 4.83694500 0.82681600 -0.74524100
H 3.92096600 -0.18520400 1.94129800
H 3.19381300 1.15456400 -1.36004700
H 3.02751000 -2.41790000 -0.78520200
```

2.4.48. Structure **34**

2.4.48.1. SMD(THF)//M06-2X/6- 31++G(d,p)

```
P  0.20698600  1.02853500  0.40136200
H  1.95993700 -0.09997000  0.15341900
O  0.05154900  1.95521500 -0.99849700
C -1.08395400  2.80312000 -1.10721900
H -1.13221300  3.50537700 -0.26788500
H -0.98974000  3.36381700 -2.04118400
H -2.01486800  2.22085600 -1.13590500
O -0.09375100  1.88590800  1.63485000
C -1.29851400 -0.05094600  0.16021900
C -2.23328400 -0.20872500  1.18723900
C -1.46688600 -0.78227600 -1.02256800
C -3.31907600 -1.07516800  1.03660200
H -2.10244000  0.36576800  2.10193300
C -2.55095500 -1.64423400 -1.18248900
H -0.74668300 -0.66510500 -1.83180000
C -3.47969100 -1.79343500 -0.14852400
H -4.04263800 -1.18688500  1.83992000
H -2.67684000 -2.19682700 -2.10988500
H -4.32342000 -2.46728900 -0.26811700
N  2.82901800 -0.74087200  0.01527500
C  3.95969100  0.13931900 -0.34896700
H  4.11874600  0.85500300  0.45895200
H  4.85577200 -0.46752100 -0.49885400
C  2.47933300 -1.67916300 -1.07275300
H  2.23448300 -1.10101800 -1.96557700
H  3.32854200 -2.33718700 -1.27119300
C  3.05072600 -1.43603300  1.30147600
H  2.14796100 -1.99469900  1.55426800
H  3.90025400 -2.11591400  1.20391100
H  1.61285000 -2.26593900 -0.76269500
H  3.24978200 -0.68952100  2.07169900
H  3.70587300  0.67139900 -1.26728300
```

2.4.49. Structure **35**

2.4.49.1. SMD(THF)//M06-2X/6- 31++G(d,p)

```
P  0.24555100  1.07553600 -0.01193500
H  -0.56726100  0.62786600 -1.05733100
O  -0.42339200  1.32638800  1.29916200
C  1.68895000 -0.00681700  0.07525100
C  1.91896900 -0.76356600  1.22604900
C  2.55944900 -0.10019200 -1.01502400
C  3.02287400 -1.61189700  1.28727300
H  1.22411100 -0.69055400  2.05733400
C  3.65869600 -0.95623600 -0.95467800
H  2.38014000  0.49273300 -1.90908000
C  3.89006400 -1.70894100  0.19720300
H  3.20635000 -2.19918500  2.18208600
H  4.33506700 -1.03115200 -1.80083200
H  4.74821100 -2.37306800  0.24540900
O  0.80004600  2.40426800 -0.76252700
C  1.69742000  3.25850700 -0.04208100
H  2.53896100  2.68893700  0.36836500
H  2.07470300  3.99155600 -0.75562500
H  1.17072100  3.76964000  0.76786000
O  -0.89293700 -1.59824500  0.13596000
C  -0.61717000 -2.18999200 -1.11151400
H  -1.31688100 -3.00432600 -1.34901800
H  -0.65190000 -1.46054000 -1.93750900
H  0.39363400 -2.61055400 -1.07645200
H  -1.76345700 -1.11453600  0.07202800
N  -3.29165300 -0.31154300 -0.00461300
C  -4.20183400 -1.26983000 -0.62260700
H  -4.10811400 -2.24059200 -0.12627500
H  -5.25245000 -0.93995500 -0.55244300
C  -3.35386800  0.97595300 -0.68737300
H  -3.05893600  0.85724000 -1.73483300
H  -4.37249300  1.39986600 -0.65668100
C  -3.58368000 -0.14867700  1.41738400
H  -2.84155500  0.52408500  1.85629800
H  -4.59432700  0.26276500  1.58022800
H  -2.67197800  1.67976200 -0.20122300
H  -3.51724800 -1.11906000  1.91854900
H  -3.94595200 -1.39232600 -1.67960700
```

2.4.50. Structure **36**

2.4.50.1. SMD(THF)//M06-2X/6-

31++G(d,p)

P	-0.19558700	0.96057100	0.69694000
H	-0.31384700	1.42840900	2.01786900
O	0.98478000	1.21001700	-0.35039500
C	-1.57419000	-0.09236900	0.09793100
C	-1.29958100	-1.34967500	-0.45232300
C	-2.90086600	0.34496300	0.16904900
C	-2.33180300	-2.14964800	-0.93869500
H	-0.27156900	-1.70008100	-0.48920000
C	-3.93816700	-0.46694300	-0.29143400
H	-3.11758300	1.32735100	0.57822400
C	-3.65437400	-1.71147000	-0.85233000
H	-2.10681000	-3.11776700	-1.37689900
H	-4.96569100	-0.12246600	-0.22036700
H	-4.46068000	-2.33962700	-1.21998000
O	-0.96230500	2.43371200	0.30234500
C	-1.14668800	2.80577700	-1.04833200
H	-1.43066800	1.95249200	-1.67986500
H	-1.95257400	3.54620400	-1.08658800
H	-0.23351100	3.24846600	-1.46094300
O	0.70029000	-0.39232400	1.34061300
C	0.17089700	-1.04448400	2.46468000
H	0.98110000	-1.57678200	2.97409800
H	-0.26959200	-0.33415700	3.18460500
H	-0.60714900	-1.77146800	2.18912000
H	1.76278500	0.50731600	-0.35049100
N	3.03189000	-0.36599500	-0.51163000
C	3.80321700	-0.24017200	0.72333200
H	3.20438100	-0.61766500	1.55523600
H	4.74936900	-0.80134300	0.66425500
C	3.77521200	0.17536900	-1.64856400
H	4.00945900	1.22737400	-1.46300100
H	4.71576800	-0.37308800	-1.81457600
C	2.65810100	-1.75884400	-0.74712400
H	2.04536100	-1.82427900	-1.65125900
H	3.54846100	-2.39448800	-0.87869500
H	3.16332000	0.10693200	-2.55244800
H	2.07708000	-2.11861500	0.10561300
H	4.03048600	0.81442400	0.90495700

2.4.51. Structure **38**

2.4.51.1. SMD(THF)//M06-2X/6-

31++G(d,p)

P	-0.43366900	-0.62677400	0.45229100
H	0.22960700	-1.81899300	0.11077900
O	0.11550400	0.62903600	1.28199200
C	-2.16245300	-0.45634100	-0.13829100
C	-2.54131400	0.68589000	-0.85295900
C	-3.11561400	-1.44563300	0.12141600
C	-3.85518000	0.84300200	-1.28972800
H	-1.79596400	1.44611000	-1.07199000
C	-4.42514100	-1.30294900	-0.33961400
H	-2.83000700	-2.32392800	0.69275800
C	-4.79762800	-0.15626900	-1.04035700
H	-4.14140500	1.73829400	-1.83395600
H	-5.15480000	-2.08362300	-0.14550800
H	-5.81871100	-0.04095600	-1.39236200
O	-0.85135500	-1.47301300	1.87532000
C	-1.54403900	-0.82355600	2.92163500
H	-2.30065500	-0.12039300	2.54683000
H	-2.05100900	-1.58954600	3.51790700
H	-0.85197500	-0.26816400	3.56441800
O	0.24065100	0.07575400	-0.99222500
C	0.17825800	-0.70034100	-2.16153600
H	0.76576200	-0.20202300	-2.93988100
H	0.59904800	-1.70703200	-2.00668300
H	-0.85264800	-0.80948100	-2.53101800
H	0.55894000	1.38391100	0.72372500
N	3.07983800	-1.91882600	-0.42470800
C	3.06323100	-1.34739200	0.91106200
H	2.72541000	-2.09527000	1.63583200
H	4.06428200	-0.98906900	1.22263100
C	3.42869500	-0.90547400	-1.40537900
H	2.69096400	-0.09766200	-1.36316200
H	4.43596700	-0.48028700	-1.22620800
C	3.99521500	-3.04478900	-0.49131700
H	3.96995700	-3.48645200	-1.49232600
H	5.03878200	-2.74950800	-0.26884900
H	3.41710000	-1.33916000	-2.41076400
H	3.69535100	-3.81035900	0.23090500
H	2.37370500	-0.49815500	0.94543100
N	1.30359000	2.69248600	0.22795900
C	1.21263400	2.92042000	-1.21187300
H	0.16260700	2.99680700	-1.50661400
H	1.73355600	3.84812400	-1.50035100
C	2.69811800	2.53808200	0.63885000
H	3.15313200	1.71087600	0.08646300
H	3.27868500	3.45444700	0.44505600
C	0.66552300	3.77991000	0.96847300
H	0.71989600	3.57439400	2.04135500
H	1.15354600	4.74711400	0.76854700
H	2.74386300	2.31226000	1.70839900
H	-0.38739100	3.84840800	0.67967000
H	1.65521300	2.07373200	-1.74113700

2.4.52. Structure **39**

2.4.52.1. SMD(THF)//M06-2X/6- 31++G(d,p)

```
P -1.23519700  0.30934000 -0.39610200
O -1.77591000  0.53073200  1.19656500
C  0.56475800 -0.13644800 -0.16219400
C  1.02240400 -0.93946300  0.88802900
C  1.50279800  0.34863300 -1.08007500
C  2.37778000 -1.24187700  1.02444400
H  0.30549600 -1.33863100  1.60014900
C  2.85955600  0.03975200 -0.95986400
H  1.16592400  0.98952500 -1.89217600
C  3.30249700 -0.75487700  0.09759100
H  2.71381300 -1.86141300  1.85227400
H  3.57013400  0.42506400 -1.68659400
H  4.35758200 -0.99396800  0.19959000
O  -0.85192300  2.04496700 -0.48195200
C  -0.23483200  2.73436800  0.57457400
H  0.58953500  2.16272700  1.03002200
H  0.18227500  3.67501100  0.18950000
H  -0.94944500  2.97471400  1.37392900
O  -1.59408700 -1.59028300 -0.01860600
C  -2.77511600 -2.00986400 -0.61723500
H  -2.90036800 -3.09721200 -0.49745400
H  -3.68013600 -1.53545600 -0.18719600
H  -2.79937900 -1.79805200 -1.70282200
H  -1.97118500 -0.36708600  1.50265200
```

2.4.53. Structure **40**

2.4.53.1. SMD(THF)//M06-2X/6- 31++G(d,p)

```
P   1.39795400  0.07977100 -0.06136900
O   1.87103400  0.16316900  1.54530200
C  -0.46106200  0.01893900  0.03833600
C  -1.13731200  0.27652900  1.23693100
C  -1.21618400 -0.26781800 -1.10358100
C  -2.52934300  0.23501900  1.29698700
H  -0.55624900  0.51518500  2.12488700
C  -2.61327800 -0.30782000 -1.05141300
H  -0.70967400 -0.45963300 -2.04895000
C  -3.27386500 -0.05863100  0.15040400
H  -3.03878900  0.43516600  2.23648000
H  -3.18294600 -0.53132000 -1.94989900
H  -4.35909700 -0.08833700  0.19513800
O   1.39048900 -1.82448200  0.31088300
C   1.18625000 -2.63282300 -0.79422600
H   1.61671200 -2.19507600 -1.71754000
H   1.66312600 -3.61521200 -0.65168000
H   0.11487000 -2.81962600 -0.99849900
O   1.36794000  1.88971500  0.01838500
C   1.00478300  2.48597600 -1.18683300
H   1.40182500  3.50922900 -1.22601300
H   1.40394800  1.94104700 -2.06376100
H   -0.09046200  2.54759800 -1.31696800
H   1.97178800 -0.75901800  1.82113900
```

2.4.54. Water **41**

2.4.54.1. SMD(THF)//M06-2X/6- 31++G(d,p)

```
O  0.000000000  0.00000000  0.11690500
H  0.000000000  0.76741200 -0.46761800
H  0.000000000 -0.76741200 -0.46761800
```

2.4.55. Structure **42**

2.4.55.1. SMD(THF)//M06-2X/6- 31++G(d,p)

```
P  1.38436000 -0.03318700  0.48619600
H  1.30801300 -0.47937000  1.80485400
O  1.91528700 -1.00481600 -0.52868600
C -0.22005200  0.64427800  0.02272200
C -0.76127600  0.33816300 -1.22799100
C -0.92604900  1.45316600  0.91853300
C -2.00978300  0.84658200 -1.58486000
H -0.21139800 -0.30248400 -1.91235600
C -2.17716700  1.95237400  0.56182400
H -0.50727500  1.68578100  1.89550900
C -2.71686800  1.64977000 -0.68980800
H -2.43250500  0.61056900 -2.55676700
H -2.73069000  2.57517400  1.25797800
H -3.69227800  2.03892800 -0.96666900
O  2.34566800  1.24143000  0.72896600
C  2.72673700  2.02359600 -0.41361000
H  1.84218000  2.37527800 -0.95600400
H  3.28222800  2.88076900 -0.03361400
H  3.36253800  1.43565600 -1.08006900
O -0.53352400 -2.18558200  1.16365400
C -1.91344200 -1.90278300  1.30509400
H -2.51136700 -2.82236900  1.34769200
H -2.04807100 -1.36331500  2.24658300
H -2.28963400 -1.27487600  0.48581800
H -0.38789800 -2.65230900  0.32042800
O  0.32716400 -3.04927000 -1.34192200
H  0.78432700 -3.88227700 -1.50464900
H  1.01706400 -2.37233200 -1.16918700
```

2.4.56. Structure **43**

2.4.56.1. SMD(THF)//M06-2X/6-

31++G(d,p)

```
P  0.84540600  0.66621600  0.49315200
H  1.12192900  0.92080700  1.84512200
O  1.81739900  0.86410200  -0.78423000
C  -0.79792600 -0.03714600  0.11203300
C  -0.90540800 -1.22296500  -0.62384300
C  -1.96018500  0.60963300  0.54458700
C  -2.15858800 -1.74633400  -0.93449300
H  -0.00662100 -1.73911000  -0.95051100
C  -3.21393200  0.06981400  0.25793300
H  -1.88158000  1.53958300  1.09984800
C  -3.31431700 -1.10500100  -0.48625900
H  -2.23195200 -2.65945900  -1.51759900
H  -4.11063100  0.57174100  0.60897100
H  -4.29073600 -1.52100200  -0.71724700
O  0.36728100  2.28305700  0.43913500
C  -0.02519600  2.89259700  -0.77916900
H  -0.62818500  2.21969100  -1.40297200
H  -0.63015100  3.76934900  -0.53080400
H  0.85081000  3.20888300  -1.35386700
O  1.57904700 -0.91753400  0.75276200
C  1.16158300 -1.62345600  1.89976500
H  1.93423300 -2.35244600  2.15999000
H  1.02705700 -0.94939500  2.76029000
H  0.21502800 -2.15252000  1.72676300
H  2.67789300 -1.72568500  -0.52380100
O  3.02126700 -1.54621300  -1.41894600
H  3.97780500 -1.66934000  -1.38900900
H  2.29787500  0.05550100  -1.06552400
```

2.4.57. Iso-propyl *hydrogeno-*

phenylphosphinate **45**

2.4.57.1. SMD(THF)//M06-2X/6-

31++G(d,p)

```
P  0.70020100  -1.00250000  -0.64367400
H  0.61948000  -1.52757400  -1.94069900
O  1.60479400  0.28128400  -0.99850800
C  2.27040600  1.10870600  -0.00287600
H  2.53171200  2.00745400  -0.56861100
O  1.21482300  -1.93845200  0.39939900
C  -0.95736400  -0.38220700  -0.27062500
C  -1.62128900  -0.83821600  0.87030800
C  -1.57862000  0.53316100  -1.12743200
C  -2.90177200  -0.36850900  1.16198100
H  -1.12949200  -1.55147100  1.52637700
C  -2.85893800  0.99756300  -0.83572900
H  -1.06234500  0.88729000  -2.01708100
C  -3.51858700  0.54763500  0.31008200
H  -3.41751600  -0.71834000  2.05120200
H  -3.34118700  1.70922400  -1.49900300
H  -4.51656500  0.91091500  0.53728700
C  3.53927700  0.41858000  0.46784400
H  4.15976700  0.13483100  -0.38682400
H  4.11479000  1.10174600  1.10036000
H  3.30010100  -0.47994600  1.04381300
C  1.34528600  1.48991800  1.14122100
H  0.43007200  1.96391800  0.77505300
H  1.07676300  0.61640900  1.74589400
H  1.86407200  2.20061200  1.79156600
```

2.4.58. Menthyl *hydrogeno*-phenylphosphinate **46**

2.4.58.1. SMD(THF)//M06-2X/6-31++G(d,p)

```
P -0.97672800 -2.01120800 0.03722400
H -1.32469500 -3.08053000 -0.79889000
O 0.27331400 -1.46016800 -0.82057500
O -0.72389700 -2.40645200 1.45443500
C -2.27282900 -0.76352900 -0.12183500
C -2.96742000 -0.35668200 1.01956000
C -2.57896200 -0.20472800 -1.36862100
C -3.95960000 0.61836700 0.91741700
H -2.71965400 -0.79817300 1.98121400
C -3.56784100 0.77059400 -1.46723100
H -2.04107300 -0.52493900 -2.25885400
C -4.25591000 1.18219800 -0.32283400
H -4.49865300 0.93732400 1.80433900
H -3.80240000 1.20983800 -2.43207500
H -5.02649000 1.94343100 -0.40215800
C 0.77236500 -0.08966400 -0.76459000
H -0.03046100 0.55032300 -1.15272100
C 1.93607100 -0.06095600 -1.71793400
C 1.13710800 0.34640900 0.66069400
H 1.69440900 -0.15616600 -2.77489800
C 3.20622900 0.06517600 -1.32427500
H 0.40234200 -0.10788000 1.33714100
C 2.49972400 -0.23917400 1.04818300
C 0.99079400 1.87791300 0.86908000
H 3.99259600 0.09577600 -2.07940500
C 3.64193500 0.16440100 0.11337000
H 2.41384100 -1.33489900 1.02799900
H 2.74221400 0.04101200 2.08003400
H 1.56502100 2.11790800 1.77516200
H 3.92196000 1.20981600 0.31329900
C 4.88535600 -0.69437900 0.35914100
H 4.67474000 -1.74783700 0.14244100
H 5.71979000 -0.37640100 -0.27478500
H 5.20565100 -0.62050600 1.40377500
C 1.51356800 2.77436800 -0.26037300
H 2.57523500 2.62918000 -0.47026900
H 0.96079200 2.60753800 -1.19270100
H 1.37027000 3.82436900 0.01722200
C -0.47651600 2.22937200 1.14277800
H -0.85972700 1.68750900 2.01394900
H -0.59240700 3.30204800 1.33199000
H -1.11215100 1.97422000 0.28375500
```

2.4.59. *tert*-butyl *hydrogeno*-phenylphosphinate **47**

2.4.59.1. SMD(THF)//M06-2X/6-31++G(d,p)

```
P -0.35603300 -1.12222500 -0.78548800
H -0.26618800 -1.37978700 -2.16010000
O -0.68149700 -2.30846900 0.06141400
C 1.21315200 -0.34654500 -0.33039500
C 2.04065100 -0.97153900 0.60504400
C 1.60696600 0.85770400 -0.92471800
C 3.25883500 -0.38798300 0.95320900
H 1.72214100 -1.90544600 1.06018800
C 2.82530100 1.43641200 -0.57750000
H 0.96016900 1.34582100 -1.65041300
C 3.64960300 0.81320800 0.36212000
H 3.90178300 -0.87017300 1.68337500
H 3.13190800 2.37195500 -1.03560800
H 4.59863600 1.26667500 0.63301200
O -1.44031400 0.06258200 -0.86569300
C -2.17962600 0.60528800 0.27668400
C -3.32742200 -0.34827300 0.58556700
H -2.94528500 -1.31688200 0.91907300
H -3.95845500 0.07354300 1.37428700
H -3.94179000 -0.50044500 -0.30718700
C -1.26879900 0.78562400 1.48692800
H -0.87829300 -0.17365900 1.84284900
H -0.42878100 1.44886900 1.25830400
H -1.84748100 1.23317900 2.30076500
C -2.69501100 1.94883200 -0.21779000
H -3.31912200 1.81321800 -1.10609500
H -3.29566900 2.42757100 0.56131500
H -1.86048500 2.60966800 -0.47210300
```

2.4.60. Adamantyl *hydrogeno*-phenylphosphinate **48**

2.4.60.1. SMD(THF)//M06-2X/6-

31++G(d,p)

P	1.31588400	1.67479300	-0.41822800
H	1.70141700	2.36112800	-1.57756800
O	0.01938600	0.93594700	-1.02782400
O	1.12350000	2.54081300	0.78202200
C	2.53448000	0.36654100	-0.15608400
C	3.11526400	0.20977100	1.10451800
C	2.89187000	-0.48505400	-1.20800400
C	4.04942900	-0.80506400	1.31553100
H	2.83334800	0.88216000	1.91038800
C	3.82730100	-1.49433700	-0.99495800
H	2.43933600	-0.36169600	-2.18975700
C	4.40442200	-1.65348700	0.26747700
H	4.50147100	-0.92976300	2.29479600
H	4.10746400	-2.15468300	-1.80989700
H	5.13514000	-2.43993000	0.43120100
C	-0.60507500	-0.19725700	-0.37501100
H	0.15824200	-0.98053300	-0.26323800
C	-1.71995800	-0.68860300	-1.29989900
C	-1.17645900	0.17307400	0.99914300
H	-1.28313300	-0.92835700	-2.27692700
C	-2.79320100	0.40095700	-1.44877500
C	-2.34261300	-1.94867200	-0.67469000
H	-0.36543300	0.53666400	1.64109300
C	-2.24970900	1.25993700	0.84166700
C	-1.79910600	-1.09268200	1.61099200
H	-3.58562500	0.03794100	-2.11579400
H	-2.35914300	1.29562300	-1.90966600
C	-3.37708200	0.74494900	-0.06901400
H	-1.58506600	-2.73746900	-0.57778500
H	-3.12883800	-2.33073900	-1.33771300
C	-2.92774900	-1.60731300	0.70442800
H	-1.80173200	2.16819300	0.42211900
H	-2.64953500	1.51959000	1.83026300
H	-1.03243000	-1.86859300	1.73739600
H	-2.18991500	-0.85627800	2.60861300
H	-4.14439500	1.52038200	-0.17922700
C	-4.00009600	-0.51645400	0.55092300
H	-3.37332300	-2.50650300	1.14659700
H	-4.43336700	-0.27775400	1.53130300
H	-4.81614000	-0.88320600	-0.08582200

2.4.61. *Iso*-propanol **49**

2.4.61.1. SMD(THF)//M06-2X/6-31++G(d,p)

C	0.00000100	0.04945900	0.35414500
H	0.00000900	0.14304500	1.44814900
C	1.26097100	-0.67957100	-0.08319800
H	1.28576700	-0.75905500	-1.17571100
H	2.15414000	-0.13794900	0.24227000
H	1.29397600	-1.68987700	0.33737600
C	-1.26098200	-0.67955000	-0.08319000
H	-1.29399200	-1.68986100	0.33736900
H	-2.15413800	-0.13791900	0.24229500
H	-1.28579100	-0.75901800	-1.17570500
O	-0.00000400	1.35845400	-0.23127100
H	0.00012400	2.02096700	0.46757900

2.4.62. Menthol **50**

2.4.62.1. SMD(THF)//M06-2X/6-
31++G(d,p)

```
O  0.22792100  2.54142200  0.44524100
C  0.47722400  1.31206700  -0.25112300
H  1.40637600  1.42594100  -0.82982500
C  -0.66408000  1.13615200  -1.21840600
C  0.62696000  0.13371700  0.72627900
H  -0.70088000  1.84031800  -2.04794000
C  -1.60574400  0.19636600  -1.09495400
H  1.12457300  0.54287300  1.61739700
C  -0.75759900  -0.34103300  1.18402400
C  1.56091400  -0.99153500  0.20730500
H  -2.39132900  0.12873900  -1.84871300
C  -1.67078800  -0.78962600  0.04188000
H  -1.25035000  0.49700100  1.69643000
H  -0.65121900  -1.14796400  1.91940700
H  1.33051900  -1.88725200  0.80193200
H  -1.33407800  -1.76928000  -0.32990300
C  -3.11418500  -0.95806200  0.52415100
H  -3.16752900  -1.68389400  1.34257800
H  -3.51149100  -0.00391600  0.88896200
H  -3.76438400  -1.30964400  -0.28398000
C  1.40677400  -1.36850800  -1.27214600
H  0.39846300  -1.69810000  -1.53143400
H  1.66174600  -0.52733800  -1.92753700
H  2.09475100  -2.18689300  -1.51133900
C  3.02403200  -0.62120800  0.47399800
H  3.20805900  -0.46056600  1.54145600
H  3.69969900  -1.41147700  0.12957800
H  3.29753000  0.29974800  -0.05658800
H  1.02513200  2.77035500  0.94154700
```

2.4.63. *tert*-butanol **51**

2.4.63.1. SMD(THF)//M06-2X/6-
31++G(d,p)

```
C  -0.00695900  0.00000300  0.01582600
C  0.67044500  -1.25666800  -0.52766500
H  0.19434400  -2.15260200  -0.11684300
H  0.60448800  -1.29629800  -1.61979100
H  1.73213400  -1.27278600  -0.25330400
C  -1.49323900  -0.00019200  -0.31449700
H  -1.97558300  -0.88864800  0.10529600
H  -1.97585900  0.88803800  0.10545700
H  -1.64672700  -0.00011800  -1.39789500
C  0.67010600  1.25688800  -0.52758800
H  0.19379200  2.15267300  -0.11669000
H  1.73179300  1.27325000  -0.25323500
H  0.60412500  1.29658300  -1.61971100
O  0.06259400  -0.00002400  1.44808600
H  0.99462300  -0.00008500  1.70557100
```

2.4.64. 1-adamantanol **52**

2.4.64.1. SMD(THF)//M06-2X/6-

31++G(d,p)

```

C  0.74060100 -0.69945000  1.25564300
H  1.12222500 -0.17952700  2.14377800
H  1.13893400 -1.72430200  1.27101300
C  1.24612800  0.02192000 -0.00004700
C  -0.79677500 -0.72494800  1.26115700
H  -1.14970600 -1.24022000  2.16217100
C  -1.32311100  0.71977600  1.24946000
H  -0.98292200  1.24979000  2.14867400
H  -2.42064500  0.71875500  1.26522900
C  0.71749400  1.45670800 -0.00976100
H  1.10007100  1.97279400 -0.89975800
H  1.09979100  1.98478600  0.87331600
C  -0.81962900  1.44331000 -0.00989500
H  -1.19040900  2.47472600 -0.01700900
C  -1.32283100  0.70251000 -1.25937600
H  -2.42036400  0.70138300 -1.27537800
H  -0.98237600  1.22015900 -2.16566200
C  0.74077600 -0.71661400 -1.24582500
H  1.13920800 -1.74154600 -1.24707100
H  1.12247500 -0.20880900 -2.14090400
C  -1.29873000 -1.46287600  0.00990600
H  -0.94123900 -2.50103300  0.01707500
H  -2.39596200 -1.49559600  0.01004700
C  -0.79659300 -0.74226700 -1.25124800
H  -1.14934200 -1.26978800 -2.14522300
O  2.67015200  0.10554900 -0.00070700
H  3.02506000 -0.79437600  0.00528000

```

2.4.65. Structure **TS1**

2.4.65.1. PM6

```

P   0.00000000  0.00000000  0.00000000
H   1.44959000  0.00000000  0.00000000
O  -0.82743900  1.24858300  0.00000000
C  -0.31067800 -1.04377400  1.51816400
C   0.38153600 -2.23364500  1.72943000
C  -1.24213600 -0.57108300  2.44039500
C   0.14184600 -2.96396900  2.90023000
H   1.09741900 -2.61967400  1.00203600
C  -1.47573800 -1.30184200  3.61213000
H  -1.78974000  0.36239900  2.26909300
C  -0.78349000 -2.49564100  3.83936200
H   0.67335800 -3.89631400  3.07854400
H  -2.19446200 -0.94031000  4.34466300
H  -0.96556100 -3.06372800  4.75093400
O  -0.92763900 -1.57991600 -0.89192700
C  -2.36719400 -1.51452100 -0.84070500
H  -2.74011200 -0.51566200 -1.09547900
H  -2.73678900 -2.26394000 -1.54880900
H  -2.65526400 -1.78851500  0.18324300
O   0.34747900 -0.15010500 -1.92746500
C  -0.12604500  0.94775000 -2.71562600
H   0.65233400  1.72087400 -2.68810300
H  -0.24870900  0.56998300 -3.73533400
H  -1.06807000  1.36080300 -2.32782000
H  -0.52121000 -1.22110300 -1.98113300

```

2.4.65.2. SMD(THF)//M06-2X/6-

31++G(d,p)

```

P   -0.94935   0.37480   -0.46679
H   -0.94773   0.19708   -1.86004
O   -1.30002   1.62090   0.29296
C    0.89135   0.27848   -0.26260
C    1.62826   -0.55881  -1.10619
C    1.55730   1.02637   0.71115
C    3.01289   -0.65751  -0.97349
H    1.11960   -1.13945  -1.87499
C    2.94281   0.92756   0.84982
H    0.98153   1.68726   1.35282
C    3.67065   0.08459   0.00928
H    3.57895   -1.30731  -1.63475
H    3.45479   1.51045   1.61022
H    4.74913   0.00981   0.11535
O   -1.01261   -1.40091   0.19162
C   -0.46574   -1.75611   1.47862
H   -0.71300   -0.99647   2.22437
H   -0.89921   -2.71737   1.75693
H   0.61436   -1.84999   1.36928
O   -2.71625   -0.26188  -0.60551
C   -3.77372   0.44903   0.01417
H   -3.90555   1.42961   -0.45261
H   -4.69048   -0.13468  -0.11922
H   -3.59656   0.59898   1.08526
H   -2.05729   -1.33635   0.07213

```

2.4.66. Structure TS2

2.4.66.1. PM6

P	0.00000000	0.00000000	0.00000000
H	1.44263000	0.00000000	0.00000000
O	-0.86734000	1.37001900	0.00000000
C	-0.70587300	-1.49645200	-0.79677500
C	-0.69148600	-2.69579400	-0.08014000
C	-1.23644000	-1.42529800	-2.08281000
C	-1.22335200	-3.84740200	-0.66687600
H	-0.27879900	-2.75216100	0.93238600
C	-1.77151200	-2.58367400	-2.66418700
H	-1.22568600	-0.48375400	-2.65365800
C	-1.76419100	-3.78844100	-1.95792500
H	-1.21825700	-4.78914500	-0.12218700
H	-2.18955900	-2.54066600	-3.66818000
H	-2.17951100	-4.68803500	-2.41188400
O	-0.11650800	-0.39072000	1.64688100
C	-1.40280200	-0.19331500	2.26139600
H	-1.18122200	-0.29980000	3.33240400
H	-1.80041900	0.81198100	2.05968100
H	-2.10297100	-0.97180800	1.93703200
O	0.16532600	0.88908600	-1.87023700
C	1.37081700	1.38493500	-2.40215600
H	2.03784500	0.54364000	-2.62355700
H	1.11938400	1.90311600	-3.33702700
H	1.85345400	2.08680000	-1.71325300
H	-0.67508200	1.80291700	-1.10435300

2.4.66.2. SMD(THF)//M06-2X/6-

31++G(d,p)

P	1.11399	-0.35878	-0.19852
H	1.72608	-0.11191	-1.42678
O	1.93327	-0.29803	1.14620
C	-0.63987	0.08113	-0.10025
C	-1.10946	0.98636	0.85661
C	-1.53822	-0.54750	-0.96872
C	-2.47258	1.25868	0.94214
H	-0.41134	1.48010	1.52453
C	-2.89935	-0.25318	-0.89571
H	-1.17649	-1.26792	-1.69707
C	-3.36637	0.64550	0.06256
H	-2.83717	1.95572	1.69039
H	-3.59283	-0.73216	-1.58011
H	-4.42746	0.86821	0.12551
O	1.00528	-1.96871	-0.48182
C	0.54678	-2.82598	0.56526
H	-0.39318	-2.46138	0.99629
H	0.37944	-3.80888	0.12222
H	1.30183	-2.90098	1.35243
O	1.58541	1.65881	0.10204
C	2.51273	2.20322	-0.80588
H	3.40554	1.56797	-0.92309
H	2.05141	2.33156	-1.79455
H	2.84552	3.18770	-0.45724
H	2.02517	0.84775	0.97773

2.4.66.3. CPCM(THF)//M06-2X/6-

31++G(d,p)

P	-1.11244	0.36156	-0.19719
H	-1.72982	0.12438	-1.42450
O	-1.92700	0.30608	1.15068
C	0.63836	-0.08538	-0.10259
C	1.10419	-0.99554	0.85154
C	1.53918	0.54556	-0.96679
C	2.46644	-1.27104	0.93817

H	0.40229	-1.48885	1.51537
C	2.89943	0.24848	-0.89236
H	1.17865	1.27050	-1.69084
C	3.36268	-0.65553	0.06272
H	2.82868	-1.97116	1.68396
H	3.59498	0.72939	-1.57244
H	4.42286	-0.87973	0.12709
O	-0.99695	1.97161	-0.47950
C	-0.52880	2.82961	0.56299
H	0.44353	2.49246	0.93965
H	-0.42206	3.82413	0.13034
H	-1.25005	2.85437	1.38346
O	-1.59745	-1.64801	0.10074
C	-2.52374	-2.19977	-0.80669
H	-3.42267	-1.57302	-0.91155
H	-2.06394	-2.31055	-1.79712
H	-2.83910	-3.19010	-0.46272
H	-2.03210	-0.84091	0.97995

2.4.66.4. SMD(THF)//B3LYP/6-

31++G(d,p)

P	-1.12300	0.33678	-0.21527
H	-1.70415	-0.02962	-1.43146
O	-1.95476	0.29409	1.13959
C	0.64461	-0.03820	-0.07869
C	1.19617	-0.49998	1.12502
C	1.47010	0.16832	-1.19464
C	2.56718	-0.75317	1.20920
H	0.56105	-0.66675	1.98910
C	2.83933	-0.09990	-1.10818
H	1.05300	0.53444	-2.12909
C	3.38886	-0.55759	0.09355
H	2.99151	-1.10815	2.14411
H	3.47374	0.05408	-1.97648
H	4.45386	-0.76194	0.16080
O	-1.12810	1.93646	-0.60237
C	-0.66352	2.93411	0.32635
H	0.32927	2.68380	0.71653
H	-0.60458	3.87266	-0.22877
H	-1.36827	3.04371	1.15611
O	-1.52380	-1.74654	0.22621
C	-2.37816	-2.44714	-0.64966
H	-3.26810	-1.86175	-0.94440
H	-1.84617	-2.73583	-1.57012
H	-2.73827	-3.37045	-0.17289
H	-2.02204	-0.81676	1.07056

2.4.66.5. CPCM(THF)//B3LYP/6-

31++G(d,p)

P	-1.11845	0.33998	-0.21661
H	-1.70259	-0.01715	-1.43369
O	-1.94822	0.29696	1.13850
C	0.64678	-0.04078	-0.08085
C	1.19275	-0.52385	1.11711
C	1.47719	0.18633	-1.18907
C	2.56316	-0.77948	1.20262
H	0.55210	-0.70370	1.97406
C	2.84544	-0.08581	-1.10231
H	1.06402	0.57302	-2.11644
C	3.38916	-0.56576	0.09340
H	2.98407	-1.14946	2.13275
H	3.48359	0.08278	-1.96454
H	4.45331	-0.77188	0.16129
O	-1.11677	1.94112	-0.59675
C	-0.66484	2.93436	0.34372
H	0.36311	2.73203	0.66257
H	-0.70044	3.89197	-0.17736

H	-1.32401	2.96263	1.21554
O	-1.53482	-1.74177	0.21661
C	-2.39466	-2.44341	-0.65707
H	-3.27871	-1.85044	-0.95002
H	-1.86357	-2.73374	-1.57600
H	-2.75854	-3.36143	-0.17585
H	-2.02698	-0.81440	1.06464

2.4.67. Structure **TS3**

2.4.67.1. PM6

P	0.00000000	0.00000000	0.00000000
H	1.44201224	0.00000000	0.00000000
O	-0.81053771	1.41452950	0.00000000
C	-0.38287918	-0.56796990	1.74210864
C	0.03886164	-1.82931095	2.16026552
C	-1.06487254	0.28682584	2.60276025
C	-0.22452457	-2.24064972	3.47129764
H	0.56387082	-2.51075976	1.48730733
C	-1.32691534	-0.12652597	3.91653671
H	-1.40168829	1.27644953	2.27205411
C	-0.90575999	-1.38704576	4.34773176
H	0.09960554	-3.22207846	3.81090669
H	-1.85703540	0.53524891	4.59857965
H	-1.10760261	-1.70827482	5.36916187
O	-0.53743092	-1.33275786	-0.85812369
C	-1.96603832	-1.53567196	-0.78295581
H	-2.52364391	-0.64974277	-1.11217560
H	-2.12165766	-2.35962559	-1.49561356
H	-2.26514151	-1.84941940	0.22601024
O	0.28678773	0.86162844	-1.80944012
C	-0.15016455	0.36256623	-3.05319526
H	-1.24298189	0.36472082	-3.11486160
H	0.27177633	1.02513494	-3.81943774
H	0.23166384	-0.65640535	-3.18960659
H	-0.59375030	1.82166342	-1.09825540

2.4.67.2. SMD(THF)//M06-2X/6-

31++G(d,p)

P	0.85305	-0.25737	-0.40159
H	0.94775	-0.16231	-1.78638
O	1.17239	-1.61047	0.34532
C	-0.96734	-0.20384	-0.23342
C	-1.68723	0.60926	-1.11588
C	-1.65072	-0.92465	0.75079
C	-3.07326	0.71314	-1.00863
H	-1.16620	1.16500	-1.89422
C	-3.03762	-0.82307	0.85750
H	-1.09605	-1.56820	1.42752
C	-3.74841	-0.00308	-0.01945
H	-3.62577	1.34501	-1.69759
H	-3.56350	-1.38497	1.62368
H	-4.82854	0.07397	0.06422
O	1.28220	1.14297	0.26567
C	0.57759	1.69334	1.39030
H	0.45500	0.94754	2.18069
H	1.20054	2.50928	1.75786
H	-0.39808	2.08067	1.08635
O	2.89537	-0.59067	-0.67369
C	3.87889	0.19911	-0.05835
H	3.69672	0.33537	1.01906
H	4.86211	-0.27563	-0.17724
H	3.92570	1.19634	-0.51547
H	2.24360	-1.49741	0.05974

2.4.68. Structure **TS4**

2.4.68.1. PM6

P	0.00000000	0.00000000	0.00000000
H	1.45760880	0.00000000	0.00000000
O	-0.28446000	1.59811996	0.00000000
C	-0.36428107	-0.90573348	1.56430028
C	-0.49357007	-0.18413688	2.74972937
C	-0.48246406	-2.29362313	1.53724600
C	-0.74017486	-0.87501012	3.94244707
H	-0.41200806	0.90626603	2.77096642
C	-0.73046602	-2.97861705	2.73329207
H	-0.38813455	-2.85972156	0.60673912
C	-0.85766308	-2.26899784	3.93198665
H	-0.84224008	-0.32674158	4.87740304
H	-0.82489855	-4.06302272	2.72966210
H	-1.05014548	-2.80417577	4.86166779
O	-0.04095233	-0.96472407	-1.34716654
C	-1.26169242	-1.27062120	-2.05728386
H	-1.74393178	-0.35558748	-2.42831666
H	-0.87818206	-1.88472283	-2.88319175
H	-1.95724860	-1.83225745	-1.42552150
O	-2.03376477	0.31859454	-0.33467468
C	-3.07458793	-0.02110874	0.54973860
H	-4.00368711	0.36251756	0.10874618
H	-3.13295767	-1.11179725	0.64198579
H	-2.92087380	0.42866194	1.53703583
H	-1.45363314	1.66865059	-0.16942814

2.4.68.2. SMD(THF)//M06-2X/6-

31++G(d,p)

P	1.08828	0.00328	-0.97342
H	1.05875	0.49844	-2.28541
O	1.69768	-1.41912	-1.26993
C	-0.64559	0.07282	-0.49032
C	-1.41703	-1.09141	-0.44285
C	-1.21973	1.31251	-0.19647
C	-2.76401	-1.01242	-0.09687
H	-0.96765	-2.05548	-0.66707
C	-2.56681	1.38425	0.15813
H	-0.62171	2.21989	-0.24001
C	-3.33781	0.2232	0.20696
H	-3.36483	-1.91602	-0.06247
H	-3.01253	2.34623	0.39214
H	-4.38698	0.28025	0.48101
O	1.91499	1.26045	-0.42137
C	2.07497	1.63243	0.95668
H	2.88427	1.06021	1.40801
H	2.31741	2.69632	0.94034
H	1.15359	1.47026	1.52066
O	1.49601	-0.96812	0.90668
C	0.66522	-1.20961	2.00577
H	1.25558	-1.20653	2.93393
H	-0.11562	-0.43955	2.10774
H	0.15450	-2.18186	1.93562
H	1.71630	-1.67767	-0.19241

2.4.69. Structure **TS5**

2.4.69.1. PM6

P	0.00000000	0.00000000	0.00000000
H	1.44654000	0.00000000	0.00000000
O	-0.55177960	1.40008328	0.00000000
C	-0.69047116	-1.03380331	1.35270253
C	-1.64352805	-0.42822581	2.17512084
C	-0.28840657	-2.35266912	1.55498614
C	-2.19725641	-1.15950036	3.23091646
H	-1.96028610	0.60928912	2.01117739
C	-0.84871972	-3.08072324	2.61284604
H	0.44214453	-2.83334508	0.89171578
C	-1.79777517	-2.48361532	3.44772332
H	-2.93646148	-0.69950525	3.88364212
H	-0.54528567	-4.11179649	2.78222817
H	-2.23001263	-3.05141372	4.27163603
O	-1.10765063	-0.32224714	-1.63192805
C	-2.52729079	-0.13272926	-1.43900026
H	-2.97167029	-0.20305646	-2.43755406
H	-2.94382100	-0.88249599	-0.76205247
H	-2.65216788	0.88820458	-1.03884897
O	0.36913529	-1.75992842	-0.99057618
C	1.50955187	-1.86678937	-1.82991375
H	1.44971455	-2.85862450	-2.29743067
H	1.51806197	-1.09260675	-2.60431891
H	2.41628097	-1.80992630	-1.21640342
H	-0.80129242	-1.43612414	-1.77618302

2.4.69.2. SMD(THF)//M06-2X/6-

31++G(d,p)

P	1.01425	-0.24032	-0.69686
H	1.26721	0.67417	-1.75467
O	1.35207	-1.55925	-1.33306
C	-0.72777	0.11850	-0.34405
C	-1.66567	-0.85692	-0.69322
C	-1.15118	1.32396	0.22483
C	-3.02366	-0.6327	-0.46438
H	-1.33087	-1.78955	-1.14146
C	-2.50917	1.54444	0.45058
H	-0.42669	2.08843	0.49294
C	-3.44504	0.56691	0.10835
H	-3.74980	-1.39398	-0.73554
H	-2.83778	2.48110	0.89223
H	-4.50236	0.74298	0.28564
O	1.35776	-0.85274	1.07726
C	0.47485	-1.68749	1.79678
H	0.99019	-2.03556	2.69728
H	-0.43972	-1.15624	2.08801
H	0.21299	-2.55578	1.18236
O	1.88828	1.07436	0.30983
C	3.15123	1.58196	-0.14287
H	3.42126	2.41850	0.50291
H	3.91668	0.80212	-0.10157
H	3.02959	1.93654	-1.16952
H	1.82913	0.34109	1.16599

2.4.70. Structure **TS6**

2.4.70.1. SMD(THF)//M06-2X/6- 31++G(d,p)

```
P -0.94935200  0.37480300 -0.46679000
H -0.94773100  0.19707600 -1.86003600
O -1.30001700  1.62090000  0.29296300
C  0.89134500  0.27848400 -0.26260000
C  1.62826000 -0.55880700 -1.10618600
C  1.55730100  1.02636800  0.71114800
C  3.01288600 -0.65751400 -0.97348600
H  1.11960500 -1.13945400 -1.87499400
C  2.94281100  0.92755900  0.84981600
H  0.98153400  1.68725800  1.35282200
C  3.67065400  0.08458800  0.00927500
H  3.57895000 -1.30731200 -1.63475100
H  3.45478700  1.51044600  1.61022200
H  4.74913400  0.00980600  0.11534700
O -1.01260800 -1.40091200  0.19161500
C -0.46574400 -1.75610900  1.47861800
H -0.71300100 -0.99647000  2.22437200
H -0.89921300 -2.71737100  1.75693200
H  0.61436300 -1.84999000  1.36928000
O -2.71625400 -0.26188200 -0.60551000
C -3.77372100  0.44902900  0.01417400
H -3.90554500  1.42960900 -0.45261300
H -4.69048200 -0.13468400 -0.11921500
H -3.59656000  0.59897700  1.08525800
H -2.05728500 -1.33635300  0.07212600
```

2.4.71. Structure **TS7**

2.4.71.1. SMD(THF)//M06-2X/6- 31++G(d,p)

```
P -0.95493600  0.37292300 -0.43767100
H -0.95817900  0.24000700 -1.83665200
O -1.30672500  1.59488800  0.35989000
C  0.88843200  0.28123200 -0.25342400
C  1.55803400  0.99269500  0.74525400
C  1.62373200 -0.51282200 -1.13884500
C  2.94543100  0.89985400  0.86649500
H  0.98348000  1.62184400  1.41918100
C  3.01051100 -0.60573200 -1.02339100
H  1.11263700 -1.06332200 -1.92791300
C  3.67178500  0.09949000 -0.01611700
H  3.46029400  1.45451500  1.64578900
H  3.57506500 -1.22190600 -1.71729600
H  4.75187200  0.02974500  0.07611400
O -2.71752900 -0.27230100 -0.58389600
C -3.79294300  0.47567600 -0.04693500
H -3.89724500  1.43132500 -0.57035900
H -4.70885100 -0.10730700 -0.18929000
H -3.65788100  0.67941500  1.02076900
O -1.01168300 -1.40693600  0.19296700
C -0.42709100 -1.78962900  1.45548600
H -0.87903000 -2.73995800  1.74182900
H  0.64457600 -1.91500900  1.30354800
H -0.62354400 -1.03051800  2.21645400
H -2.05900200 -1.34246300  0.10007000
```

2.4.72. Structure **TS8**

2.4.72.1. SMD(THF)//M06-2X/6-

31++G(d,p)

P	1.15895	0.18999	-0.17275
H	1.62949	0.46789	-1.46859
O	2.00950	0.17025	1.22136
C	-0.64106	-0.10476	-0.04393
C	-1.43795	0.76141	0.71590
C	-1.24013	-1.19560	-0.68675
C	-2.80596	0.52943	0.84643
H	-0.98343	1.61694	1.20564
C	-2.61389	-1.40826	-0.57964
H	-0.62784	-1.87849	-1.26442
C	-3.39757	-0.55102	0.19212
H	-3.41036	1.19756	1.45267
H	-3.07023	-2.24988	-1.09210
H	-4.46594	-0.72431	0.28377
O	1.51542	-1.44371	-0.44850
C	2.50953	-2.20189	0.21328
H	2.27775	-2.34025	1.27441
H	2.53899	-3.18034	-0.27455
H	3.50044	-1.74025	0.12739
O	1.03417	1.91078	0.06435
C	0.53784	2.68539	-1.00051
H	0.78785	3.73174	-0.80615
H	0.99411	2.39534	-1.95991
H	-0.55292	2.59565	-1.09938
H	2.06030	1.07183	1.57337

2.4.72.2. CPCM(THF)//M06-2X/6-

31++G(d,p)

P	-1.34320	0.06163	-0.08500
H	-1.88839	-0.15459	-1.36357
O	-2.13468	0.25681	1.32126
C	0.46655	-0.00753	0.01703
C	1.07162	-0.04315	1.27631
C	1.25211	-0.06409	-1.13691
C	2.45932	-0.11931	1.37878
H	0.46033	-0.00685	2.17399
C	2.64057	-0.14788	-1.03028
H	0.78902	-0.04078	-2.12071
C	3.24459	-0.17149	0.22614
H	2.92691	-0.14019	2.35815
H	3.24779	-0.19288	-1.92872
H	4.32514	-0.23340	0.30794
O	-1.51209	1.73541	-0.34084
C	-0.46748	2.65486	-0.59129
H	0.02286	2.46711	-1.55481
H	-0.92047	3.64850	-0.62103
H	0.29392	2.63692	0.19717
O	-1.51464	-1.65730	0.19926
C	-1.08907	-2.53768	-0.81269
H	-1.38535	-2.17920	-1.81168
H	0.00148	-2.66549	-0.80223
H	-1.56248	-3.50779	-0.64637
H	-2.34077	-0.61755	1.68693

2.4.72.3. SMD(THF)//B3LYP/6-

31++G(d,p)

P	-1.15013	-0.16561	-0.16022
H	-1.62255	-0.43675	-1.46290
O	-1.98184	-0.12725	1.26352
C	0.66406	0.09850	-0.04207
C	1.45777	-0.78676	0.70757

C	1.28173	1.18432	-0.68697
C	2.83457	-0.57910	0.82653
H	0.99634	-1.63711	1.19765
C	2.66325	1.37358	-0.58972
H	0.67983	1.88199	-1.25680
C	3.44204	0.49713	0.17212
H	3.43170	-1.26333	1.42326
H	3.12799	2.21097	-1.10312
H	4.51464	0.65123	0.25482
O	-1.49864	1.48352	-0.44664
C	-2.49667	2.27043	0.19436
H	-2.50684	3.23939	-0.31583
H	-3.49489	1.82216	0.10678
H	-2.27517	2.43143	1.25566
O	-1.08164	-1.90974	0.08160
C	-0.71166	-2.73263	-1.01077
H	-1.21832	-2.42727	-1.94094
H	0.37304	-2.71869	-1.18958
H	-1.01542	-3.75844	-0.77862
H	-2.05213	-1.03652	1.59879

2.4.72.4. CPCM(THF)//B3LYP/6-

31++G(d,p)

P	1.31667	-0.09931	-0.06563
H	1.88012	0.18924	-1.32596
O	2.08623	-0.40782	1.34778
C	-0.50061	0.01758	0.02528
C	-1.14990	-0.15138	1.25798
C	-1.25494	0.31114	-1.12054
C	-2.53952	-0.03121	1.33982
H	-0.57464	-0.37897	2.15059
C	-2.64591	0.43296	-1.03297
H	-0.76976	0.44017	-2.08418
C	-3.29001	0.26172	0.19564
H	-3.03481	-0.16697	2.29689
H	-3.22211	0.66035	-1.92512
H	-4.37000	0.35504	0.26194
O	1.47259	-1.76993	-0.43451
C	0.42494	-2.66670	-0.78517
H	-0.08066	-2.37138	-1.71389
H	0.88884	-3.64501	-0.93986
H	-0.32507	-2.75551	0.00985
O	1.55534	1.61368	0.33933
C	1.38564	2.59551	-0.66647
H	1.85648	2.29166	-1.61577
H	0.32371	2.80378	-0.85840
H	1.86887	3.51614	-0.32661
H	2.31765	0.44590	1.75281

2.4.73. Structure **TS9**

2.4.73.1. SMD(THF)//M06-2X/6-

31++G(d,p)

```
P  1.19375500  0.11622200  0.12995400
H  1.86599800  0.03791800 -1.11083900
O  1.80792200  0.41486700  1.61190600
C  -0.62288200 -0.07642000  0.07405100
C  -1.20354200 -1.28926500 -0.31579000
C  -1.45579800  0.98946900  0.43948200
C  -2.59050400 -1.42865600 -0.35424500
H  -0.57392200 -2.13175400 -0.57960600
C  -2.84101000  0.84017000  0.42844000
H  -1.01599700  1.93571300  0.73889000
C  -3.41110900 -0.36693700  0.02349300
H  -3.02738500 -2.37154100 -0.66942900
H  -3.47413400  1.66934500  0.72959400
H  -4.49107200 -0.48024900  0.00461800
O  1.17277700  1.83913000 -0.09790600
C  0.87190100  2.33201200 -1.38115900
H  1.34581900  1.72671800 -2.17037700
H  1.26050500  3.35108500 -1.45703100
H  -0.21054000  2.34946600 -1.56853700
O  1.50263200 -1.53010800  0.38316700
C  2.18860100 -2.26110300 -0.61207700
H  3.24082500 -1.95554200 -0.68692700
H  1.72534100 -2.15895700 -1.60366000
H  2.15442200 -3.31532800 -0.32588900
H  1.81322200  1.37306600  1.75938700
```

2.4.73.2. SMD(THF)//B3LYP/6-

31++G(d,p)

```
P      1.18002   -0.07134   -0.14467
H      1.85265   -0.01839    1.10364
O      1.75426   -0.29751   -1.67446
C      -0.65154    0.06344   -0.06453
C      -1.46042   -1.05459   -0.33696
C      -1.27327    1.28500    0.24735
C      -2.85317   -0.95078   -0.30645
H      -0.99617   -2.00399   -0.57882
C      -2.66691    1.38238    0.29837
H      -0.67075    2.16479    0.43736
C      -3.46050    0.26643    0.01794
H      -3.46199   -1.82214   -0.53195
H      -3.13001    2.33320    0.54763
H      -4.54391    0.34471    0.04976
O      1.48195    1.59827   -0.35035
C      2.10792    2.32671    0.69939
H      2.24025    3.35240    0.34222
H      1.50141    2.35613    1.61627
H      3.09773    1.91930    0.94985
O      1.24970   -1.82056    0.01627
C      1.14915   -2.39470    1.30805
H      1.74764   -1.84028    2.04915
H      0.10955   -2.42972    1.66360
H      1.53705   -3.41688    1.25492
H      1.78135   -1.25404   -1.84418
```

2.4.74. Structure **TS10**

2.4.74.1. SMD(THF)//M06-2X/6-

31++G(d,p)

```
P      1.01818    0.04645    0.20598
H      1.15968   -0.34585   -1.17192
O      1.00313    0.53467    1.81199
C      -0.81042    0.04180    0.06115
C      -1.36268   -0.34480   -1.16575
C      -1.67229    0.39755    1.10910
C      -2.74519   -0.37742   -1.34914
H      -0.70993   -0.62136   -1.99036
C      -3.05295    0.36490    0.92701
H      -1.25319    0.70068    2.06111
C      -3.59208   -0.02181   -0.30133
H      -3.15680   -0.67917   -2.30768
H      -3.70987    0.64326    1.74580
H      -4.66900   -0.04418   -0.44072
O      1.86826    1.43288   -0.13284
C      2.25562    1.72309   -1.47248
H      2.92327    0.95357   -1.87293
H      2.78823    2.67508   -1.43966
H      1.38271    1.82494   -2.12560
O      1.71219   -1.37223    0.67907
C      1.92285   -2.40148   -0.28245
H      2.57048   -2.06602   -1.09935
H      0.97453   -2.76159   -0.69653
H      2.41197   -3.22148    0.24622
H      1.68955    1.19180    1.97944
```

2.4.74.2. CPCM(THF)//M06-2X/6-

31++G(d,p)

```
P      1.01826    0.04652    0.20595
H      1.15983   -0.34652   -1.17173
O      1.00342    0.53542    1.81174
C      -0.81033    0.04178    0.06116
C      -1.67216    0.39847    1.10882
C      -1.36262   -0.34588   -1.16539
C      -3.05283    0.36571    0.92678
H      -1.25302    0.70240    2.06055
C      -2.74514   -0.37862   -1.34872
H      -0.7099   -0.62314   -1.98979
C      -3.59199   -0.02205   -0.30120
H      -3.70970    0.64483    1.74535
H      -3.15679   -0.68119   -2.30699
H      -4.66891   -0.04450   -0.44055
O      1.71210   -1.37204    0.67976
C      1.92299   -2.40159   -0.28136
H      2.41136   -3.22169    0.24786
H      0.97483   -2.76137   -0.69614
H      2.57141   -2.06659   -1.09782
O      1.86815    1.43290   -0.13361
C      2.25492    1.72280   -1.47348
H      2.92225    0.95309   -1.87410
H      1.38170    1.82463   -2.12620
H      2.78767    2.67473   -1.44112
H      1.68909    1.19350    1.97858
```

2.4.74.3. SMD(THF)//B3LYP/6-

31++G(d,p)

```
P      1.00666    0.07728    0.19407
H      1.15343   -0.40622   -1.15803
O      1.01900    0.60480    1.81490
C      -0.83708   -0.01337    0.05955
C      -1.67986    1.02118    0.50043
```

C	-1.40948	-1.13461	-0.56102
C	-3.06556	0.92671	0.33718
H	-1.26490	1.92119	0.94802
C	-2.79604	-1.24289	-0.69904
H	-0.77356	-1.93077	-0.94024
C	-3.62700	-0.21008	-0.25224
H	-3.70313	1.74171	0.66885
H	-3.22520	-2.12640	-1.16378
H	-4.70430	-0.28687	-0.37086
O	1.87356	-1.23585	0.73273
C	2.42914	-2.18306	-0.19210
H	3.14413	-2.77944	0.38034
H	1.65806	-2.84743	-0.59714
H	2.95689	-1.69500	-1.01830
O	1.69632	1.52584	-0.23296
C	2.04807	1.77943	-1.60277
H	2.79380	1.06656	-1.97036
H	1.16950	1.75812	-2.25739
H	2.47711	2.78432	-1.62161
H	0.13408	0.82282	2.13220

2.4.74.4. CPCM(THF)//B3LYP/6-

31++G(d,p)

P	1.00924	0.04322	0.19495
H	1.16565	-0.32654	-1.18721
O	1.00227	0.50521	1.82833
C	-0.82633	0.03985	0.05679
C	-1.69124	0.39200	1.10985
C	-1.38491	-0.34095	-1.17497
C	-3.07588	0.35914	0.92988
H	-1.27126	0.69118	2.06185
C	-2.77102	-0.37380	-1.35587
H	-0.73526	-0.61244	-2.00276
C	-3.61934	-0.02354	-0.30203
H	-3.73141	0.63372	1.75151
H	-3.18415	-0.66992	-2.31577
H	-4.69679	-0.04648	-0.43893
O	1.71672	-1.39533	0.65903
C	1.98286	-2.42402	-0.30544
H	2.50820	-2.03331	-1.18321
H	2.61798	-3.15642	0.19701
H	1.05625	-2.91195	-0.62644
O	1.86458	1.45677	-0.11075
C	2.29923	1.78277	-1.43902
H	2.88584	0.97223	-1.88289
H	1.44802	2.01385	-2.08766
H	2.92833	2.66989	-1.34309
H	1.72123	1.12611	2.00534

2.4.75. Structure **TS10b**

2.4.75.1. SMD(THF)//M06-2X/6-31++G(d,p)

P	-1.27915	0.02216	0.12295
H	-1.79965	-0.05718	-1.19436
O	-1.98281	0.12896	1.59484
C	0.53723	0.00003	0.12294
C	1.21298	-0.15388	-1.09306
C	1.27294	0.14304	1.30332
C	2.60756	-0.16938	-1.12575
H	0.65474	-0.25869	-2.02118
C	2.66619	0.12340	1.26856
H	0.78019	0.27524	2.26360
C	3.33557	-0.03332	0.05490
H	3.12162	-0.28809	-2.07481
H	3.22689	0.23281	2.19198
H	4.42102	-0.04687	0.03051
O	-1.44668	1.72535	0.00121
C	-1.09099	2.32468	-1.22094
H	-1.57342	3.30453	-1.27198
H	-0.00437	2.46211	-1.30702
H	-1.43300	1.73368	-2.08699
O	-1.49606	-1.67513	0.22697
C	-1.21093	-2.44827	-0.91328
H	-0.13310	-2.62756	-1.02719
H	-1.71483	-3.41218	-0.80254
H	-1.58249	-1.97517	-1.83737
H	-1.35533	0.17376	2.32896

2.4.76. Structure **TS11**

2.4.76.1. SMD(THF)//M06-2X/6-

31++G(d,p)

P	-1.03477	0.05326	-0.27239
H	-1.12324	0.23353	-1.66131
O	-2.67184	0.12091	0.11714
C	0.81994	-0.02001	-0.08303
C	1.60371	0.51893	-1.10493
C	1.45019	-0.57084	1.03657
C	2.99756	0.50171	-1.01771
H	1.13003	0.95677	-1.98194
C	2.84097	-0.57659	1.13325
H	0.85449	-1.00613	1.83460
C	3.61947	-0.04330	0.10419
H	3.59437	0.91677	-1.82522
H	3.31840	-1.00540	2.00997
H	4.70311	-0.05534	0.17654
O	-0.97749	-1.61007	-0.05248
C	-2.04610	-2.52504	-0.23552
H	-2.56174	-2.36319	-1.19194
H	-1.60644	-3.52442	-0.25650
H	-2.76307	-2.48633	0.59238
O	-0.89604	1.57868	0.37753
C	-1.93624	2.55058	0.44069
H	-1.44642	3.50764	0.63760
H	-2.48441	2.61263	-0.50476
H	-2.63754	2.32590	1.24688
H	-3.19006	-0.6402	-0.16907

2.4.77. Structure **TS12**

2.4.77.1. SMD(THF)//M06-2X/6-

31++G(d,p)

P	0.97470	-0.35735	-0.17948
H	0.74599	-1.39715	-1.11876
O	1.15099	0.35690	1.32378
C	-0.88092	-0.26969	0.08046
C	-1.65438	-1.05645	-0.77795
C	-1.54313	0.56129	0.99882
C	-3.04970	-1.01489	-0.73984
H	-1.16652	-1.71989	-1.49010
C	-2.93487	0.60660	1.04129
H	-0.96443	1.17327	1.68091
C	-3.69262	-0.18189	0.17198
H	-3.62979	-1.63776	-1.41446
H	-3.43038	1.25739	1.75635
H	-4.77762	-0.14768	0.21067
O	1.32726	0.86451	-1.19532
C	0.72226	2.14892	-1.04358
H	0.76232	2.48497	-0.00325
H	1.29507	2.83549	-1.66916
H	-0.31751	2.12922	-1.38481
O	2.45738	-1.14606	-0.07191
C	3.61583	-0.64646	0.57571
H	3.57226	-0.80425	1.66133
H	4.46962	-1.20960	0.19215
H	3.78260	0.41540	0.35304
H	2.05794	0.49358	1.62450

2.4.78. Structure **TS13**

2.4.78.1. SMD(THF)//M06-2X/6-

31++G(d,p)

P	1.02474	-0.41140	-0.16757
H	1.19711	-0.52895	-1.55617
O	0.73679	-1.98077	0.35377
C	-0.81973	-0.19649	-0.02191
C	-1.64381	-0.66921	-1.04534
C	-1.39910	0.40086	1.10113
C	-3.03046	-0.53430	-0.95668
H	-1.20554	-1.14050	-1.92310
C	-2.78495	0.52031	1.20039
H	-0.76725	0.78400	1.89974
C	-3.60318	0.05710	0.16886
H	-3.66193	-0.89421	-1.76404
H	-3.22615	0.98086	2.07977
H	-4.68210	0.15837	0.24192
O	1.29001	1.23533	0.06516
C	0.55165	2.19534	-0.67686
H	-0.33042	2.53569	-0.12559
H	1.21903	3.04428	-0.85063
H	0.22768	1.80389	-1.64999
O	2.58069	-0.65773	0.41431
C	3.65825	0.20343	0.06954
H	3.66873	1.09774	0.69575
H	4.57434	-0.37087	0.23134
H	3.61097	0.50581	-0.98326
H	1.57252	-2.44208	0.51711

2.4.79. Structure **TS14**

2.4.79.1. SMD(THF)//M06-2X/6-

31++G(d,p)

P	-0.93992	0.48237	-0.20890
H	-0.63568	1.57788	-1.06635
O	-1.14797	1.15435	1.26259
C	0.90921	0.15896	-0.11742
C	1.51488	-1.03898	-0.50400
C	1.72549	1.24925	0.20748
C	2.90667	-1.15348	-0.54589
H	0.90000	-1.89216	-0.77723
C	3.11380	1.13371	0.19274
H	1.27128	2.20138	0.47847
C	3.70846	-0.07132	-0.18818
H	3.36170	-2.08959	-0.85726
H	3.73138	1.98372	0.46848
H	4.79051	-0.16145	-0.21325
O	-1.31001	-1.12569	0.00959
C	-0.92025	-1.80743	1.19678
H	-0.07392	-1.32992	1.69960
H	-1.76976	-1.83214	1.88803
H	-0.64286	-2.83058	0.92939
O	-2.44956	0.68397	-0.92432
C	-3.60823	-0.06567	-0.57371
H	-3.6838	-0.21858	0.50875
H	-4.47197	0.51307	-0.91215
H	-3.60682	-1.04056	-1.06742

2.4.80. Structure **TS15**

2.4.80.1. SMD(THF)//M06-2X/6-

31++G(d,p)

P	1.02517	-0.45934	-0.45025
H	0.74548	-0.95382	-1.75844
O	2.37451	-1.44496	-0.61155
C	-0.80093	-0.11349	-0.26246
C	-1.66851	-1.21067	-0.30334
C	-1.33876	1.17307	-0.16579
C	-3.04844	-1.03181	-0.21427
H	-1.26854	-2.21918	-0.40500
C	-2.72133	1.35612	-0.09416
H	-0.67712	2.03458	-0.14947
C	-3.57772	0.25546	-0.10953
H	-3.70939	-1.89345	-0.23562
H	-3.12897	2.36078	-0.02457
H	-4.65238	0.40014	-0.04914
O	1.54315	1.05540	-0.70678
C	2.90126	1.39294	-0.41685
H	3.58564	0.86933	-1.08988
H	2.98977	2.46915	-0.56995
H	3.15003	1.15458	0.62284
O	1.25393	-0.67099	1.21058
C	0.59410	0.12879	2.18227
H	1.12376	-0.03391	3.12413
H	0.64074	1.19473	1.93090
H	-0.45226	-0.16719	2.30702
H	2.86506	-1.54367	0.21764

2.4.81. Structure **TS16**

2.4.81.1. SMD(THF)//M06-2X/6-

31++G(d,p)

P	1.04908	0.07941	-0.71998
H	1.17035	0.50884	-2.05615
O	1.23116	-1.53075	-1.27872
C	-0.69643	-0.03205	-0.23436
C	-1.05818	-0.41348	1.06119
C	-1.69182	0.25427	-1.17378
C	-2.40534	-0.51113	1.41092
H	-0.29205	-0.62821	1.80173
C	-3.03713	0.15496	-0.82278
H	-1.41913	0.55689	-2.18259
C	-3.39519	-0.22898	0.47011
H	-2.68008	-0.80452	2.41981
H	-3.80519	0.37671	-1.55784
H	-4.44335	-0.30551	0.74370
O	1.99736	-0.26904	0.56430
C	2.33584	-1.57982	1.02025
H	1.45309	-2.21604	1.11700
H	3.04577	-2.05400	0.34075
H	2.79827	-1.43758	1.99963
O	1.28278	1.73102	-0.41293
C	1.23840	2.29033	0.88707
H	2.13351	2.03513	1.46188
H	1.18309	3.37638	0.77053
H	0.35244	1.95584	1.44336
H	0.93586	-1.60956	-2.19491

2.4.82. Structure **TS17**

2.4.82.1. SMD(THF)//M06-2X/6-

31++G(d,p)

P	1.07174	0.09818	-0.46339	P	1.28312	0.28070	-0.00361
H	1.02844	0.33791	-1.85608	H	2.59690	0.46869	-0.48887
O	1.62867	-0.20158	1.09734	O	1.56205	0.79531	1.52498
C	-0.72241	-0.01867	-0.16009	C	-0.52703	-0.15887	0.08036
C	-1.25764	-0.61069	0.98983	C	-1.36434	0.36220	1.07116
C	-1.58891	0.49951	-1.12974	C	-1.08795	-0.97802	-0.90761
C	-2.63978	-0.67983	1.16648	C	-2.72921	0.06366	1.08255
H	-0.59407	-1.01894	1.74581	H	-0.97319	1.02467	1.83981
C	-2.96904	0.44117	-0.94833	C	-2.45106	-1.26598	-0.90726
H	-1.18118	0.95452	-2.02956	H	-0.45292	-1.40114	-1.68093
C	-3.49541	-0.15119	0.20033	C	-3.27679	-0.74766	0.09178
H	-3.04771	-1.14355	2.05971	H	-3.36219	0.47237	1.86494
H	-3.63324	0.85296	-1.70220	H	-2.86770	-1.90235	-1.68274
H	-4.57108	-0.20079	0.34191	H	-4.33834	-0.97664	0.09733
O	1.49986	1.71803	-0.41018	O	1.00719	1.66085	-0.91689
C	1.57007	2.51992	0.76038	C	-0.17884	2.44560	-0.98556
H	2.44457	2.27175	1.37117	H	-0.47441	2.81397	0.00231
H	0.65177	2.44238	1.35964	H	-1.01110	1.88938	-1.42821
H	1.66626	3.55557	0.42775	H	0.05623	3.30035	-1.62406
O	1.69762	-1.36902	-0.91933	O	1.56504	-1.38021	-0.02113
C	1.95290	-2.47670	-0.05951	C	2.90084	-1.85693	-0.09037
H	2.16765	-3.32516	-0.71369	H	2.85272	-2.92480	-0.31351
H	1.07997	-2.71132	0.55832	H	3.42233	-1.71383	0.86288
H	2.81119	-2.28643	0.58770	H	3.46835	-1.35608	-0.88433
H	1.39352	0.47777	1.74148	H	1.04875	0.30334	2.18358

2.4.83. Structure **TS18**

2.4.83.1. SMD(THF)//M06-2X/6-

31++G(d,p)

P	1.28312	0.28070	-0.00361
H	2.59690	0.46869	-0.48887
O	1.56205	0.79531	1.52498
C	-0.52703	-0.15887	0.08036
C	-1.36434	0.36220	1.07116
C	-1.08795	-0.97802	-0.90761
C	-2.72921	0.06366	1.08255
H	-0.97319	1.02467	1.83981
C	-2.45106	-1.26598	-0.90726
H	-0.45292	-1.40114	-1.68093
C	-3.27679	-0.74766	0.09178
H	-3.36219	0.47237	1.86494
H	-2.86770	-1.90235	-1.68274
H	-4.33834	-0.97664	0.09733
O	1.00719	1.66085	-0.91689
C	-0.17884	2.44560	-0.98556
H	-0.47441	2.81397	0.00231
H	-1.01110	1.88938	-1.42821
H	0.05623	3.30035	-1.62406
O	1.56504	-1.38021	-0.02113
C	2.90084	-1.85693	-0.09037
H	2.85272	-2.92480	-0.31351
H	3.42233	-1.71383	0.86288
H	3.46835	-1.35608	-0.88433
H	1.04875	0.30334	2.18358

2.4.84. Structure **TS19**

2.4.84.1. SMD(THF)//M06-2X/6-

31++G(d,p)

P	1.00134	0.50735	-0.36091
H	2.21019	1.24846	-0.32029
O	0.65368	1.50822	-1.66290
C	-0.79722	0.11809	-0.10770
C	-1.74317	1.14183	0.02188
C	-1.21854	-1.21171	-0.01244
C	-3.08777	0.84054	0.24155
H	-1.43574	2.18339	-0.03959
C	-2.56435	-1.51364	0.19544
H	-0.49222	-2.01287	-0.11304
C	-3.50150	-0.48842	0.32566
H	-3.81082	1.64440	0.34558
H	-2.88059	-2.55106	0.25690
H	-4.54877	-0.72369	0.49113
O	1.16674	0.26293	1.30649
C	2.37138	0.53598	1.99985
H	2.88904	-0.39762	2.24457
H	3.04960	1.16802	1.40976
H	2.12477	1.06224	2.92590
O	1.50012	-0.87784	-1.06051
C	2.65360	-1.52597	-0.52731
H	2.42617	-1.99429	0.43559
H	2.94222	-2.29525	-1.24503
H	3.48509	-0.82056	-0.40711
H	-0.21787	1.35190	-2.05711

2.4.85. Structure **TS20**

2.4.85.1. SMD(THF)//M06-2X/6-

31++G(d,p)

P	-0.44232	0.69891	-0.34293
H	-1.13179	0.70205	-1.55357
O	-1.10601	1.26961	0.96892
C	0.75336	-0.64536	-0.12416
C	0.62295	-1.58285	0.90556
C	1.85428	-0.70354	-0.98581
C	1.59142	-2.57032	1.07079
H	-0.23716	-1.54445	1.56502
C	2.80862	-1.70864	-0.83160
H	1.96857	0.03593	-1.77333
C	2.67950	-2.63844	0.19909
H	1.49208	-3.29257	1.87522
H	3.65469	-1.75745	-1.51009
H	3.42760	-3.41541	0.32527
O	0.55176	1.91130	-0.80788
C	1.49971	2.45686	0.12580
H	1.66083	1.75740	0.95563
H	2.44524	2.55566	-0.41642
O	-1.97467	-0.64507	0.17166
C	-3.09317	-0.66134	-0.68680
H	-3.35892	0.36301	-1.00279
H	-2.83678	-1.22395	-1.59655
H	-1.83583	0.37248	0.93480
C	1.01889	3.79854	0.63862
H	0.07094	3.68196	1.17051
H	1.75891	4.22203	1.32511
H	0.87592	4.49722	-0.19091
C	-4.28873	-1.30122	-0.00179
H	-4.56355	-0.73544	0.89423
H	-5.15252	-1.32361	-0.67435
H	-4.05300	-2.32726	0.29628

2.4.85.2. SMD(THF)//B3LYP/6-

31++G(d,p)

P	-0.09020	0.95871	-0.14562
H	-0.68527	1.34446	-1.34906
O	-0.46750	1.64965	1.23711
C	0.30836	-0.80567	-0.05243
C	0.34221	-1.46633	1.18369
C	0.61372	-1.50409	-1.23034
C	0.67765	-2.82162	1.23816
H	0.10279	-0.93022	2.09687
C	0.93851	-2.86214	-1.17020
H	0.59549	-0.99857	-2.19247
C	0.97222	-3.52123	0.06312
H	0.70374	-3.33061	2.19757
H	1.16612	-3.40229	-2.08492
H	1.22713	-4.57644	0.10813
O	1.34598	1.65970	-0.52955
C	2.47417	1.64680	0.38132
H	2.21063	2.22148	1.27547
H	2.68460	0.61288	0.68119
O	-2.14911	0.42266	0.30195
C	-3.16233	0.92319	-0.54662
H	-3.21629	2.02628	-0.49659
H	-2.92448	0.66810	-1.59496
H	-1.49641	1.23933	1.17168
C	3.66880	2.25571	-0.32664
H	3.46124	3.28768	-0.62875
H	4.52964	2.26309	0.35166
H	3.93790	1.67722	-1.21680
C	-4.52671	0.33761	-0.19125

H	-4.80882	0.60271	0.83448
H	-5.30042	0.72039	-0.86933
H	-4.50906	-0.75550	-0.26879

2.4.86. Structure **TS21**

2.4.86.1. SMD(THF)//M06-2X/6-

31++G(d,p)

P	-0.20627800	0.83261200	-0.35369900
H	-2.00312900	-0.23072100	-0.14538800
O	-0.11507900	1.72982500	1.07399200
C	0.98779000	2.61283100	1.22997100
H	1.15344600	3.20161300	0.32047900
H	0.75836400	3.28994400	2.05760900
H	1.90532700	2.05936700	1.46936800
O	0.00857700	1.75667000	-1.55757100
C	1.39730200	-0.10610500	-0.16317400
C	2.41907600	0.05041300	-1.10326600
C	1.58403600	-1.00432400	0.89433000
C	3.61274500	-0.66521000	-0.98485300
H	2.26419400	0.74911600	-1.92270600
C	2.77395600	-1.72135000	1.02015100
H	0.79522300	-1.13678500	1.63462900
C	3.79145900	-1.55235500	0.07700700
H	4.40253700	-0.53225900	-1.71953700
H	2.91117000	-2.41126200	1.84860200
H	4.71845600	-2.11117300	0.17073200
C	-3.97132400	0.32570500	-0.43967200
H	-3.77465900	0.62085400	-1.47158500
H	-4.97729000	-0.09031200	-0.34893400
C	-3.11654700	-1.08959200	1.37448300
H	-3.01512500	-0.19666100	1.99369200
H	-4.09546800	-1.54872500	1.52996100
C	-2.99228000	-1.86791500	-0.94923900
H	-2.18331600	-2.54044800	-0.65892900
H	-3.95515900	-2.37734600	-0.86779300
H	-2.32430900	-1.79960800	1.61792700
H	-2.83329000	-1.52030000	-1.97118800
H	-3.85881100	1.19032300	0.21686700

2.4.87. Structure **TS22**

2.4.87.1. SMD(THF)//M06-2X/6- 31++G(d,p)

```

P -0.18248000  1.02642700  0.54842700
H -0.20866300  1.36549300  1.91754200
O  0.90617900  1.31959800 -0.48162400
C -1.55223500 -0.09527800  0.05395300
C -1.30473300 -1.12699300 -0.85704200
C -2.83919200  0.05536800  0.57608000
C -2.32831400 -1.98890900 -1.24807500
H -0.30134900 -1.24935200 -1.25792800
C -3.86148800 -0.82153800  0.20711600
H -3.04272100  0.86861500  1.26758600
C -3.60898300 -1.84152800 -0.70976500
H -2.12985500 -2.77804100 -1.96813000
H -4.85557400 -0.70198700  0.62872400
H -4.40575800 -2.51769300 -1.00639000
O -1.15315400  2.45179900  0.37496000
C -1.48251400  2.87002700 -0.92689200
H -1.91358100  2.05323400 -1.52775200
H -2.23127300  3.66684000 -0.85467400
H -0.60274000  3.25310300 -1.45863500
O  0.77364100 -0.43808700  1.14252200
C  0.26268700 -1.17198400  2.21455200
H  1.07587600 -1.69993200  2.72884600
H -0.22770600 -0.52010800  2.96065700
H -0.48027300 -1.91781700  1.88859200
H  2.15190600 -0.18050500  0.09851300
N  3.08412000 -0.41609200 -0.31484900
C  3.65446700 -1.51022800  0.50160000
H  2.95506900 -2.34708500  0.49826300
H  4.61307500 -1.81510500  0.07573000
C  3.91324700  0.80975900 -0.26206000
H  4.00457400  1.12302500  0.77900500
H  4.89860300  0.59059400 -0.67988000
C  2.83406400 -0.83908600 -1.71159700
H  2.30428900 -0.03178000 -2.21679700
H  3.79032700 -1.04516300 -2.19827500
H  3.40565000  1.58532800 -0.83392000
H  2.21936500 -1.74028500 -1.69885500
H  3.79374400 -1.14928500  1.52122400

```

2.4.88. Structure **TS24**

2.4.88.1. SMD(THF)//M06-2X/6- 31++G(d,p)

```

P -1.18756700  0.45147900 -0.41732400
O -1.76609800  0.50092700  1.14715000
C  0.57946300 -0.08518800 -0.16461900
C  0.99732200 -0.83389400  0.93928100
C  1.52697200  0.27213300 -1.12900200
C  2.33346800 -1.20867800  1.08235000
H  0.26329100 -1.13291300  1.68239000
C  2.86508800 -0.10519200 -0.99648700
H  1.21787800  0.86014000 -1.99171900
C  3.27205300 -0.84560900  0.11376100
H  2.64351500 -1.78905900  1.94758900
H  3.58792000  0.18160400 -1.75595200
H  4.31220600 -1.14044400  0.22259400
O -0.83485700  2.12405700 -0.49301800
C -0.21040400  2.79337100  0.58509600
H  0.68207100  2.25874600  0.93956000
H  0.09723000  3.78439200  0.23394700
H -0.89953600  2.91274800  1.42892000
O -1.70070200 -1.70990800  0.13001900
C -2.76397500 -2.12064600 -0.64427900
H -3.12402600 -3.12845300 -0.35948100
H -3.65135500 -1.45203200 -0.57732200
H -2.51599300 -2.17675500 -1.72504700
H -1.98635700 -0.46855000  1.22456900

```

2.4.89. Structure **TS25**

2.4.89.1. SMD(THF)//M06-2X/6- 31++G(d,p)

```
P  1.38497300 -0.00021800  0.03523000
O  1.67565700  0.00024500  1.68716200
C -0.46515400 -0.00026900  0.07810900
C -1.18087000  0.00033800  1.28243200
C -1.18279300 -0.00051100 -1.12324800
C -2.57463700  0.00045000  1.28391000
H -0.63175800  0.00069000  2.22014600
C -2.58123800 -0.00032800 -1.12672100
H -0.64633500 -0.00079300 -2.07143200
C -3.28174700  0.00009400  0.07790300
H -3.11437300  0.00085500  2.22776700
H -3.12004900 -0.00055300 -2.07080200
H -4.36825800  0.00016400  0.08010700
O  1.35474400 -1.87440000  0.15452300
C  1.18192500 -2.49117000 -1.07585200
H  1.70289800 -1.95561700 -1.89575800
H  1.58630700 -3.51419800 -1.05025900
H  0.11902500 -2.57085800 -1.37394000
O  1.35341200  1.87480200  0.15418300
C  1.18263500  2.49098000 -1.07665500
H  1.58615200  3.51437800 -1.05075700
H  1.70556300  1.95554700 -1.89542200
H  0.12027100  2.56983000 -1.37708000
H  2.62673900  0.00114600  1.84277800
```

2.4.90. Structure **TS26**

2.4.90.1. SMD(THF)//M06-2X/6- 31++G(d,p)

```
P  0.97467300  0.65483800  0.45939700
H  1.34336700  0.68441700  1.80329200
O  1.96368200  0.60670200 -0.74534000
C -0.70874500  0.08168300  0.09421200
C -0.92453500 -0.87039500 -0.90692400
C -1.79274200  0.62146500  0.79056300
C -2.22185200 -1.27637300 -1.21141300
H -0.08140900 -1.29824200 -1.44519400
C -3.08904300  0.19554300  0.49955600
H -1.62644500  1.37597300  1.55480700
C -3.30362800 -0.74840800 -0.50426200
H -2.38743700 -2.00850400 -1.99585100
H -3.92931200  0.60891300  1.04931400
H -4.31383900 -1.07179400 -0.73735600
O  0.67620100  2.28352300  0.51805800
C  0.32227600  2.97456400 -0.67457900
H -0.48855600  2.46491700 -1.21034700
H -0.01887200  3.96988700 -0.38237500
H  1.18759200  3.06361000 -1.33764600
O  1.48981100 -1.26313900  0.79380800
C  0.73986200 -2.04521300  1.69512600
H  1.38590200 -2.79901400  2.15702000
H  0.33969000 -1.40455000  2.49329500
H -0.10163000 -2.54563900  1.19949200
H  1.96608800 -1.71997200 -0.19465400
O  2.41526700 -1.67008600 -1.31931600
H  3.33789500 -1.94748600 -1.37436000
H  2.27760700 -0.44827400 -1.14173500
```

2.4.91. A1: Triethylammonium

2.4.91.1. SMD(DMSO)//M06-2X/6-

31++G(d,p)

```

N -0.00063200 -0.00075600 -0.18928100
C  0.02615900  1.43808900  0.25001400
H -0.84166900  1.91257900 -0.20667700
H -0.10562500  1.42630300  1.33556000
C  1.29040700  2.16740100 -0.16547000
H  1.49461900  2.02712400 -1.23203700
H  1.13450500  3.23505300  0.00847900
H  2.16520800  1.85937700  0.41001000
C  1.22987200 -0.74201400  0.25763500
H  2.07720800 -0.22176900 -0.18730500
H  1.27459600 -0.62927900  1.34445100
C  1.23779500 -2.19824500 -0.16902400
H  1.02523700 -2.29683400 -1.23863800
H  2.23966700 -2.59589400  0.01140200
H  0.52958700 -2.80855900  0.39425800
C  -1.25968000 -0.69399700  0.25662200
H -1.23490700 -1.68783900 -0.18905100
H -1.18421200 -0.79019400  1.34338900
C  -2.52436700  0.02978900 -0.16736900
H -3.37027600 -0.63739400  0.01621700
H -2.69473200  0.94909600  0.39572300
H -2.50667700  0.26201700 -1.23722500
H  0.00077700 -0.00462600 -1.21804000

```

2.4.91.2. SMD(THF)//M06-2X/6-

31++G(d,p)

```

N  0.00033800  0.00068900 -0.17883600
C  -1.28448500  0.64637000  0.26888400
H -2.09078500  0.04991000 -0.15629900
H -1.30855800  0.54856300  1.35790900
C  -1.41702500  2.08905300 -0.18185500
H -1.22763100  2.18743400 -1.25556900
H -2.44583200  2.40650100  0.00379100
H -0.75635900  2.76639300  0.36172800
C  1.20434000  0.78979500  0.26573600
H  1.09258200  1.78473300 -0.16399300
H  1.13066300  0.86571100  1.35432100
C  2.52002100  0.17851000 -0.17944600
H  2.51282200 -0.04302700 -1.25184500
H  3.30960900  0.91164300  0.00207400
H  2.77591400 -0.72854900  0.37110800
C  0.08420800 -1.43672000  0.26088900
H  0.99838800 -1.83621400 -0.17682400
H  0.19377700 -1.41519900  1.34886500
C  -1.10707200 -2.26779000 -0.17864900
H -0.86717500 -3.31880400 -0.00058700
H -2.01506800 -2.03508900  0.38010200
H -1.30291100 -2.14753300 -1.24929300
H -0.00172300  0.00339500 -1.20698800

```

2.4.92. A2: Acetic acid

2.4.92.1. SMD(DMSO)//M06-2X/6-

31++G(d,p)

```

C -0.08652601  0.11888904  0.00000000
O -0.63180835  1.20090486  0.00000000
C  1.39164607 -0.11986450  0.00000000
H  1.67007021 -0.70200039  0.88255442
H  1.67007021 -0.70200039 -0.88255442
H  1.91894077  0.83272267  0.00000000
O -0.78754065 -1.02858219  0.00000000
H -1.73461872 -0.80393448  0.00000000

```

2.4.92.2. SMD(THF)//M06-2X/6-

31++G(d,p)

```

C -0.08719915  0.11952320  0.00000000
O -0.63172834  1.20099811  0.00000000
C  1.39167090 -0.11974454  0.00000000
H  1.66924597 -0.70127933  0.88312825
H  1.66924597 -0.70127933 -0.88312825
H  1.91818973  0.83320956  0.00000000
O -0.78707594 -1.02920092  0.00000000
H -1.73333498 -0.80417809  0.00000000

```

2.4.93. B2: Acetate

2.4.93.1. SMD(DMSO)//M06-2X/6-

31++G(d,p)

C	0.19302700	0.00001300	-0.00000300
O	0.70781800	1.14909300	0.00000000
C	-1.34603200	-0.04725800	-0.00000200
H	-1.73079700	0.47866900	-0.88052000
H	-1.72402900	-1.07227200	-0.00009600
H	-1.73076300	0.47848400	0.88064100
O	0.80513400	-1.09926900	0.00000000

2.4.93.2. SMD(THF)//M06-2X/6-

31++G(d,p)

C	0.19557610	0.00024685	0.00000000
O	0.70413547	1.15125313	0.00000000
C	-1.34585488	-0.04961599	0.00000000
H	-1.73055526	0.47653584	-0.88046305
H	-1.72146631	-1.07564520	0.00000000
H	-1.73055526	0.47653584	0.88046305
O	0.80638170	-1.09887282	0.00000000

2.4.94. A3: Oxopyridinic acid

2.4.94.1. SMD(DMSO)//M06-2X/6-

31++G(d,p)

C	0.00000000	1.17354106	0.28614156
C	0.00000000	1.19426278	-1.09768544
C	0.00000000	-0.00000000	-1.81411820
C	0.00000000	-1.19426278	-1.09768544
C	0.00000000	-1.17354106	0.28614156
H	0.00000000	2.05738419	0.91075938
H	0.00000000	2.15583367	-1.59903964
H	0.00000000	0.00000000	-2.89830620
H	0.00000000	-2.15583367	-1.59903964
H	0.00000000	-2.05738419	0.91075938
N	0.00000000	0.00000000	0.96924180
O	0.00000000	-0.00000000	2.26418180

2.4.94.2. SMD(THF)//M06-2X/6-

31++G(d,p)

C	0.01000101	-0.23616069	1.18897103
C	-0.00524382	1.14539131	1.20709087
C	-0.01195465	1.84292118	0.00000000
C	-0.00524382	1.14539131	-1.20709087
C	0.01000101	-0.23616069	-1.18897103
H	0.02421388	-0.87385359	2.06507610
H	-0.00487881	1.65667342	2.16196281
H	-0.01865652	2.92776618	0.00000000
H	-0.00487881	1.65667342	-2.16196281
H	0.02421388	-0.87385359	-2.06507610
N	0.00586901	-0.86270082	0.00000000
O	0.09673484	-2.23165984	0.00000000
H	-0.82048920	-2.56941872	0.00000000

2.4.95. B3: Oxypyridine

2.4.95.1. SMD(DMSO)//M06-2X/6-
31++G(d,p)

```
C  0.000000000  1.17354106  0.28614156
C  0.000000000  1.19426278  -1.09768544
C  0.000000000  -0.00000000  -1.814111820
C  0.000000000  -1.19426278  -1.09768544
C  0.000000000  -1.17354106  0.28614156
H  0.000000000  2.05738419  0.91075938
H  0.000000000  2.15583367  -1.59903964
H  0.000000000  0.00000000  -2.89830620
H  0.000000000  -2.15583367  -1.59903964
H  0.000000000  -2.05738419  0.91075938
N  0.000000000  0.00000000  0.96924180
O  0.000000000  -0.00000000  2.26418180
```

2.4.95.2. SMD(THF)//M06-2X/6-

31++G(d,p)

```
C  0.000000000  1.17362486  0.28622820
C  0.000000000  1.19400607  -1.09743380
C  0.000000000  -0.00000000  -1.81436798
C  0.000000000  -1.19400607  -1.09743380
C  0.000000000  -1.17362486  0.28622820
H  0.000000000  2.05610376  0.91258733
H  0.000000000  2.15555414  -1.59879365
H  0.000000000  0.00000000  -2.89847498
H  0.000000000  -2.15555414  -1.59879365
H  0.000000000  -2.05610376  0.91258733
N  0.000000000  0.00000000  0.97091502
O  0.000000000  -0.00000000  2.26190202
```

2.4.96. A4: Protonated quinuclidine

2.4.96.1. SMD(DMSO)//M06-2X/6-
31++G(d,p)

```
C  -1.40376213  -0.23878977  0.74007274
C  0.000000000  -0.00000000  -1.31214132
C  -1.43958599  0.01714180  -0.77700197
H  -1.64568671  -1.27131810  0.99859498
H  -2.05467190  0.43316748  1.30051771
H  -2.04120084  -0.75795846  -1.25855548
H  -1.90480595  0.98459329  -0.98905755
C  0.90867907  -1.09629878  0.74007274
H  1.92383712  -0.78954745  0.99859498
H  0.65220191  -1.99598180  1.30051771
C  0.70494776  -1.25528893  -0.77700197
H  1.67701170  -1.38875255  -1.25855548
H  0.09972017  -2.14190699  -0.98905755
H  0.000000000  -0.00000000  -2.40432082
C  0.73463823  1.23814713  -0.77700197
H  1.80508578  1.15731370  -0.98905755
H  0.36418914  2.14671101  -1.25855548
C  0.49508306  1.33508855  0.74007274
H  1.40246999  1.56281433  1.30051771
H  -0.27815042  2.06086555  0.99859498
N  -0.00000000  -0.00000000  1.22244125
H  -0.00000000  -0.00000000  2.24610933
```

2.4.97. B4: Quinuclidine

2.4.97.1. SMD(DMSO)//M06-2X/6-
31++G(d,p)

```
C  1.31235057  0.43706054 -0.78785375
C  0.00000000  0.00000000  1.29018400
C  1.29533963  0.62583859  0.75322876
H  2.04569652 -0.32242293 -1.08096354
H  1.58263145  1.36922021 -1.29526207
H  2.16900889  0.14937045  1.21138461
H  1.32736484  1.69009714  1.01562354
C  -0.27766976 -1.35505920 -0.78785375
H  -1.30207471 -1.61041369 -1.08096354
H  0.39446376 -2.05520915 -1.29526207
C  -0.10567770 -1.43471632  0.75322876
H  -0.95514584 -1.95310202  1.21138461
H  0.79998463 -1.99458024  1.01562354
H  0.00000000  0.00000000  2.38470481
C  -1.18966193  0.80887773  0.75322876
H  -2.12734948  0.30448311  1.01562354
H  -1.21386305  1.80373158  1.21138461
C  -1.03468081  0.91799866 -0.78785375
H  -1.97709521  0.68598894 -1.29526207
H  -0.74362181  1.93283662 -1.08096354
N  -0.00000000 -0.00000000 -1.29080151
```

2.4.98. A5: Oxime

2.4.98.1. SMD(DMSO)//M06-2X/6-
31++G(d,p)

```
C      0.04658     0.92332     0.00159
N      0.10169     2.20498    -0.01579
O     -1.13964     2.81407     0.07374
H     -0.92727     3.75831     0.05080
C     -1.21236     0.12764     0.05358
C     -1.36157    -0.86520     1.02853
C     -2.23226     0.33572    -0.88176
C     -2.52706    -1.62846     1.07999
H     -0.56549    -1.03795     1.74837
C     -3.38810    -0.44104    -0.83956
H     -2.11546     1.10056    -1.64310
C     -3.54012    -1.42009     0.14385
H     -2.63964    -2.38980     1.84593
H     -4.17114    -0.28159    -1.57472
H     -4.44389    -2.02126     0.17723
C     1.35619     0.21578    -0.03889
C     2.50368     0.80527     0.50909
C     1.45692    -1.04113    -0.64830
C     3.73204     0.15429     0.43330
H     2.42404     1.77028     1.00031
C     2.68901    -1.68882    -0.72548
H     0.57359    -1.50880    -1.07424
C     3.82892    -1.09316    -0.18644
H     4.61415     0.61743     0.86546
H     2.75767    -2.65894    -1.20856
H     4.78747    -1.60040    -0.24379
```

2.4.99. B5: Deprotonated oxime

2.4.99.1. SMD(DMSO)//M06-2X/6-

31++G(d,p)

C	0.02681	0.93805	-0.00305
N	0.07357	2.25619	0.00284
O	-1.02616	2.93864	0.05613
C	1.33484	0.24201	-0.04031
C	1.48767	-0.99732	-0.68969
C	2.48079	0.80858	0.54938
C	2.72599	-1.63320	-0.75720
H	0.62569	-1.46397	-1.15958
C	3.72072	0.17751	0.47467
H	2.38665	1.75301	1.07654
C	3.85415	-1.04966	-0.17806
H	2.81057	-2.58679	-1.27173
H	4.58572	0.64098	0.94191
H	4.81903	-1.54542	-0.23030
C	-1.22829	0.14637	0.04009
C	-2.37588	0.53165	-0.67508
C	-1.30327	-1.02534	0.81378
C	-3.54215	-0.23155	-0.62506
H	-2.34454	1.43952	-1.26568
C	-2.47097	-1.78445	0.87128
H	-0.43301	-1.34439	1.38241
C	-3.59925	-1.39176	0.14928
H	-4.41314	0.08323	-1.19395
H	-2.49887	-2.68275	1.48200
H	-4.51069	-1.98124	0.18936

2.4.100. C1-AC

2.4.100.1. SMD(THF)//M06-2X/6-

31++G(d,p)

P	0.37535300	1.34027800	-0.48329100
H	0.13348500	1.45750300	-1.85597100
O	-0.83295000	1.49764300	0.38821400
C	1.23913200	-0.21689900	-0.20506500
C	0.68977000	-1.16777600	0.65959700
C	2.45387500	-0.46928100	-0.85443400
C	1.36020300	-2.37140100	0.87721400
H	-0.25862800	-0.96901400	1.15308900
C	3.11772600	-1.67321000	-0.63527700
H	2.88076000	0.27228400	-1.52575000
C	2.57018700	-2.62243400	0.23114700
H	0.93705600	-3.11047700	1.55056000
H	4.05993900	-1.87130400	-1.13689500
H	3.08991000	-3.56062400	0.40198900
O	1.49033600	2.49292000	-0.34697100
C	2.08020100	2.72423600	0.94484400
H	2.49170400	1.79622000	1.35514300
O	-2.72659400	-0.37465200	1.26600100
C	-3.45885800	-0.77520400	0.11460500
H	-4.18959000	-1.50734900	0.47903700
H	-2.10600700	0.32812400	0.99573200
C	-2.55294200	-1.45514900	-0.90690800
H	-3.13739100	-1.84425700	-1.74761600
H	-1.82106400	-0.74168000	-1.30727300
H	-2.00872400	-2.28665700	-0.44843800
C	-4.20190900	0.40888100	-0.49348900
H	-4.81349300	0.09548300	-1.34619900
H	-4.85598600	0.87471100	0.24972500
H	-3.48568900	1.16282000	-0.84249600
H	1.33817400	3.13917200	1.63114400
H	2.88459600	3.44301200	0.79222100

2.4.101. C1-TS

2.4.101.1. SMD(THF)//M06-2X/6- 31++G(d,p)

```

P -0.28425800  0.97576000 -0.12079200
H -1.01538500  0.94790200 -1.30885700
O -0.94503100  1.36277800  1.25350400
C  1.10146500 -0.18938800 -0.06579600
C  1.20957700 -1.16058800  0.93440500
C  2.10465800 -0.06812700 -1.03325200
C  2.31862100 -2.00326800  0.96459700
H  0.42586800 -1.26160600  1.67806200
C  3.20131500 -0.92901300 -1.01311200
H  2.03222700  0.69904800 -1.79938700
C  3.31086000 -1.89239900 -0.01142500
H  2.40578600 -2.75135600  1.74671400
H  3.97181800 -0.83867100 -1.77264700
H  4.16956700 -2.55693500  0.01048700
O  0.49979800  2.35113800 -0.54648400
C  1.37023100  2.97746700  0.39649200
H  2.09681400  2.26477700  0.80465300
O  -1.57978000 -0.59274200  0.35669800
C  -2.67822200 -0.84135700 -0.50202600
H  -2.30356000 -0.82529000 -1.54076700
H  -1.57355300  0.37502800  1.16369500
C  -3.75192600  0.23372800 -0.35736900
H  -4.59208900  0.03600100 -1.03092300
H  -4.13085700  0.25058000  0.67141000
H  -3.35738900  1.22853700 -0.59285100
C  -3.22987700 -2.23024600 -0.21253500
H  -4.03995600 -2.48150300 -0.90543900
H  -2.44081300 -2.98140800 -0.31012900
H  -3.62222600 -2.27195000  0.80977500
H  0.79262600  3.41523300  1.21521500
H  1.90487700  3.76496600 -0.13674500

```

2.4.102. C1-TBP

2.4.102.1. SMD(THF)//M06-2X/6- 31++G(d,p)

```

P -0.45515100  1.07087000 -0.03248000
H -1.14395000  1.21077300 -1.24701600
O -0.64987100  1.85524100  1.39057000
C  0.87107400 -0.18735800 -0.04021700
C  0.90460400 -1.19389400  0.93084000
C  1.87439300 -0.14088400 -1.01474200
C  1.93579700 -2.13225100  0.93558200
H  0.12184700 -1.24142500  1.68212900
C  2.88865400 -1.09711400 -1.02738600
H  1.86257400  0.64964600 -1.75957700
C  2.92406400 -2.08974200 -0.04825600
H  1.96296600 -2.90080700  1.70272200
H  3.65509300 -1.06056800 -1.79600400
H  3.72035900 -2.82866100 -0.05093400
O  0.50181300  2.33759400 -0.61433500
C  1.55361300  2.88713900  0.16085300
H  2.08512600  2.12110000  0.74057100
O  -1.68752700 -0.01648200  0.51253300
C  -2.25903200 -0.89949900 -0.44760600
H  -1.55493000 -1.03033100 -1.28758600
H  -1.28612500  1.36881500  1.93630100
C  -3.56069600 -0.31122500 -0.97722600
H  -4.00240600 -0.96668100 -1.73490500
H  -4.27673100 -0.19516200 -0.15631800
H  -3.39481500  0.67207900 -1.42859700
C  -2.47675400 -2.25187700  0.21323500
H  -2.92950200 -2.95489900 -0.49304800
H  -1.52981500 -2.67366600  0.56183300
H  -3.14778900 -2.14220900  1.07208500
H  1.17155900  3.64447900  0.85270100
H  2.26416500  3.35387400 -0.52775900

```

2.4.103. C3-AC

2.4.103.1. SMD(THF)//M06-2X/6- 31++G(d,p)

```

P -0.07256500  0.42871300  0.60892200
H  0.39288500  0.05462100  1.87605700
O  0.96757200  0.41970800  -0.47198500
C -1.45661400  -0.66997600  0.24429900
C -1.40722700  -1.49108700  -0.88446300
C -2.55745800  -0.71989800  1.10675600
C -2.46623300  -2.35691700  -1.15647400
H -0.54595700  -1.44600300  -1.54553900
C -3.61165300  -1.58751700  0.83317100
H -2.59309700  -0.08085000  1.98600700
C -3.56503500  -2.40452200  -0.29881600
H -2.43244500  -2.99370600  -2.03500000
H -4.46805900  -1.62688600  1.49918200
H -4.38809800  -3.08043700  -0.51117400
O -0.68306000  1.85872400  1.00248700
C -1.06463800  2.87851300  0.03097500
O  2.77191900  -1.71769000  -0.75200300
C  3.91501000  -1.33826800  0.00261400
H  4.56015900  -2.22505300  0.01401700
H  2.14522600  -0.97007100  -0.73611700
C  3.53534000  -0.98574400  1.43745500
H  4.42839200  -0.80767400  2.04593300
H  2.92618700  -0.07392700  1.45471800
H  2.96138200  -1.79826800  1.89422800
C  4.65695600  -0.19234600  -0.67603900
H  5.57277900  0.06263200  -0.13213000
H  4.92550600  -0.46293200  -1.70158900
H  4.01955100  0.69958000  -0.71075300
H -1.69230200  3.55081100  0.62212600
C -1.88156500  2.30550500  -1.11474300
H -1.28138800  1.62983600  -1.73446500
H -2.76329800  1.76984700  -0.75164100
H -2.21834700  3.13020500  -1.75009700
C  0.17666200  3.61745700  -0.43791100
H -0.11815600  4.48352500  -1.03839900
H  0.75651900  3.97265500  0.41853700
H  0.80831700  2.96425400  -1.04665800

```

2.4.104. C3-TS

2.4.104.1. SMD(THF)//M06-2X/6- 31++G(d,p)

```

P  0.22829700  0.62041300  0.32268400
H  1.03056400  0.66196600  1.46361700
O  0.65225900  1.34029200  -1.01474200
C -0.70516700  -0.92073500  0.16229300
C -0.64472300  -1.69326700  -1.00064500
C -1.54401000  -1.29956700  1.21383500
C -1.43785900  -2.83228400  -1.11527300
H  0.01827900  -1.40342800  -1.80993300
C -2.31480600  -2.45680700  1.10699000
H -1.60434400  -0.68738700  2.10981400
C -2.26839100  -3.21751000  -0.06070900
H -1.40276500  -3.424666300  -2.02449900
H -2.95770700  -2.75499700  1.92947000
H -2.87837800  -4.11168800  -0.14977600
O -0.88633400  1.62109800  0.97140200
C -1.92562700  2.33067900  0.25576900
O  1.91712300  -0.41889400  -0.40823300
C  3.09636700  -0.38927900  0.36941700
H  2.81972300  -0.59481500  1.41975200
H  1.53476500  0.60760100  -1.08600500
C  3.76923600  0.98032300  0.30908700
H  4.67945000  0.99726600  0.91730500
H  4.04230500  1.21887200  -0.72596600
H  3.10342100  1.76932400  0.67700500
C  4.03297700  -1.49516300  -0.09867600
H  4.93333700  -1.53851300  0.52370300
H  3.52877100  -2.46476500  -0.05082900
H  4.33669100  -1.31471700  -1.13601500
H -2.66989500  2.53376000  1.03273700
C -2.58386800  1.50688900  -0.84253700
H -1.87509400  1.27153400  -1.64354800
H -3.00733200  0.57644200  -0.45439200
H -3.39837900  2.09539300  -1.27633600
C -1.37400200  3.64966500  -0.26207100
H -2.18850000  4.25626300  -0.67067300
H -0.90020600  4.20936600  0.54956700
H -0.63430400  3.47336900  -1.04754100

```

2.4.105. C3-TBP

2.4.105.1. SMD(THF)//M06-2X/6- 31++G(d,p)

```

P  0.11218600  0.90524500  -0.17069200
H  -0.33956900  1.47529000  -1.37130000
O  0.72424300  1.58672100  1.18527700
C  -0.08606500  -0.90671800  -0.12069100
C  -0.61613600  -1.53073300  1.01202200
C  0.30342900  -1.68174800  -1.21755800
C  -0.72657200  -2.91964200  1.05982900
H  -0.93984400  -0.93046900  1.85794000
C  0.15767800  -3.06814200  -1.18421200
H  0.73284100  -1.20059900  -2.09201800
C  -0.34665500  -3.68885700  -0.04106900
H  -1.12003800  -3.39970300  1.95102400
H  0.44803800  -3.66291600  -2.04512600
H  -0.44589800  -4.76993500  -0.00834500
O  1.62390500  0.93097800  -0.91956700
C  2.92221200  0.65964700  -0.37361200
O  -1.45327400  1.22480500  0.52163300
C  -2.58884400  1.06375500  -0.31797800
H  -2.31047900  0.46017300  -1.19933400
H  -0.00721600  1.80707800  1.78291200
C  -3.06795600  2.43090100  -0.78973500
H  -3.92471400  2.33486900  -1.46462500
H  -3.36825000  3.03649100  0.07239300
H  -2.26940000  2.96083300  -1.31912900
C  -3.66484200  0.31485600  0.45346300
H  -4.55917700  0.18249700  -0.16410800
H  -3.30698900  -0.67169200  0.76203400
H  -3.94357500  0.87992700  1.34964900
H  3.50092500  0.32051000  -1.24276100
C  2.96749200  -0.44842400  0.67500100
H  2.38715600  -0.18214300  1.56344200
H  2.59586400  -1.39795200  0.28120400
H  4.00905700  -0.59443000  0.98032200
C  3.55676500  1.94715700  0.14033300
H  4.61559900  1.77810700  0.36365000
H  3.48625500  2.73188400  -0.61902100
H  3.05459600  2.29116100  1.04807900

```

2.4.106. D1-AC

2.4.106.1. SMD(THF)//M06-2X/6- 31++G(d,p)

```

P  2.36022700  -1.26130100  -0.62919400
H  1.83294900  -1.08480800  -1.91547600
O  3.86167200  -1.67078900  -1.03905500
O  1.63170000  -2.24563300  0.23579300
C  2.45551800  0.37412700  0.12171000
C  2.04101500  0.54843800  1.44506300
C  2.89716100  1.46702100  -0.63193000
C  2.06780600  1.82007700  2.01551300
H  1.69104600  -0.30845400  2.01495000
C  2.91526900  2.73718800  -0.06039100
H  3.21512800  1.33089300  -1.66340700
C  2.50039700  2.91152800  1.26136600
H  1.74486900  1.96010300  3.04253300
H  3.24698000  3.59002900  -0.64453200
H  2.51111000  3.90361300  1.70315300
C  4.80172600  -1.93448600  0.01807100
H  4.85906400  -1.08354200  0.70516200
O  -1.06252500  -2.05760600  -0.54399100
C  -1.30231000  -0.76913400  0.02619700
H  -0.33745000  -0.25765600  0.13714100
C  -1.92969500  -0.90527600  1.39591600
C  -2.19564500  0.03168700  -0.92851100
H  -1.27164600  -1.21192100  2.20882700
C  -3.23043700  -0.70131500  1.62879300
H  -1.80873200  -0.14486100  -1.94275700
C  -3.61486700  -0.54497700  -0.83264400
C  -2.12736100  1.55426500  -0.67375500
H  -3.62171900  -0.81841000  2.64027400
C  -4.22570000  -0.33470600  0.55594500
H  -3.55412600  -1.62472800  -1.02373400
H  -4.27182100  -0.12325500  -1.60080100
H  -2.41145300  1.74900300  0.37046000
H  -4.48189000  0.72999500  0.68079200
C  -5.51668600  -1.13946500  0.72287600
H  -6.24660600  -0.86635900  -0.04689400
H  -5.31463400  -2.21306100  0.63348800
H  -5.97471100  -0.96170300  1.70184600
C  -0.70950200  2.10119000  -0.88304900
H  -0.00471600  1.74810200  -0.12445500
H  -0.32274300  1.80660300  -1.86829900
H  -0.70804200  3.19596200  -0.83915700
C  -3.10309000  2.30934200  -1.58034000
H  -4.14652300  2.05624900  -1.37070800
H  -2.99272300  3.39066900  -1.44666000
H  -2.90566300  2.08095400  -2.63595100
H  -0.20222200  -2.36530800  -0.20895500
H  5.77004300  -2.08251800  -0.45877600
H  4.51444900  -2.83686900  0.56288500

```

2.4.107. D1-TS

2.4.107.1. SMD(THF)//M06-2X/6- 31++G(d,p)

```

P -1.77616200 -1.45140800 0.55228600
H -1.08183900 -1.59324900 1.74603300
O -3.22123100 -1.82696800 1.22319600
O -1.65838700 -2.49921900 -0.61600800
C -2.06256600 0.24984700 0.03610700
C -2.18543000 0.56519200 -1.31976100
C -2.26731600 1.23144700 1.01043300
C -2.51476200 1.86585300 -1.69937700
H -2.03222600 -0.20245000 -2.07429700
C -2.58965700 2.53172300 0.62484400
H -2.18207900 0.98426600 2.06637600
C -2.71661800 2.84748900 -0.72794500
H -2.61444000 2.11093900 -2.75240900
H -2.74203200 3.29607300 1.38067200
H -2.97261400 3.85996500 -1.02560500
C -4.38454400 -1.87805500 0.39550400
H -4.56344900 -0.91118200 -0.08958900
O 0.22487100 -1.37944900 -0.16466500
C 1.02592900 -0.32505400 -0.65653500
H 0.39266600 0.39966200 -1.19084800
C 2.01281000 -0.88648300 -1.65597800
C 1.73284500 0.38870500 0.51263600
H 1.60304900 -1.19233200 -2.61849000
C 3.31672100 -1.03811100 -1.40636700
H 0.99134100 0.47161500 1.32380600
C 2.88184500 -0.50936000 0.99002000
C 2.17112400 1.82444900 0.14614700
H 3.97014800 -1.44461400 -2.17957000
C 3.95662600 -0.69439500 -0.08536200
H 2.46056200 -1.49524200 1.22856500
H 3.33327000 -0.12175700 1.90992800
H 2.70227000 1.78687800 -0.81695000
H 4.50778200 0.25111700 -0.21246400
C 4.97070700 -1.76624300 0.32035000
H 5.44844600 -1.50936400 1.27203000
H 4.47778700 -2.73809000 0.43931600
H 5.75749500 -1.87660600 -0.43360900
C 0.95902400 2.74985200 -0.00454000
H 0.20485600 2.35806500 -0.69401400
H 0.47579900 2.89396000 0.97015400
H 1.26457100 3.73589900 -0.37171500
C 3.11436100 2.42881500 1.19087900
H 4.07379500 1.90679400 1.24781900
H 3.32249500 3.47838400 0.95579700
H 2.65393200 2.39694300 2.18708100
H -0.58740400 -2.17455700 -0.80166000
H -5.22731000 -2.11121200 1.04749500
H -4.28304000 -2.65773000 -0.36465300

```

2.4.108. D1-TBP

2.4.108.1. SMD(THF)//M06-2X/6- 31++G(d,p)

```

P 1.13560800 -1.46924000 -0.27786800
H 0.21246500 -1.49370800 -1.32423300
O 2.25620700 -1.93813700 -1.46245800
O 1.53100700 -2.75996600 0.63660600
C 1.98375300 0.09896400 0.11554100
C 2.12749500 0.51094300 1.44452000
C 2.50203400 0.89295000 -0.91246900
C 2.78686000 1.70232900 1.74274200
H 1.72073500 -0.10099200 2.24596700
C 3.13154000 2.10120200 -0.61561900
H 2.41438200 0.56283500 -1.94388300
C 3.27847000 2.50407600 0.71162600
H 2.90766000 2.00892700 2.77745100
H 3.51501700 2.72211400 -1.41983600
H 3.77970100 3.43952900 0.94262300
C 3.59750800 -2.23899000 -1.12333400
H 3.97821500 -1.59493700 -0.31900700
O -0.16330800 -1.20732500 0.85495600
C -0.97677500 -0.03396200 0.91390000
H -0.38497600 0.76211700 1.38448200
C -2.11921500 -0.36565300 1.84341200
C -1.48112700 0.46996500 -0.45478000
H -1.86054400 -0.48728200 2.89415000
C -3.38199400 -0.52561400 1.43937600
H -0.65667800 0.42125000 -1.17963600
C -2.60334600 -0.46166200 -0.92923600
C -1.87583400 1.96396600 -0.38537500
H -4.15553500 -0.75162500 2.17435500
C -3.81932800 -0.42417700 0.00144300
H -2.21487100 -1.49023600 -0.94423700
H -2.90665400 -0.22286000 -1.95449200
H -2.51554100 2.11602900 0.49655900
H -4.33736600 0.53957700 -0.12424200
C -4.81674800 -1.53339800 -0.33955800
H -5.14548400 -1.45496200 -1.38143700
H -4.35760000 -2.51910300 -0.20149500
H -5.70439200 -1.48062100 0.29980500
C -0.63400500 2.85474700 -0.24908600
H 0.01967900 2.56643300 0.58064100
H -0.03951000 2.81034000 -1.17041300
H -0.92496300 3.89917900 -0.09275500
C -2.65108000 2.41115400 -1.62792500
H -3.62477500 1.92239800 -1.72265700
H -2.82559700 3.49210600 -1.59780400
H -2.07471900 2.19365200 -2.53652500
H 0.95922700 -2.77940100 1.41968200
H 4.21367400 -2.07695900 -2.01295900
H 3.69383200 -3.28281900 -0.80599100

```

2.4.109. D2-AC

2.4.109.1. SMD(THF)//M06-2X/6- 31++G(d,p)

```

P -1.15324700 -0.67023900 -0.91408200
H -1.55416300 -0.94245300 -2.22752000
O 0.35432800 -0.20500900 -1.21853700
O -1.32577100 -1.81264600 0.04199400
C -2.03110700 0.80869700 -0.37123800
C -2.80437100 0.76108900 0.79184900
C -1.94569200 1.99137100 -1.11544000
C -3.49093700 1.89970200 1.21275800
H -2.85803300 -0.16277600 1.36142800
C -2.63610100 3.12470700 -0.69362000
H -1.34272200 2.02602200 -2.02008700
C -3.40742900 3.07724000 0.46989800
H -4.09009400 1.86762600 2.11743500
H -2.57404300 4.04326900 -1.26886800
H -3.94565500 3.96220000 0.79645400
C 1.18171300 0.30420200 -0.12368100
H 0.50575000 0.74231300 0.62436200
C 2.02896800 1.39548300 -0.71567900
C 1.98294300 -0.84680300 0.49514500
H 1.51069400 2.31390400 -0.98595100
C 3.34522600 1.27695900 -0.91275300
H 1.328222800 -1.72508900 0.44818200
C 3.20467900 -1.15516600 -0.37834600
C 2.28398800 -0.62793500 2.00101600
H 3.89492800 2.12170000 -1.32929100
C 4.13928000 0.03496300 -0.60701800
H 2.84194800 -1.48950500 -1.36064900
H 3.76398900 -1.99307700 0.05424900
H 3.09709600 -1.32324100 2.25384400
H 4.72495800 0.22161200 0.30561000
C 5.13418900 -0.25588800 -1.73376800
H 4.60745200 -0.41867900 -2.68097500
H 5.83284500 0.57592700 -1.87212100
H 5.71776600 -1.15528500 -1.51056200
C 2.73762700 0.78152900 2.40190700
H 3.64257200 1.10580500 1.88418100
H 1.95464500 1.52438000 2.20832900
H 2.94604600 0.80341800 3.47713900
C 1.06132300 -1.01635200 2.84023800
H 0.76171600 -2.05236600 2.65348000
H 1.27244900 -0.90786700 3.90951200
H 0.20172700 -0.37544500 2.60594900
O -3.51000000 -3.46477500 -0.44663300
C -4.47750000 -2.43685700 -0.43207600
H -5.42508600 -2.86223500 -0.77406500
H -2.65842700 -3.05344300 -0.21519000
H -4.21671400 -1.60910200 -1.10875500
H -4.63041200 -2.02623200 0.57535700

```

2.4.110. D2-TS

2.4.110.1. SMD(THF)//M06-2X/6- 31++G(d,p)

```

P 1.28676700 -0.75048700 1.12417600
H 1.52875600 -0.62999800 2.48601300
O -0.22998500 -0.15136600 1.22028700
O 1.06647900 -2.15543500 0.44332600
C 2.10457800 0.48619000 0.10274000
C 2.34432400 0.23437400 -1.25050900
C 2.47409400 1.70858800 0.67042300
C 2.95142800 1.21194700 -2.03754000
H 2.06451700 -0.72208100 -1.68624800
C 3.09203300 2.67756600 -0.11857700
H 2.28274000 1.90687300 1.72268000
C 3.32757400 2.43033200 -1.47162900
H 3.13557800 1.01871600 -3.08990300
H 3.38682100 3.62498300 0.32230800
H 3.80632900 3.18779100 -2.08503300
C -1.03152200 -0.02718700 0.01650400
H -0.41471000 -0.32030100 -0.84375500
C -1.40383900 1.42525600 -0.12117400
C -2.23592700 -0.96962800 0.11733800
H -0.59715800 2.10406400 -0.39702200
C -2.63848000 1.89101900 0.08651600
H -1.87064900 -1.85579800 0.65053500
C -3.31767000 -0.33147700 0.99777600
C -2.72648100 -1.47729500 -1.26367200
H -2.83370600 2.95574800 -0.04615400
C -3.80368900 1.03639300 0.51136100
H -2.89718400 -0.19952400 2.00471500
H -4.16809200 -1.01715400 1.09554800
H -3.73953200 -1.87375200 -1.10468700
H -4.46423000 0.90003400 -0.35826400
C -4.62155800 1.74624300 1.59421000
H -4.00318900 1.94180400 2.47775800
H -5.01083900 2.70425000 1.23355100
H -5.47221400 1.12998200 1.90413100
C -2.81027800 -0.42683000 -2.37797100
H -3.46847300 0.40962300 -2.13324700
H -1.82162600 -0.01491100 -2.61414200
H -3.19298800 -0.89509500 -3.29143700
C -1.84218300 -2.63602500 -1.73823100
H -1.83825200 -3.45790800 -1.01487000
H -2.19465800 -3.02835100 -2.69827600
H -0.80330600 -2.30976800 -1.87173900
O 3.12084900 -1.79976500 1.28202100
C 4.35967700 -1.46605900 0.71372500
H 4.64770400 -0.43582900 0.96937100
H 2.14835800 -2.40640800 0.63483700
H 4.35968200 -1.55032700 -0.38352600
H 5.13760200 -2.13728000 1.10140800

```

2.4.111. D2-TBP

2.4.111.1. SMD(THF)//M06-2X/6- 31++G(d,p)

```

P -1.38841100 -1.01999000 -0.86492000
H -1.44821100 -1.03350400 -2.26833300
O 0.12374700 -0.29963300 -1.08373900
O -0.75298700 -2.11446400 0.16788800
C -2.18634500 0.41033500 -0.06488900
C -3.01762100 0.22699600 1.04537600
C -1.98954500 1.69655000 -0.57522700
C -3.62086500 1.32442200 1.65622700
H -3.19492500 -0.77396800 1.43030400
C -2.61809100 2.79159600 0.01879300
H -1.34139100 1.84063100 -1.43543400
C -3.42560900 2.60705200 1.14009900
H -4.25052200 1.17808900 2.52890000
H -2.47135200 3.78637800 -0.39136800
H -3.90644100 3.45973300 1.61038600
C 0.95981700 0.07909000 0.02342000
H 0.35012000 0.08522100 0.93965900
C 1.44135000 1.48511300 -0.24103400
C 2.11254700 -0.92518300 0.18426300
H 0.69528500 2.27292300 -0.14885200
C 2.69663300 1.79392400 -0.57972000
H 1.68576600 -1.90002900 -0.07341100
C 3.20442800 -0.62948300 -0.85156500
C 2.61950400 -1.05822700 1.64358200
H 2.96099600 2.83971300 -0.74318100
C 3.79437100 0.77970600 -0.76570300
H 2.75910100 -0.74537600 -1.84978300
H 4.00501200 -1.37569600 -0.77143800
H 3.60417500 -1.54523000 1.58588800
H 4.46798100 0.83947300 0.10273900
C 4.62822400 1.10687700 -2.00789000
H 4.00187200 1.09524000 -2.90738100
H 5.08930700 2.09716600 -1.92748400
H 5.42854700 0.37130400 -2.14266200
C 2.79497200 0.25132600 2.42342600
H 3.49397000 0.94510100 1.95157100
H 1.83757800 0.77244300 2.54431500
H 3.17415400 0.03009000 3.42749300
C 1.69229900 -1.98330200 2.44017400
H 1.60216400 -2.96521600 1.96423400
H 2.07021300 -2.12977300 3.45820300
H 0.68395700 -1.55857400 2.51289700
O -2.82566100 -1.99843500 -0.84586700
C -3.89223400 -1.58628700 -1.66656500
H -3.53488900 -1.19594700 -2.63338000
H -1.43594400 -2.75593300 0.41712000
H -4.49494900 -0.80490100 -1.18393800
H -4.52921200 -2.45228600 -1.86612800

```

2.4.112. E1-AC

2.4.112.1. SMD(THF)//M06-2X/6- 31++G(d,p)

```

P -0.58134800 1.08425900 0.31391400
H -0.11161800 1.06647400 1.63240200
O 0.47956900 1.01270700 -0.74245300
C -1.80809200 -0.22535800 0.14780000
C -1.62380900 -1.21884700 -0.81719300
C -2.92901100 -0.25194700 0.98641400
C -2.56503100 -2.23975200 -0.94637500
H -0.74938200 -1.18810500 -1.46107000
C -3.86511600 -1.27419900 0.85469800
H -3.07096200 0.52258200 1.73637900
C -3.68183900 -2.26618300 -0.11169400
H -2.42572000 -3.01203500 -1.69626200
H -4.73643400 -1.29777500 1.50169200
H -4.41399100 -3.06175500 -0.21309800
O -1.40694900 2.46454800 0.37896000
C -2.08239100 2.90573600 -0.81217800
H -2.78208300 2.14119600 -1.16608600
H -2.63343700 3.80500200 -0.53896300
H -1.35600100 3.13803300 -1.59465300
O 2.41859100 -1.03215000 -0.56694600
C 3.55183200 -0.46516700 0.08936100
H 1.77371800 -0.31953700 -0.72943700
C 3.10561200 0.26735500 1.35656200
H 2.54513400 -0.41212400 2.00813200
H 3.96836500 0.64948000 1.91298300
H 2.46224000 1.11653200 1.09949200
C 4.26153200 0.50193100 -0.85953200
H 5.14957300 0.93925000 -0.39028600
H 4.57110800 -0.02232300 -1.76963400
H 3.58787200 1.31828200 -1.14449400
C 4.46116200 -1.63566500 0.44022500
H 3.94773100 -2.32744400 1.11612300
H 4.73976700 -2.18304700 -0.46618900
H 5.37555500 -1.28484600 0.92923000

```

2.4.113. E1-TS

2.4.113.1. SMD(THF)//M06-2X/6- 31++G(d,p)

```

P -0.00364500 -1.14003500 0.10476900
H -0.75838100 -1.16764800 1.27208700
O -0.57461200 -1.68790300 -1.25671500
C 1.20824400 0.20389300 0.02368300
C 1.24969100 1.08360700 -1.06193000
C 2.14222600 0.32314800 1.05793400
C 2.22321400 2.07797000 -1.11066600
H 0.51519400 0.99597900 -1.85557300
C 3.10002600 1.33645800 1.01704000
H 2.12388700 -0.37302900 1.89230900
C 3.14297800 2.21018800 -0.06848000
H 2.25893100 2.75585300 -1.95802800
H 3.81612000 1.43523800 1.82719500
H 3.89449800 2.99362000 -0.10471400
O 0.95828200 -2.37311800 0.60142800
C 1.92676100 -2.90670400 -0.30212300
H 2.53081200 -2.11153700 -0.75576100
H 2.57851300 -3.56143500 0.27832800
H 1.43470300 -3.48131300 -1.09168900
O -1.44903700 0.23463700 -0.53209000
C -2.62275900 0.62290200 0.16882200
H -1.31416800 -0.79840900 -1.26916000
C -3.49206900 -0.59717100 0.49005300
H -2.96768300 -1.30687200 1.13930400
H -4.41210700 -0.29369800 1.00102200
H -3.77094000 -1.11838400 -0.43281200
C -3.39478700 1.58196900 -0.73716600
H -4.30885500 1.93678500 -0.24832000
H -2.77215600 2.44763600 -0.98525100
H -3.67359000 1.07931900 -1.66957300
C -2.20218400 1.34508300 1.45061100
H -1.65005100 0.67881200 2.12275000
H -1.55695200 2.19563600 1.20597000
H -3.07820900 1.71697700 1.99271400

```

2.4.114. E1-TBP

2.4.114.1. SMD(THF)//M06-2X/6- 31++G(d,p)

```

P 0.21271700 1.12540100 0.01639300
H 0.92391100 1.31128000 1.20561600
O 0.32992600 1.96123000 -1.38679700
C -1.04790100 -0.20105300 -0.01211100
C -0.98852500 -1.20433800 -0.98639700
C -2.07990200 -0.22526700 0.93204900
C -1.95194400 -2.20970600 -1.02303000
H -0.17741500 -1.20176500 -1.70795800
C -3.02591100 -1.25071100 0.91488600
H -2.14237700 0.55970200 1.67998200
C -2.96692300 -2.24018000 -0.06571700
H -1.90315100 -2.97583500 -1.79136500
H -3.81310000 -1.27037400 1.66305300
H -3.70966800 -3.03269100 -0.08480600
O -0.81444600 2.31841600 0.64966800
C -1.89757700 2.84074300 -0.09878600
H -2.40964200 2.06606200 -0.68470700
H -2.61434500 3.26988400 0.60786100
H -1.55517000 3.62352800 -0.78345400
O 1.48092200 0.11965300 -0.59385700
C 2.39702200 -0.63394200 0.21565300
H 0.98658700 1.52601600 -1.95121800
C 3.47168200 0.30190900 0.77522800
H 3.05717000 1.02328200 1.48649800
H 4.24438500 -0.27300900 1.29627900
H 3.94455100 0.85554000 -0.04241300
C 3.03298200 -1.63626400 -0.74345700
H 3.77547800 -2.25019400 -0.22296100
H 2.26720500 -2.29684500 -1.16324200
H 3.52907800 -1.11245300 -1.56670600
C 1.69685300 -1.39348500 1.34877200
H 1.21179300 -0.72239000 2.06516800
H 0.94364000 -2.08226100 0.95413100
H 2.43996100 -1.97911700 1.89969600

```

2.4.115. E2-AC

2.4.115.1. SMD(THF)//M06-2X/6- 31++G(d,p)

```

P  0.22525700  0.73095500 -0.71190100
H -0.04210500  1.01272500 -2.05839400
O  0.00170300  1.88394000  0.22163300
C -0.78181500 -0.70667100 -0.28634800
C -1.75771200 -0.59276500  0.70727600
C -0.59623500 -1.92059700 -0.95776800
C -2.54156300 -1.69837200  1.03709700
H -1.90149700  0.35618700  1.21868900
C -1.38303200 -3.02141400 -0.62711900
H  0.16540900 -2.00978300 -1.72907100
C -2.35326500 -2.90933700  0.37132000
H -3.29809400 -1.61210300  1.81094000
H -1.23887700 -3.96550100 -1.14349300
H -2.96351000 -3.76967000  0.62975300
O  1.73465800  0.22163200 -0.87813600
C  2.68511100  0.01975600  0.22402700
O -2.54479900  2.88698600  0.63895000
C -3.01509400  2.57639200 -0.65561000
H -4.06997900  2.85951000 -0.70594600
H -2.47333700  3.12858600 -1.43567500
H -2.94487800  1.50046000 -0.87765100
H -1.60178700  2.64372200  0.65692000
C  3.24823900  1.38276600  0.60536300
H  2.46317200  2.02725600  1.00998100
H  4.02923300  1.26185000  1.36262100
H  3.68650700  1.86973300 -0.27114700
C  2.01020900 -0.65627900  1.41246600
H  1.21908300 -0.02929000  1.83744700
H  1.58617300 -1.62489000  1.13016000
H  2.75847600 -0.82305000  2.19316900
C  3.75760500 -0.87787900 -0.37299500
H  4.21152000 -0.40283700 -1.24770600
H  4.54045600 -1.06356900  0.36843300
H  3.32799300 -1.83771000 -0.67634700

```

2.4.116. E2-TS

2.4.116.1. SMD(THF)//M06-2X/6- 31++G(d,p)

```

P  -0.22194000 -0.98784900 -0.32348500
H  -0.19087100 -1.68113100 -1.53268700
O  -0.71017800 -1.69625000  1.00130300
C   1.08606900  0.24792500 -0.14440000
C   1.90998400  0.25903500  0.98371400
C   1.22775000  1.23031700 -1.12805700
C   2.86446100  1.26159400  1.13349400
H   1.80298300 -0.51127700  1.74104300
C   2.20297500  2.21817600 -0.98695600
H   0.57672200  1.23043600 -1.99849900
C   3.01524000  2.23792200  0.14626600
H   3.49618000  1.27687900  2.01632400
H   2.31992700  2.97520600 -1.75637100
H   3.76669300  3.01334400  0.26161700
O  -1.49507300 -0.07896200 -0.77911500
C  -2.35283900  0.74346800  0.06374700
O   1.23940700 -2.44291200  0.15737000
C   1.29855200 -3.53841800 -0.71819100
H   1.67720500 -3.22778000 -1.70323800
H   1.98051400 -4.30221800 -0.32445800
H   0.31439700 -4.01318000 -0.86730100
H   0.20877600 -2.35914100  0.95425500
C  -3.44123000 -0.15278400  0.64636200
H  -3.00877400 -0.89369600  1.32305300
H  -4.16533400  0.45284400  1.20084300
H  -3.96955500 -0.67459500 -0.15772800
C  -1.57355500  1.44445700  1.17399400
H  -1.10822800  0.72516900  1.85514600
H  -0.80114300  2.10395100  0.76724500
H  -2.26948700  2.05503600  1.75782400
C  -2.94989100  1.76823800 -0.89217700
H  -3.48669700  1.26602400 -1.70271000
H  -3.65116800  2.41674100 -0.35807900
H  -2.16138900  2.39053500 -1.32725300

```

2.4.117. E2-TBP

2.4.117.1. SMD(THF)//M06-2X/6- 31++G(d,p)

```

P  0.17800900  1.18549400 -0.29051500
H  0.25266700  1.69517600 -1.59645200
O  0.93698500  1.66185600  1.07685500
C -1.03989500 -0.15440900 -0.08889200
C -1.91120700 -0.14886200  1.00407300
C -1.11316100 -1.18741900 -1.02718400
C -2.82466700 -1.18690500  1.17617300
H -1.87340300  0.66644500  1.72195000
C -2.05151700 -2.20831800 -0.87306900
H -0.43076600 -1.19706600 -1.87261900
C -2.89948200 -2.21477400  0.23456200
H -3.48469900 -1.18878600  2.03844800
H -2.11356400 -3.00165100 -1.61221900
H -3.62128800 -3.01614100  0.36196800
O  1.48281100  0.22985800 -0.75566300
C  2.33777200 -0.64305800  0.01014600
O -0.97737500  2.44674600  0.06327400
C -1.99873300  2.66044100 -0.87933400
H -2.81441000  1.93282100 -0.76666700
H -2.40100500  3.66645500 -0.73193100
H -1.61934200  2.59311300 -1.91221400
H  0.40825900  2.35131800  1.50788500
C  3.52250400  0.16757800  0.53643700
H  3.19294000  0.89611300  1.28005600
H  4.26261100 -0.49719100  0.99497400
H  4.00382300  0.70246000 -0.28887600
C  1.62232900 -1.34990800  1.16427600
H  1.20955700 -0.63540700  1.88161500
H  0.81720500 -1.99683200  0.80371200
H  2.34783400 -1.97746300  1.69256400
C  2.82550600 -1.67958800 -1.00017700
H  3.34664200 -1.18599800 -1.82667100
H  3.51343300 -2.38750200 -0.52663900
H  1.97731100 -2.23862100 -1.40895300

```

2.4.118. E3-AC

2.4.118.1. SMD(THF)//M06-2X/6- 31++G(d,p)

```

P  0.36113700 -0.33405400  0.58415000
H -0.13860700 -0.23198200  1.88918500
O -0.67348300 -0.63680900 -0.45971100
C  1.23793600  1.20852000  0.25412600
C  0.85072600  2.00161800 -0.82823300
C  2.29618600  1.60679800  1.07863800
C  1.53198800  3.18905100 -1.09451800
H  0.02763600  1.68275400 -1.46205500
C  2.97240200  2.79441000  0.81104500
H  2.59680900  0.98862600  1.92143400
C  2.59100200  3.58291600 -0.27701000
H  1.23664300  3.80422400 -1.93883300
H  3.79678300  3.10374100  1.44616600
H  3.12150900  4.50720500 -0.48614800
O  1.46752100 -1.46268900  0.85102100
C  2.18469600 -2.20764900 -0.19208900
O -3.04585500  0.87774500 -0.56213200
C -4.04957700  0.06606900  0.04601800
H -2.22576600  0.35245100 -0.61312000
C  1.27405500 -3.33376900 -0.66428500
H  0.37415600 -2.92965100 -1.13593000
H  1.80478300 -3.95669000 -1.39107300
H  0.97832700 -3.96170300  0.18173300
C  2.58228300 -1.29343500 -1.34592000
H  1.70482800 -0.89261400 -1.86454300
H  3.20256400 -0.46181800 -0.99816200
H  3.16169700 -1.87383300 -2.07030000
C  3.41590600 -2.74839500  0.51789100
H  3.12535700 -3.36224900  1.37550100
H  4.00054300 -3.36577600 -0.17063400
H  4.04680300 -1.92651000  0.87065800
C -4.36277000 -1.12512900 -0.86089000
H -3.46142000 -1.72945100 -1.01450800
H -5.13469200 -1.76640800 -0.42150900
H -4.71386100 -0.77522500 -1.83723100
C -3.56113800 -0.42374500  1.41118600
H -3.27905700  0.42766300  2.04004600
H -4.34142300 -0.99353100  1.92711800
H -2.68672100 -1.07306700  1.28907500
C -5.27362100  0.95936700  0.20215000
H -5.03978800  1.81751200  0.84096400
H -5.59579500  1.33489300 -0.77465700
H -6.10425300  0.40650600  0.65250800

```

2.4.119. E3-TS

2.4.119.1. SMD(THF)//M06-2X/6- 31++G(d,p)

```

P -0.03188800 -0.66552600 -0.16974400
H 0.62647300 -1.06251900 -1.32670900
O 0.10927300 -1.48464700 1.17163900
C -0.23488000 1.12794700 -0.04512100
C 0.09533600 1.82223700 1.12101500
C -0.78778900 1.80558300 -1.13440100
C -0.14513000 3.19149200 1.20082600
H 0.53856300 1.29230500 1.95835800
C -1.00132600 3.18248700 -1.06082300
H -1.05835300 1.26226200 -2.03629500
C -0.68866300 3.87276700 0.10928700
H 0.09886900 3.73011400 2.11149600
H -1.42215600 3.70963300 -1.91173300
H -0.86744600 4.94213200 0.17218600
O -1.48832200 -1.12325700 -0.74871700
C -2.73426300 -1.28573700 -0.01520100
O 1.93990500 -0.36690700 0.53379000
C 3.13906900 -0.66507200 -0.16058400
H 1.19909500 -1.18597200 1.23057700
C -2.75405300 -2.69198300 0.57613200
H -1.96584500 -2.80559100 1.32455800
H -3.72263300 -2.88415200 1.04914300
H -2.60006400 -3.43457200 -0.21307400
C -2.90583200 -0.23436500 1.07951300
H -2.12163300 -0.31291600 1.83906200
H -2.90321900 0.77894800 0.66639500
H -3.86860600 -0.39782100 1.57398100
C -3.81904300 -1.12717500 -1.07391300
H -3.68688500 -1.86793700 -1.86840600
H -4.80777200 -1.26816600 -0.62655700
H -3.77551700 -0.12700200 -1.51689100
C 4.30194700 -0.36857600 0.78726100
H 4.22933200 -0.99563500 1.68259800
H 5.26683400 -0.56275200 0.30551100
H 4.27237300 0.68029800 1.09993200
C 3.18049200 -2.14038100 -0.57705500
H 2.37606000 -2.38454400 -1.27938000
H 4.13162200 -2.38145100 -1.06402200
H 3.07512900 -2.78495800 0.30318900
C 3.22640700 0.24525100 -1.38845600
H 2.40316400 0.05220100 -2.08574900
H 3.17357400 1.29451500 -1.07866700
H 4.16688400 0.08810500 -1.92791200

```

2.4.120. E3-TBP

2.4.120.1. SMD(THF)//M06-2X/6- 31++G(d,p)

```

C 0.11404400 3.79596000 -0.08247400
C -0.42016300 3.09533800 -1.16540600
C -0.49341700 1.70382800 -1.12885900
C 0.00552000 1.00438300 -0.02719900
C 0.55437000 1.70732000 1.04810500
C 0.59164000 3.10132700 1.02901700
P -0.06453300 -0.81602800 0.02243300
O -1.69619200 -0.89187100 -0.58276800
C -2.87666900 -0.85312900 0.23017500
C -2.84242800 0.28361300 1.25778900
O 0.36029000 -1.56528300 -1.36853100
O 1.48145100 -1.04784200 0.67458600
C 2.78914200 -0.92633200 0.08290500
C 3.70344300 -0.53942400 1.24452200
C 3.20070000 -2.29128100 -0.47057900
C 2.88354600 0.13943400 -1.01361100
C -4.01995700 -0.61181700 -0.75167900
C -3.07222800 -2.20352600 0.92709100
H -0.49591000 -1.36422800 1.23507400
H -0.94162600 1.15963900 -1.95556300
H 0.95579800 1.16269500 1.89822100
H -0.79074800 3.63368100 -2.03288800
H 1.00432100 3.64236200 1.87558500
H 0.15584000 4.88103300 -0.10474600
H -0.43757500 -1.67884600 -1.90821800
H 2.56563900 -2.57326600 -1.31342300
H 4.24314500 -2.26805000 -0.80676900
H 3.10617500 -3.05375900 0.30964200
H 2.20495800 -0.07471400 -1.84366900
H 2.66410400 1.13821600 -0.62463400
H 3.90654800 0.14735000 -1.40464500
H 3.64025300 -1.28822900 2.04058100
H 4.74435500 -0.47030200 0.91195100
H 3.40424600 0.43074400 1.65498400
H -4.04876800 -1.40879400 -1.50161000
H -4.98150200 -0.58861700 -0.22823300
H -3.87925200 0.34420100 -1.26672100
H -2.29012600 -2.40080900 1.66683500
H -4.03557700 -2.22780500 1.44726500
H -3.05827300 -3.00901400 0.18561000
H -2.04167100 0.15433300 1.99378500
H -2.70506400 1.25164800 0.76566300
H -3.79095800 0.30676800 1.80436500

```

2.4.121. F1-AC

2.4.121.1. SMD(THF)//M06-2X/6-

31++G(d,p)

```
P -1.87749500  1.10549600  0.31802600
H -1.40887500  1.10826200  1.63725700
O -0.81263500  1.01845500  -0.73376400
C -3.10179500  -0.20789500  0.16671300
C -2.89501500  -1.22833300  -0.76478300
C -4.24290800  -0.21010300  0.97819300
C -3.83474500  -2.25112400  -0.88930300
H -2.00200000  -1.21752000  -1.38302500
C -5.17739200  -1.23452100  0.85142800
H -4.40142800  0.58492900  1.70296400
C -4.97245600  -2.25263500  -0.08279100
H -3.67818100  -3.04419700  -1.61370400
H -6.06443700  -1.23958700  1.47714200
H -5.70376200  -3.04947200  -0.18070500
O -2.70733300  2.48455000  0.36072500
C -3.38036300  2.90645400  -0.83856100
H -4.07765700  2.13534400  -1.18295400
H -3.93393500  3.80864300  -0.58044500
H -2.65248800  3.12849900  -1.62268900
O  0.61642700  -1.28849000  0.07585600
H  0.35332100  -0.43749900  -0.31589000
C  2.02215300  -1.34478200  0.26352700
H  2.22065600  -2.36934300  0.60657700
C  2.51595100  -0.36344300  1.34073100
C  2.80040700  -1.10303500  -1.04032100
H  1.94171400  -0.54168400  2.25894000
C  2.32107000  1.08621700  0.86735200
C  4.01119300  -0.61800000  1.59471800
H  2.42607400  -1.79939000  -1.80099900
C  2.60204900  0.34805200  -1.51078000
C  4.29453500  -1.35647000  -0.78151500
H  2.66763900  1.77629800  1.64803000
H  1.25833100  1.29903300  0.69589800
C  3.11160200  1.31768000  -0.43121900
H  4.16432500  -1.64546900  1.95101700
H  4.37273600  0.05687400  2.38168500
C  4.80524400  -0.38993000  0.29844700
H  1.54409000  0.54900300  -1.72305300
H  3.15030800  0.50588700  -2.44884800
H  4.45042200  -2.39483000  -0.45960200
H  4.85962100  -1.21530900  -1.71221200
H  2.96800300  2.35115300  -0.76941500
C  4.60465100  1.05808200  -0.17636000
H  5.87036500  -0.57483300  0.48344400
H  5.17770000  1.23273100  -1.09709600
H  4.98313200  1.75664100  0.58188800
```

2.4.122. F1-TS

2.4.122.1. SMD(THF)//M06-2X/6-

31++G(d,p)

```
P  1.49990800  -1.14545000  0.15433900
H  0.75792800  -1.28355600  1.32693800
O  0.97157400  -1.68507900  -1.22656600
C  2.56466200  0.31882900  0.09290000
C  2.44820900  1.25307100  -0.94071000
C  3.54682400  0.48079400  1.07531300
C  3.31425300  2.34236800  -0.99096200
H  1.67838300  1.13051800  -1.69542700
C  4.39721700  1.58566100  1.03420600
H  3.65098200  -0.25521800  1.86787800
C  4.28370100  2.51299500  -0.00061900
H  3.22757600  3.06312600  -1.79824400
H  5.15121800  1.71520600  1.80441300
H  4.95094900  3.36900300  -0.03716700
O  2.58140500  -2.28964000  0.60743800
C  3.58698400  -2.69952900  -0.32055200
H  4.11565200  -1.83603900  -0.74192100
H  4.29642000  -3.31872700  0.23048800
H  3.13980300  -3.28163900  -1.13079700
O  -0.12816200  0.06863600  -0.35667600
H  0.12328200  -0.88117400  -1.15043500
C  -1.25314200  0.07327900  0.49410900
H  -0.89588300  0.00481300  1.53953700
C  -2.19554600  -1.11505900  0.22771200
C  -2.03301400  1.38897300  0.34373100
H  -1.62656500  -2.04984300  0.33171200
C  -2.77778700  -1.01151400  -1.19140400
C  -3.33928900  -1.08520000  1.25381600
H  -1.34037200  2.21989900  0.52608800
C  -2.60751600  1.48524500  -1.07759300
C  -3.17657200  1.41232200  1.36964200
H  -3.44020700  -1.86703600  -1.37787700
H  -1.97846100  -1.05536900  -1.94208500
C  -3.55883500  0.30509000  -1.33247600
H  -2.93568200  -1.17618700  2.27098000
H  -4.00576400  -1.94170000  1.08891400
C  -4.12493700  0.22910400  1.11690100
H  -1.78974000  1.47546100  -1.80827200
H  -3.14577700  2.43502000  -1.19522700
H  -2.77040200  1.35490600  2.38849100
H  -3.72519500  2.35999900  1.29097800
H  -3.97389100  0.37865400  -2.34507500
C  -4.70076000  0.33320800  -0.30455100
H  -4.94138100  0.24738100  1.84918100
H  -5.27399300  1.26425400  -0.40817500
H  -5.39274900  -0.49918000  -0.49032600
```

2.4.123. F1-TBP

2.4.123.1. SMD(THF)//M06-2X/6- 31++G(d,p)

```
P -1.45181900 1.28589900 0.11657200
H -0.82968700 1.63925600 1.32352200
O -1.64854900 2.16272600 -1.25089700
C -2.14171300 -0.40429300 0.03703800
C -1.84994900 -1.23110100 -1.05306900
C -2.98500100 -0.87437700 1.04953700
C -2.40239800 -2.50809600 -1.13527900
H -1.18550400 -0.87547200 -1.83557900
C -3.51070300 -2.16455700 0.98353200
H -3.23268700 -0.22855900 1.88705500
C -3.22524700 -2.97968100 -0.11197400
H -2.18083700 -3.13729600 -1.99228900
H -4.15068200 -2.52800900 1.78200800
H -3.64419700 -3.98010700 -0.16948000
O -2.82471700 1.99935800 0.79508900
C -4.04408500 2.07980800 0.07633500
H -4.18775500 1.22181000 -0.59318600
H -4.86059300 2.09193000 0.80473700
H -4.08154000 2.99705000 -0.52035600
O 0.09851800 0.83149800 -0.51346100
H -0.88624100 2.01657500 -1.83156400
C 1.00937100 0.20222400 0.37414200
H 0.48555500 -0.07807600 1.30654300
C 2.15710200 1.16235300 0.72401200
C 1.57566900 -1.07721100 -0.25867100
H 1.72663800 2.07186500 1.16409500
C 2.93801100 1.51488200 -0.55136900
C 3.09297900 0.47710200 1.73164700
H 0.74190600 -1.74565700 -0.50315500
C 2.35837700 -0.71752800 -1.53036700
C 2.51396600 -1.75476400 0.75284000
H 3.74942400 2.21229900 -0.30470100
H 2.27591800 2.01792700 -1.26591900
C 3.51354400 0.23295300 -1.17546200
H 2.54470700 0.23499200 2.65195200
H 3.90529500 1.16214500 2.00733500
C 3.66843900 -0.80539500 1.11015000
H 1.68837600 -0.24188600 -2.25688000
H 2.75133600 -1.63334200 -1.99152300
H 1.95640900 -2.02708100 1.65893300
H 2.90914700 -2.68426800 0.32281400
H 4.07379500 0.48600600 -2.08385300
C 4.44926900 -0.45063700 -0.16586400
H 4.33775300 -1.29358900 1.82897300
H 4.87596600 -1.36154500 -0.60694000
H 5.28696800 0.21580700 0.07996800
```

2.4.124. F2-AC

2.4.124.1. SMD(THF)//M06-2X/6- 31++G(d,p)

```
P 1.124750 -1.074320 -0.525590
H 1.503455 -1.630058 -1.753794
O 1.283134 -1.994495 0.648098
C 2.041490 0.464962 -0.313568
C 2.959911 0.578264 0.734425
C 1.849347 1.531377 -1.200521
C 3.681595 1.760134 0.897647
H 3.110201 -0.256176 1.414974
C 2.572341 2.710021 -1.033393
H 1.137673 1.442522 -2.017945
C 3.486284 2.823436 0.016219
H 4.394536 1.849923 1.711555
H 2.421925 3.538989 -1.718104
H 4.049392 3.743120 0.145078
O -0.374113 -0.650621 -0.905382
O 3.865214 -2.868193 1.193198
C 4.273991 -2.785372 -0.155803
H 4.186961 -1.763084 -0.555271
H 5.327505 -3.073084 -0.207583
H 3.702405 -3.464965 -0.802792
H 2.918453 -2.641138 1.208890
C -1.195061 0.028969 0.083912
H -0.536717 0.463606 0.850658
C -2.158758 -0.970108 0.729527
C -1.966397 1.143476 -0.623678
H -1.571442 -1.761511 1.209133
C -3.085649 -1.564859 -0.341614
C -2.992346 -0.213599 1.777583
H -1.246003 1.829267 -1.086225
C -2.891658 0.537506 -1.690501
C -2.804104 1.887363 0.429965
H -3.773680 -2.277365 0.130725
H -2.497990 -2.118940 -1.082839
C -3.876158 -0.438365 -1.026252
H -2.336487 0.204098 2.552689
H -3.675440 -0.915253 2.272364
C -3.786389 0.910764 1.095034
H -2.298740 0.017227 -2.451782
H -3.439046 1.344325 -2.194427
H -2.147531 2.335769 1.187102
H -3.351254 2.706017 -0.053908
H -4.539358 -0.865227 -1.78093
C -4.711542 0.310141 0.024658
H -4.384089 1.444523 1.843334
H -5.292505 1.108615 -0.455895
H -5.427600 -0.378653 0.492158
```

2.4.125. F2-TS

2.4.125.1. SMD(THF)//M06-2X/6-

31++G(d,p)

P	1.41606700	-1.09613500	-0.24485000
H	1.66712000	-1.75699500	-1.44677800
O	1.21044000	-1.89958700	1.09645300
C	2.18416500	0.53375900	-0.09100100
C	2.97480800	0.85860100	1.01506400
C	1.94897300	1.48426400	-1.08901700
C	3.52142100	2.13479300	1.12340900
H	3.16638800	0.11457300	1.78185000
C	2.51751600	2.75415600	-0.98797400
H	1.32561200	1.23473800	-1.94390100
C	3.29847100	3.08007200	0.12016100
H	4.12804500	2.38997700	1.98680900
H	2.34465300	3.48748900	-1.76962000
H	3.73472700	4.07105000	0.20376400
O	-0.10178300	-0.69271500	-0.68236200
O	3.28889400	-1.93746600	0.23430400
C	3.72180100	-2.95126500	-0.63751600
H	2.95457300	-3.72665200	-0.79660400
H	3.98560800	-2.52866700	-1.61769300
H	4.61446300	-3.44360900	-0.23338700
H	2.31775200	-2.20537200	1.03556400
C	-0.98557200	-0.01739600	0.23539600
H	-0.39297600	0.42859100	1.04875000
C	-1.99198900	-1.01902700	0.81513200
C	-1.71829400	1.08771400	-0.53133900
H	-1.43550700	-1.79607800	1.35062700
C	-2.81226700	-1.63866500	-0.32728900
C	-2.93113800	-0.27133500	1.77726400
H	-0.97520400	1.78658900	-0.93437600
C	-2.53700800	0.46248900	-1.67165600
C	-2.65841100	1.82156400	0.43972000
H	-3.53092200	-2.35705300	0.08783800
H	-2.15123400	-2.18882700	-1.00651100
C	-3.55622000	-0.53101700	-1.09119400
H	-2.35708800	0.16677800	2.60466800
H	-3.64239100	-0.98248400	2.21635700
C	-3.68229700	0.83290400	1.01803400
H	-1.86942900	-0.04828400	-2.37527900
H	-3.05612900	1.25588300	-2.22486600
H	-2.07938300	2.28007700	1.25227000
H	-3.17129600	2.63216700	-0.09340400
H	-4.13959500	-0.97616000	-1.90627300
C	-4.49711700	0.20832200	-0.12667900
H	-4.35416700	1.36094500	1.70549000
H	-5.04683600	0.99252600	-0.66422700
H	-5.23926600	-0.49064600	0.28141900

2.4.126. F2-TBP

2.4.126.1. SMD(THF)//M06-2X/6-

31++G(d,p)

P	1.385014	-1.428649	-0.203683
H	1.468532	-2.034575	-1.468734
O	0.818217	-2.029608	1.206002
C	2.073437	0.254750	-0.083720
C	2.842850	0.617445	1.026993
C	1.853244	1.182660	-1.104770
C	3.360782	1.906795	1.128646
H	3.037190	-0.109810	1.810936
C	2.397294	2.464886	-1.016500
H	1.254868	0.902914	-1.967471
C	3.142239	2.830099	0.104314
H	3.941830	2.188746	2.001564
H	2.233585	3.178360	-1.818525
H	3.556239	3.831291	0.179321
O	-0.168033	-0.970926	-0.680414
O	2.890700	-2.202244	0.205785
C	3.939941	-2.096676	-0.725795
H	3.574917	-2.188172	-1.761788
H	4.468773	-1.137951	-0.632809
H	4.647459	-2.909695	-0.542341
H	1.545665	-2.456550	1.684563
C	-1.006454	-0.178430	0.161014
H	-0.390053	0.302991	0.937310
C	-2.083244	-1.034183	0.847039
C	-1.680050	0.919629	-0.675508
H	-1.584086	-1.824226	1.415397
C	-3.021977	-1.648174	-0.202404
C	-2.888075	-0.126600	1.791558
H	-0.899527	1.505153	-1.175582
C	-2.618472	0.293337	-1.718189
C	-2.486613	1.824252	0.270060
H	-3.776342	-2.268112	0.300305
H	-2.452651	-2.301876	-0.874083
C	-3.703745	-0.530965	-1.007404
H	-2.224767	0.303896	2.553895
H	-3.645886	-0.721225	2.318352
C	-3.563613	0.995611	0.987865
H	-2.045290	-0.347524	-2.398980
H	-3.078929	1.088240	-2.319977
H	-1.816423	2.290418	1.004774
H	-2.954777	2.634616	-0.304017
H	-4.379034	-0.970243	-1.752012
C	-4.504318	0.375730	-0.057892
H	-4.136513	1.642096	1.663879
H	-5.004196	1.169540	-0.629244
H	-5.288380	-0.207762	0.443380

RESUME

La thèse consiste en l'étude de la racémisation d'*hydrogénophénylphosphinates d'alkyle*, des molécules centrées sur un phosphore stéréogénique. Pour cela, nous avons synthétisé les composés d'intérêt puis étudié leur cinétique de racémisation en utilisant l'HPLC chirale et la RMN du phosphore. La première étude théorique (SMD//M06-2X/6-31++G**) sur l'enantiomérisation d'un phosphinate d'alkyle après une S_N2 par un alcool a montré comme mécanisme le plus favorable une *syn*-addition de l'alcool sur la double liaison P=O du phosphinate à l'opposé du groupement alkoxy. Les études cinétiques d'inversion du phosphinate d'éthyle dans l'éthanol à reflux ont montré une barrière de 135 kJ.mol⁻¹ en moyenne, en excellent accord avec ce modèle (136 kJ.mol⁻¹). L'ajout de base lors de l'étude cinétique ont montré une accélération de l'inversion avec une barrière maximum mesurée à 121,5 kJ.mol⁻¹ montrant un effet de catalyse basique. Les modèles cinétiques et théoriques réalisés à ce jour ont suggéré que la base activerait l'alcool pour faciliter son addition. Les premiers résultats sur l'influence du groupement alkyle ont montré une dépendance globale de l'inversion à la taille du groupement, mais certains modèles DFT, notamment avec l'adamantyle, n'étaient pas en accord avec cette hypothèse.

ABSTRACT

This thesis is about the racemization of alkyl *hydrogeno-phenylphosphinate*, a molecule centered on a stereogenic phosphorus atom. We have synthetized compounds of interest, and studied their kinetic of racemization with chiral HPLC and phosphorus NMR. The first theoretical study (SMD//M06-2X/6-31++G**) about the enantiomerization of alkyl phosphinate after an S_N2 with an alcohol have shown that the most favored mechanism was a *syn*-addition of the alcohol onto the double bond P=O on the opposite side of the alkoxy group. Kinetic studies with ethyl phosphinate in ethanol under reflux have shown an inversion barrier around 135 kJ.mol⁻¹, in excellent agreement with this model (136 kJ.mol⁻¹). The addition of a basic compound during kinetic measurements has shown a decreasing of the barrier to 121.5 kJ.mol⁻¹, showing a catalytic effect. Kinetic and theoretical models have suggested that the mechanism would go through an activation of the alcohol by the basic compound which would facilitate its addition. The first tests about the nature of the alkyl group of phosphinate and alcohol have shown a general dependency of the barrier with the hindrance, but some DFT models, especially with adamantyl, have been in disagreement with this hypothesis.